

**UNIVERSIDADE FEDERAL DE MINAS GERAIS (UFMG)**  
**Escola de Engenharia**  
**Departamento de Engenharia Nuclear**  
**Programa de Pós-Graduação em Ciências e Técnicas Nucleares**

João Gabriel de Oliveira Marques

**THERMODYNAMIC ANALYSIS OF A NOVEL TRIGENERATION PROCESS OF  
HYDROGEN, ELECTRICITY AND DESALINATED WATER: THE CASE OF Na-O-H  
CYCLE, GEN-IV NUCLEAR REACTORS AND MED INSTALLATION**

Belo Horizonte

2021

João Gabriel de Oliveira Marques

**THERMODYNAMIC ANALYSIS OF A NOVEL TRIGENERATION PROCESS OF  
HYDROGEN, ELECTRICITY AND DESALINATED WATER: THE CASE OF Na-O-H  
CYCLE, GEN-IV NUCLEAR REACTORS AND MED INSTALLATION**

Doctoral thesis presented to the Graduate Program in Nuclear Science and Technology of the Nuclear Engineering Department of the Federal University of Minas Gerais (UFMG), as a partial requirement to obtain the title of Doctor in Nuclear Science and Technology.

Advisor: Prof. Dra. Antonella Lombardi Costa

Co-advisor: Prof. Dra. Cláudia Pereira Bezerra Lima

Concentration Area: Nuclear and Energy Engineering

Research Line: Technological, Socio-Energetic and Environmental Assessment of Energy Production Systems

Belo Horizonte

2021

## LIBRARY CATALOG

M357t Marques, João Gabriel de Oliveira.  
Thermodynamic analysis of a novel trigeneration process of hydrogen, electricity and desalinated water [recurso eletrônico] : the case of Na-O-H cycle, gen-IV nuclear reactors and med installation / João Gabriel de Oliveira Marques. - 2021.  
1 recurso online (227 f.: il., color.) : pdf.  
Orientadora: Antonella Lombardi Costa.  
Coorientadora: Cláudia Pereira Bezerra Lima.  
Tese (doutorado) - Universidade Federal de Minas Gerais, Escola de Engenharia.  
Apêndices: f. 221-227.  
Bibliografia: f. 196-220.  
Exigências do sistema: Adobe Acrobat Reader.  
1. Engenharia nuclear - Teses. 2. Reatores nucleares - Teses. 3. Dessalinização da água - Teses. 4. Eletricidade - Teses. I. Costa, Antonella Lombardi. II. Lima, Cláudia Pereira Bezerra. III. Universidade Federal de Minas Gerais. Escola de Engenharia. IV. Título.

CDU: 621.039(043)

## APPROVAL DOCUMENT



**UNIVERSIDADE FEDERAL DE MINAS GERAIS**

**PROGRAMA DE PÓS-GRADUAÇÃO EM CIÊNCIAS E TÉCNICAS NUCLEARES**



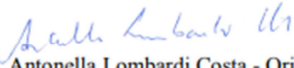
### FOLHA DE APROVAÇÃO

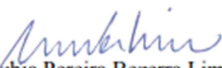
**THERMODYNAMIC ANALYSIS OF A NOVEL TRIGENERATION PROCESS OF HYDROGEN, ELECTRICITY AND DESALINATED WATER: THE CASE OF Na-O-H CYCLE, GEN-IV NUCLEAR REACTORS AND MED INSTALLATION**

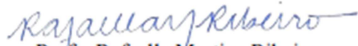
### **JOÃO GABRIEL DE OLIVEIRA MARQUES**

Tese submetida à Banca Examinadora designada pelo Colegiado do Programa de Pós-Graduação em CIÊNCIAS E TÉCNICAS NUCLEARES, como requisito parcial para obtenção do grau de Doutor em CIÊNCIAS E TÉCNICAS NUCLEARES, área de concentração ENGENHARIA NUCLEAR E DA ENERGIA.


Aprovada em 18 de junho de 2021, pela banca constituída pelos membros:

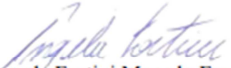
  
Profª. Antonella Lombardi Costa - Orientadora  
Departamento de Engenharia Nuclear - UFMG

  
Profª. Cláudia Pereira Bezerra Lima - Coorientadora  
Departamento de Engenharia Nuclear - UFMG

  
Profª. Rafaella Martins Ribeiro  
Universidade Federal do Rio de Janeiro

  
Prof. Paulo Roberto Lopes Barbieri  
CEFET/MG

  
Prof. André Guimarães Ferreira  
CEFET/MG

  
Profª. Ângela Fortini Macedo Ferreira  
Universidade Federal de Minas Gerais

Belo Horizonte, 18 de junho de 2021.

## INTERNATIONAL EXAMINER: EVALUATION FORM



### UNIVERSIDADE FEDERAL DE MINAS GERAIS

Nuclear Engineering Department  
Graduate Program in Nuclear Science and Technology  
Av. Antônio Carlos, 6627, Pampulha, Escola de Engenharia, Bloco 4  
CEP 31270-901 Belo Horizonte, Minas Gerais, Brazil  
[poscctn@nuclear.ufmg.br](mailto:poscctn@nuclear.ufmg.br) / tel +55 31 34096666



### Thesis Evaluation - External Examiner

Thesis Title: THERMODYNAMIC ANALYSIS OF A NOVEL TRIGENERATION PROCESS OF HYDROGEN, ELECTRICITY AND DESALINATED WATER: THE CASE OF Na-O-H CYCLE, GEN-IV NUCLEAR REACTORS AND MED INSTALLATION

Student: João Gabriel de Oliveira Marques

Advisor(s): Prof. Dr. Antonella Lombardi Costa / Prof. Dr. Cláudia Pereira

External Examiner: Prof. Dr. Ing. Sümer Şahin

University/Institution: Nişantaşı University and Bahçeşehir University, İstanbul, Türkiye

Date: May 11, 2021

Overall rating: **Excellent**

A handwritten signature in blue ink, appearing to read "Aline dos Santos Silva".

Aline dos Santos Silva  
Secretária do Programa de Pós-graduação  
em Ciências e Técnicas Nucleares/UFMG

---

Secretary of the Graduate Program in Nuclear Science and Technology

## RELATED PUBLICATIONS

MARQUES, João G. O.; COSTA, Antonella L.; PEREIRA, Cláudia. Na-O-H thermochemical water splitting cycle: A new approach in hydrogen production based on sodium cooled fast reactor. **International Journal of Hydrogen Energy**, v. 43, n. 16, p. 7738-7753, 2018.

MARQUES, João G. O.; COSTA, Antonella L.; PEREIRA, Cláudia. Produção de água dessalinizada via processo MED (Multi-Effect Distillation) utilizando o calor rejeitado pelo condensador da usina PWR Angra 2. **Anais da Quarta Semana de Engenharia Nuclear e Ciências das Radiações – IV SENCIR**, 2018.

MARQUES, João G. O.; COSTA, Antonella L.; PEREIRA, Cláudia. Gibbs free energy ( $\Delta G$ ) analysis for the Na-O-H (sodium-oxygen-hydrogen) thermochemical water splitting cycle. **International Journal of Hydrogen Energy**, v. 44, n. 29, p. 14536-14549, 2019.

MARQUES, J. G. O.; COSTA, A. L.; PEREIRA, C. Thermodynamic analysis of a Na-OH thermochemical cycle coupled to a Gas Turbine Modular Helium Reactor (GT-MHR). **In: IOP Conference Series: Earth and Environmental Science**. IOP Publishing, p. 012002, 2019.

MARQUES, João G. O.; COSTA, Antonella L.; PEREIRA, Cláudia. Exergy analysis for the Na-O-H (sodium-oxygen-hydrogen) thermochemical water splitting cycle. **International Journal of Hydrogen Energy**, v. 45(20), p. 11424-11437, 2020.

MARQUES, João G. O.; COSTA, Antonella L.; PEREIRA, Cláudia. Thermodynamic study of a novel trigeneration process of hydrogen, electricity and desalinated water: The case of Na-OH thermochemical cycle, SCWR nuclear power plant and MED desalination installation. **Energy Conversion and Management**, v. 209, p. 112648, 2020.

## ACKNOWLEDGMENTS

I thank God, my lord and savior who gave me this opportunity.

I thank my family, where I find support to continue my journey and who encourages me in good and bad times. In particular: Adriana, Conceição, Adaniela, Adailton, Anderson, Andréia, Janete, Norma, Maura, Ícaro, Bárbara, Emanuel, Lucas, Felipe, Geraldo, Márcio, Rodrigo, Ênio, Andrei, Duda, Sofia, Laura, Valentina, Matheus, Rafael, Nathália, Alan, Geraldo e Hélio.

To my teachers and advisors, Antonella and Cláudia, for the opportunity, support and teachings.

To my UFMG friends, especially Márcia, Wallen, Michel, Fidelis, Patrícia, Esther, Janine, Guerra, Dani, Estephanie, Maurício, Sarah, Jonusan, Angelina, Renato, Caio, Bebel, Karina, Jéssica, Igor, Mariana, Raphagalo, Edelize e Keila for their friendship throughout this journey.

To the Graduate Program in Nuclear Science and Technology (PCTN) of the Nuclear Engineering Department (DEN) of the Federal University of Minas Gerais (UFMG) for the opportunity, for the personal and academic developments.

I thank Coordenação de Aperfeiçoamento de Pessoal de Nível Superior - Brazil (CAPES) for the scholarship. Additionally, I am grateful to FAPEMIG (Fundação de Amparo à Pesquisa do Estado de Minas Gerais) and CNPq (Conselho Nacional de Desenvolvimento Científico e Tecnológico) for their support to DEN and PCTN, both from UFMG.

To the professors and assistants of the postgraduate program who somehow contributed to the development of this work, Arno (Bão), Dr. Clarysson, Maria Auxiliadora (Dôra), Tarcísio, Telma, Sônia, Carlos, Aline, Thales and Adriana.

Anyway, I would like to thank everyone who somehow contributed to the realization of this work.

## RESUMO

O hidrogênio ( $H_2$ ) é uma substância com uma ampla gama de aplicações. Ele pode ser obtido de acordo com diferentes processos, incluindo o ciclo termoquímico Na-O-H (sódio-oxigênio-hidrogênio) que quebra moléculas de água por meio de reações químicas cíclicas sustentadas por uma fonte de calor. Nesse contexto, os reatores nucleares de quarta geração (GEN-IV) são opções energéticas adequadas para atender a esse tipo de processos, pois são projetados para fornecer eletricidade em conjunto com aplicações que demandam altas temperaturas. Ao mesmo tempo, água potável poderia ser obtida por meio do processo de dessalinização MED (*Multi-Effect Distillation*) que reutiliza o calor residual de sistemas térmicos. Ainda, a produção de  $H_2$  a partir do ciclo Na-O-H através do calor fornecido por reatores GEN-IV acoplados a uma unidade MED possibilita a trigerção de eletricidade,  $H_2$  e  $H_2O$ , três importantes insumos para a sociedade. Então, o primeiro objetivo principal desta tese é avaliar o desempenho térmico de um novo processo de trigerção, considerando três tecnologias GEN-IV de 1000 MW como fontes de calor para o ciclo Na-O-H e instalação MED. Este objetivo é desenvolvido através da implementação de balanços de massa, energia, entropia e exergia no software *Engineering Equation Solver* (EES) para determinar a quantidade desses três insumos. De acordo com os resultados, o processo avaliado tem potencial para produzir cerca de 5 kg/s de  $H_2$ , 400 MW de eletricidade e 800 kg/s de água. Tais valores obtidos são teóricos e maximizados em função de todas as simplificações consideradas na pesquisa. No segundo objetivo principal é investigado se existem outras variações (b, c, d ou e) do ciclo Na-O-H que apresentam desempenho térmico superior à forma clássica desse sistema, variação (a), avaliada no primeiro objetivo. Os resultados indicaram que a variação (e) apresenta eficiência energética de aproximadamente 77% enquanto a variação (a) apresenta eficiência próxima de 52%. No terceiro objetivo principal são estabelecidos os limites termodinâmicos para ciclos termoquímicos partir de sistemas semelhantes ao Na-O-H. Os resultados mostraram que todos os ciclos termoquímicos devem ter variação de entalpia superior a 283,83 kJ para produzir 1 mol de  $H_2$ . Finalmente, concluiu-se que o processo de trigerção de  $H_2$ , água e eletricidade avaliado no trabalho tem potencial para atender a demanda por tais insumos pelo desenvolvimento futuro dos sistemas analisados.

**Palavras-chave:** Trigerção de  $H_2$ , Eletricidade e Água Dessalinizada; Ciclo Na-O-H; Reatores Nucleares GEN-IV; Dessalinização MED; Performance Térmica; Software EES.



## ABSTRACT

Hydrogen ( $H_2$ ) is a substance with a wide range of important applications like  $NH_3$  production.  $H_2$  can be obtained according to different processes, including the Na-O-H (sodium-oxygen-hydrogen) thermochemical cycle that breaks water through cyclic chemical reactions sustained by a heat source at specified temperature levels. In this context, GEN-IV (Generation IV) nuclear reactors are suitable energy options for these kind of processes because they are designed to provide electricity together with high temperature applications. At the same time, water could be get by means of MED (Multi-Effect Distillation), a desalination method that harvest waste heat from thermal systems to get fresh water from saline one. Then,  $H_2$  production from Na-O-H cycle through the heat supplied by GEN-IV reactors coupled to a MED unit enables the trigeneration of electricity,  $H_2$  and  $H_2O$ , three important goods for society. Therefore, the first main aim of this thesis is to evaluate the thermal performance of this trigeneration process, a new one, considering three  $1000\text{ MW}_{th}$  GEN-IV technologies as the heat sources for both Na-O-H cycle plus a MED installation. This goal is developed by implementing mass, energy, entropy and exergy balances in the Engineering Equation Solver (EES) software to determine the amount of  $H_2$ , electricity and desalinated  $H_2O$  acquired. Consonant with preliminary results, this trigeneration process has potential to produce around  $5\text{ kg/s}$  of  $H_2$ ,  $400\text{ MW}_e$  and  $800\text{ kg/s}$  of  $H_2O$ . These are theoretical and maximized values in function of all simplifications considered in the research. In the second main aim is investigated if there are other variations (b, c, d and e) of the Na-O-H cycle that have higher thermal performance when compared to its classic form, variation (a), evaluated in the first main objective. According to the results, variation (e) has energy efficiency around 77% while variation (a) has energy efficiency near 52%. In the third main aim is established the thermodynamic limits (the minimum requirements of enthalpy change and other thermodynamic parameters) for thermochemical water splitting cycles starting from systems similar to the Na-O-H cycle. The results showed that all thermochemical cycles must have enthalpy change superior to  $283.83\text{ kJ}$  to produce 1 mol of  $H_2$  gas. As it is being demonstrated in this study, it is possible to conclude that the trigeneration process of  $H_2$ , water and electricity has potential to attempt the demand for such goods through more research and development of the systems analyzed.

**Keywords:** Trigeneration of  $H_2$ , Electricity and Desalinated Water; Na-O-H Thermochemical Cycle; GEN-IV Nuclear Reactors; MED Desalination; Thermal Performance; EES software.

## CHARTS LIST

CHART 1 – Cu-Cl cycle: 3-step variation.....	45
CHART 2 – Cu-Cl cycle: 4-step variation.....	45
CHART 3 – Cu-Cl cycle: 5-step variation.....	46
CHART 4 – Examples of thermochemical cycles: high temperature processes.....	46
CHART 5 – Examples of thermochemical cycles: pure cycles x hybrid processes.....	47
CHART 6 – Examples of thermochemical cycles: safety and environmental issues cycles.....	47
CHART 7 – Examples of thermochemical cycles: economic processes.....	48
CHART 8 – Examples of thermochemical cycles: complex processes.....	48
CHART 9 – Brief description of 19 selected hydrogen production methods.....	53
CHART 10 – Key benefits and critical challenges of selected hydrogen production methods....	56
CHART 11 – Technology summary of selected H <sub>2</sub> production methods.....	57
CHART 12 – Summary of some studies about thermochemical cycles.....	87
CHART 13 – Summary of some studies about MED installation.....	90
CHART 14 – Mass flow rate relations for the chemicals in the Na-O-H production unit.....	105
CHART 15 – Mass balances for the control volumes in the Na-O-H production unit.....	105
CHART 16 – Energy balances for the control volumes in the Na-O-H production unit.....	105
CHART 17 – Exergy balances for the control volumes in the Na-O-H production unit.....	106
CHART 18 – Mass balances for the control volumes in the GT-MHR power plant.....	108
CHART 19 – Energy balances for the control volumes in the GT-MHR power plant.....	108
CHART 20 – Exergy balances for the control volumes in the GT-MHR power plant.....	109
CHART 21 – Mass balances for the control volumes in the SFR power plant.....	111
CHART 22 – Energy balances for the control volumes in the SFR power plant.....	112
CHART 23 – Exergy balances for the control volumes in the SFR power plant.....	112
CHART 24 – Mass balances for the control volumes in the SCWR power plant.....	115
CHART 25 – Energy balances for the control volumes in the SCWR power plant.....	115
CHART 26 – Exergy balances for the control volumes in the SCWR power plant.....	115
CHART 27 – Mass balances for each effect in the MED desalination plant.....	118
CHART 28 – Energy balances for each effect in the MED desalination plant.....	119
CHART 29 – Exergy balances for each effect in the MED desalination plant.....	119
CHART 30 – Summary of the input and output variables.....	125

## FIGURES LIST

FIGURE 1 – Pyrolysis process scheme.....	36
FIGURE 2 – Schematic illustration of a basic water electrolysis system.....	38
FIGURE 3 – Conceptual set up of three electrolysis cell technologies.....	39
FIGURE 4 – Flowchart of the four-step Mg-Cl cycle.....	43
FIGURE 5 – Scheme of a H <sub>2</sub> production unit based on the 4-step Cu-Cl cycle and SCWR.....	44
FIGURE 6 – Schematic view of the steps in the Na-O-H cycle.....	50
FIGURE 7 – Schematic view of a GT-MHR power plant.....	61
FIGURE 8 – Schematic view of a SFR power plant.....	63
FIGURE 9 – Schematic view of a SCWR power plant.....	65
FIGURE 10 – Possible desalination routes using nuclear energy.....	68
FIGURE 11 – Schematics of a single-effect MED desalination system.....	69
FIGURE 12 – Schematic diagram of a three-effect MED desalination system.....	70
FIGURE 13 – The first law of thermodynamics for a water heater.....	73
FIGURE 14 – Definition of exergy.....	74
FIGURE 15 – An air reservoir at dead state.....	75
FIGURE 16 – Example: exergy efficiency for a water heater.....	77
FIGURE 17 – $\Delta G$ for three water flow cases .....	81
FIGURE 18 – $\Delta G$ for a generic chemical reaction considering four distinct situations.....	81
FIGURE 19 – EES software example.....	91
FIGURE 20 – Main steps of methodology chapter.....	92
FIGURE 21 – Simplified diagram of the trigeneration cases analyzed.....	101
FIGURE 22 – System A: Na-O-H hydrogen production unit.....	104
FIGURE 23 – System B: GT-MHR power plant.....	107
FIGURE 24 – System C: SFR power plant.....	111
FIGURE 25 – System D: SCWR power plant.....	114
FIGURE 26 – System E: six-effect MED desalination plant.....	117
FIGURE 27 – Algorithm flowchart of the modeling process performed in EES software.....	124
FIGURE 28 – EES software results for SCWR nuclear power plant .....	126
FIGURE 29 – Scheme of a hypothetical self-sustainable thermochemical water splitting cycle...190	
FIGURE 30 – Scheme of a self-sustainable thermochemical cycle without H <sub>2</sub> production.....	190
FIGURE 31 – Scheme of actual thermochemical water splitting cycles.....	191

## GRAPHS LIST

GRAPH 1 – GWP and AP of selected hydrogen production methods.....	54
GRAPH 2 – Production cost of selected hydrogen production methods.....	54
GRAPH 3 – Energy and exergy efficiencies of selected hydrogen production methods.....	55
GRAPH 4 – World water feed quality used in desalination.....	66
GRAPH 5 – Desalination industry by technology and users.....	67
GRAPH 6 – Common brine disposal approaches in Australia.....	69
GRAPH 7 – Specific heat ( $C_p$ ) of the chemicals in the hydrogen production step.....	128
GRAPH 8 – Enthalpy change for the hydrogen production step ( $\Delta H_1$ ).....	129
GRAPH 9 – Enthalpy change for the metal separation step ( $\Delta H_2$ ).....	130
GRAPH 10 – Specific heat ( $C_p$ ) of the chemicals in the metal separation step.....	130
GRAPH 11 – Enthalpy change for the hydrolysis step ( $\Delta H_3$ ).....	131
GRAPH 12 – Specific heat ( $C_p$ ) of the chemicals in the hydrolysis step.....	132
GRAPH 13 – Entropy change for the hydrogen production step ( $\Delta S_1$ ).....	133
GRAPH 14 – Entropy change for the metal separation step ( $\Delta S_2$ ).....	134
GRAPH 15 – Entropy change for the hydrolysis step ( $\Delta S_3$ ).....	135
GRAPH 16 – Gibbs free energy for the hydrogen production step ( $\Delta G_1$ ).....	136
GRAPH 17 – Gibbs free energy of the metal separation step ( $\Delta G_2$ ).....	137
GRAPH 18 – Gibbs free energy of the hydrolysis step ( $\Delta G_3$ ).....	139
GRAPH 19 – Exergy efficiency and exergy destroyed for the hydrogen production step.....	140
GRAPH 20 – Exergy of reactants and products for the hydrogen production step.....	141
GRAPH 21 – Exergy efficiency and exergy destroyed for the metal separation step.....	142
GRAPH 22 – Exergy of reactants and products for the metal separation step.....	142
GRAPH 23 – Exergy efficiency and exergy destroyed for the hydrolysis step.....	143
GRAPH 24 – Exergy of reactants and products for the hydrolysis step.....	144
GRAPH 25 – Electricity generated and thermal efficiency in each trigeneration case.....	145
GRAPH 26 – Exergy destroyed for every NPP's in each trigeneration case.....	147
GRAPH 27 – Exergy efficiency for every NPP's in each trigeneration case.....	147
GRAPH 28 – Hydrogen production in each trigeneration case.....	150
GRAPH 29 – Amount of water required in each trigeneration case to produce $H_2$ .....	151

GRAPH 30 – Desalinated water produced in the MED plant in each trigeneration case.....	154
GRAPH 31 – Sea water mass flow rate required in each trigeneration case.....	155
GRAPH 32 – Heat supplied to the MED plant in each trigeneration case.....	156
GRAPH 33 – Exergy destroyed in the MED plant in each trigeneration case.....	158

## TABLES LIST

TABLE 1 – Coefficients in Eq. (46) to (49) for the chemicals in the Na-O-H cycle.....	95
TABLE 2 – Data at standard state for the chemicals in the NaOH cycle.....	95
TABLE 3 – Standard chemical exergy for the substances in the Na-O-H cycle.....	99
TABLE 4 – Thermodynamic properties of helium in the GT-MHR power plant.....	110
TABLE 5 – Thermodynamic properties of Na and water/steam in the SFR power plant.....	113
TABLE 6 – Thermodynamic properties of water/steam in the SCWR power plant.....	116
TABLE 7 – Calculated thermodynamic properties for the Na-O-H cycle.....	127
TABLE 8 – Pressure ranges for vacuum conditions.....	137
TABLE 9 – Chemical, physical and total exergy for the substances in the Na-O-H cycle.....	139
TABLE 10 – Mass flow rate for every chemical in the Na-O-H cycle in function of H <sub>2</sub> .....	152
TABLE 11 – Standards enthalpy of formation and entropy for Na compounds.....	163
TABLE 12 – $\Delta H_{a,i}^0$ , $S_{a,i}^0$ , $G_{a,i}^0$ and $\eta_a$ for (Na-O-H) <sub>a</sub> and its chemical reactions.....	173
TABLE 13 – $\Delta H_{b,i}^0$ , $\Delta S_{b,i}^0$ , $G_{b,i}^0$ and $\eta_b$ for (Na-O-H) <sub>b</sub> and its chemical reactions.....	174
TABLE 14 – $\Delta H_{c,i}^0$ , $\Delta S_{c,i}^0$ , $\Delta G_{c,i}^0$ and $\eta_c$ for (Na-O-H) <sub>c</sub> and its chemical reactions.....	175
TABLE 15 – $\Delta H_{d,i}^0$ , $\Delta S_{d,i}^0$ , $\Delta G_{d,i}^0$ and $\eta_d$ for (Na-O-H) <sub>d</sub> and its chemical reactions.....	175
TABLE 16 – $\Delta H_{e,i}^0$ , $\Delta S_{e,i}^0$ , $\Delta G_{e,i}^0$ , and $\eta_e$ for (Na-O-H) <sub>e</sub> and its chemical reactions.....	176
TABLE 17 – $\Delta H_i^0$ , $\Delta S_i^0$ , $\Delta G_i^0$ and $\eta_i$ for all variations of the Na-O-H cycle.....	177
TABLE 18 – Standards enthalpy of formation and entropy for Li compounds.....	182
TABLE 19 – Standards enthalpy of formation and entropy for K compounds.....	182
TABLE 20 – Standards enthalpy of formation and entropy for Rb compounds.....	183
TABLE 21 – Standards enthalpy of formation and entropy for Cs compounds.....	183
TABLE 22 – $\Delta H_i^0$ , $\Delta S_i^0$ , $\Delta G_i^0$ and $\eta_i$ for all Li-O-H cycle variations.....	185
TABLE 23 – $\Delta H_i^0$ , $\Delta S_i^0$ , $\Delta G_i^0$ and $\eta_i$ for all K-O-H cycle variations.....	185
TABLE 24 – $\Delta H_i^0$ , $\Delta S_i^0$ , $\Delta G_i^0$ and $\eta_i$ for all Rb-O-H cycle variations.....	186
TABLE 25 – $\Delta H_i^0$ , $\Delta S_i^0$ , $\Delta G_i^0$ and $\eta_i$ for all Cs-O-H cycle variations.....	186
TABLE 26 – $\Delta H_{a,i}^0$ , $S_{a,i}^0$ , $G_{a,i}^0$ and $\eta_a$ for (Li-O-H) <sub>a</sub> and its chemical reactions.....	221
TABLE 27 – $\Delta H_{b,i}^0$ , $\Delta S_{b,i}^0$ , $G_{b,i}^0$ and $\eta_b$ for (Li-O-H) <sub>b</sub> and its chemical reactions.....	221
TABLE 28 – $\Delta H_{c,i}^0$ , $\Delta S_{c,i}^0$ , $\Delta G_{c,i}^0$ and $\eta_c$ for (Li-O-H) <sub>c</sub> and its chemical reactions.....	222
TABLE 29 – $\Delta H_{d,i}^0$ , $\Delta S_{d,i}^0$ , $\Delta G_{d,i}^0$ and $\eta_d$ for (Li-O-H) <sub>d</sub> and its chemical reactions.....	222

TABLE 30 – $\Delta H^0_{e,i}$ , $\Delta S^0_{e,i}$ , $\Delta G^0_{e,i}$ , and $\eta_e$ for $(\text{Li-O-H})_e$ and its chemical reactions.....	222
TABLE 31 – $\Delta H^0_{a,i}$ , $S^0_{a,i}$ , $G^0_{a,i}$ and $\eta_a$ for $(\text{K-O-H})_a$ and its chemical reactions.....	223
TABLE 32 – $\Delta H^0_{b,i}$ , $\Delta S^0_{b,i}$ , $G^0_{b,i}$ and $\eta_b$ for $(\text{K-O-H})_b$ and its chemical reactions.....	223
TABLE 33 – $\Delta H^0_{c,i}$ , $\Delta S^0_{c,i}$ , $\Delta G^0_{c,i}$ and $\eta_c$ for $(\text{K-O-H})_c$ and its chemical reactions.....	223
TABLE 34 – $\Delta H^0_{d,i}$ , $\Delta S^0_{d,i}$ , $\Delta G^0_{d,i}$ and $\eta_d$ for $(\text{K-O-H})_d$ and its chemical reactions.....	223
TABLE 35 – $\Delta H^0_{e,i}$ , $\Delta S^0_{e,i}$ , $\Delta G^0_{e,i}$ , and $\eta_e$ for $(\text{K-O-H})_e$ and its chemical reactions.....	224
TABLE 36 – $\Delta H^0_{a,i}$ , $S^0_{a,i}$ , $G^0_{a,i}$ and $\eta_a$ for $(\text{Rb-O-H})_a$ and its chemical reactions.....	224
TABLE 37 – $\Delta H^0_{b,i}$ , $\Delta S^0_{b,i}$ , $G^0_{b,i}$ and $\eta_b$ for $(\text{Rb-O-H})_b$ and its chemical reactions.....	224
TABLE 38 – $\Delta H^0_{c,i}$ , $\Delta S^0_{c,i}$ , $\Delta G^0_{c,i}$ and $\eta_c$ for $(\text{Rb-O-H})_c$ and its chemical reactions.....	225
TABLE 39 – $\Delta H^0_{d,i}$ , $\Delta S^0_{d,i}$ , $\Delta G^0_{d,i}$ and $\eta_d$ for $(\text{Rb-O-H})_d$ and its chemical reactions.....	225
TABLE 40 – $\Delta H^0_{e,i}$ , $\Delta S^0_{e,i}$ , $\Delta G^0_{e,i}$ , and $\eta_e$ for $(\text{Rb-O-H})_e$ and its chemical reactions.....	225
TABLE 41 – $\Delta H^0_{a,i}$ , $S^0_{a,i}$ , $G^0_{a,i}$ and $\eta_a$ for $(\text{Cs-O-H})_a$ and its chemical reactions.....	226
TABLE 42 – $\Delta H^0_{b,i}$ , $\Delta S^0_{b,i}$ , $G^0_{b,i}$ and $\eta_b$ for $(\text{Cs-O-H})_b$ and its chemical reactions.....	226
TABLE 43 – $\Delta H^0_{c,i}$ , $\Delta S^0_{c,i}$ , $\Delta G^0_{c,i}$ and $\eta_c$ for $(\text{Cs-O-H})_c$ and its chemical reactions.....	226
TABLE 44 – $\Delta H^0_{d,i}$ , $\Delta S^0_{d,i}$ , $\Delta G^0_{d,i}$ and $\eta_d$ for $(\text{Cs-O-H})_d$ and its chemical reactions.....	226
TABLE 45 – $\Delta H^0_{e,i}$ , $\Delta S^0_{e,i}$ , $\Delta G^0_{e,i}$ , and $\eta_e$ for $(\text{Cs-O-H})_e$ and its chemical reactions.....	227

## ABBREVIATIONS

B-MED – Boosted Multi-Effect Distillation  
BPC – British Petroleum Company  
CV – Control Volume  
DB-MED – Distributed Boosted Multi-Effect Distillation  
DEC – Discrete Ericsson Cycle  
EAEC – European Atomic Energy Community  
EES – Engineering Equation Solver  
ESCWA – Economic and Social Commission for Western Asia  
FFP – Fossil Fired Plant  
F-MED – Flash Multi-Effect Distillation  
GEN – Generation of Nuclear Power Plants  
GFR – Gas Cooled Fast Reactor  
GIF – Generation-IV International Forum  
GT-MHR – Gas Turbine – Modular Helium Reactor  
IRENA – International Renewable Energy Agency  
LFR – Lead Cooled Fast Reactor  
LT-MED – Low-Temperature Multi-Effect Distillation  
LWR – Light Water Reactor  
MED – Multi-Effect Distillation  
MSF – Multi-Stage Flash  
MSR – Molten Salt Reactor  
NEA – Nuclear Energy Agency  
NERAC – Nuclear Energy Research Advisory Committee  
NPP – Nuclear Power Plant  
NSW – New South Wales Government  
OECD – Organization for Economic Co-operation and Development  
PT-CSP – Parabolic Trough Concentrated Solar Power  
PWR – Pressurized Water Reactor  
RO – Reverse Osmosis



SCWR – Supercritical Water Reactor

SFR – Sodium Cooled Fast Reactor

UN – United Nations

UNICEF – United Nations International Children's Emergency Fund

VHTR – Very High Temperature Reactor

### CHEMICAL ELEMENTS AND SUBSTANCES

Al	Aluminium
Al <sub>2</sub> O <sub>3</sub>	Dialuminium trioxide
AlBr <sub>3</sub>	Aluminium tribromide
Br	Bromine
Br <sub>2</sub>	Bromine
Cl	Chlorine
Cl <sub>2</sub>	Chlorine gas
CO <sub>2</sub>	Carbon dioxide
Cu	Copper
Cu <sub>2</sub> OCl <sub>2</sub>	Copper oxychloride
CuCl	Copper chloride
CuCl <sub>2</sub>	Copper (II) chloride
Cs	Cesium
Cs <sub>2</sub> O	Dicesium oxide
Cs <sub>2</sub> O <sub>2</sub>	Dicesium peroxide
CsH	Cesium hydride
CsOH	Cesium hydroxide
Eu	Europium
Eu <sub>2</sub> O <sub>3</sub>	Dieuropium trioxide
EuO	Europium oxide
Fe	Ferrous
Fe <sub>3</sub> O <sub>4</sub>	Ferrous (III) oxide (IV)
FeBr <sub>2</sub>	Ferrous bromide
H	Hydrogen

H <sub>2</sub>	Hydrogen gas
H <sub>2</sub> O	Water
H <sub>2</sub> SO <sub>4</sub>	Sulfuric acid
HBr	Hydrogen bromide
HCl	Hydrochloric acid
Hg	Mercury
HgO	Mercury oxide
HI	Hydrogen iodide
I	Iodine
I <sub>2</sub>	Iodine gas
K	Potassium
K <sub>2</sub> O	Dipotassium oxide
K <sub>2</sub> O <sub>2</sub>	Dipotassium peroxide
KH	Potassium hydride
KOH	Potassium hydroxide
Li	Lithium
Li <sub>2</sub> O	Dilithium oxide
Li <sub>2</sub> O <sub>2</sub>	Dilithium peroxide
LiH	Lithium hydride
LiOH	Lithium hydroxide
Mg	Magnesium
MgCl <sub>2</sub>	Magnesium chloride
MgO	Magnesium oxide
MgOHCl	Magnesium chloride hydroxide
Mo	Molybdenum
MoO	Molybdenum oxide
MoO <sub>2</sub>	Molybdenum dioxide
Na	Sodium
Na <sub>2</sub> O	Disodium oxide
Na <sub>2</sub> O <sub>2</sub>	Disodium peroxide
NaH	Sodium hydride

NaOH	Sodium hydroxide
NH <sub>3</sub>	Ammonia
O	Oxygen
O <sub>2</sub>	Oxygen gas
Rb	Rubidium
Rb <sub>2</sub> O	Dirubidium oxide
Rb <sub>2</sub> O <sub>2</sub>	Dirubidium peroxide
RbH	Rubidium hydride
RbOH	Rubidium hydroxide
S	Sulfur
Si	Silicon
SiO	Silicon oxide
SiO <sub>2</sub>	Silicon dioxide
SO <sub>2</sub>	Sulfur dioxide
SO <sub>3</sub>	Sulfur trioxide
Sr	Strontium
Sr(OH) <sub>2</sub>	Strontium hydroxide (II)
Sr <sub>3</sub> U <sub>2</sub> O <sub>8</sub>	Strontium (III) uranium (II) oxide (VIII)
Sr <sub>3</sub> U <sub>2</sub> O <sub>9</sub>	Strontium (III) uranium (II) oxide (IX)
Sr <sub>3</sub> UO <sub>6</sub>	Strontium (III) uranium oxide (VI)
SrI <sub>2</sub>	Strontium iodide (II)
SrO	Strontium oxide
U	Uranium
W	Tungsten
WO <sub>2</sub>	Tungsten dioxide
WO <sub>3</sub>	Tungsten Trioxide

### **THERMODYNAMIC VARIABLES**

$\dot{m}$	Mass flow rate [kg/s]
$\dot{Q}$	Heat rate [MW]
$\dot{W}$	Power [MW]

$h$	Specific enthalpy [kJ/kg]
$\bar{h}$	Specific molar enthalpy [kJ/mol]
$s$	Specific entropy [kJ/kg·K]
$\bar{s}$	Specific molar entropy [kJ/mol·K]
$\dot{S}_G$	Entropy generation [kW/K]
$\eta$	Thermal efficiency
$T$	Temperature [°C; K]
$\Delta\bar{h}$	Sensible molar enthalpy difference [kJ/mol]
$\Delta G$	Gibbs free energy [kJ]
$\Delta H$	Enthalpy change [kJ]
$\Delta S$	Entropy change [kJ/K]
$p$	Pressure [kPa; bar; atm]
$N$	Number of moles [mol]
$e$	Specific exergy [kJ/mol; kJ/kg]
$\bar{e}$	Specific molar exergy [kJ/mol; kJ/kg]
$E$	Exergy [kJ]
$\dot{E}$	Exergy rate [MW]
$\varepsilon$	Exergy efficiency [-]
$E_D$	Exergy destroyed [kJ]
$\dot{E}_D$	Exergy destroyed rate [MW]
$b$	Salt concentration [%]
$y$	Percentage of working fluid from NPP's directed to the Na-O-H plant [ $0 < y < 1$ ]
$x$	quality

### SUBSCRIPTS

in	inlet
out	outlet
P	Products
R	Reactants
0	Dead state
i	Thermodynamic states, chemical reactions [1, 2, 3,...]

ph	Physical
ch	Chemical
th	Thermal
e	Electric

### **SUPERSCRIPTS**

·	Rate
—	Molar base
0	Standard reference state

### **PHYSICAL STATES OF SUBSTANCES**

(aq)	Aqueous
(g)	Gas
(l)	Liquid
(s)	Solid

## SUMMARY

<b>1 INTRODUCTION</b> .....	25
<b>1.1 Aims</b> .....	29
<b>1.2 Systems and trigeneration cases analyzed</b> .....	31
<b>2 THEORETICAL FUNDAMENTS AND LITERTURE REVIEW</b> .....	32
<b>2.1 Conventional and prevailing hydrogen production routes</b> .....	32
<i>2.1.1 Methane Steam Reforming</i> .....	32
<i>2.1.2 Partial oxidation</i> .....	34
<i>2.1.3 Methane cracking</i> .....	34
<i>2.1.4 Pyrolysis and gasification</i> .....	36
<i>2.1.5 Water electrolysis</i> .....	38
<b>2.2 Thermochemical water splitting cycles of hydrogen production</b> .....	40
<i>2.2.1 Basic concepts and currently examples</i> .....	40
<i>2.2.2 Variations of a same thermochemical cycle</i> .....	45
<i>2.2.3 Categories of thermochemical water splitting cycles</i> .....	46
<i>2.2.4 Classic form of the Na-O-H (sodium-oxygen-hydrogen) thermochemical cycle</i> .....	49
<i>2.2.5 Comparative studies among thermochemical cycles and other H<sub>2</sub> production methods</i> .....	52
<b>2.3 Generation IV Nuclear Reactors</b> .....	57
<i>2.3.1 General aspects of GEN-IV nuclear reactors</i> .....	57
<i>2.3.2 Gas Turbine – Modular Helium Reactor (GT-MHR)</i> .....	60
<i>2.3.3 Sodium Cooled Fast Reactor (SFR)</i> .....	62
<i>2.3.4 Supercritical Water Reactor (SCWR)</i> .....	64
<b>2.4 Multi-Effect Distillation (MED) desalination process</b> .....	66
<b>2.5 Physical principles</b> .....	70
<i>2.5.1 Conservation of mass for control volumes</i> .....	71
<i>2.5.2 The first law of thermodynamics for control volumes</i> .....	71
<i>2.5.3 The second law of thermodynamics for control volumes</i> .....	73
<i>2.5.4 Exergy analysis for control volumes</i> .....	74

2.5.5 Enthalpy change for chemical reactions .....	77
2.5.6 Entropy change for chemical reactions .....	78
2.5.7 Gibbs free energy ( $\Delta G$ ) .....	79
2.5.8 Exergy analysis for chemical reactions .....	83
2.6 Literature review .....	84
2.7 Basic aspects and literature review about Engineering Equation Solver (EES) software .....	91
<b>3 METHODOLOGY TO EVALUATE THE TRIGENERATION CASES .....</b>	<b>92</b>
3.1 Defining thermodynamic properties for the chemicals of the Na-O-H cycle .....	93
3.2 Determining operational conditions for the Na-O-H cycle .....	96
3.2.1 Gibbs free energy analysis for the Na-O-H cycle .....	96
3.2.2 Exergy analysis for the Na-O-H cycle .....	98
3.3 Thermodynamic modeling of control volumes and systems .....	101
3.3.1 Modeling of system A – Na-O-H hydrogen production unit .....	103
3.3.2 Modeling of system B – GT-MHR power plant .....	107
3.3.3 Modeling of system C – SFR power plant .....	110
3.3.4 Modeling of system D – SCWR power plant .....	113
3.3.5 Modeling of system E – MED desalination plant .....	116
3.4 Model limitations, simplifications and assumptions .....	120
3.5 Simulations in EES software of the trigeneration cases: flowchart, inputs and outputs .....	120
<b>4 RESULTS AND DISCUSSIONS ABOUT THE TRIGENERATION CASES .....</b>	<b>127</b>
4.1 Verifying input source data .....	127
4.2 Enthalpy change analysis for the Na-O-H cycle .....	128
4.3 Entropy change analysis for the Na-O-H cycle .....	132
4.4 Gibbs free energy analysis for the Na-O-H cycle .....	135
4.5 Exergy analysis for the Na-O-H cycle .....	139
4.6 Thermal aspects of electricity generation in each trigeneration case .....	145
4.7 Thermal aspects of hydrogen production in each trigeneration case .....	149

4.8 Thermal aspects of desalinated water production in each trigeneration case.....	153
4.9 The best option to trigenerate H <sub>2</sub> , electricity and desalinated water.....	159
<b>5 THERMODYNAMIC STUDY ABOUT VARIATIONS OF THE Na-O-H CYCLE.....</b>	<b>160</b>
5.1 The reciprocal ternary system Na-NaOH-Na <sub>2</sub> O-NaH and its chemical reactions.....	160
5.2 Generic thermochemical water splitting cycle.....	161
5.3 Thermodynamic modeling of variations of the Na-O-H cycle.....	162
5.3.1 Modeling Na-O-H cycle – variation (a) – (Na-O-H) <sub>a</sub> .....	163
5.3.2 Modeling Na-O-H cycle – variation (b) – (Na-O-H) <sub>b</sub> .....	165
5.3.3 Modeling Na-O-H cycle – variation (c) – (Na-O-H) <sub>c</sub> .....	166
5.3.4 Modeling Na-O-H cycle – variation (d) – (Na-O-H) <sub>d</sub> .....	169
5.3.5 Modeling Na-O-H cycle – variation (e) – (Na-O-H) <sub>e</sub> .....	170
5.4 Analyzing the results of all variations of the Na-O-H thermochemical cycle.....	172
5.4.1 Analyzing variation (a) of the Na-O-H cycle.....	173
5.4.2 Analyzing variation (b) of the Na-O-H cycle.....	174
5.4.3 Analyzing variation (c) of the Na-O-H cycle.....	174
5.4.4 Analyzing variation (d) of the Na-O-H cycle.....	175
5.4.5 Analyzing variation (e) of the Na-O-H cycle.....	176
5.4.6 Comparing all variations of the Na-O-H cycle.....	176
<b>6 THERMODYNAMIC LIMITS FOR THERMOCHEMICAL CYCLES.....</b>	<b>178</b>
6.1 Generic metal-oxygen-hydrogen (M-O-H) cycle and its variations.....	179
6.1.1 Lithium-oxygen-hydrogen (Li-O-H) cycle and its variations.....	180
6.1.2 Potassium-oxygen-hydrogen (K-O-H) cycle and its variations.....	181
6.1.3 Rubidium-oxygen-hydrogen (Rb-O-H) cycle and its variations.....	181
6.1.4 Cesium-oxygen-hydrogen (Cs-O-H) cycle and its variations.....	181
6.2 Thermodynamic modeling of the cycles Li-O-H, K-O-H, Rb-O-H and Cs-O-H.....	181
6.3 Modeling thermal decomposition of water (thermolysis).....	183
6.4 Results for the cycles Li-O-H, K-O-H, Rb-O-H and water thermolysis.....	184
6.4.1 Results for the Li-O-H cycle and its variations.....	184
6.4.2 Results for the K-O-H cycle and its variations.....	185



<i>6.4.3 Results for the Rb-O-H cycle and its variations</i> .....	185
<i>6.4.4 Results for the Cs-O-H cycle and its variations</i> .....	186
<i>6.4.5 Comparing the results of the thermochemical cycles and water thermolysis</i> .....	186
<b>6.5 Thermodynamic limits for thermochemical cycles operating at standard conditions</b> ...	188
<b>6.6 Thermodynamic limits for thermochemical cycles operating at actual conditions</b> .....	189
<b>6.7 Impossibility of a self-sustainable thermochemical water splitting cycle of H<sub>2</sub> production</b> .....	189
<b>7 FINAL CONCLUSIONS</b> .....	192
<b>7.1 Suggestions for future works</b> .....	194
<b>REFERENCES</b> .....	196
<b>APPENDIX</b> .....	221
<b>Results of all chemical reactions for all variations of the Li-O-H cycle</b> .....	221
<b>Results of all chemical reactions for all variations of the K-O-H cycle</b> .....	222
<b>Results of all chemical reactions for all variations of the Rb-O-H cycle</b> .....	224
<b>Results of all chemical reactions for all variations of the Cs-O-H cycle</b> .....	225

## 1 INTRODUCTION

Energy is an essential matter nowadays and it probably will be for the next generations. It covers several sectors of society like natural resources and environment, economics, international relations among countries (OZCAN and DINCER, 2016a), domestic policy, decision making in both industries and public sector beyond many others. Furthermore, Al-Zareer *et al.* (2017a) claim energy is a key appeal to maintain most of ours prevailing and basic living standards such as hot water, air conditioning, agriculture, water treatment, electricity, driving means of transportation, food conservation, chemicals processing and medical treatment.

In this context, Corumlu *et al.* (2018) believe the global future need for energy will rise due to specific circumstances, for instance, increasing the living standards and quality life of people together with industrialization growth. This line of reasoning comprises the desire of many developing countries that wish to achieve the same development standards as in developed ones. Currently, the global demand for energy is mainly accomplished by utilizing fossil fuels such as coal, natural gas and oil. Proven this fact, source data from British Petroleum Company (BPC, 2018) reveals that more than 70% of all primary energy consumption and near 60% of all electricity generated worldwide in 2017 came from those resources.

Despite their clear importance in modern world, society and many researchers like Sorgulu and Dincer (2018) hope fossil fuels expenditure must drop in the future just not to attend resource management strategies, because they are finite resources and may exhaust sometime, but also to reduce the environmental impacts in soil, in water and air pollutions, particularly CO<sub>2</sub> emission, related to their extraction, processing, transportation and usage. This panorama could reduce the dependency of countries on foreign fossil fuels because energy resources represent security concerns and autonomy for any nation, especially when a state depends on energy appeal from other countries. Hirayama *et al.* (2018) share this same viewpoint. Farther environmental and political preoccupations, some stages of fossil fuels life cycle, such as coal mining, can cause either impact on human health as analyzed by Shandro *et al.* (2011) or social problems like the dispossession of communities in India as Ghosh (2016) discussed in his research.

The overall environmental concerns in addition to a possible energy shortage in the future has led scientists to seek clean and sustainable energy alternatives which have technical feasibility and availability (GONDAL *et al.*, 2018) to complement or even partially replace fossil ones (SAGIR *et al.*, 2018). To sustain such line of thinking, Sorgulu and Dincer (2018) draw attention to the annual investment increasing in the energy sector all over the world, around U\$ 1.8 trillion per year, to find sustainable and renewable energy options while subsidies related to fossil fuels consumption dropped from U\$ 500 billion to U\$ 325 billion respectively considering the years 2014 and 2015. One sustainable energy option under research is the hydrogen ( $H_2$ ).

Hydrogen is a substance with a wide range of applications such as refining agent in oil industry (LIKKASIT *et al.*, 2018), reducer in metals processing (VOGL *et al.*, 2018), propellant for space rockets (BETELIN *et al.*, 2014) and even medicine for medical care (OHTA, 2014). Besides that, Dimitriou *et al.* (2018) pointed out hydrogen is a highly efficient combustible which can be converted into electricity in fuel cells or combustion engines. In a complementary manner, hydrogen is considered a clean and environmentally friendly alternative firing when compared to fossil ones because its combustion mainly releases water. All these characteristics attract the attention of many countries to use hydrogen as fuel or energy option, especially Japan, where there are around 80  $H_2$  refueling stations and it estimated that such number may reach 320 by the year 2025 (HIRAYAMA *et al.*, 2018). The end use of  $H_2$  as combustible in the automotive sector by replacing fossil ones is considered a promising approach of it in the next decades.

However, the most relevant application of  $H_2$  nowadays is ammonia ( $NH_3$ ) production, the key chemical needed to get some important substances such as urea and nitrates employed to make fertilizers, one of the pillars of food and agriculture industries, two vital activities for human subsistence. Around 70% of all  $NH_3$  generated worldwide is designated for such applications (BICER *et al.*, 2016). The making of chemicals, including  $NH_3$  itself, represents around 65% of the final usage of  $H_2$  according to source data from the International Renewable Energy Agency (IRENA, 2018). Still, from this same data, the end use of  $H_2$  as refining agent in oil and other industries represents 25% while its consumption as firing accounts a negligible percentage of all its efforts.

Contrasting all its good features and applications previously described, hydrogen is not freely available in nature, but it normally exists aggregated to other elements like oxygen in water and carbon in hydrocarbons. In this way, some technique, based on the substance used as hydrogen source, must be employed to get it, sometimes demanding a great amount of energy. There are many hydrogen production methods described in the literature as introduced in the studies of Joshi *et al.* (2010), Dufour *et al.* (2012) in addition to Ansarifar and Shams (2018). Among them are coal gasification analyzed by Yilmaz *et al.* (2019a), oil partial oxidation studied by Sengodan *et al.* (2018) and methane steam reforming assessed by Haseli (2019) and many other scientists. All these technics produce H<sub>2</sub> by consuming non-renewable fossil resources and they account more than 90% of all H<sub>2</sub> produced worldwide (IRENA, 2018). In an alternative route, hydrogen is obtained without using fossil fuels through thermochemical cycles.

Thermochemical water splitting cycles or just thermochemical cycles are processes in which H<sub>2</sub> and O<sub>2</sub> gases are indirectly generated over decomposing H<sub>2</sub>O molecules by means of cyclic chemical reactions whose required heat is supplied from some thermal energy system, preferably low-carbon options to reduce the use of fossil resources. There are several thermochemical procedures under research in the literature as listed in the works of Yalçın (1989), Abanades *et al.* (2006), Balta *et al.* (2009) besides Yan and Hino (2011). Among the most recurrent and studied ones are: the sulfur-iodine (S-I), the copper-chlorine (Cu-Cl) and the magnesium chlorine (Mg-Cl). From such studies, the cycles S-I, Cu-Cl and Mg-Cl respectively require operational temperatures around 900 °C, 450-500 °C and 500-530 °C.

Contributing to the development of thermochemical methods, Miyaoka *et al.* (2012) proposed a new cycle composed by three chemical reactions whose substances are formed by combining the elements Na (sodium), O (oxygen) and H (hydrogen). Such system is named Na-O-H (sodium-oxygen-hydrogen). It has potential to operate near 400-500 °C under vacuum or low pressure condition and it has simpler chemical reactions than many of the existing thermochemical ones. The low temperature requirement of a thermochemical process facilitates H<sub>2</sub> production because it enables the use of different energy systems, including nuclear power plants (NPP's). So, there are some NPP's capable to provide heat considering the temperature limits required by the Na-O-H cycle. Among them are: Gas Turbine Modular Helium Reactor (GT-MHR), Sodium Cooled

Fast Reactor (SFR) and Supercritical Water Reactor (SCWR). They all belong to the Generation IV Nuclear Reactors (GEN-IV) which are designed to achieve high temperature applications, including H<sub>2</sub> production.

It is known that NPP's, like most thermal power cycles, release a great amount of heat to the environment through their condensers or coolers during electricity generation. Normally, this kind of energy has low temperature (low exergy), making it a not appropriate thermal source to produce work. However, such waste heat could be reused to secure potable H<sub>2</sub>O through a relatively low temperature desalination method known as Multi-Effect Distillation (MED) whose operational temperature lies near 55-70 °C (KHALID *et al.*, 2016). This system could be coupled to a NPP in order to replace its condenser and then harvest the wasted heat.

Then, in such approach, the already available fresh H<sub>2</sub>O would be saved to be used in essential human activities, for instance, drinking and agriculture, while desalinated water would serve as hydrogen source in the Na-O-H system. Still, water obtained through this method could supply the already existing lack of potable water in the world. Kaminski *et al.* (2018), using source data from the United Nations International Children's Emergency Fund (UNICEF, 2015), estimate that 663 million of people worldwide, one in ten, lack direct access to drinkable H<sub>2</sub>O; one third of the global population lives without access to a toilet or improved sanitation conditions. From these facts, it is perceptible that the problem of water scarcity also affects essential human needs like basic sanitation and just not only the direct availability of drinkable one.

Considering everything discussed until now, it is verified that H<sub>2</sub> production based on the techniques Na-O-H thermochemical cycle through the heat supplied by a GEN-IV nuclear reactor coupled to a MED desalination unit allows the attaining of electricity, H<sub>2</sub> and H<sub>2</sub>O. These three products express key goods presently, what justifies the development of a thesis covering this trigeneration process, a task never done before which guarantees novelty for a research covering it. This newness is mainly justified because the Na-O-H cycle is a recent method that was not properly evaluated since Miyaoka *et al.* (2012) introduced it for the first time while the GEN-IV and MED desalination ones are relatively well-known technologies under development and they are a way to achieve an end that is H<sub>2</sub> making. Then, all the novelty aspects of this research are intrinsically related to the Na-O-H cycle and not to the other two systems (MED and GEN-IV).

So, it becomes necessary to figure out if this new trigeneration process, considering its possible cases, has satisfactory thermal aspects aiming an actual implementation of it in the future. Additionally, it is important to investigate if the Na-O-H system has other configurations that may have superior thermal aspects when compared to its conventional version introduced by Miyaoka *et al.* (2012). Each variation of it consists of the same chemical elements and substances used in the traditional Na-O-H cycle but with different chemical steps. Then, extrapolating from the thermal aspects of the Na-O-H cycle and its variations, they are established the thermodynamic limits for thermochemical water splitting cycles of H<sub>2</sub> making. All these thoughts are explored during the thesis development in function of its three main aims described next.

### 1.1 Aims

This research has three main aims, each one with its respective specific objectives. They are presented briefly now and then developed at specific chapters of the work with more details.

*(i) First main aim: evaluating three trigeneration cases of H<sub>2</sub>, electricity and desalinated water*

The first main aim of this thesis is to evaluate the thermal performance of three trigeneration cases of electricity, H<sub>2</sub> and desalinated water. H<sub>2</sub> comes from a hydrogen production unit based on the Na-O-H thermochemical water splitting cycle whose required heat is provided by three different NPP's (GT-MHR, SFR and SCWR), what distinguish every case. Fresh water is secured in a MED desalination facility that replaces the condensers or coolers in each NPP. It was considered a 1000 MW<sub>th</sub> for each NPP because this amount of heat is a common value adopted in different studies covering nuclear reactors like Al-Hamadi *et al.* (2020) and Kim *et al.* (2009).

This aim is achieved athwart the following steps or specific objectives that represent the main phases of methodology in chapter 3 which results are presented and discussed over chapter 4.

- i.a) Definition of proper source data (thermodynamic properties and states, boundary conditions, equations and similar) to develop the next steps.
- i.b) Establishment of specific theoretical operational conditions (pressure and temperature) in which the three chemical reactions of the sodium-oxygen-hydrogen cycle,

and consequently a H<sub>2</sub> production unit based on such cycle are able to proceed. It is done through a Gibbs free energy study followed by an exergy analysis related to this system;

- i.c) Application of mass, energy, entropy and exergy balances for the systems (Na-O-H hydrogen production unit, NPP's and MED facility) and their constituent devices (nuclear reactors, turbines, chemical reactors and etc.) to assess their thermal performances (energy and exergy) in addition to the amount of hydrogen, electricity and fresh water produced in each trigeneration case;

Step “i.b” is directly related to the understanding of the basic thermodynamic behavior of the sodium-oxygen-hydrogen cycle in addition to its possible theoretical operational conditions. Step “i.c” covers the overall thermodynamic features of the analyzed technologies. All the NPP's and their thermodynamic cycles, as well as the hydrogen production unit and the desalination plant are evaluated according to the steps “i.b” and “i.c” implemented in the Engineering Equation Solver (EES) software (KLEIN, 2019), available at Federal University of Minas Gerais (UFMG), as reported in methodology section. Steps “i.b” and “i.c” are developed considering the classic form of the Na-O-H cycle introduced in the research of Miyaoka *et al.* (2012).

This proposed research provides a first insight on many technologies under study that still even exist in industrial scale, but only on experimental or theoretical ones. The first main aim also let comprehend if all of the technologies under study are able to provide H<sub>2</sub>, electricity and H<sub>2</sub>O with satisfactory thermal performances, especially the Na-O-H system when compared to other thermochemical cycles or the traditional and prevailing H<sub>2</sub> production methods represented by methane steam reforming, water electrolysis plus few others.

(ii) Second main aim: investigating variations of the Na-O-H cycle to improve its thermal aspects

The second main goal of this work is to analyze different variations (a, b, c, d and e) of the Na-O-H system to determine if one of them has better thermal aspects when compared to the traditional form of this cycle, variation (a), initially proposed by Miyaoka *et al.* (2012). Such aim is accomplished in chapter 5 by comparing the enthalpy ( $\Delta H$ ), entropy ( $\Delta S$ ) and Gibbs free energy ( $\Delta G$ ) changes plus energy efficiency ( $\eta$ ) for all modes of the Na-O-H trial, considering standard conditions ( $T_0 = 25$  °C and  $p_0 = 1$  bar) for all its configurations.

*(iii) Third main aim: establishing thermodynamic limits for thermochemical cycles*

Finally, in the third aim of this research are established the thermodynamic limits (the minimum requirements of enthalpy, entropy and Gibbs free energy changes plus the maximum energy efficiency) for thermochemical water splitting cycles of hydrogen production after analyzing and comparing the values of  $\Delta H$ ,  $\Delta S$ ,  $\Delta G$  and  $\eta$  among different thermochemical cycles (Li-O-H, K-O-H, Rb-O-H and Cs-O-H) with their respective variations and the direct thermal decomposition of water (thermolysis). These new procedures are analogous to the Na-O-H one, but they have compounds based on chemical elements of the Group 1A of the periodic table like lithium (Li), potassium (K), rubidium (Rb) and cesium (Cs) instead of sodium (Na). Some of these processes are actual ones while others are hypothetical ones as it is explained later in the thesis. This final aim is developed in chapter 6 considering standard conditions of temperature and pressure for all systems under attention, combined with many of the concepts first introduced in chapter 5.

## 1.2 Systems and trigeneration cases analyzed

The systems analyzed in the work are:

- System A: Na-O-H hydrogen production unit;
- System B: Gas Turbine Modular Helium Reactor (GT-MHR) nuclear power plant;
- System C: Sodium Cooled Fast Reactor (SFR) nuclear power plant;
- System D: Supercritical Water Reactor (SCWR) nuclear power plant;
- System E: Multi-Effect Distillation (MED) desalination facility.

Using these technologies, it is possible to compare three trigeneration cases. Each one constituted by a hydrogen production facility based on the Na-O-H thermochemical cycle, a desalination installation (MED) plus a nuclear power plant (GT-MHR, SFR or SCWR) that produces electricity and supplies heat to the other two processes. Such cases are:

- Case 1: Na-O-H cycle + GT-MHR + MED facility (Systems A + B + E);
- Case 2: Na-O-H cycle + SFR + MED facility (Systems A + C + E);
- Case 3: Na-O-H cycle + SCWR + MED facility (Systems A + D + E).

Then, in chapter 2 are introduced the basic thermodynamic fundamentals employed to develop the work in addition to the literature review.



## **2 THEORETICAL FUNDAMENTS AND LITERATURE REVIEW**

This chapter is divided into seven parts. In the first one, 2.1, they are commented about the traditional and prevailing H<sub>2</sub> production methods while in section 2.2 are introduced the main aspects of thermochemical water splitting cycles. The general features, including thermodynamic cycles, related to the Generation IV nuclear power plants chosen as the driven heat sources to perform the work are described during item 2.3. The technology employed to produce fresh water is the MED desalination explained in topic 2.4. The basic thermodynamic fundamentals needed to develop the thesis are first studied in section 2.5. During subject 2.6 is presented a literature review about studies covering hydrogen production through thermochemical cycles coupled to different energy systems, including NPP's. Additionally, some references about different MED desalination technics using low grade waste heat are also discussed. Finally, in the seventh and last portion of chapter 2 is shown how mathematical equations and thermodynamic properties are implemented in the Engineering Equation Solver (EES) software. It is the tool employed in the methodology to model and to evaluate the technologies under attention.

### **2.1 Conventional and prevailing hydrogen production routes**

There are a wide variety of possible hydrogen production methods available nowadays. Throughout this section are presented some of the conventional and prevailing ones, focusing attention on processes that require any type of energy resource. This overview over other H<sub>2</sub> routes allows understanding the choice of the Na-O-H cycle to develop the study.

#### ***2.1.1 Methane Steam Reforming***

Known as catalytic steam reforming, methane steam reforming (MSR), steam methane reforming (SMR) or just steam reforming is the main technology employed currently to produce H<sub>2</sub> gas. It happens due to some interesting aspects like its relatively simplicity and low costs, suitable for industrial large scale production in addition to high efficiency conversion of methane (CH<sub>4</sub>) into hydrogen (TUNA *et al.*, 2018). Such route accounts around 50% of all H<sub>2</sub> produced worldwide considering source data from IRENA (2018).

MSR proceeds when natural gas, mostly composed of methane, reacts with water steam to produce hydrogen and carbon oxides as explanation from Ricca *et al.* (2017). Such chemical process happens as in Equations (1) or (2) provided by Chaichi *et al.* (2018) and Shin *et al.* (2017).



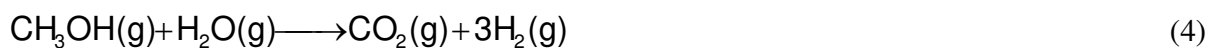
According to a study published by IEA (2006), the gaseous products in Equation (1) contains about 12% of carbon monoxide (CO) which can be turned into additional H<sub>2</sub> plus CO<sub>2</sub> after CO reacting with water in a reaction known as water-gas shift shown in Equation (3).



Based on the research performed by Tuna *et al.* (2018), the final concentration of H<sub>2</sub>, CO<sub>2</sub> and CO in Equations (1), (2) and (3) are directly affected by different aspects such as reactants concentration, pressure and temperature inside the chemical chamber where the reaction occurs as well as the chemical and physical properties of the catalyst used to support the process.

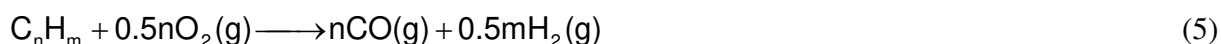
Methane steam reforming normally takes place at temperatures close to 800 °C (IEA, 2006), but Yun *et al.* (2018) plus Shin *et al.* (2017) highlight that new low temperature reformer units that operate around 400-500 °C have been developed to reduce energy losses and increase the thermal efficiency of the process by using a special catalyst that reduces its temperature requirement.

Traditionally, steam reforming refers to getting H<sub>2</sub> starting from the reaction between CH<sub>4</sub> and H<sub>2</sub>O as in Equations (1) or (2). However, the expression steam reforming can be associated to the reaction between water steam and other fuels or chemicals to obtain gaseous H<sub>2</sub> like in methanol steam reforming (JI *et al.*, 2018) presented in Equation (4), steam reforming of glycerol (AMAN *et al.*, 2018) and steam reforming of acetic acid (OMONIYI and DUPONT, 2018).



### 2.1.2 Partial oxidation

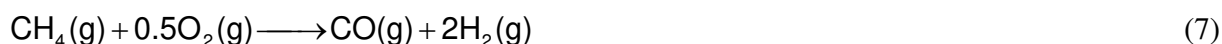
In the words of Sengodan *et al.* (2018), “partial oxidation (POX) is a process in which methane, natural gas or hydrocarbon is heated in the presence of a stoichiometric amount of pure oxygen” producing carbon oxide (CO) and H<sub>2</sub> as in Equation (5), where C<sub>n</sub>H<sub>m</sub> is a generic hydrocarbon.



He *et al.* (2018) explain that POX is naturally exothermic, releases heat, because it has negative enthalpy change. In this way, it can be thermally self-sustained. This gas mixture of CO and H<sub>2</sub> is sometimes referred as syngas. In the case of propane (C<sub>3</sub>H<sub>8</sub>), its partial oxidation is described by Equation (6) and it has negative enthalpy change equal to 497 kJ/mol (HE *et al.*, 2018).



Similarly, partial oxidation of methane has negative enthalpy change about 35.6 kJ/mol and it happens according to Equation (7) from Sengodan *et al.* (2018).



Usually, POX of hydrocarbons is performed in the presence of a catalyst to decrease the temperature required to carry out the process (HOGNON *et al.*, 2018). As discussed in the last section, the majority of all hydrogen produced nowadays comes from steam reforming. However, Hognon *et al.* (2018) pointed out that such route is a high endothermic reaction. So, these same researchers consider partial oxidation as a good candidate to replace or complement MSR and then equilibrate the thermal balance because POX occurs in a thermally self-sustaining way.

### 2.1.3 Methane cracking

Methane cracking consists of breaking the CH<sub>4</sub> molecules into elemental carbon (C) and H<sub>2</sub> gas, without carbon dioxide emissions, through a very high temperature heat source in the absence of oxygen gas as can be seen in Equation (8) from Weger *et al.* (2017). If this reaction happens in

the presence of O<sub>2</sub> also will be formed carbon oxides instead pure elemental carbon, what contributes to climate changes like global warming.



Based on the study developed by Amin *et al.* (2011), the separation of C and H<sub>2</sub> can be easily done by absorption technics or membrane separation of the gaseous phase (H<sub>2</sub>) to produce a volume near to 99% of pure hydrogen segregated from solid carbon. This same group of researchers believes that such approach is much simpler than the separation of two gaseous products (CO or CO<sub>2</sub> and H<sub>2</sub>) as in the traditional steam reforming technique.

The element C resulting after the separation step have potential to be used in many important applications with economic value like the production of carbon nanotubes suggested by Weger *et al.* (2017) and even the capture and storing of CO<sub>2</sub> proposed by Amin *et al.* (2011) in order to reduce potential climate effects referring to the presence of carbon dioxides on atmosphere.

In relation to its energy consumption, Amin *et al.* (2011) point out that methane cracking has enthalpy of formation of 74.8 kJ/mol at 298 K, in contrast to 253.2 kJ/mol at 298 K of MSR. According to these same authors, the energy required in this cracking reaction can be supplied burning about 15% in weight of the H<sub>2</sub> obtained in the process itself.

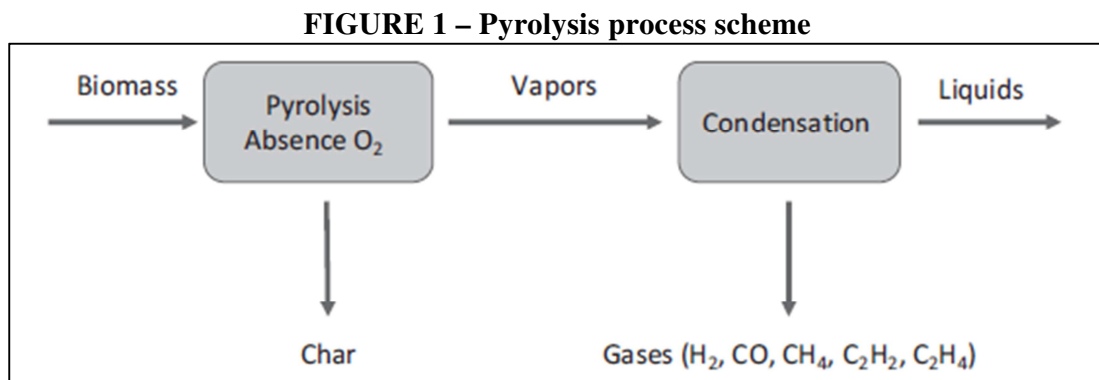
Instead its low energy requirements compared to other hydrogen routes, CH<sub>4</sub> cracking reaction demands very high temperature limits, close to 1200 °C, a consequence of the strong bond between carbon and hydrogen atoms (ABBAS and DAUD, 2010). However, this limit can be reduced due to the catalyst employed as explanation and examples given in the study developed by Zhou and Basset (2016). The high temperature levels involved in methane cracking limit the energy options capable to achieve its maximum temperature requirement. According to Abbas and Daud (2010), the main energy sources employed in methane cracking are solar and plasma.

Due to its interesting characteristics such as very low carbon oxides emissions and the possibility to capture CO<sub>2</sub>, Weger *et al.* (2017) think that methane cracking is a potential bridge between the current carbon-intensive energy technologies based on fossil resources and the expected future

low-carbon energy systems. At the same time, Abánades *et al.* (2013) accredit methane cracking is a technology that already proved its scientific viability, but it must be developed considering industrial questions, for example, reliability, continuity, sustainability and economic aspects. In such context, those authors suggest that some innovative technology must be developed to overcome the gap between laboratory and industrial scales.

#### 2.1.4 Pyrolysis and gasification

Quispe *et al.* (2017) define pyrolysis as “a thermal process where organic matter or biomass is decomposed in the presence of high temperatures and absence of oxygen”. Vegetables and their oils, woods, agriculture and municipal organic wastes are all examples of biomass. In Figure 1 (QUISPE *et al.*, 2017) is represented a scheme of a traditional pyrolysis process.



Source: Quispe *et al.* (2017).

The co-products formed in a pyrolysis are: bio-oil or liquids that compose the condensable part of a vapor mixture; non-condensable gas mixture (syngas) including H<sub>2</sub>, carbon oxides (CO and CO<sub>2</sub>) and hydrocarbons (CH<sub>4</sub>, C<sub>2</sub>H<sub>2</sub> and etc); solid residue also known as char or bio-char (WANG *et al.*, 2016). The gas mixture or syngas can be burned to supply the heat required in the process or cover other industrial applications while char or bio-char can supplement or replace coal as an energy resource or even be a means to capture and store CO<sub>2</sub>, as suggest by Quispe *et al.* (2017). According to the study of Peters *et al.* (2014), the final fractions and composition of each co-product is directly affected by biomass itself and the operational conditions in which the reaction is performed.

Pyrolysis is usually classified into three different categories: slow, intermediate and fast. Each one is defined in function of some aspects like heating rate, residence time, feed rate and reaction temperature (QUISPE *et al.*, 2017). Still, these same researchers classify as slow and intermediate pyrolysis when it proceeds at temperatures below 500 °C and fast pyrolysis when it happens at temperatures between 500 and 700 °C.

Despite being a natural and renewable resource with potential to reduce important environmental impacts such as global warming by decreasing the burning of fossil fuels, Peters *et al.* (2014) think biomass is a heterogeneous solid fuel with relatively low density, what makes its transportation difficult and consequently reduces its potential for industrial applications. Due to this reason, such authors explain that biomass is converted into bio-oil that has heating value or energy content close to its precursor organic matter but with higher density in liquid phase and thus facilitating its handle and usage.

In contrast, Duman and Yanik (2017) list some inappropriate aspects of bio-oil that diminish its direct application, including low calorific value, corrosiveness, highly viscosity and water content. Peters *et al.* (2014) credit bio-oil has potential to be an important energy carrier in the future if pyrolysis becomes an efficient technology. Therefore, even producing H<sub>2</sub>, a high content energy fuel, the main target of pyrolysis is to obtain bio-oil and char as highlighted by Duman and Yanik (2017).

Similar to pyrolysis, gasification is a thermochemical process which converts solid materials, such as biomass, wood and coal, into a gas mixture rich in high-quality hydrogen fuel (AIDYN *et al.*, 2018) by heating them in order to remove their water content and volatile products. According to Bläsing and Müller (2018), “a general advantage of co-gasification is that it allows for the use wood in larger, more efficient coal driven plants and weaken some environmental and commercial problems, e.g. CO<sub>2</sub> emission and costs because of transport distance”.

Then, based on the last two paragraphs and depending on the circumstances, pyrolysis and gasification processes could be employed in a combined way where the first method would produce a bio-char that would be used to produce H<sub>2</sub> gas through gasification because the main aim of pyrolysis is not to generate hydrogen gas but bio-oil and char.

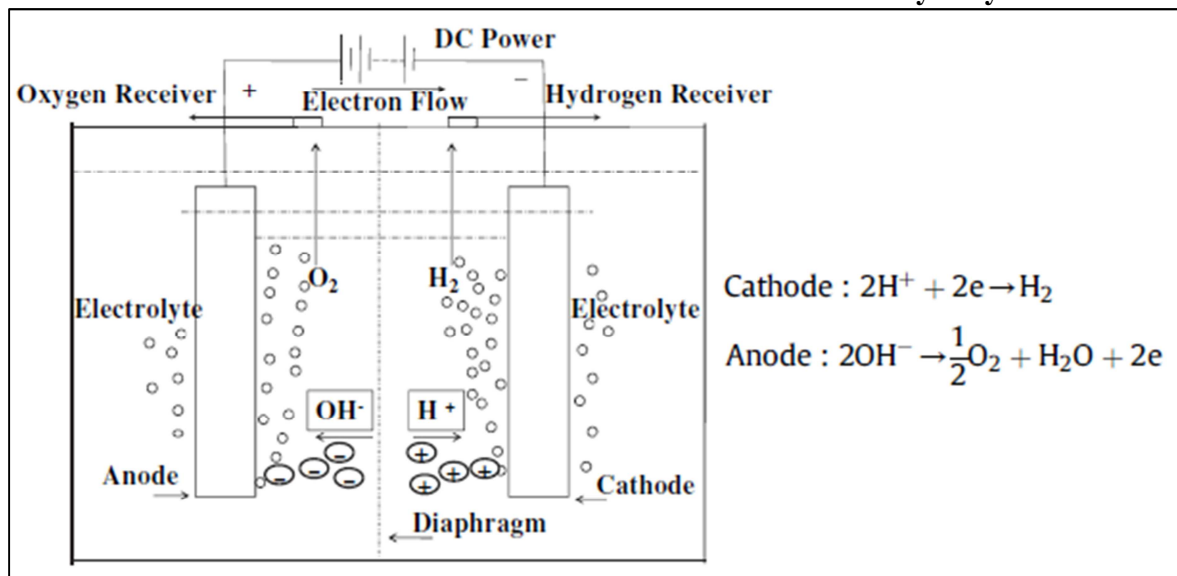
### 2.1.5 Water electrolysis

Water electrolysis is an electrochemical reaction that separates H<sub>2</sub>O molecules into O<sub>2</sub> and H<sub>2</sub> through an electric current according to Equation (9) exhibited by Chakik *et al.* (2017). Authors like Dobó and Palotas (2017) considered it as one of the simplest methods to make H<sub>2</sub>.



A traditional electrolysis device or electrolyzer consists of a cathode, an anode, a power supply of direct current (DC) plus an electrolyte (solution with free moving ions like K<sup>+</sup>, Na<sup>+</sup> or Cl<sup>-</sup>) as shown in Figure 2 adapted from Zeng and Zhang (2010). The reactions that occur in cathode and anode also are described in this same figure. The chemical, physical and electrical properties of all agents involved in electrolysis influence its overall efficiency (CHAKIK *et al.*, 2017).

**FIGURE 2 – Schematic illustration of a basic water electrolysis system**



Source: adapted from Zeng and Zhang (2010).

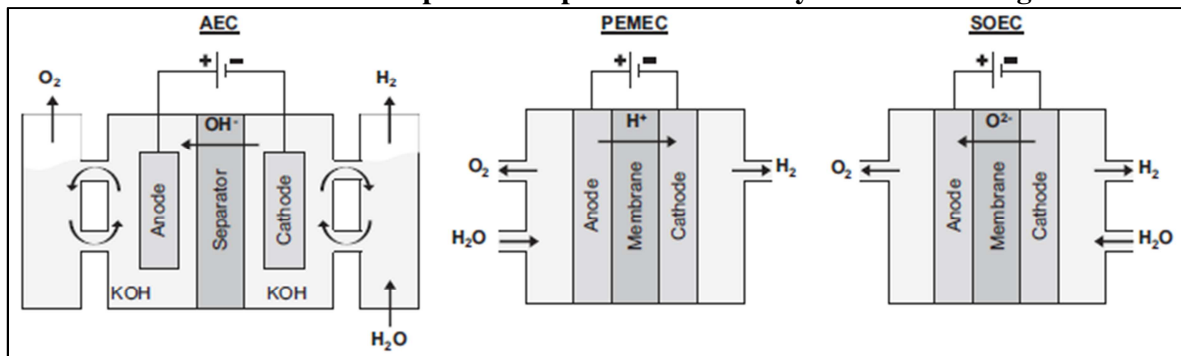
Zeng and Zhang (2010) explain that when an electric current is applied in water in the presence of an electrolyte, electrons flow from the negative region of the apparatus (anode) to the positive region where hydrogen ions or protons (H<sup>+</sup>) of water consume electrons to produce H<sub>2</sub> gas. At the same time, to maintain the electrical charge (electrons transfer) and consequently electrolysis itself, hydroxide ions (anions OH<sup>-</sup>) flow from the electrolyte solution to anode where they release

the electrons required to keep the electrochemical reaction (ZENG and ZHANG, 2010). Both oxygen and hydrogen formed during the process are collected in specific receivers.

Based on the study of Chakik *et al.* (2017), they concluded that water electrolysis is a simple, ecological and relatively clean technology with easy maintenance aspects. Additionally, it can produce high purity hydrogen (PATEL *et al.*, 2018). However, Chakik *et al.* (2017) draw attention to the fact that such method needs to improve its economic and energy performances in order to be a competitive technology. Dobó and Palotas (2017) concluded in their research that due to economic reasons related to electrolysis, the majority of all hydrogen produced nowadays comes from fossil resources. Additionally, among the main limitations related to electrolysis are its high energy dissipation caused by joule effect plus parasitic reactions within water/electrolyte solution (CHAKIK *et al.*, 2017). All these facts contributes to the relatively low amount of H<sub>2</sub> produced worldwide through this route, merely around 4% (IRENA, 2018), and the need of an electric potential higher than the theoretical value of around 1.23 V (PATEL *et al.*, 2018).

There are many different electrolysis approaches. The procedure described in Figure 2 is the classic model based on Alkaline Electrolysis Cells (AEC) and it is used for industrial applications. In contrast, other two methods, PEMEC (Proton Exchange Membrane Electrolysis Cells) and SOEC (Solid Oxide Electrolysis Cells) are relatively new electrolysis technologies under development and less mature than alkaline electrolysis (SCHMDIT *et al.*, 2017). In a simple way, both PEMEC and SOEC uses a solid material as electrolyte instead an electrolytic fluid like in AEC. According to explanation provided from Schmdit *et al.* (2017), PEMEC uses a polymer as electrolyte while SOEC employs a solid ion-conducting ceramic. The differentiation between these three processes is schematized in Figure 3 (SCHMDIT *et al.*, 2017).

**FIGURE 3 – Conceptual set up of three electrolysis cell technologies**



Source: Schmdit *et al.* (2017).



## 2.2 Thermochemical water splitting cycles of hydrogen production

This subject covers the main aspects of thermochemical water splitting cycles of H<sub>2</sub> making.

### 2.2.1 Basic concepts and currently examples

One possible direct way to produce hydrogen without the need of fossil fuels like in MSR or POX routes or another non-renewable resource is by splitting H<sub>2</sub>O molecules into H<sub>2</sub> and O<sub>2</sub> gases through a heat source as in Equation (10). Such process is known as water thermolysis (BAYKARA, 2004 and ACAR *et al.*, 2016).



Çelik and Yildiz (2017) pointed out that such reaction only occurs at extremely high temperatures supplied by some thermal source, like heat at 2200 °C as Dincer and Acar (2015) imply. This makes its application difficult with nuclear reactors and the most of energy systems, because their working fluids and materials cannot reach that level of temperature to sustain the reaction.

On the other hand, hydrogen is also gained from water splitting by electrolysis. In this route, H<sub>2</sub>O is directly cracked into hydrogen and oxygen by consuming electricity instead of heat in Equation (10). As already is known, electricity generation from thermal sources has relatively low energy efficiency, ordinarily around 35-40%. Additionally, producing electrical work is more expensive than heat because the first one necessarily requires an energy conversion method, like a Rankine or Brayton power cycles, to change heat into electricity. Forsberg (2003) thinks these drawbacks can make electrolysis a not competitive option to produce H<sub>2</sub> in large scale, except where electricity is available at low cost. So, to surpass the problems related to thermolysis and electrolysis were proposed thermochemical water splitting cycles.

A thermochemical cycle consists of a sequence of cyclic chemical reactions supplied by a thermal energy source to indirectly decompose water into H<sub>2</sub> and O<sub>2</sub> based on more viable temperature ranges than the traditional thermolysis method (ÇELIK and YILDIZ, 2017). Dincer

(2012) emphasizes that all the chemicals (reactants and products) involved in this kind of procedure are recycled in a closed loop, except H<sub>2</sub>O that is a consumable resource and the source of H<sub>2</sub>. Still, such methods could need electricity or not to ensue (YAN and HINO, 2011). When thermochemical procedures only need heat, they are named pure cycles. In contrast, when these techniques demand heat and electricity (electrochemical process), they are referred hybrid ones.

There are many thermochemical processes under research and development that are referenced in the literature. Among the most recurrent and promising cycles are: the sulfur-iodine (S-I) studied by Zhou *et al.* (2017), Kasahara *et al.* (2017), Ying *et al.* (2017) and Xu *et al.* (2018); the copper-chlorine (Cu-Cl) evaluated by Ozbilen *et al.* (2016a), Ozbilen *et al.* (2016b), Wu *et al.* (2017), Sayyaadi and Boroujeni (2017) plus Ouagued *et al.* (2018); and the magnesium chlorine (Mg-Cl) analyzed by Ozcan and Dincer (2016b), Ozcan and Dincer (2016c), Ozcan and Dincer (2017) in addition to Ozcan and Dincer (2018). Each procedure is composed by a well-defined number of chemical reactions or steps that occur at specific conditions of pressure and temperature with chemical compounds of sulfur-iodine, copper-chlorine and magnesium-chlorine in its respective cycle. All the main steps involved in these three routes are described in the following paragraphs of this subsection. Each technic is more adequate to operate consonant the heat source available in function of the maximum operational temperature required by every thermochemical method.

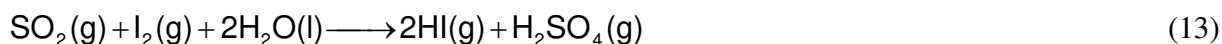
The S-I cycle is described based on Equations (11), (12), (13) and (14) adapted from Dincer and Acar (2015). The first reaction of this system consists of an aqueous solution of H<sub>2</sub>SO<sub>4</sub> (sulfuric acid) heated up at 300-500 °C to generate two gaseous products, H<sub>2</sub>O (water) and SO<sub>3</sub> (sulfur trioxide), as in Equation (11).



In the next step, H<sub>2</sub>O(g) and SO<sub>3</sub>(g) are separated from each other by a heating process at around 800-900 °C. After that, SO<sub>3</sub>(g) is decomposed into O<sub>2</sub>(g) and SO<sub>2</sub>(g) (sulfur dioxide) as proposed by Equation (12).



Then, in Equation (13),  $\text{SO}_2(\text{g})$  spontaneously reacts exothermically with iodine ( $\text{I}_2$ ) and water, the source of  $\text{H}_2$ , at low temperatures to produce HI (hydrogen iodide) and  $\text{H}_2\text{SO}_4$ .

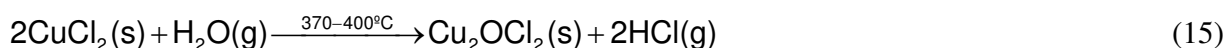


Finally,  $\text{H}_2$  is produced by HI decomposition, Equation (14), at temperatures near to 425-450 °C.



It is noticeable that the highest level of temperature in the S-I procedure happens at around 800-900 °C during  $\text{SO}_3$  decomposition in Equation (12), restricting its application because there are few energy systems capable to supply heat at that level of temperature. In contrast, the copper-chlorine (Cu-Cl) cycle has more viable temperature ranges than the sulfur-iodine one. Ozbilen *et al.* (2013) characterize the Cu-Cl cycle as a sequence of chemical reactions using different compounds of copper and chlorine in a recyclable closed loop at specific conditions of pressure and temperature. It happens with the need of very low or none electrical power (DINCER, 2012). There are three variations of this cycle (3-step, 4-step and 5-step), each one based on a well-defined number of steps represented by a single chemical reaction. All these variants are encountered in the studies of Al-Zareer *et al.* (2017b), Wu *et al.* (2017) beyond other authors. Only the 3-step cycle is introduced at this moment with the purpose to exemplify it in accordance with Equations (15), (16) and (17) adapted from Ozbilen *et al.* (2013) and Al-Zareer *et al.* (2017a).

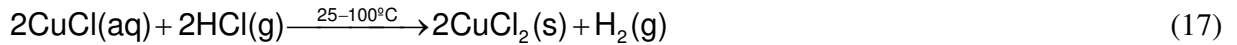
The first step in the Cu-Cl cycle is hydrolysis represented by Equation (15). It occurs when  $\text{H}_2\text{O}$  reacts with copper (II) chloride ( $\text{CuCl}_2$ ) forming copper oxychloride ( $\text{Cu}_2\text{OCl}_2$ ) and hydrochloric acid (HCl).



The next step, Equation (16), consists in heating up  $\text{Cu}_2\text{OCl}_2$ , decomposing it into CuCl (copper chloride) and oxygen.

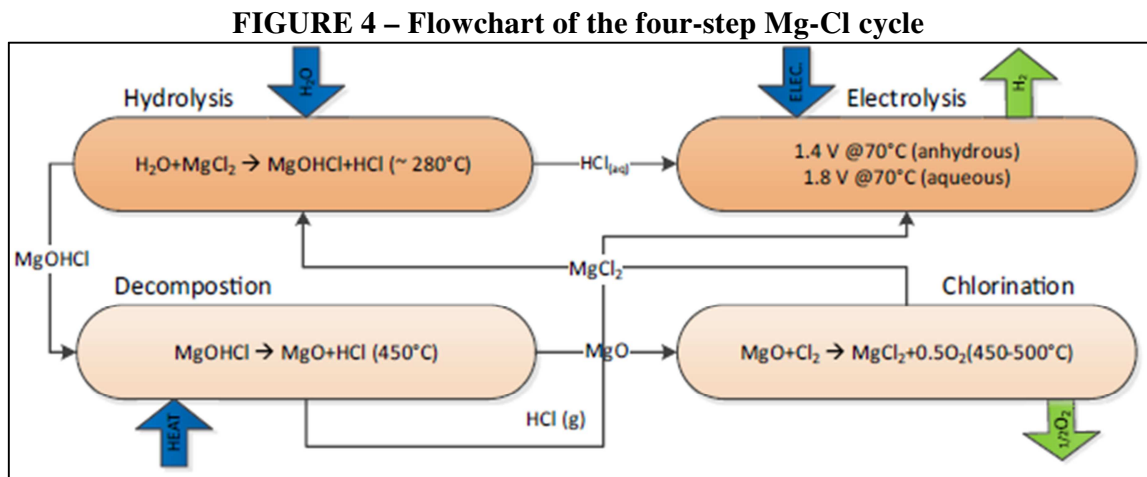


Closing the cycle, CuCl reacts with HCl to form hydrogen and CuCl<sub>2</sub>, as in Equation (17).



Analyzing previous information, the highest level of temperature in the copper-chlorine cycle occurs at about 500-550 °C during oxygen production in Equation (16), making such route suitable to operate together with different energy systems.

Additionally, the hybrid four-step Mg-Cl, one possible variation of the magnesium-chlorine cycle, has its maximum operational temperature close to 450 °C (OZCAN and DINCER, 2016b plus OZCAN and DINCER, 2018), characterizing it as another viable H<sub>2</sub> production method. All the steps of this cycle are drafted in Figure 4 from Ozcan and Dincer (2016b). The chemical compounds of Mg and Cl involved in this system are: magnesium chloride (MgCl<sub>2</sub>); magnesium chloride hydroxide (MgOHCl); hydrochloric acid (HCl) and magnesium oxide (MgO). The flowchart in Figure 4 also could be drafted for the cycles Cu-Cl and S-I to emphasize the recyclability of their chemical substances in each cycle.

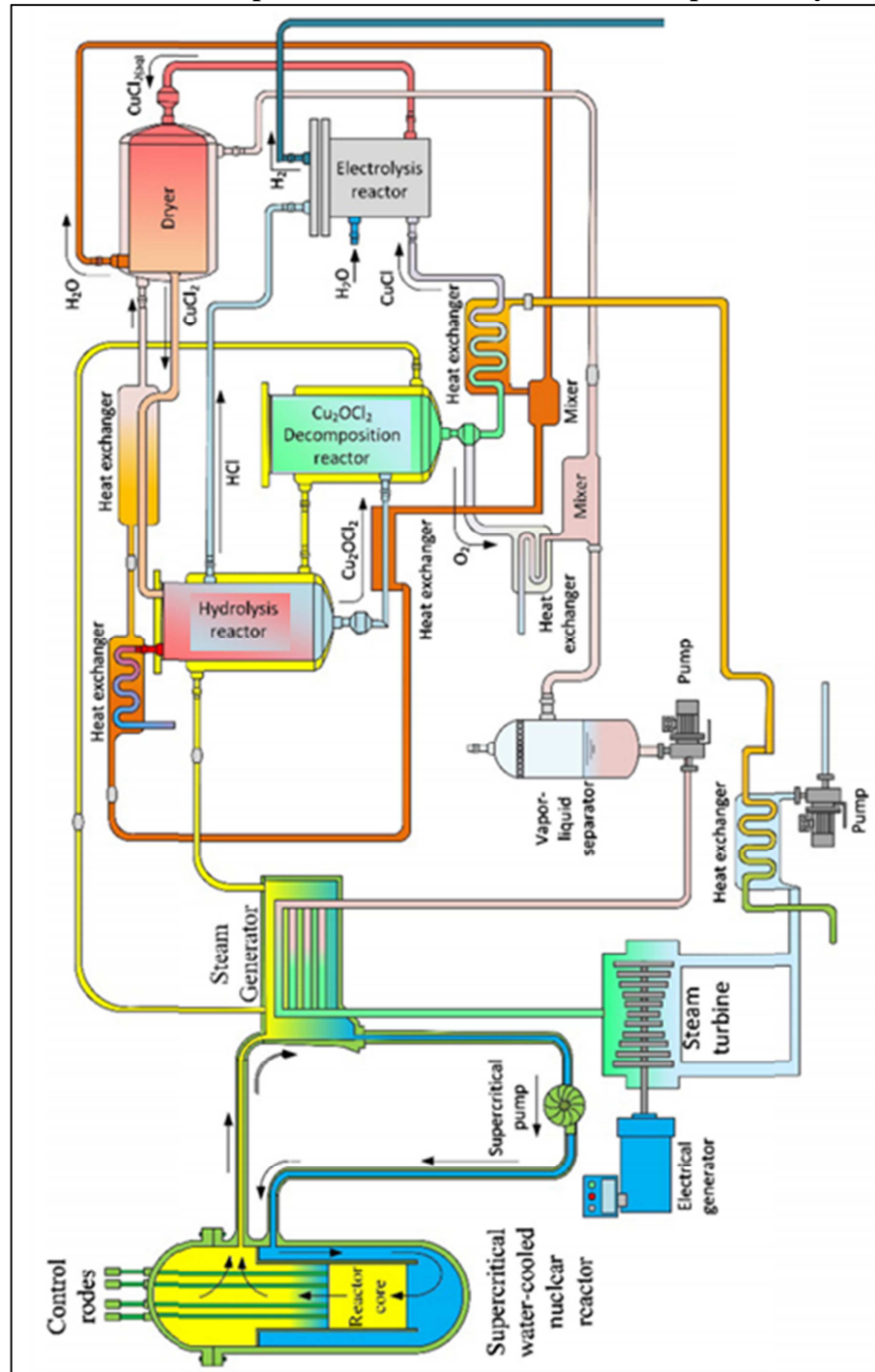


Source: adapted from Ozcan and Dincer (2016b).

In contrast to Cu-Cl and Mg-Cl which have relatively low and viable temperature ranges, there are thermochemical trials that demand temperatures higher than 1000 °C. This is verifiable through the literature review study performed by Yalçın (1989) and Abanades *et al.* (2006) concerning many thermochemical cycles.

Figure 5 adapted from Al-Zareer *et al.* (2017a) illustrates a  $H_2$  production installation with the main devices (pumps, chemical reactors, turbines and etc.) needed to its operation. It is based on the 4-step Cu-Cl cycle coupled to a NPP, in this case a Supercritical Water Reactor (SCWR).

**FIGURE 5 – Scheme of a  $H_2$  production unit based on the 4-step Cu-Cl cycle and SCWR**



Source: adapted from Al-Zareer *et al.* (2017a).

### 2.2.2 Variations of a same thermochemical cycle

A same thermochemical cycle may have different configurations or variations with many purposes like increasing its thermal performance, lowering the operational temperature of its chemical reactions or just reducing the number of chemical steps to facilitate the practical implementation of the process.

In Charts 1, 2 and 3 adapted from Wu *et al.* (2017) are present 3 variations (3-step, 4-step and 5-step) of the Cu-Cl procedure. According to the research performed by those scientists, the 4-step version of the copper-chlorine cycle with a CuCl/HCl electrolyzer “has a high possibility of commercialization due to the lower grade heat requirement, the less number of equipment and the higher energy efficiency” when compared to its two other versions. So, later in Chapter 5 are proposed other configurations for the Na-O-H cycle in order to discover if they have better thermal aspects (enthalpy, entropy and Gibbs free energy changes plus energy efficiency) when compared to the classic form of this cycle introduced and discussed in section 2.2.4.

**CHART 1 – Cu-Cl cycle: 3-step variation**

Cu-Cl cycle: 3 step	
#1 Hydrolysis	$2\text{CuCl}_{2(aq)} + \text{H}_2\text{O}_{(g)} \rightarrow \text{CuO} \cdot \text{CuCl}_{2(s)} + 2\text{HCl}_{(g)}$ 400 °C, 1 atm
#2 O <sub>2</sub> production	$\text{CuO} \cdot \text{CuCl}_{2(s)} \rightarrow 2\text{CuCl}_{(l)} + 0.5\text{O}_{2(g)}$ 500 °C, 1 atm
#3 Electrolysis	$2\text{CuCl}_{(l)} + 2\text{HCl}_{(l)} \rightarrow 2\text{CuCl}_{2(aq)} + \text{H}_{2(g)}$ 100 °C, 24 bar

Source: adapted from Wu *et al.* (2017).

**CHART 2 – Cu-Cl cycle: 4-step variation**

Cu-Cl cycle: 4-step	
#1 Drying	$\text{CuCl}_{2(aq)} \rightarrow \text{CuCl}_{2(s)}$ 100 °C, 1 atm
#2 Hydrolysis	$2\text{CuCl}_{2(s)} + \text{H}_2\text{O}_{(g)} \rightarrow \text{CuO} \cdot \text{CuCl}_{2(s)} + 2\text{HCl}_{(g)}$ 400 °C, 1 atm
#3 O <sub>2</sub> production	$\text{CuO} \cdot \text{CuCl}_{2(s)} \rightarrow 2\text{CuCl}_{(l)} + 0.5\text{O}_{2(g)}$ 500 °C, 1 atm
#4 Electrolysis	$2\text{CuCl}_{(l)} + 2\text{HCl}_{(l)} \rightarrow 2\text{CuCl}_{2(aq)} + \text{H}_{2(g)}$ 100 °C, 24 bar

Source: adapted from Wu *et al.* (2017).

**CHART 3 – Cu-Cl cycle: 5-step variation**

Cu-Cl cycle: 5-step	
#1	$\text{CuCl}_{2(aq)} \rightarrow \text{CuCl}_{2(s)}$
Drying	100 °C, 1 atm
#2	$2\text{CuCl}_{2(s)} + \text{H}_2\text{O}_{(g)} \rightarrow \text{CuO}_{(s)} + \text{CuCl}_{2(s)} + 2\text{HCl}_{(g)}$
Hydrolysis	400 °C, 1 atm
#3	$\text{CuCl}_{2(s)} \rightarrow \text{CuCl}_{(l)} + 0.5\text{Cl}_{2(g)}$
O <sub>2</sub> production-1	500 °C, 1 atm
#4	$\text{CuO}_{(s)} + 0.5\text{Cl}_{2(g)} \rightarrow \text{CuCl}_{(l)} + 0.5\text{O}_{2(g)}$
O <sub>2</sub> production-2	500 °C, 1 atm
#5	$2\text{CuCl}_{(l)} + 2\text{HCl}_{(l)} \rightarrow 2\text{CuCl}_{2(aq)} + \text{H}_{2(g)}$
Electrolysis	100 °C, 24 bar

Source: adapted from Wu *et al.* (2017).

### 2.2.3 Categories of thermochemical water splitting cycles

In order to complement information about the thermochemical cycles exemplified in section 2.2.1 and also to understand the choice of the Na-O-H trial over other thermochemical processes, they are presented some categories of this kind of hydrogen production route.

#### (i) Thermochemical cycles: high temperature processes

This category is composed by cycles that demand very high temperatures to proceed, normally above 1500 °C. This fact limits their application because few energy systems are able to meet such requirements. Some of these thermochemical technics are exemplified in Chart 4 adapted from Abanades *et al.* (2006).

**CHART 4 – Examples of thermochemical cycles: high temperature processes**

Thermochemical Cycle	Chemical Reactions	Temperature
Cycle Mo/MoO <sub>2</sub> :	$\text{MoO}_2 (s) \rightarrow \text{Mo} + \text{O}_2$	(3713 °C)
	$\text{Mo} + 2\text{H}_2\text{O} \rightarrow \text{MoO}_2 (s) + 2\text{H}_2$	(1543 °C)
Cycle SiO <sub>2</sub> /SiO:	$\text{SiO}_2 \rightarrow \text{SiO}(g) + \frac{1}{2}\text{O}_2$	(2977 °C)
	$\text{SiO} (g) + \text{H}_2\text{O} \rightarrow \text{SiO}_2 + \text{H}_2$	(2656 °C)
Cycle W/WO <sub>3</sub> :	$\text{WO}_3(s) \rightarrow \text{W} + \frac{3}{2}\text{O}_2$	(3910 °C)
	$\text{W} + 3\text{H}_2\text{O} \rightarrow \text{WO}_3 (s) + 3\text{H}_2$	(884 °C)

Source: adapted from Abanades *et al.* (2006).

(ii) Thermochemical cycles: pure cycles x hybrid cycles

Some thermochemical cycles claim simultaneously heat and electricity to occur, the hybrid ones. In Chart 5 (adapted from ABANADES *et al.*, 2006) are presented two examples of them. Depending on the trial under analysis, the use of electricity can reduce its temperature requirements and then facilitating its overall proceeding or increase its thermal performance.

**CHART 5 – Examples of thermochemical cycles: pure cycles x hybrid processes**

Thermochemical Cycle	Chemical Reactions	Temperature
<i>Cycle 80:</i> US-Chlorine	$\text{H}_2\text{O} + \text{Cl}_2 \rightarrow 2\text{HCl} + \frac{1}{2}\text{O}_2$ $2\text{HCl} + 2\text{CuCl} (\text{s}) \rightarrow 2\text{CuCl}_2 (\text{s}) + \text{H}_2$ $2\text{CuCl}_2 (\text{s}) \rightarrow 2\text{CuCl} (\text{s}) + \text{Cl}_2$	(700 °C) (200 °C) (electrochemical, 300 °C)
<i>Cycle 287:</i> Argonne Cu, Cl	$2\text{Cu} + 2\text{HCl} \rightarrow \text{H}_2(\text{g}) + 2\text{CuCl}$ $4\text{CuCl} \rightarrow 2\text{Cu} + 2\text{CuCl}_2$ $2\text{CuCl}_2 + \text{H}_2\text{O} \rightarrow \frac{1}{2}\text{O}_2(\text{g}) + 2\text{HCl} + 2\text{CuCl}$	(430 °C) (electrochemical, 25–75 °C) (< 550 °C)

Source: adapted from Abanades *et al.* (2006).

(iii) Thermochemical cycles: safety and environmental issues processes

Safety and environmental issues processes consist of toxic, corrosive or even non-environmentally friendly chemicals like cadmium (Cd), mercury (Hg) or sulfuric acid (H<sub>2</sub>SO<sub>4</sub>). Some processes based on these chemicals are exhibited in Chart 6 using information adapted from Abanades *et al.* (2006). These authors highlight that the levels of toxicity, corrosiveness or environmental issues related to the substances contained in the cycles will define their use.

**CHART 6 – Examples of thermochemical cycles: safety and environmental issues cycles**

Thermochemical Cycle	Chemical Reactions	Temperature
<i>Cycle HgO/Hg:</i>	$\text{Hg} (\text{g}) + \text{H}_2\text{O} \rightarrow \text{HgO} (\text{s}) + \text{H}_2$ $\text{HgO}(\text{s}) \rightarrow \text{Hg} + \frac{1}{2}\text{O}_2$	(360 °C) (600 °C)
<i>Cycle 17:</i> FeBr <sub>2</sub> GIRIO	$3\text{FeBr}_2 (\text{l}) + 4\text{H}_2\text{O} \rightarrow \text{Fe}_3\text{O}_4 (\text{s}) + 6\text{HBr} (\text{g}) + \text{H}_2$ $\text{Fe}_3\text{O}_4 + 8\text{HBr} \rightarrow 3\text{FeBr}_2 + 4\text{H}_2\text{O} + \text{Br}_2$ $\text{H}_2\text{O} + \text{Br}_2 \rightarrow 2\text{HBr} + \frac{1}{2}\text{O}_2$	(850 °C) (250 °C) (650 °C)
<i>Cycle 261:</i>	$2\text{Al}_2\text{O}_3 + 6\text{Br}_2 (\text{l}) \rightarrow 4\text{AlBr}_3 + 3\text{O}_2$ $4\text{AlBr}_3 + 6\text{WO}_3 (\text{s}) \rightarrow 2\text{Al}_2\text{O}_3 + 6\text{Br}_2 + 6\text{WO}_2 (\text{s})$ $6\text{WO}_2 (\text{s}) + 6\text{H}_2\text{O} \rightarrow 6\text{WO}_3 + 6\text{H}_2$	(700 °C) (1500 °C) (150 °C)

Source: adapted from Abanades *et al.* (2006).



(iv) Thermochemical cycles: economic processes

According to Abanades *et al.* (2006), economic procedures employ heavy chemical “*elements which are not abundant*” on earth, making H<sub>2</sub> production not favorable due to cost issues. Chart 7 (adapted from ABANADES *et al.*, 2006) adduces classic examples of economic cycles.

**CHART 7 – Examples of thermochemical cycles: economic processes**

Thermochemical Cycle	Chemical Reactions	Temperature
Cycle 31: Eu, Sr	$2\text{EuO} + \text{H}_2\text{O} \rightarrow \text{Eu}_2\text{O}_3 (\text{s}) + \text{H}_2$	(390 °C)
	$\text{I}_2(\text{g}) + \text{SrO}(\text{s}) \rightarrow \text{SrI}_2(\text{s}) + \frac{1}{2}\text{O}_2$	(323 °C)
	$\text{Eu}_2\text{O}_3 (\text{s}) + \text{SrI}_2 (\text{l}) \rightarrow 2\text{EuO} + \text{I}_2 (\text{g}) + \text{SrO} (\text{s})$	(1000 °C)
Cycle 182: Sr, U	$\text{Sr}_3\text{U}_2\text{O}_8 + 3\text{Sr}(\text{OH})_2 \rightarrow 2\text{Sr}_3\text{UO}_6 + 2\text{H}_2\text{O} + \text{H}_2$	(600 °C)
	$2\text{SrUO}_6 + 3\text{H}_2\text{O} \rightarrow \text{Sr}_3\text{U}_2\text{O}_9 + 3\text{Sr}(\text{OH})_2$	(90 °C)
	$\text{Sr}_3\text{U}_2\text{O}_9 \rightarrow \text{Sr}_3\text{U}_2\text{O}_8 + \frac{1}{2}\text{O}_2$	(600 °C)

Source: adapted from Abanades *et al.* (2006).

(v) Thermochemical cycles: complex processes

Complex processes cover cycles whose chemicals formed during reactions have more than one substance mixed each other in a same physical phase like two liquids or three gaseous products. This characteristic could make such methods unfeasible because in practical situations can be very difficult to separate many substances when they are mixed in a same physical phase, impacting on the recycling of their chemicals. Some complexity methods are typified in Chart 8 adapted from Abanades *et al.* (2006).

**CHART 8 – Examples of thermochemical cycles: complex processes**

Thermochemical Cycle	Chemical Reactions	Temperature
Cycle 1: IS Cycle (Ispra Mark 16)	$\text{H}_2\text{SO}_4(\text{g}) \rightarrow \text{H}_2\text{O}(\text{g}) + \text{SO}_2(\text{g}) + \frac{1}{2}\text{O}_2(\text{g})$	(800–1000 °C)
	$\text{I}_2(\text{l}) + \text{SO}_2(\text{aq}) + 2\text{H}_2\text{O}(\text{l}) \rightarrow \text{H}_2\text{SO}_4(\text{aq}) + 2\text{HI}(\text{l})$	(120 °C)
	$2\text{HI}(\text{l}) \rightarrow \text{I}_2(\text{l}) + \text{H}_2(\text{g})$	(450 °C)
Cycle 30: THEME S-3	$\text{SO}_2 + \text{H}_2\text{O} + \text{I}_2 \rightarrow \text{SO}_3 + 2\text{HI}$	(200 °C)
	$\text{SO}_3 \rightarrow \text{SO}_2 + \frac{1}{2}\text{O}_2$	(900 °C)
	$2\text{HI} \rightarrow \text{H}_2 + \text{I}_2$	(450 °C)

Source: adapted from Abanades *et al.* (2006).

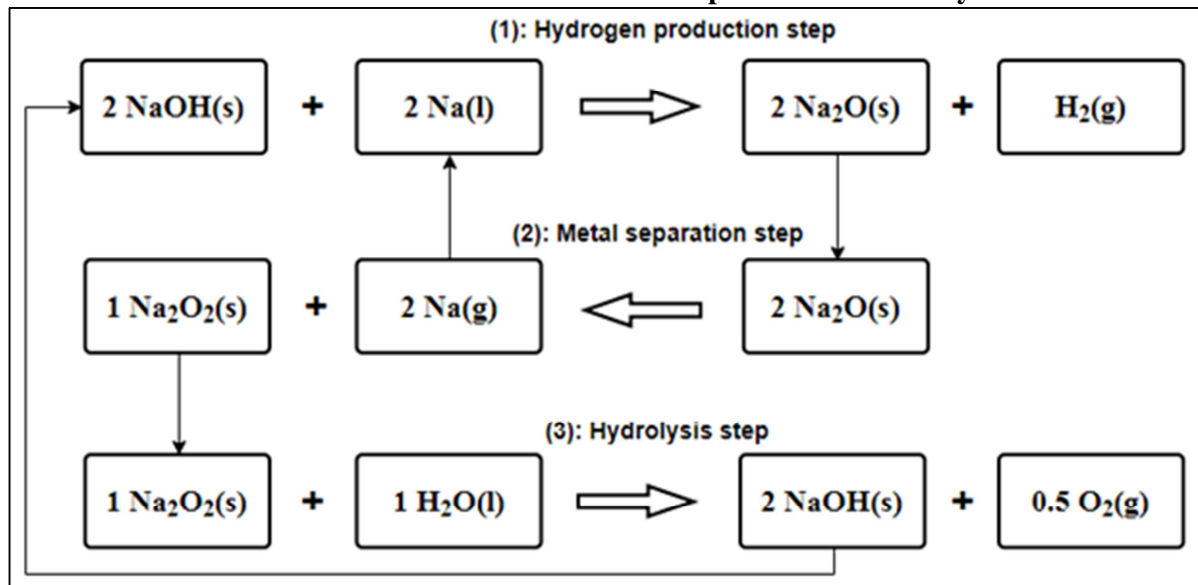
So, based on the characteristics of each category of thermochemical cycles discussed in items (i) to (v), it concludes the Na-O-H system avoids some of the problems related to those methods, including: a relatively low operational temperature around 400-500 °C, at low pressure, a value far below than the above 1500 °C related to high temperature ones; it does not demand electricity, only heat, in contrast to hybrid cycles; it does not have two or more chemicals formed and mixed each other in a same physical phase in contrast to complexity procedures; it does not demand heavy and non-abundant elements that can impact on economic questions. All these features make the Na-O-H system a potential thermochemical trial and because of that, combined with the scarce information about it available in the literature due to its newness aspect; this system was chosen as the hydrogen production route to develop the work. However, the sodium-oxygen-hydrogen technic demands sodium, a corrosive and explosive substance when it reacts with water, demanding special attention to handle with it. Beyond that, such system is not a patented one, like many thermochemical ones introduced by Yalçin (1989), what could facilitate its development and application in the future. Such approach is described in the next topic.

#### ***2.2.4 Classic form of the Na-O-H (sodium-oxygen-hydrogen) thermochemical cycle***

Miyaoka *et al.* (2012) proposed a new thermochemical method whose constituent elements are sodium (Na), oxygen (O) and hydrogen (H). Because of this, it is named Na-O-H cycle. It is composed by relatively simpler chemical reactions than most of the existing thermochemical processes like those ones addressed in section 2.2.3. Additionally, it has potential to operate at temperatures around 500 °C under vacuum or low pressure condition, enabling H<sub>2</sub> production over various heat sources, including GEN-IV nuclear power plants. The classic form of this thermochemical cycle consisting of three chemical reactions schematized in Figure 6 adapted from Marques *et al.* (2019) and described over the next paragraphs considering the experiment carried out by Miyaoka *et al.* (2012).

Reaction 1 (hydrogen production step) happens when solid sodium hydroxide (NaOH) and liquid sodium (Na) react to produce hydrogen gas (H<sub>2</sub>) and solid disodium oxide (Na<sub>2</sub>O) as in Equation (18). Such step was experimentally performed by those researchers under 0.1 MPa in Argon atmosphere at 300 and 350 °C in a closed system.

**FIGURE 6 – Schematic view of the steps in the Na-O-H cycle**



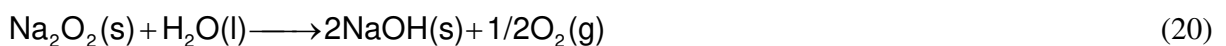
Source: adapted from Marques *et al.* (2019).



In metal separation step or reaction 2, Equation (19), sodium oxide is endothermically decomposed into solid disodium peroxide ( $\text{Na}_2\text{O}_2$ ) and sodium vapor ( $\text{Na}$ ). Miyaoka *et al.* (2012) dispatched this reaction at 400 and 500 °C under vacuum or low pressure atmosphere to facilitate its proceeding. Additionally,  $\text{Na(g)}$  was separated from the reaction field by cooling and condensing it.

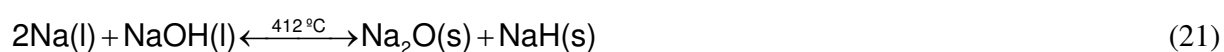


Finally, in reaction 3 or oxygen generation by hydrolysis step, Equation (20), sodium peroxide and liquid water ( $\text{H}_2\text{O}$ ) exothermically react to form solid sodium hydroxide and oxygen gas ( $\text{O}_2$ ). During the experiment, sodium peroxide and water were heated at 100 °C and 0.1 MPa under argon ( $\text{Ar}$ ) atmosphere in a closed system (MIYAOKA *et al.*, 2012). In the Na-O-H system, water is the source of hydrogen and it is consumed during the process while the other chemicals are recycled in a closed loop, like any thermochemical cycle.



The temperature limits for Equations (18), (19) and (20) could be investigated according to changes in their Gibbs free energy ( $\Delta G$ ) as that one performed over section 3.2.1 which results are in item 4.4. In actual situations may happen differences between theoretical and experimental values, causing variations in system behavior, like the increase in its operational temperature.

From the paper of Miyaoka *et al.* (2012),  $H_2$  production in Equation (18) has low yield at 300 and 350 °C under argon atmosphere. One possible explanation for that is because at temperatures close to 340°C and beyond, solid sodium hydroxide becomes liquid. Then, when liquid NaOH and liquid sodium react, they might form a solid solution as explanation in the research of Xu *et al.* (2006) or even different compounds like sodium hydride (NaH) as in Equation (21) and experimental data both from the research of Myles and Cafasso (1977), instead of producing hydrogen as indicated by Equation (18). Additionally, Gnanasekaran (1999) concluded that the solubility of  $H_2$  gas in liquid sodium enhances with temperature, increasing the possibility to form NaH instead releasing  $H_2$  when NaOH reacts with Na in Equation (18).



To avoid such problems and to maximize the probability to form  $H_2$  and not NaH or other products, Xu *et al.* (2006) suggested that the reaction between Na(l) and NaOH(s) should be performed below the melting point of NaOH that is 323 °C (LIDE, 2004). Besides that, Xu *et al.* (2006) performed an experimental analysis and concluded the reaction between solid sodium hydroxide and sodium releases hydrogen at around 275 °C under very low pressure. Endothermic processes, like Equation (18), usually have their rates or yields improved just increasing their operational temperature or giving them more heat. However, with the explanations provided in the last two paragraphs, Equation (18) should be performed at temperatures closes to 275 °C instead 300 or 350 °C to promote hydrogen production than other chemicals. Moreover, Miyaoka *et al.* (2012) explain that the yield of Equation (18) and consequently the releasing of hydrogen could be improved through some non-equilibrium techniques, including a proper catalyst.

In relation to Equation (19), Miyaoka *et al.* (2012) inferred that the metal separation phase has low yielding and such reaction could achieve very high yielding if non-equilibrium techniques, such as a catalyst, were used. The yield of Equations (18) and (19) could be improved if the gaseous products were removed from the reaction field insofar as they are formed instead of

keeping them inside reactor chamber. Finally, in Equation (20) all reactants turn into products when the reaction is performed at 100 °C suggested in the practical research performed by Miyaoka *et al.* (2012).

Proceeding Equation (19) under a vacuum condition can restrict its application only for small scale plants because producing extremely low pressures for large scale operations can become impractical due to some aspect. One of them is a possible difficulty to hold and operate the system at a vacuum simultaneously with the chemical process that happens inside the chemical chamber as well as the need for special materials to handle this situation, what can increase the costs related to the system. Then, the Na-O-H cycle could be more suitable to operate in small scale situations. Yet, a specific study of this aspect of the sodium-oxygen-hydrogen thermochemical process should be developed to investigate and consequently elucidate its technical and economic viability under very low pressures or at very high vacuum atmosphere.

### ***2.2.5 Comparative studies among thermochemical cycles and other H<sub>2</sub> production methods***

In this part of chapter 2 are shortly described the results of some comparative studies available in the literature, specially the one performed by Dincer and Acar (2015), to show the performance of thermochemical cycles when compared to other H<sub>2</sub> production routes, specially the conventional ones, considering environmental, economics, thermal and viability viewpoints. The values lodged over this section are mean ones covering different technologies. In this way could exist some deviations in them if other studies about a certain method were considered.

#### ***(i) Definition and description of the hydrogen production process under comparison***

In Chart 9 adapted from Dincer and Acar (2015) is introduced a brief description of the 19 methods under comparison, each one identified according to the initials M1 to M19. Such nomenclature is also used in topics ii and iii of section 2.2.5. Among the 19 methods assessed, **M4** and **M13** received especial attention because they are related to one of the subjects of this thesis, the Na-O-H thermochemical cycle. **M4** refers to the pure thermochemical water splitting cycles (only demand heat), in such comparative they are represented by the S-I cycle; while **M13** covers hybrid thermochemical ones (need both heat and electricity) represented by the Cu-Cl process in the comparative research under attention.

**CHART 9 – Brief description of 19 selected hydrogen production methods**

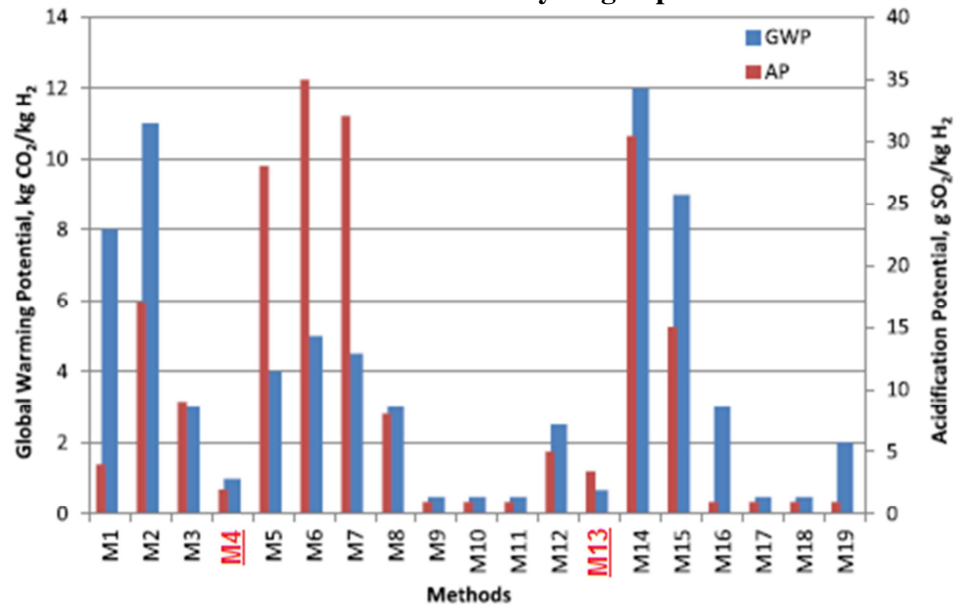
M1	Electrolysis	Direct current is used to split water into O <sub>2</sub> and H <sub>2</sub> (electrochemical reaction)
M2	Plasma arc decomposition	Cleaned natural gas is passed through plasma arc to generate H <sub>2</sub> and carbon soot
M3	Thermolysis	Thermal decomposition of water (steam) at temperatures over 2500 K
M4	<b>Thermochemical process - water splitting</b>	<b>Cyclical chemical reactions (net reaction: water splitting into H<sub>2</sub>)</b>
M5	Thermochemical process - biomass conversion	Thermocatalytic conversion
M6	Thermochemical process - Gasification	Conversion of biomass into syngas
M7	Thermochemical process - Reforming	Conversion of liquid biomass (biofuels) into H <sub>2</sub>
M8	PV electrolysis	PV panels are used to generate electricity
M9	Photocatalysis	Water is split into H <sub>2</sub> by using the electron-hole pair generated by the photocatalyst
M10	Photoelectrochemical	A hybrid cell simultaneously produces current and voltage upon absorption of light
M11	Dark fermentation	Biological systems are used to generate H <sub>2</sub> in the absence of light
M12	High temperature electrolysis	Electrical and thermal energy are used together to drive water splitting at high temperatures
M13	<b>Hybrid thermochemical cycles</b>	<b>Electrical and thermal energy are used together to drive cyclical chemical reactions</b>
M14	Coal gasification	Conversion of coal into syngas
M15	Fossil fuels reforming	Fossil fuels are converted to H <sub>2</sub> and CO <sub>2</sub>
M16	Biophotolysis	Biological systems (microbes, bacteria, etc.) are used to generate H <sub>2</sub>
M17	Photofermentation	Fermentation process activated by exposure to light
M18	Artificial photosynthesis	Chemically engineered systems mimic photosynthesis to generate H <sub>2</sub>
M19	Photoelectrolysis	Photoelectrodes and external electricity are used to drive water electrolysis

Source: adapted from Dincer and Acar (2015).

*(ii) Environmental, economics and thermal comparison*

In Graph 1 (DINCER and ACAR, 2015) is shown the GWP (Global Warming Potential) related to CO<sub>2</sub> emissions and the AP (Acidification Potential) measured in SO<sub>2</sub> emissions of different H<sub>2</sub> technologies considered in analysis. GWP and AP are determined per each 1 kg of H<sub>2</sub> produced. **M4** and **M13**, pure and hybrid thermochemical cycles, respectively, present relatively low and inferior GWP (mean value around 1 kg CO<sub>2</sub>/kg H<sub>2</sub>) and AP (mean value near to 1 g SO<sub>2</sub>/kg H<sub>2</sub>) when compared to other conventional H<sub>2</sub> processes like M1 (electrolysis) that has GWP = 8 kg CO<sub>2</sub>/kg H<sub>2</sub> and AP = 1.5 g SO<sub>2</sub>/kg H<sub>2</sub> or M15 (fossil fuels reforming) that have GWP = 9 kg CO<sub>2</sub>/kg H<sub>2</sub> and AP = 5.5 g SO<sub>2</sub>/kg H<sub>2</sub>. The lowest values of GWP and AP usually are associated to biological routes like M11 (dark fermentation) and M17 (Photofermentation).

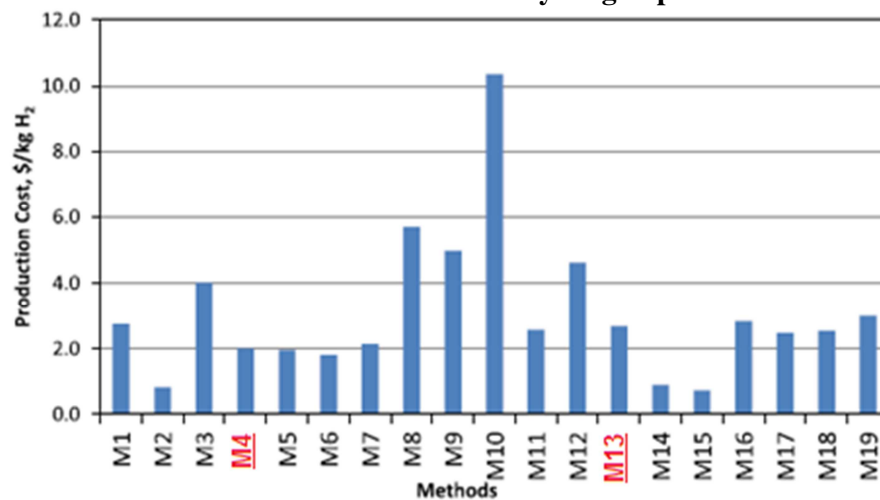
**GRAPH 1 – GWP and AP of selected hydrogen production methods**



Source: Dincer and Acar (2015).

Still, Graph 2 from Dincer and Acar (2015) presents the production cost in American dollars (\$) for the 19 H<sub>2</sub> processes under comparison. As can be seen in it, thermochemical water splitting cycles (M4) have production cost equal to 2.0 \$/kg H<sub>2</sub> that is little inferior than electrolysis (M1) that is 2.5 \$/kg H<sub>2</sub>, but superior to coal gasification (M14) and fossil fuel reforming (M15) that have production cost lower than 1 \$/kg H<sub>2</sub>. The highest production costs usually are related to photo or biological process such as M9 (Photocatalysis) or M10 (Photoelectrochemical) while the lowest ones are associated with conventional routes like M14 and M15.

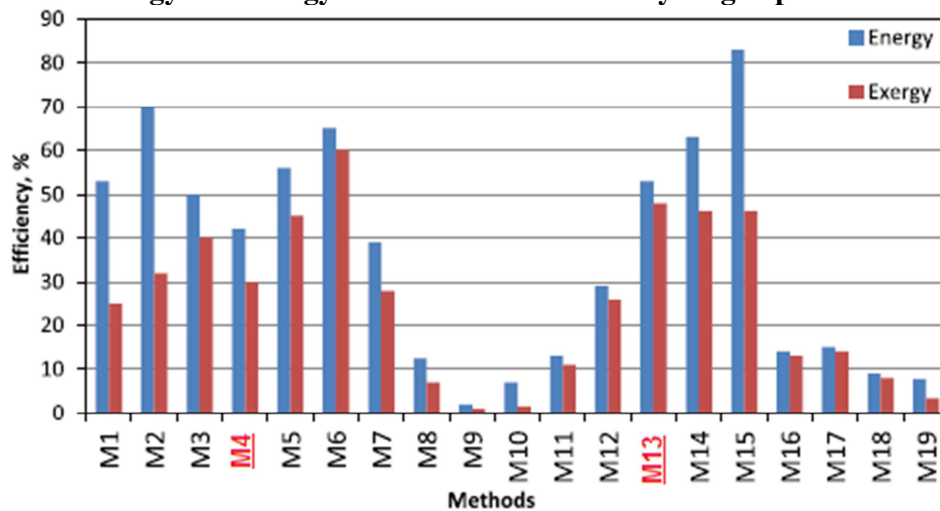
**GRAPH 2 – Production cost of selected hydrogen production methods**



Source: Dincer and Acar (2015).

Finally, the energy and exergy efficiencies of the nineteen H<sub>2</sub> production procedures evaluated in the research of Dincer and Acar (2015) are shown in Graph 3. After analyzing such diagram, it is possible to note that thermochemical cycles (M4) have respectively, energy and exergy efficiencies equal to 42% and 30% while hybrid cycles (M13) have energy efficiency around 52% and exergy efficiency 48%. As discussed in section 2.2.3, the use of electricity in thermochemical cycles can increase their thermal performance. M5 (biomass conversion), M6 (biomass gasification), M13 (hybrid cycles), M14 (coal gasification), M15 (fossil fuels reforming) are responsible for the highest values of energy and exergy efficiency in Graph 3.

**GRAPH 3 – Energy and exergy efficiencies of selected hydrogen production methods**



Source: Dincer and Acar (2015).

(iii) Key benefits, technical challenges and maturity of some hydrogen production technologies

Closing section 2.2, in Chart 10 (adapted from DINCER and ACAR, 2015) are exposed some key benefits and critical challenges of some hydrogen production routes, including thermochemical cycles; while in Chart 11 adapted from Holladay *et al.* (2009) are exhibited the maturity status (commercial, near term or long term) of some H<sub>2</sub> technologies. After analyzing these two charts, it concludes that thermochemical cycles are in the beginning of their development; they are not mature technologies and they are not ready to be used in commercial applications; they are long term ones that are expected to be ready for industrial applications in future. All these considerations justify the great number of recent publications about thermochemical cycles because such studies aim to contribute to the development of this kind of technology. Some of these research materials are being analyzed in the literature review, section 2.6.



**CHART 10 – Key benefits and critical challenges of selected hydrogen production methods**

	Fossil fuel reforming	Biofuel reforming	Coal and biomass gasification	Thermochemical method	Water electrolysis	Photoelectrochemical method
Critical challenges						
High capital costs	High capital costs	High reactor costs	High reactor costs	Cost effective reactor	Low system efficiency	Effective photocatalytic material
Design	High operation and maintenance costs	System efficiency	System efficiency	Long-term technology	High capital costs	Low system efficiency
High operation and maintenance costs	Design	Feedstock impurities	Feedstock impurities	Effective and durable materials	System integration	Cost effective reactor
Major R&D Needs	Feedstock quality	Carbon capture and storage	Carbon capture and storage		Design issues	Long-term technology
Efficiency and cost	Hydrogen yield and efficiency	Low cost and efficient purification	Low cost and efficient purification	Robust, low cost materials	Durable and cheap materials	Durable and efficient photocatalyst
Low cost and efficient purification	Low temperature production	Co-fed gasifiers	Co-fed gasifiers	Ease of manufacture and application	Corrosive-resistant membranes	Low cost materials
Feedstock pre-treatment	Low cost and efficient purification	Carbon capture and storage	Carbon capture and storage	System optimization	Durable, active, and cheap catalysts	Active, stable, and cheap supporting materials
Optimization	Optimization	Hydrogen quality	Hydrogen quality	High volume, low cost, flexible system design	Large scale applications	High volume production
Automated process control	Regional best feedstock	Cost of feedstock preparation	Cost of feedstock preparation	Efficient heat transfer	Storage and production rate	System control
Reliability	Feedstock pre-treatment	Tolerance for impurities	Tolerance for impurities	Reliability	Reliability	Power losses
Key benefits	Viability	Low cost syngas production	Low cost syngas production	Clean and sustainable	No pollution with renewable energy sources	Low operation temperature
Most viable approach	Existing infrastructure	Abundant and cheap feedstock	Abundant and cheap feedstock	Recycled chemicals	Existing infrastructure	Clean and sustainable
Lowest current cost	Existing infrastructure				Integration with fuel cells	

Source: adapted from Dincer and Acar (2015).

**CHART 11 – Technology summary of selected H<sub>2</sub> production methods**

Technology	Feed stock	Maturity
Steam reforming	Hydrocarbons	Commercial
Partial oxidation	Hydrocarbons	Commercial
Autothermal reforming	Hydrocarbons	Near term
Plasma reforming	Hydrocarbons	Long term
Aqueous phase reforming	Carbohydrates	Med. term
Ammonia reforming	Ammonia	Near term
Biomass gasification	Biomass	Commercial
Photolysis	Sunlight + water	Long term
Dark fermentation	Biomass	Long term
Photo fermentation	Biomass + sunlight	Long term
Microbial electrolysis cells	Biomass + electricity	Long term
Alkaline electrolyzer	H <sub>2</sub> O + electricity	Commercial
PEM electrolyzer	H <sub>2</sub> O + electricity	Near term
Solid oxide electrolysis cells	H <sub>2</sub> O + electricity + heat	Med. Term
Thermochemical water splitting	H <sub>2</sub> O + heat	Long term
Photoelectrochemical water splitting	H <sub>2</sub> O + sunlight	Long term

Source: adapted from Holladay *et al.* (2009).

## 2.3 Generation IV Nuclear Reactors

In this chapter, the Generation IV Nuclear Reactors are introduced. Firstly, the general aspects of this group are discussed. Next, three technologies were selected and then described focusing on their main ordinary features, especially thermodynamic cycles because they are key information needed to accomplish the first main aim of this thesis.

### 2.3.1 General aspects of GEN-IV nuclear reactors

Nuclear power plants are classified into four distinct generations considering their evolutionary aspects over time. Based on information provided by NERAC (Nuclear Energy Research Advisory Committee) and GIF (Generation-IV International Forum) in 2002 plus the research conducted by Locatelli *et al.* (2013), such generations are:

- Generation I (1950 – 1970): it corresponds to the early prototypes or concepts of many different nuclear reactors;
- Generation II (1970 – 1995): it represents the first commercial power plants, including nuclear reactors cooled by light water (LWR's), whose maximum exponent are Pressurized Water Reactors (PWR's) like Angra II in operation in Brazil;

- Generation III/III+ (1995 – 2030): they are the natural evolution of GEN-II by incorporation better environmental, economics, efficiency and safety aspects;
- Generation IV (2030+): it is a step above compared to GEN-III due to its unique features, reported later in this section.

Abram and Ion (2008) reported that the GEN-IV initiative was proposed as a necessity to sustain the advancement of a new generation of nuclear power plants. In this same line of thinking, as reported by Kelly (2014), it happened because at the end of the twentieth century, electricity generation from NPP's was considered a mature technology; due to this fact, most of the nuclear research programs were not causing much enthusiasm, especially in United States, bringing to the need of the development of novel nuclear energy systems. So, several nations established in the year 2000 the International Generation IV Initiative to promote and support an international collaboration to develop the next concept in nuclear power plants, the GEN-IV nuclear reactors (ABRAM and ION, 2008).

All activities associated with these new systems are guided by the Generation-IV International Forum (GIF), whose active participating members must affirm an agreement among them. The founding members who signed GIF chart in July 2001 are Argentina, Brazil, Canada, France, Japan, Republic of Korea, Republic of South Africa, United Kingdom and United States while Switzerland, Russia, China and the Euratom or EAEC (European Atomic Energy Community) signed GIF deal between 2002 and 2006 (KELLY, 2014). This same author explains that the Organization for Economic Co-operation and Development (OECD) provides technical consulting and support to GIF through the Nuclear Energy Agency (NEA).

They were proposed eight main goals for the GEN-IV nuclear reactors during the first forum. Such aims were divided into four categories: sustainability; economics; safety and reliability; proliferation resistance and physical protection. NERAC and GIF (2002) highlight that all objectives are equally important and none of them should receive more or less attention or be considered more special than others. The GEN-IV aims are exposed in this section from NERAC and GIF (2002):

*“Sustainability–1: Generation IV nuclear energy systems will provide sustainable energy generation that meets clean air objectives and promotes long-term availability of systems and effective fuel utilization for worldwide energy production”.*

*“Sustainability–2: Generation IV nuclear energy systems will minimize and manage their nuclear waste and notably reduce the long-term stewardship burden, thereby improving protection for the public health and the environment”.*

*“Economics–1: Generation IV nuclear energy systems will have a clear life-cycle cost advantage over other energy sources”.*

*“Economics–2: Generation IV nuclear energy systems will have a level of financial risk comparable to other energy projects”.*

*“Safety and Reliability–1: Generation IV nuclear energy systems operations will excel in safety and reliability”.*

*“Safety and Reliability–2: Generation IV nuclear energy systems will have a very low likelihood and degree of reactor core damage”.*

*“Safety and Reliability–3: Generation IV nuclear energy systems will eliminate the need for offsite emergency response”.*

*“Proliferation Resistance and Physical Protection–1: Generation IV nuclear energy systems will increase the assurance that they are a very unattractive and the least desirable route for diversion or theft of weapons-usable materials, and provide increased physical protection against acts of terrorism”.*

Beyond all the characteristics introduced above, the GEN-IV systems are designed so that their coolants achieve great temperatures allied with high power density in order to meet high temperature applications, further electricity generation, like hydrogen production (NERAC and GIF, 2002) or even sea water desalination, what is in agreement with the first main aim proposed in this research.

Initially, GIF identified six nuclear technologies capable to achieve those eight objectives (NEA, 2014) and also high temperature applications. They are: Gas Cooled Fast Reactor (GFR); Lead Cooled Fast Reactor (LFR); Molten Salt Reactor (MSR); Sodium Cooled Fast Reactor (SFR); Supercritical Water Cooled Reactor (SCWR); Very High Temperature Reactor (VHTR). Additionally to these systems, Locatelli *et al.* (2013) considerer the Gas Turbine Modular Helium Reactor (GT-MHR) as a system capable to accomplish the targets proposed by GIF as any GEN-IV technology. GT-MHR is similar to a High Temperature Reactor (HTR).

Then, in this thesis work, only three of these systems were considered: GT-MHR, SFR and SCWR. The other remaining ones, GFR, LFR, MSR and VHTR, were not evaluated because there were not found in the literature enough thermodynamic and technical information in the manner required to perform a proper study matching the proposed aim. Due to this reason, in the next subsections are being only described the technologies GT-MHR, SFR and SCWR. The way in which each NPP is coupled to the Na-O-H hydrogen production unit in addition to a MED desalination plant to grant three different trigeneration cases of H<sub>2</sub>, electricity and H<sub>2</sub>O is being explained in chapter 3.

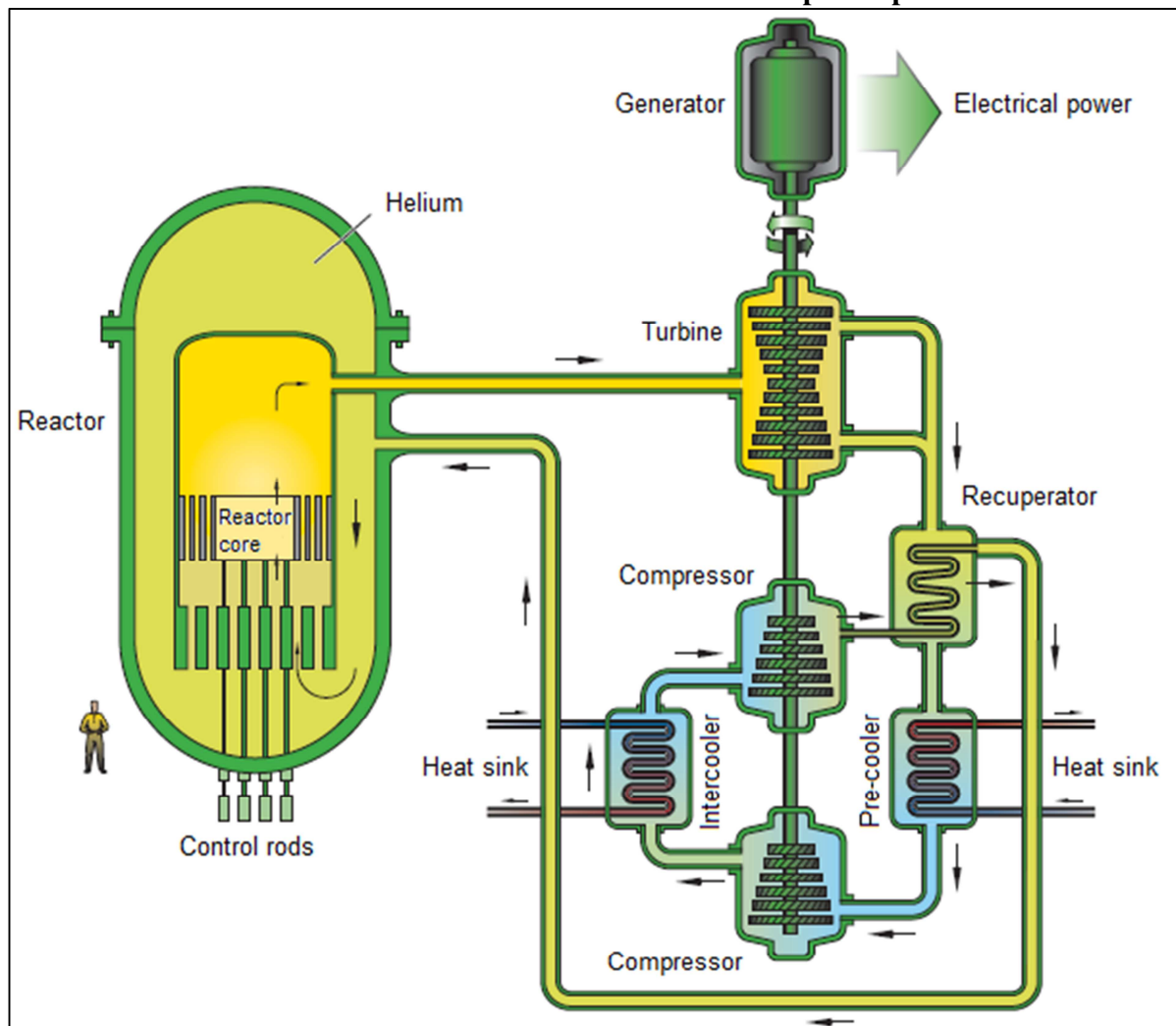
### **2.3.2 Gas Turbine – Modular Helium Reactor (GT-MHR)**

Gas Turbine Modular Helium Reactor (GT-MHR) is a technology with high energy efficiency, around 45%, due to the lofty temperature achieved by its coolant working fluid, in this case helium (He) (MOHAMMADKHANI *et al.*, 2014). Besides that, Zare and Mahmoudi (2015) highlight other important features of it, for example, low cost, safety and proliferation resistance. Sahin *et al.* (2012) believe proliferation resistance is possible because the system is designed to burn some special nuclear materials, like the weapon-grade plutonium coming from spent nuclear fuels from other NPP's. GT-MHR is under development depending on the collaboration among Framatome (France), Fuji Electric (Japan), General Atomics (USA) and Ministry of Atomic Energy of Russia as Sahin *et al.* (2012) report in their study.

Usually, a Gas Turbine Modular Helium Reactor consists of a thermodynamic Brayton power cycle represented in Figure 7 (adapted from NERAC and GIF, 2002). As it can be seen, helium coolant at high temperature (850 °C) and high pressure (8 MPa) flows through a gas turbine to produce electricity (ZARE and MAHMOUDI, 2015). Then, the coolant flows inside recuperator,

a heat exchanger design to preheat helium in a counter-flow before it reaches reactor core in order to remove heat from fission reaction. Next, the coolant releases heat in pre-cooler to a heat sink, normally sea water, before He is compressed in two stages to be directed to a recuperator and finally reach the reactor core to begin the cycle again. There is an intercooler between the two compression steps to reduce He temperature to about 26 °C (MOHAMMADKHANI *et al.*, 2014) and consequently reduces the compression work demanded in each stage. The heat released in pre-cooler and intercooler can be used in different ways, for instance, improving GT-MHR thermal efficiency through a waste heat recovery technic like a transcritical CO<sub>2</sub> cycle studied by Wang and Dai (2016); heating applications proposed by Zare (2016) or even desalination previously suggested by Zare *et al.* (2013) and applied in this work.

**FIGURE 7 – Schematic view of a GT-MHR power plant**



Source: adapted from NERAC and GIF (2002).

### **2.3.3 Sodium Cooled Fast Reactor (SFR)**

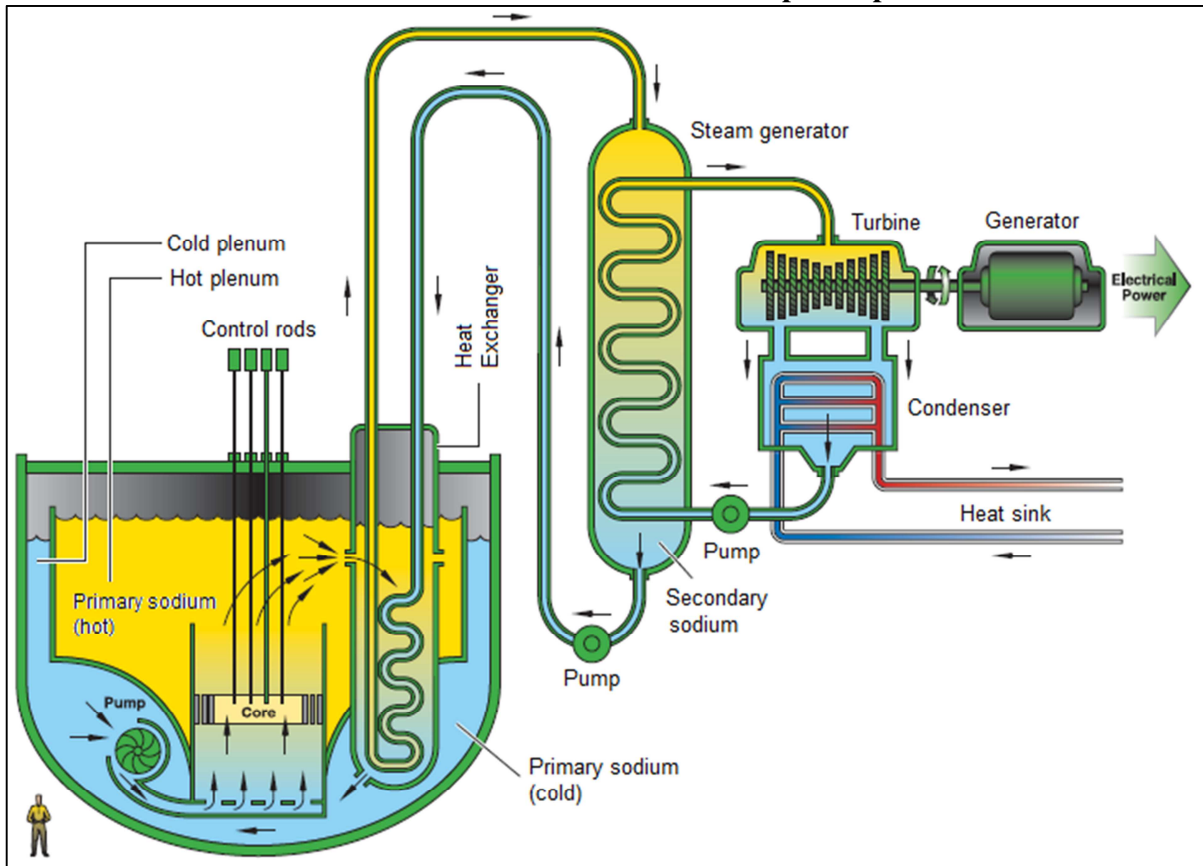
Sodium Cooled Fast Reactor (SFR) is a nuclear power installation design to burn stored spent nuclear fuels from other NPP's and also utilizing the lots of uranium 238 ( $U^{238}$ ) available in nature. Di Maio *et al.* (2014) report that SFR system is under research in many countries like U.S.A, Russia, Japan and France.

Authors like Bianchi *et al.* (2011), Jeong and Jeong (2013) and Aoto *et al.* (2014) emphasize that the recycling of spent nuclear fuels is an alternative way to enhance the security of energy supplies through a better waste management by the disposal of radioactive and weapon-base plutonium materials besides increasing the energy extract from uranium utilization. Because of these features, SFR is considered a potential sustainable energy option (CHEN *et al.*, 2018).

In accordance to Aoto *et al.* (2014), SFR could achieve raised power density with low amount of coolant because it uses liquid sodium (Na), a metal with high thermal conductivity. Complementing its great thermal conductivity, Na has low melting point (98 °C) and high boiling temperature (883 °C), making it a good coolant candidate in the advice of Lim *et al.* (2018). A schematic view of a SFR is introduced in Figure 8 adapted from NERAC and GIF (2002).

As shown in Figure 8, SFR has three coolant loops: a primary one containing liquid sodium; an intermediate one or secondary sodium loop plus a third one composed by a traditional Rankine steam plant where electrical power is produced. Such approach is found in many studies like the one presented by Zhong *et al.* (2018). In Na first loop, coolant removes heat from reactor core and then transfers such energy to liquid Na in the second loop through an intermediate heat exchanger. After that, sodium coolant in the secondary circuit causes water boiling in a steam generator. Regarding to information from Khalid *et al.* (2016), steam generated at high pressure (17 MPa) and elevated temperature (510 °C) is directed to a turbine to produce electricity. Then, steam at low pressure (15 kPa) and low temperature (50 °C) is condensed, pumped to finally return to steam generator to begin the thermodynamic cycle again. SFR has thermal efficiency ranging from around 35% to 45% depending on its physical or thermodynamic configuration as can be verified in the paper published by Ahn and Lee (2014).

**FIGURE 8 – Schematic view of a SFR power plant**



Source: adapted from NERAC and GIF (2002).

Despite the good thermal properties of Na, Lim *et al.* (2018) draw attention to the fact that it extremely reacts with water or even air, causing fume, fire and explosion. Still, in the opinion of Di Maio *et al.* (2014), the use of liquid metals as coolants in energy systems has many disadvantages, inclusive the corrosion and consequent compromising of its structural integrity.

To avoid the violent reaction between sodium and water and to reduce potential accidents in the installation and in the nuclear reactor itself, there is an intermediate heat exchanger, the secondary sodium loop, placed between first sodium loop and the steam plant (YOO *et al.*, 2017). Other configurations of SFR can solve such problem through using working fluids whose do not react with sodium, including He and CO<sub>2</sub> as proposed by Ahn and Lee (2014).



### ***2.3.4 Supercritical Water Reactor (SCWR)***

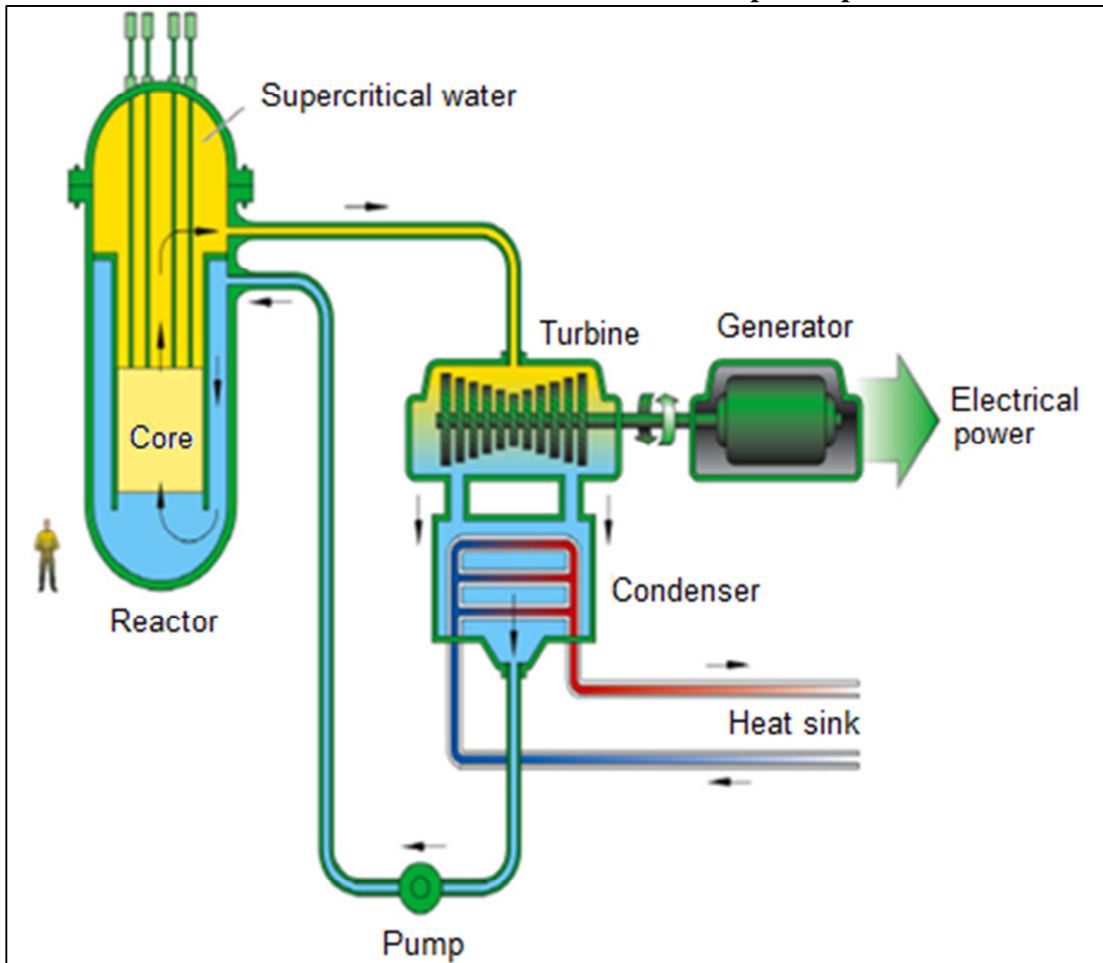
Ruzickova *et al.* (2014) characterize Supercritical Water Reactor (SCWR) as a nuclear power plant whose coolant operates above water critical point (22.1 MPa and 374 °C). Still, these same authors relate that GIF identified important technical features and advantages of it compared to the conventional water cooled reactors (GEN-II and GEN-III), making the SCWR a potential GEN-IV candidate. Among these advantages emphasized by many scientists like Su *et al.* (2013) are its high thermodynamic efficiency, higher than 40%, due to the lofty pressure and temperature operational conditions achieved by water coolant; relatively simple system design and operation beyond the possibility to apply technology and knowledge from the well-known supercritical water fossil fired power plants (SCW-FFP's).

Schulenberg and Visser (2013) clarify in their research that SCWR follows the basic principle of the SCW-FFP's that is to increase steam temperature and consequently its enthalpy to improve turbine output power and then enhance its overall thermal efficiency. Based on information from the article printed by Schulenberg *et al.* (2014), a usual SCWR plant operates at around 25 MPa with an outlet temperature about 500 °C or above.

Ruzickova *et al.* (2014) credit the high thermal efficiency with better economic aspects in addition to plant simplification as a consequence of the single-phase coolant (water at supercritical condition) coupled directly to the energy conversion system (supercritical steam turbine), what avoids the use of many components like intermediate heat exchangers, steam generators and dryers like in the SFR NPP or in the common steam power cycles.

In this way, a SCWR installation operates consonant a traditional thermodynamic Rankine cycle where supercritical water flows directly from reactor core outlet to generate electrical power in a steam turbine. After leaving turbine, steam is condensed into liquid water, pumped, pre-heated and directed to reactor core where it will be turned again into supercritical water after receiving heat released from the nuclear fuel. This thermodynamic cycle is represented in Figure 9 adapted from NERAC and GIF (2002).

**FIGURE 9 – Schematic view of a SCWR power plant**



Source: adapted from NERAC and GIF (2002).

According to the research published by Podila and Rao (2015), the design proposed for the SCWR is based on the previous experience and knowledge of Canada, a GIF participating member, acquired during development and operation of Pressurized Heavy Water Reactors (PHWR's) by the country together with the extensive worldwide knowledge about fossil fired power plants which also operate at supercritical condition (RUZICKOVA *et al.*, 2014, SCHULENBERG *et al.*, 2014). In contrast, the evolution of a viable nuclear core design plus the development of structural materials for it and for the nuclear fuel are one of the major challenges related to SCWR development in the opinion of Ruzickova *et al.* (2014).

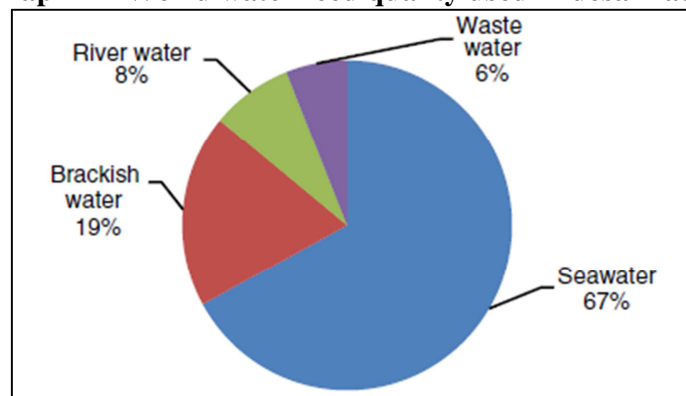
## 2.4 Multi-Effect Distillation (MED) desalination process

Water is a vital resource to almost all life forms on earth. Moreover, it is essential to maintain many key anthropogenic activities such as agriculture and industry. In the thinking of Miller *et al.* (2015), the enhanced in the living standards of people together with population growth caused an increase in water consumption, especially in developing countries during the second half of the last century for the purpose of attending their industrial and domestic necessities.

It is estimated that around 20% of the global population lives in places where water is scarce or even it is not available to the public (MILLER *et al.*, 2015). Still, United Nations (UN) foresee by the year 2025 around 1800 million people worldwide will suffer lack of potable water (SHARON and REDDY, 2015). Due to these facts and expectations, some researchers like Miller *et al.* (2015) believe water will be a precious commodity traded in global market such as some of the classical ones, including petroleum, ores and grains. So, desalination became an important option to increase the availability of fresh water in places where it is not accessible considering the current and the future panorama of this resource.

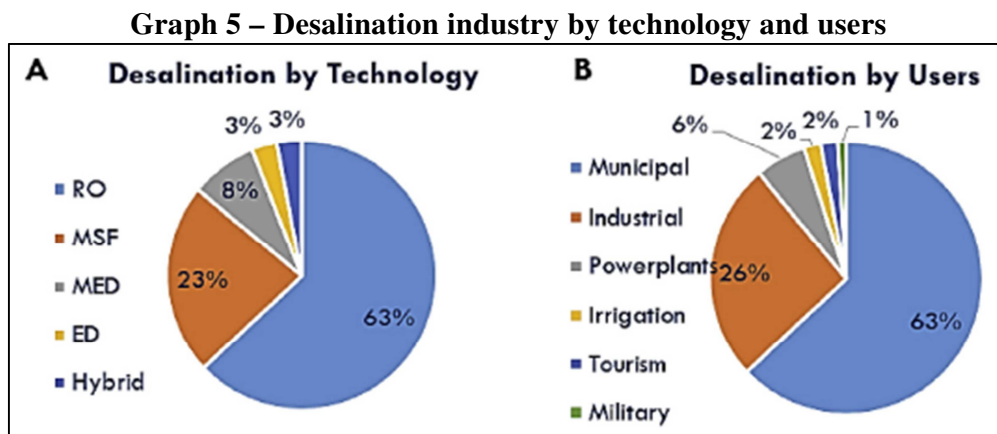
In the words of Abdelkareem *et al.* (2018), desalination is a method to remove salt from saline water to get fresh one. Otherwise, it can be understood as a process to separate potable H<sub>2</sub>O from a saline solution. Different options (river water, brackish water and waste one), beyond seawater, are able to be used as input water sources in desalination processes aiming the production of fresh one as presented in Graph 4 from the research of Mezher *et al.* (2011) based on the Economic and Social Commission for Western Asia (ESCWA, 2019) source data.

**Graph 4 – World water feed quality used in desalination**



Source: Mezher *et al.* 2011 based on ESCWA (2019).

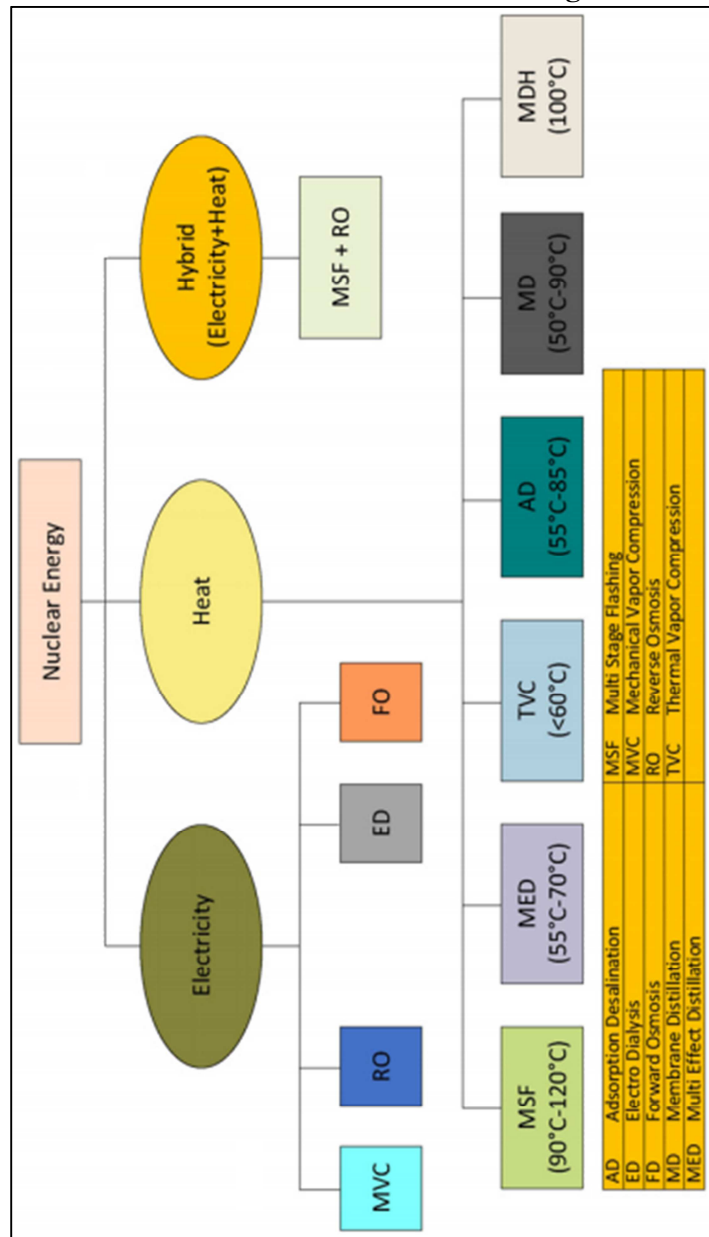
There are many desalination technologies described in the literature. Each one bases on a specific physical principle. Among them are: Reverse Osmosis (RO) studied by Anis *et al.* (2019) and Qasim *et al.* (2019), Multi-Stage Flash (MSF) evaluated by Thabit *et al.* (2019) and Deyab (2019) in addition to Multi-Effect Distillation (MED) analyzed by Micari *et al.* (2019) and Goodarzi *et al.* (2019). RO produces fresh water mainly consuming electricity while both MSF and MED secure drinkable H<sub>2</sub>O using the heat provided by some thermal energy system. Reverse Osmosis accounts around 62% of all desalinated H<sub>2</sub>O production rate worldwide while both MSF and MED contribute to 10 % and 14 % (ALKAISI *et al.*, 2017). Such percentages of every desalination technology together with the main users of desalinated water are exhibited in Graph 5 adapted from the research of Gude (2016). As noted in it, municipal user (63%) and industry one (26%) demands around 90% of all desalinated water produced worldwide.



Source: adapted from Gude 2016.

However, this thesis work is developed focusing only on the MED system because it allows the use of low grade waste heat like the energy rejected by thermal power plants. This condition totally agrees with the first main aim of thesis which is to trigenerate H<sub>2</sub>O, electricity and H<sub>2</sub>; the desalinated water, the source of hydrogen in the Na-O-H thermochemical cycle, must be attained by harvesting to a MED plant the waste heat, mainly at around 40-70 °C, released from the condensers or coolers of certain types of NPP's. Corroborating this statement, Figure 10 from Khalid *et al.* (2016) schematizes possible desalination routes using nuclear energy. According to it, a MED installation can work using a thermal energy source at 55-70 °C.

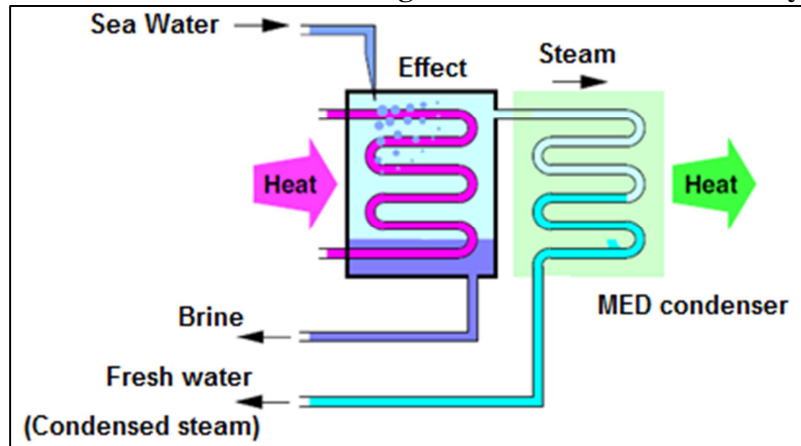
**FIGURE 10 – Possible desalination routes using nuclear energy**



Source: adapted from Khalid *et al.* (2016).

A MED desalination unit composed by a single-effect is drafted in Figure 11 adapted from Brogioli *et al.* (2018). In it, energy released from a heat source distills or produces fresh water by boiling saturated steam, almost free of salts, from saline seawater that enters the effect in the form of spray. Consequently, it is produced brine, a solution whose salt concentration is higher than seawater. Then, the steam cooled in the MED condenser corresponds to the drinkable water produced in this single-effect MED desalination system.

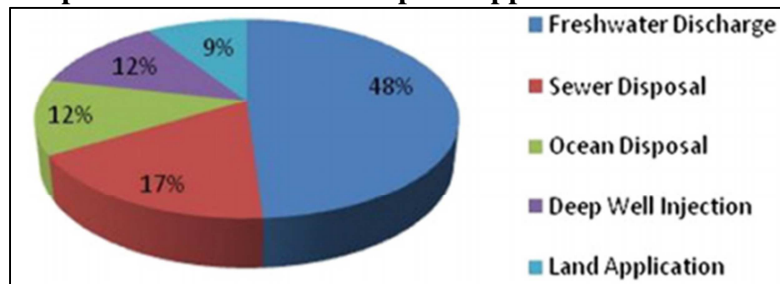
**FIGURE 11 – Schematics of a single-effect MED desalination system**



Source: adapted from Brogioli *et al.* (2018).

The distillation of fresh water from a saline solution is able to proceed at low temperatures, around 50-70 °C, as described in the studies of Mabrouk *et al.* (2015) and Piacentino (2015). It happens because the process is performed in low pressure environment achieved by a vacuum pump, what reduces the boiling point of sea water that is higher than 100 °C under atmosphere pressure. The amount of fresh H<sub>2</sub>O produced in the effect corresponds to the mass flow rate of distilled and condensed steam in it. In general, a MED unit has a recovery rate “R” (ratio between the fresh water produced and the sea water entering the system) around 35-40% as found in some studies in the literature like the one performed by Dastgerdi *et al.* (2016). Sea water with salt concentration of 3.5% or 35,000 ppm (parts per million), brine with saline concentration near 5% or 50,000 ppm in addition to steam and fresh water with salt concentration close to 0.2% (200 ppm) or even below. Talebbeydokhti *et al.* (2017) highlight that these salt concentrations represent typical values for a MED plant. About brine discharge, Burn *et al.* (2015) use source data from New South Wales Government (NSW, 2011) to illustrate in Graph 6 how such solution is managed in Australia.

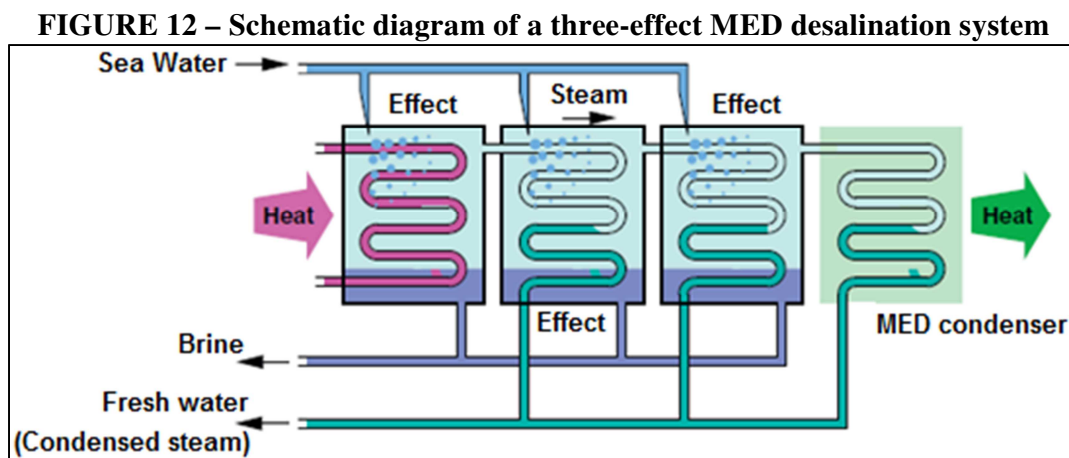
**Graph 6 – Common brine disposal approaches in Australia**



Source: adapted from Burn *et al.* 2015 using source data from NSW (2011).

The mass flow rate of steam produced in the first effect of Figure 11 can be used as the heat source in a next desalination stage by its own condensation to succeed more steam (fresh water) and brine from sea water that enters in a possible second effect. In this way, it is possible to build a MED plant composed by multi-effects depending on the temperature difference between each effect, ordinarily 2-4 °C (GABRIEL *et al.*, 2015 and AHMADI *et al.*, 2017), combined with the temperature of the heat source at the first effect.

In Figure 12, adapted from Brogioli *et al.*, (2018), is represented a simplified version of a MED plant composed by three effects plus a MED condenser necessary to cool steam formed in the last desalination stage. Figure 12 corresponds to the traditional approach of such system. Other innovative and improved configurations of MED installations are assessed in the works of Christ *et al.* (2015a) and Christ *et al.* (2015b). The thesis is developed considering the classic design of a MED technology due to the extensive information covering it available in the literature.



Source: adapted from Brogioli *et al.* (2018).

## 2.5 Physical principles

In this subject are introduced the basic physical principles and fundamentals needed to model later in methodology chapter the systems and cases previously defined in section 1.2. The physical principles and equations lodged are described in details in many thermodynamic books like the ones written by Çengel and Boules (2002), Borgnakke and Sonntag (2009), Moran *et al.* (2011) in addition to Klein and Nellis (2011).

### 2.5.1 Conservation of mass for control volumes

The principle of mass conservation, a matter balance, accounts the mass flow rate through control volumes (CV's). A control volume is a delimited region of the space where mass, energy, entropy and exergy flows are accounted. Engineering devices like pumps, turbines and heat exchangers can be modeled as CV's. Then, this principle is applied in many practical situations such as the determination of how much water flows in a pump station, the amount of cooling fluid flowing inside a radiator or the amount of petroleum that gushes during an oil-well perforation.

Equation (22) expresses this physical law for a generic CV operating at steady state conditions, which means its properties and conditions do not vary in time. This equation considers the total sum of mass flow rate in ( $\dot{m}_{in}$ ) and out ( $\dot{m}_{out}$ ) of the CV as Çengel and Boules (2005) explain.

$$\sum \dot{m}_{in} = \sum \dot{m}_{out} \quad (22)$$

So, a mass balance is applied for all the devices analyzed in the work during chapter 3 to determine the total mass flow rate of H<sub>2</sub>, desalinated H<sub>2</sub>O and other through each one of them.

### 2.5.2 The first law of thermodynamics for control volumes

The first law of thermodynamics is an energy conservation balance. One of its applications is to determine the total amount of energy exchanged during certain situations, for example, the heat released in cooling processes or the electricity generated by a turbine in a NPP. Equation (23) expresses its general form for control volumes operating at steady state. This equation neglects changes in potential and kinetic energies, a common approach in many practical situations.

$$\dot{Q} - \dot{W} = \sum \dot{m}_{out} h_{out} - \sum \dot{m}_{in} h_{in} \quad (23)$$

In Equation (23),  $\dot{Q}$  is the heat transfer rate,  $\dot{W}$  represents the net rate at which work is transferred to or from the device, and  $h$  is the specific thermodynamic property enthalpy outgoing (out) or incoming (in) the CV. Enthalpy is computed for a well-defined thermodynamic state; it is a function of two independent thermodynamic properties like  $p$  and  $T$ . So,  $h$  can be understood as the specific energy (kJ/kg) of matter defined in function of its physical state ( $p$  and  $T$  or others).



In relation to heat transfer rates, when it is positive ( $\dot{Q}$  superior to 0), the system receives thermal energy and its internal energy increases; a water heating process illustrates this kind of situation. Unlikely, when the heat transfer rate is negative ( $\dot{Q}$  inferior to 0), the system releases thermal energy and its internal energy decreases, like in a water cooling process. In relation to work, it is positive ( $\dot{W}$  superior to 0) when the system realizes work and its internal energy decreases; it is the case of a turbine that produces work by using some kind of hot working fluid. On the contrary, it is negative ( $\dot{W}$  inferior to 0) when work is added to the system and its internal energy increases; it is the case when water flows through a pump.

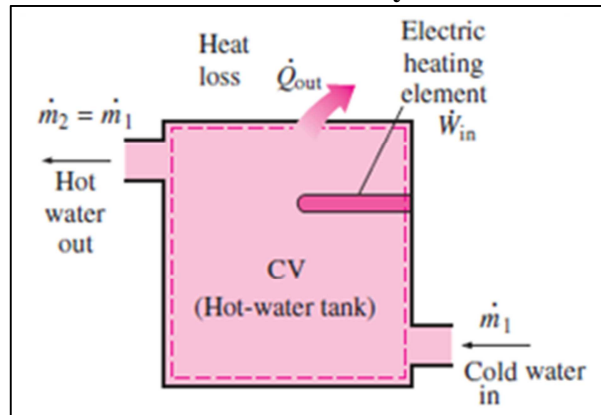
Farther, the thermal efficiency ( $\eta$ ) of an energy system is defined by the ratio between the useful energy effect produced, like the work rate generated in a power plant ( $\dot{W}$ ), and the energy supplied to the system to produce such effect, which include the thermal power released by some kind of fuel ( $\dot{Q}$ ). Equation (24) is the classic formula to account  $\eta$  of a system.

$$\eta = \frac{\dot{W}}{\dot{Q}} \quad (24)$$

Figure 13 from Çengel and Boules (2005) exemplifies an application of the first law of thermodynamics, in which an energy balance is used to determine the input power ( $\dot{W}_{in}$ ) supplied by an electrical resistance to heat a cold water stream considering the thermodynamic conditions at inlet ( $h_{cold}$ ) and outlet ( $h_{hot}$ ) of a water tank plus the amount of heat loss through system boundaries ( $\dot{Q}_{out}$ ). Such situation is quantified according to Equation (25).

$$\dot{Q}_{out} - \dot{W}_{in} = \dot{m}_{hot} h_{hot} - \dot{m}_{cold} h_{cold} \quad (25)$$

Then, over methodology section, an energy balance is applied for all the CV assessed in chapter 3 in order to determine the energy exchanged, in the form of  $\dot{Q}$  or  $\dot{W}$ , during their operation.

**FIGURE 13 – The first law of thermodynamics for a water heater**

Source: Çengel and Boules (2005).

### 2.5.3 The second law of thermodynamics for control volumes

The second law of thermodynamics evaluates in which direction a process can proceed spontaneously. For example, heat spontaneously flows from a region at higher temperature to a region at lower one. The reverse process does not happen spontaneously unless work is consumed as in a refrigerator. So, the probable occurrence direction of a process is established employing the thermodynamic property entropy and its balance, entropy generation rate ( $\dot{S}_G$ ) quantified in Equation (26) for control volumes operating at steady state (MORAN *et al.*, 2011).

$$\dot{S}_G = \sum \dot{m}_{\text{out}} s_{\text{out}} - \sum \dot{m}_{\text{in}} s_{\text{in}} - \sum \frac{\dot{Q}}{T} \quad (26)$$

The previous formula calculates entropy generation rate considering the thermodynamic property entropy ( $s$ ) at inlet (in) and outlet (out) of the CV plus the mass flow rate ( $\dot{m}$ ) through it in addition to the absolute temperature ( $T$ ) in which a possible heat transfer rate mechanism ( $\dot{Q}$ ) from or to the system takes place. Specific entropy ( $s$ ) is defined for a well-specified thermodynamic state; it is measured in kJ/kgK. Entropy is usually defined as the degree of disorder related to a system.

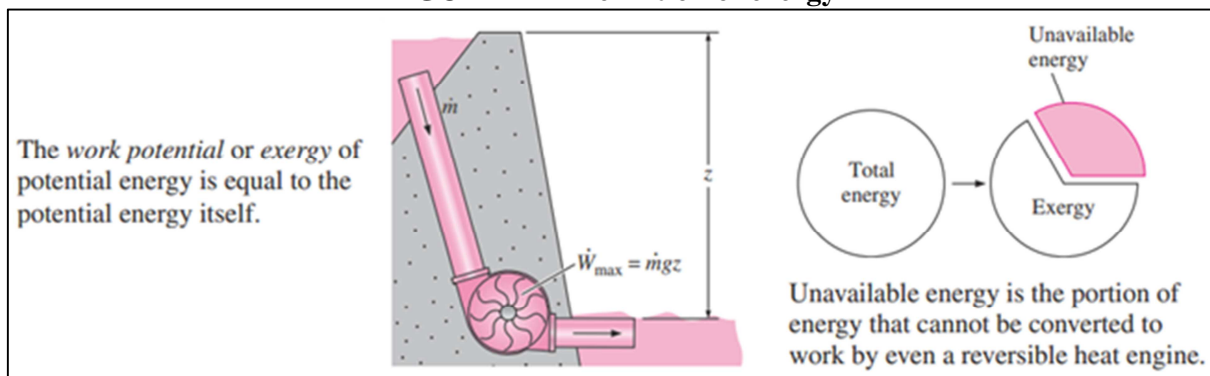
From the second law of thermodynamics, entropy generation rate must increase ( $\dot{S}_G > 0$ ) in the case of actual processes as in movement with friction. Impossible ones such as refrigerators that do not require input power must have it less than zero ( $\dot{S}_G < 0$ ). Ideal situations like motion

without friction have entropy generation rate null ( $\dot{S}_G = 0$ ). Entropy generation serve as a parameter to compare the performance of actual devices or quantify their efficiencies through an exergy analysis discussed in section 2.5.4.

#### 2.5.4 Exergy analysis for control volumes

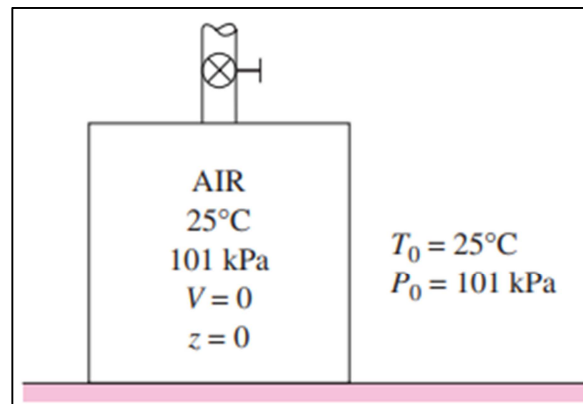
Moran *et al.* (2011) define exergy as “the maximum theoretical work obtainable from an overall system consisting of a system and its surroundings as the system comes into equilibrium with the environment or passes to the dead state”. This concept is illustrated in Figure 14 adapted from Çengel and Boules (2005). In it, exergy is defined as the useful part of some amount of energy. The unavailable energy, its portion that cannot be converted into useful work, happens in function of irreversibility such as friction inside pipes that causes pressure loss during fluid flow.

**FIGURE 14 – Definition of exergy**



Source: adapted from Çengel and Boules (2005).

The dead state occurs when a system is at equilibrium (thermodynamic, mechanical, potential and so on) with its surrounding environment (MORAN *et al.*, 2011). Figure 15 adapted from Çengel and Boules (2005) exemplifies such thermodynamic condition, where an air reservoir (system) is at the dead state because its state defined by its conditions of pressure and temperature (thermodynamic equilibrium) in addition to its high and velocity (potential and mechanical equilibrium) are the same as in the environment.

**FIGURE 15 – Air reservoir at dead state**

Source: adapted from Çengel and Boles (2005).

Tzanakakis and Angelakis (2011) classify four types of exergy. They are: kinetic, potential, physical and chemical. Potential and kinetic ones correspond respectively to the work produced by a system as consequence of changes in its height and velocity. Physical exergy is induced by pressure and temperature variations between the system the environment.

Chemical exergy is the minimum theoretical work needed to produce a pure substance starting from its basic chemical elements when products and reactants of a reaction are at the same thermodynamic state of pressure and temperature (GHARAGHEIZI *et al.*, 2014). In other words, Morosuk and Tsatsaronis (2019) define chemical exergy as the amount of energy released due to the difference in chemical composition between a substance and its surrounding environment. Calculations about chemical exergy can be found in the works of Rivero and Garfias (2006), Song *et al.*, 2012 and Oliveira (2012) in addition to many others. However, in the present research it will be used tabulated standard values of chemical exergy defined at 25 °C and 101.325 kPa (~1 bar) instead of calculating them due to their availability that saves time and resources to develop the research, but also to the relative complexity associated with this subject.

The specific physical exergy ( $e_{ph}$ ) of a generic substance is prescribed by Equation (27) considering the enthalpy difference ( $h - h_0$ ) and entropy difference ( $s - s_0$ ) when the chemical is at any temperature ( $h$  and  $s$ ) and at the dead state ( $h_0$ ,  $s_0$  and  $T_0$ ) defined in terms of  $p_0 = 1$  bar and  $T_0 = 298.15$  K (25 °C). In this way, physical exergy is too considered a thermodynamic property, like enthalpy, defined by both system ( $T, p$ ) and dead state ( $T_0, p_0$ ) conditions.

$$e_{ph} = (h - h_0) - T_0 \cdot (s - s_0) \quad (27)$$

The total specific exergy ( $e$ ) of a substance is the sum of its chemical and physical exergy as in Equation (28) while its total exergy rate is measured according to Equation (29). Equation (28) neglects potential and kinetic exergy. These two exergy types are not evaluated in this work.

$$e = e_{ch} + e_{ph} \quad (28)$$

$$\dot{E} = \dot{m} \cdot (e_{ch} + e_{ph}) \quad (29)$$

The first law of thermodynamics establishes that energy is always conserved in any process. Therefore, it is never destroyed or lost. In contrast, exergy is never conserved in any process in function of entropy generation and its irreversibility that destroy some part of it.

Equation (30) accounts the exergy destroyed in a CV due to heat transfer and work plus the sum of exergy flows in ( $\dot{E}_{in}$ ) and out ( $\dot{E}_{out}$ ) of the system. Additionally, exergy destroyed is too determined by multiplying entropy generation by dead state temperature as in Equation (31).

$$\dot{E}_D = \sum \left( 1 - \frac{T_0}{T} \right) \dot{Q} - \dot{W} + \sum \dot{E}_{in} - \sum \dot{E}_{out} \quad (30)$$

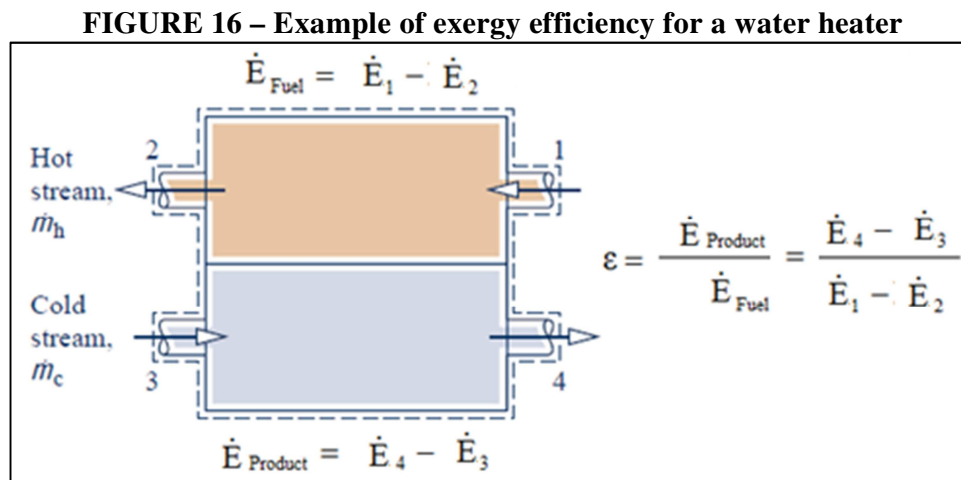
$$\dot{E}_D = \dot{S}_G T_0 \quad (31)$$

Other concepts related to exergy are: exergy rate as fuel ( $\dot{E}_{Fuel}$ ), exergy rate as product ( $\dot{E}_{Product}$ ) and exergy efficiency ( $\epsilon_i$ ).  $\dot{E}_{Fuel}$  is relative to the exergy added or supplied to a system like when a hot gas supplies energy (exergy as fuel) to heat a cold water stream in order to produce hot water ( $\dot{E}_{Product}$ ). Exergy rate as product represents some amount of the exergy supplied to a system that is recovered ( $\dot{E}_{Recovered}$ ) by it in the form of some useful effect like a heating process. Then, using both concepts, the exergy efficiency ( $\epsilon_i$ ) of a process is measured through Equation (32). Additionally, an exergy rate balance ( $\dot{E}_{Fuel} = \dot{E}_{Product} + \dot{E}_D$ ) permits to calculate the exergy efficiency of a process using the exergy destroyed in it as proposed by Equation (33).

$$\varepsilon_i = \frac{\dot{E}_{\text{Recovered}}}{\dot{E}_{\text{Supplied}}} = \frac{\dot{E}_{\text{Product}}}{\dot{E}_{\text{Fuel}}} \quad (32)$$

$$\varepsilon_i = 1 - \frac{\dot{E}_D}{\dot{E}_{\text{Fuel}}} = 1 - \frac{\dot{E}_D}{\dot{E}_{\text{Product}} + \dot{E}_D} \quad (33)$$

In Figure 16 (adapted from MORAN *et al.*, 2011) is exemplified the concepts of exergy as fuel, exergy as product and exergy efficiency. As can be seen in it, the difference between exergy flows 1 and 2 ( $\dot{E}_1 - \dot{E}_2$ ) represents exergy as fuel or the exergy supplied by a hot flow stream, while the difference between exergy flows 4 and 3 ( $\dot{E}_4 - \dot{E}_3$ ) represents exergy as product or the exergy received by the cold stream to produce a certain effect. Finally, the exergy efficiency is the ratio between exergy as fuel and product.



Source: adapted from Moran *et al.* 2011.

### 2.5.5 Enthalpy change for chemical reactions

Enthalpy change for a chemical reaction “i” ( $\Delta H_i$ ) represents the amount of energy required or released by it that is quantified as in Equation (34) (CASTELLAN, 1983). This formula considers the specific molar enthalpy ( $\bar{h}$ ) in kJ/mol of reactants (R) and products (P) involved in the process in addition to their amount of matter or number of moles (N). When enthalpy change is positive ( $\Delta H_i > 0$ ), the total enthalpy of products overcome the net enthalpy of reactants; in this

case reaction is endothermic and demands a certain quantity of heat to proceed. On the other hand, for the situation in which enthalpy change is negative ( $\Delta H_i < 0$ ), reaction is exothermic and releases heat because enthalpy of reactants is superior to products.

$$\Delta H_i = \sum_P N \cdot \bar{h} - \sum_R N \cdot \bar{h} \quad (34)$$

Additionally, for a thermochemical cycle composed by many chemical reactions, the overall enthalpy change of the process ( $\Delta H^0_{\text{cycle}}$ ) is just the sum of the enthalpy change of each chemical step, considering its endothermic and/or exothermic reactions depending on the situation, as suggested by Equation (35).

$$\Delta H_{\text{cycle}} = \sum_i^n \Delta H_i \quad (35)$$

Finally, the energy efficiency for a thermochemical cycle ( $\eta_{\text{cycle}}$ ) in Equation (36) is defined here considering the ratio between the total amount of energy related to the process, that is the net enthalpy change from Equation (35), and the total energy released during hydrogen combustion ( $\Delta H_{\text{combustion}}$ ) that is equal to 285.83 kJ/mol. It is the same value for the standard enthalpy of formation of liquid water (NIST, 2018).

$$\eta_{\text{cycle}} = \frac{(\Delta H_{\text{combustion}})_{\text{H}_2(\text{g})}}{\Delta H_{\text{cycle}}} = \frac{\text{Potential energy recovered during hydrogen combustion}}{\text{Energy required by the cycle}} \quad (36)$$

### 2.5.6 Entropy change for chemical reactions

Entropy change for a chemical reaction “i” ( $\Delta S_i$ ) establishes its most probable occurrence direction. When entropy generation or entropy change is positive ( $\Delta S_i > 0$ ), it represents real processes, reaction have potential to occur in a well-defined direction; when it is negative ( $\Delta S_i < 0$ ), it represents impossible processes, reaction cannot occur in the previous defined direction. Such variation is calculated considering the thermodynamic property molar entropy ( $\bar{s}^0$ ) and

number of moles (N) for all chemical specimens in products (P) and reactants (R) according to Equation (37) (CASTELLAN, 1983).

$$\Delta S_i = \sum_P N \cdot \bar{s} - \sum_R N \cdot \bar{s} \quad (37)$$

In Equation (38) is determined the entropy change for a thermochemical cycle ( $\Delta S^0_{\text{cycle}}$ ). It is just the sum of the entropy change in all reactions of the cycle.

$$\Delta S_{\text{cycle}} = \sum_i^n \Delta S_i \quad (38)$$

### 2.5.7 Gibbs free energy ( $\Delta G$ )

According to Hillert and Selleby (2016), chemical thermodynamics study reactions covering systems under constant conditions of temperature, pressure and content of matter. Such reactions can occur spontaneously, approaching to thermodynamic equilibrium, when their Gibbs free energy ( $\Delta G$ ) diminishes until a minimum value (HILLERT and SELLEBY, 2016).

Gibbs free energy is a parameter used to evaluate if a chemical conversion is able to proceed. It has been used to understand a wide variety of applications. Among them are biochemical metabolic activities studied by Toure and Dussap (2016); bubble nucleation from fluid particles on heated superficies due to heat transfer mechanisms analyzed in the work of Yuan *et al.* (2018); thermodynamic equilibrium during hydrogen production through combining steam and CO<sub>2</sub> methane reforming processes (DEMIDOV *et al.*, 2011); melting point of nanoparticles (LUO and HU, 2013); glycerol and methanol reforming technologies to produce H<sub>2</sub> investigated by Freitas and Guirardello (2014) and Da Silva *et al.* (2009).

Solsvik *et al.* (2016) explain that Gibbs free energy represents the effect of entropy generation on the reaction proceeding. These same scientists elucidate entropy generation of a spontaneous chemical reaction tends to increase, as expected according to the second law of thermodynamics,



what reflects on a decrease in  $\Delta G$ . In contrast, in a non-spontaneous process, there is an increase in  $\Delta G$  due to reversing the occurrence process direction. When a system is at equilibrium condition there is no changes in its Gibbs free energy,  $\Delta G$  reaches its minimum value, because changes in entropy do not occur any more (SOLSVIK *et al.*, 2016).

In this line of reasoning, a possible way to set a thermodynamic equilibrium condition or if chemical processes are able to occur spontaneously is through calculating their Gibbs free energy by applying an analytical representation of  $\Delta G$  as suggest Peng *et al.*, (2018). It can be done using Equation (39) from Yan and Hino (2011).

$$\Delta G = \Delta H - T \cdot \Delta S \quad (39)$$

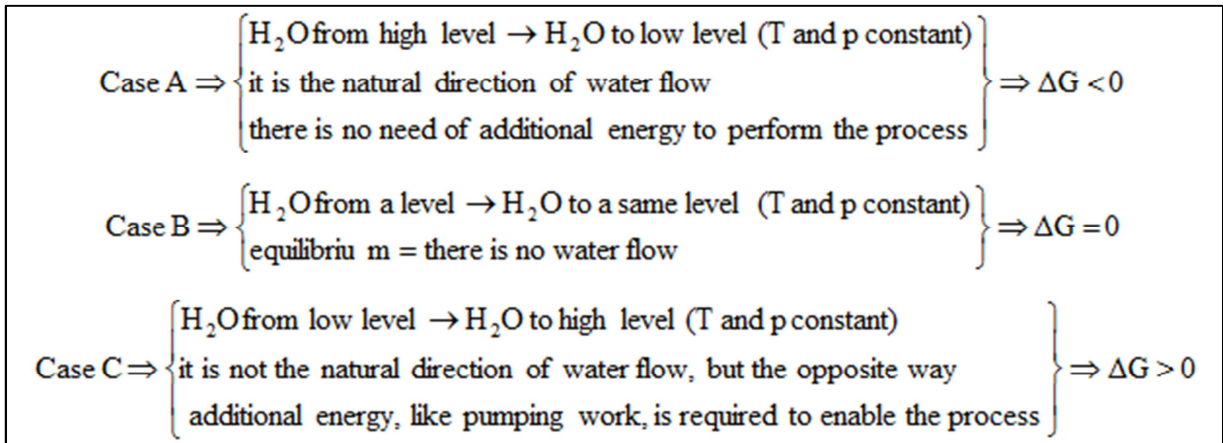
Equation (39) is the classic definition of Gibbs free energy or its change for a chemical reaction under a specified thermodynamic state of pressure (p), temperature (T) and content of matter (N).  $\Delta H$  and  $\Delta S$  respectively represent changes in enthalpy and entropy related to the products (P) and reactants (R) of reaction and they are prescribed according to Equations (34) and (37), where: N is the number of moles related to each one of the chemicals in products and reactants;  $\bar{h}$  is the total specific molar enthalpy and  $\bar{s}$  is the specific molar entropy. Both properties are measured at specific conditions of p and T in which the reaction takes place.

There are three possible values for  $\Delta G$  in any process. They are (CASTELLAN, 1983):

- $\Delta G < 0$ : the chemical reaction is able to occur spontaneously in a well-defined direction; reactants naturally turn into products. There is no need of extra energy requirements to enable it.
- $\Delta G = 0$ : the chemical reaction is at thermodynamic equilibrium; reactants and products turn into each other simultaneously and they coexist at the same time.
- $\Delta G > 0$ : the chemical reaction is not spontaneous and probably occurs in the opposite direction from that one previously defined or thought as the right way; reactants naturally do not turn into products. An additional amount of energy must be supplied to reaction to enable its proceeding.

These situations are illustrated through Figure 17 adapted from Castellan (1983) in which water flows from a specific level to another one considering three different possible cases.

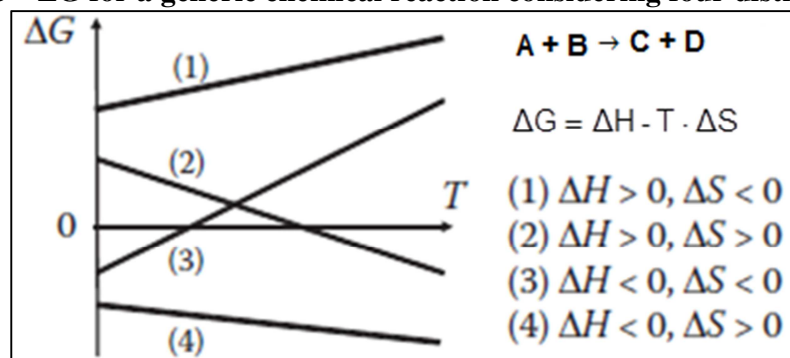
**FIGURE 17 –  $\Delta G$  for three water flow cases**



Source: adapted from Castellan (1983).

Complementing information given above, Yan and Hino (2011) show through Figure 18 the relation between enthalpy change ( $\Delta H$ ), entropy change ( $\Delta S$ ) and Gibbs free energy ( $\Delta G$ ) for a generic chemical reaction as a function of its temperature considering four different situations.

**FIGURE 18 –  $\Delta G$  for a generic chemical reaction considering four distinct situations**



Source: adapted from Yan and Hino (2011).

As it can be seen in Figure 18, the values of  $\Delta G$  or the spontaneity or non-spontaneity of a chemical process is directly affected by its temperature. According to this graph, a reaction is spontaneous ( $\Delta G < 0$ ) like in case (4) or non-spontaneous ( $\Delta G > 0$ ) as in case (1) for any temperature condition. On the other hand, a reaction can turn from spontaneous to non-

spontaneous or vice-versa depending on the temperature range in which it is carried out like in cases (2) and (3).

Still related to Figure 18 (YAN and HINO, 2011), the values of enthalpy and entropy changes for that generic reaction also depends on temperature, despite such behavior is not explicit in the figure, what impacts on the final value of  $\Delta G$ . In this way, to perform a proper thermodynamic analysis based on Gibbs free energy, the parameters  $\Delta H$  and  $\Delta S$  and their correlated thermodynamic properties  $\bar{h}$  and  $\bar{s}$  should be expressed as a function of T and also p.

In the second step described in the methodology chapter, a Gibbs free energy analysis is carried out for each one of the three chemical reactions that composes the Na-O-H cycle in order to investigate other and maybe better operational conditions for it than those ones previously described in section 2.2.4 that were introduced by Miyaoka *et al.* (2012) when they studied such system for the first time. Those authors experimentally evaluated this thermochemical cycle only considering few specific conditions of pressure and temperature for each chemical reaction. If there are better operating conditions of T and p for the Na-O-H cycle than those presented before, the energy and economic potentials to produce hydrogen through this system could be improved, what justifies a  $\Delta G$  study.

### 2.5.8 Exergy analysis for chemical reactions

In this subsection, the main concepts of exergy analysis for control volumes introduced in subsection 2.5.4 in order to obtain the exergy destroyed and exergy efficiency for chemical reactions are adapted. All equations presented are derivative from Oliveira (2012). Exergy destruction in a chemical reaction is the difference between the total exergy of reactants ( $E_R$ ) and products ( $E_P$ ) as in Equation (40) adapted from Equation (30). Additionally, exergy destroyed in a chemical process can be calculated by Equation (31) considering its entropy generation ( $S_{G,i}$ ) or difference ( $\Delta S_i$ ) in Equation (37).

$$E_D = E_R - E_P \quad (40)$$

The total exergy of reactants and products are obtained from Equations (41) and (42) by multiplying the total specific exergy ( $\bar{e}$ ) from Equation (28) and the respective number of moles ( $N$ ) related to the chemicals in products and in reactants of reaction.

$$E_{R,i} = \sum_R (N \cdot \bar{e}) \quad (41)$$

$$E_{P,i} = \sum_P (N \cdot \bar{e}) \quad (42)$$

Finally, the exergy efficiency of a chemical process ( $\epsilon_i$ ), Equation (43), is the ratio between the total exergy of products and reactants in Equations (41) and (42) or the relation between exergy destroyed from Equations (31) or (40) and exergy of products or reactants as can be demonstrated in Equation (44) similarly to Equation (33).

$$\epsilon_i = \frac{E_P}{E_R} = \frac{\sum_P (N \cdot \bar{e})}{\sum_R (N \cdot \bar{e})} \quad (43)$$

$$\epsilon_i = 1 - \frac{E_D}{E_R} = 1 - \frac{E_D}{E_P + E_D} \quad (44)$$

## 2.6 Literature review

The literature review is performed by describing some recent researches covering thermodynamic and economic aspects of hydrogen production units based on thermochemical cycles, specially the Cu-Cl and Mg-Cl, coupled to some energy systems that can be NPP's or others. Such studies are references to develop the work because their methodology is close to that one adopted in the thesis. Beyond that, the results of those works are used to evaluate the thermodynamic and economic aspects of the Na-O-H cycle when compared to different cogeneration processes of hydrogen and electricity based on other H<sub>2</sub> thermochemical procedures under development.

Additionally, they are assessed works covering different MED desalination systems under development that operate using low grade waste heat whose operational temperature lies below 100 °C in order to verify if the production costs and fresh water production rate from the trigeneration cases analyzed in the thesis are in accordance with other researches already validated and published.

### (i) Thermochemical water splitting cycles of hydrogen production

In relation to the Cu-Cl thermochemical route, Al-Zareer *et al.* (2017a) analyzed a cogeneration system composed by a hydrogen production and compression units based on a four-step version of this system whose heat and electricity demanded are supplied by a Supercritical Water Reactor (SCWR). Authors modeled the process in the software Aspen Plus through mass, energy and exergy balances. The results showed that such cogeneration method is able to produce 2.02 kg/s of compressed H<sub>2</sub> in addition to 533 MW of electricity with exergy and energy efficiencies of 56.2 % and 31.6 % respectively. Similarly, Al-Zareer *et al.* (2017b) assessed a hydrogen production and compression facilities based on an alternative version of the 5-step Cu-Cl procedure coupled to a Supercritical Water Reactor. The outputs of this research using a similar methodology such as Al-Zareer *et al.* (2017a) showed that this hybrid installation is able to yield 3.56 kg/s of compressed hydrogen with exergy and energy efficiencies of 27.8 % and 16.9 %, respectively.

Besides that, Sayyaadi (2017) proposed using an exhaust gas from a gas turbine as the heat source to drive a H<sub>2</sub> production facility based on the five-step Cu-Cl cycle. These researchers evaluated this system considering thermodynamic and economic aspects hoping to find the better optimum design of it that provides the lowest production cost allied with the highest conversion efficiency considering a plant capacity of 130,000 kg of H<sub>2</sub> per day (1.504 kg/s). According to the results, the best design choice provides a thermal efficiency of 51.3 %, exergy efficiency of 55.2 % and a cost of 4.02 US\$ per kg of H<sub>2</sub>, considering the year 2017, when is selected a Mitsubishi HI 501 F turbine model capable to generate 735 MW of electricity.

Ishaq *et al.* (2018) studied a hydrogen production installation based on the four-step Cu-Cl cycle coupled to an industrial heat recovery technology of a steel furnace. Using the first and second laws of thermodynamics, these researchers concluded that the system has exergy efficiency of 39.8% while its energy efficiency lies near 38.2%. In such condition the facility is able to make around 18 g/s (0.018 kg/s) of H<sub>2</sub>. Similar to Ishaq *et al.* (2018), Ishaq *et al.* (2019) evaluated the thermodynamic aspects of hydrogen production considering a four-step Cu-Cl cycle but now using the waste heat from furnace cement as the heat source. The final results of this research showed that the system has both energy and exergy efficiencies close to 32% and it is able to yield about 21 kg/h (0.0583 kg/s) of H<sub>2</sub>. Beyond that, Ishaq and Dincer (2019) compared the energy and exergy efficiencies of 3-step, 4-step and 5-step configurations of the Cu-Cl thermochemical cycle. They concluded that the 4-step provides the best values of exergy (75.7%) and energy efficiencies (41.9%). Besides the papers described here and cited in section 2.1.2 about the copper-chlorine cycle, there are many other works like the ones published by Bölükdemir *et al.* (2018), Vaghasia *et al.* (2018), Gabriel *et al.* (2019) and Wajda and Gabriel (2018) covering this same thermochemical method.

In relation to the Mg-Cl cycle, Balta *et al.* (2012) applied mass, energy and exergy balances to determine the energy and exergy efficiencies of a three-step magnesium-chlorine thermochemical procedure without considering a specific heat source. Such system has exergy efficiency of 34.86 % and energy efficiency of 63.63 %. In a similar way, Ozcan and Dincer (2014) applied thermodynamic principles to quantify the performance of a 3-step Mg-Cl cycle when it receives heat from a solar tower. This installation has exergy and energy efficiencies of 19.99 % and

18.8 %, respectively, for a condition when solar energy is directly applied as the heat source to produce H<sub>2</sub>. Still, Ozcan and Dincer (2016b) proposed a new configuration, 4-step, for the Mg-Cl technic. This new design enables the system to have a maximum operational temperature close to 450-500 °C instead 530 °C like in the traditional 3-step configuration. Besides that, this new magnesium-chlorine design is 13% more efficient than water electrolysis in terms of electricity consumption according to the researchers. Additionally, Ozcan and Dincer (2016c) performed a thermodynamic study related to this new arrangement of the magnesium-chlorine technic and conclude that it has an energy efficiency of 43.7 % and exergy efficiency of 52 %.

Additionally to the Cu-Cl and Mg-Cl technics, there are many recent works covering the S-I cycle, for instance, the one presented by Rodríguez *et al.* (2018), Gillis *et al.* (2018), Zhang *et al.* (2019) and Zhou *et al.* (2019). However, such researches and many of the studies about the sulphur-iodine method cover the thermodynamic aspects of its chemical reactions and not coupling it to energy systems in order to quantify the amount of H<sub>2</sub> made in this procedure plus its cost. In this way, such papers are not described here as previously done for the routes Cu-Cl and Mg-Cl.

In relation to the Na-O-H method, the first work about it was presented by Miyaoka *et al.* (2012) who proposed three chemical reactions (hydrogen production, metal separation and hydrolysis) for this system according to a first experimental study. After that, Marques *et al.* (2018a) evaluated the potential of the sodium-oxygen-hydrogen to produce hydrogen if it is coupled to a Sodium Cooled Fast Reactor (SFR) with a thermal output power of 4000 MW. They concluded that such cogeneration process is able to make around 1.321 kg/s of H<sub>2</sub>, a theoretical maximized value due to the simplifications assumed by the authors. Then, Marques *et al.* (2019) and Marques *et al.* (2020a) performed Gibbs free energy analysis ( $\Delta G$ ) plus exergy analysis to investigate theoretical operational conditions of pressure and temperature for the chemical reactions of the Na-O-H cycle to complement the first experimental information provided by Miyaoka *et al.* (2012).

In Chart 12 is summarized some of the studies and their main results described in this topic covering thermochemical water splitting cycles of hydrogen production.

**CHART 12 – Summary of some studies about thermochemical cycles**

Researchers	Systems analyzed	Main results
Al-Zareer <i>et al.</i> (2017a)	Cogeneration system composed by a H <sub>2</sub> production and compression units based on a four-step Cu-Cl cycle whose heat and electricity are supplied by a Supercritical Water Reactor.	The system has exergy efficiency equal to 56.2 % and energy efficiency equal to and 31.6 %.
Al-Zareer <i>et al.</i> (2017b)	H <sub>2</sub> production and compression facilities based on an alternative version of the 5-step Cu-Cl procedure coupled to a Supercritical Water Reactor.	This hybrid installation is able to yield 3.56 kg/s of compressed hydrogen with exergy and energy efficiencies of 27.8 % and 16.9 %, respectively.
Sayyaadi (2017)	An exhaust gas from a gas turbine as the heat source to drive a H <sub>2</sub> production facility based on the five-step Cu-Cl cycle.	The best design choice provides a thermal efficiency of 51.3 %, exergy efficiency of 55.2 % and a cost of 4.02 US\$ per kg of H <sub>2</sub> , considering the year 2017.
Ishaq <i>et al.</i> (2018)	A H <sub>2</sub> production installation based on the four-step Cu-Cl cycle coupled to an industrial heat recovery technology of a steel furnace.	It has exergy efficiency of 39.8% while its energy efficiency lies near 38.2%. The facility is able to make around 18 g/s (0.018 kg/s or 64.8 kg/h) of H <sub>2</sub> .
Balta <i>et al.</i> (2012)	A three-step version of the Mg-Cl procedure without considering a specific heat source.	Such system has exergy efficiency of 34.86 % and energy efficiency of 63.63 %.
Ozcan and Dincer (2014)	A 3-step Mg-Cl cycle coupled to a solar tower.	This installation has exergy and energy efficiencies of 19.99 % and 18.8 %, respectively.
Ozcan and Dincer (2016b)	The researchers proposed a new configuration, 4-step, for the Mg-Cl technic.	This new design enables the system to have a maximum operational temperature close to 450-500 °C instead 530 °C like in the traditional 3-step configuration.

Source: the author.



(ii) Low grade waste heat Multi-Effect Distillation (MED) system

In the research of Wang *et al.* (2011) were performed both experimental analysis and simulation covering an alternative design of a MED installation that uses waste heat in the range 65-90 °C. The authors conclude that this innovative approach has potential to increase desalinated water production rate by 25-60% when compared to the classic MED system.

Christ *et al.* (2014) investigated how a MED installation that uses sensible low grade waste heat as energy source can have its potable H<sub>2</sub>O production rate increased by means of an optimization process. The results of this research indicated that the amount of desalinated water obtained can increase around 40% depending on the temperature (50-75 °C) of the heat source and the number of desalination stages or effects (3 to 8) in the installation. Then, Christ *et al.* (2014) concluded that multi-effect distillation is a viable desalination technology while low grade waste heat is a good energy source for this kind of process.

A new design of a MED facility was assessed by Rahimi *et al.* (2014). This new configuration can have its potable water production rates enhanced by coupling a MED system to a multi-stage flashing chamber in which steam free of salts boils from saline water. In such approach, a heat source at around 75 °C enters the first effect of the MED unit and leaves it at around 64 °C. Then, the heat source goes to the flashing chamber to produce more desalinated H<sub>2</sub>O; it leaves the system at around 47 °C. The results of this research suggested that this new configuration can produce about 50% more desalinated water than the classic optimized MED installations with low increasing in pumping power consumption in addition to a reduction of 6% in capital cost.

Rahimi *et al.* (2015) assessed the classic multi-effect distillation technology in addition to its boosted (B-MED) and flash (F-MED) versions. All these system can operate by using low grade sensible heat. The authors think B-MED and F-MED are able to generate enhanced rates of desalinated water than the conventional MED installation. All the three systems (MED, B-MED and F-MED) were simulated to estimate their capital and operational costs according to a thermo-economic model developed by the researchers. The outputs of this study indicate that B-MED and F-MED plants have capital costs inferior to the regular one while their operating costs are

near to the classic MED. Finally, boosted and flash versions have production costs (1.1 US\$/m<sup>3</sup> in 2015) around 6% inferior to the regular MED system.

After comparing the classic MED and its boosted version (B-MED), Christ *et al.* (2015b) concluded that the boosted one has better economic and thermodynamic performances than the conventional version when both technologies use low temperature energy source. B-MED version has capacity to yield around 25% more desalinated water combined with a production cost (near around 1.4 US\$/m<sup>3</sup> in 2015) inferior to the convention MED design.

Similar to Rahimi *et al.* (2015), a novel distributed boosted multi-effect distillation (DB-MED) that demands waste heat at 65-90 °C was studied by Dastgerdi *et al.* (2016). This new design was compared to the classic MED in addition to its boosted version (B-MED) and the flash approach (F-MED) previously evaluated by Rahimi *et al.* (2015). According to the results found in the research carried by Dastgerdi *et al.* (2016), distributed boosted MED is able to distill more potable water than the other systems considered. Depending on the operational conditions of the process, DB-MED can make up to 40% more fresh H<sub>2</sub>O than the classic MED design.

In paper of Talebbeydokhti *et al.* (2017), they were coupled a Parabolic Trough Concentrated Solar Power (PT-CSP) to a low-temperature multi-effect distillation (LT-MED) facility. This PT-CSP power plant is a Discrete Ericsson Cycle (DEC) that operates using air as working fluid. The main goal of such study was to investigate how low grade waste heat in the range 70-80 °C provided by the CSP system influences on the desalinated water produced in the MED plant. The results showed that the LT-MED demands a specific energy consumption of 0.195 kW/(m<sup>3</sup> day of fresh water produced) when it is combined with the CSP plant. Still, the LT-MED needs 0.062 kW/(m<sup>3</sup> day of fresh water produced) when it is coupled to the innovative CSP-DEC power plant.

Finally, many researches about low grade waste heat multi-effect distillation systems indicate that the energy requirement and production cost of that kind of technology lies near 0.4-0.7 MW/(kg/s) (DASTGERDI *et al.*, 2016 and TALEBBEYDOKHTI *et al.*, 2017) and 1 to 2 US\$/m<sup>3</sup> (Youssef *et al.*, 2014 plus PINTO and MARQUES, 2017) depending on system design in addition to their operational conditions such as the temperature limits of the heat source

considered in the first stage of the MED system. This specific energy consumption is defined as the ration between the heat (kW) supplied to the first desalination stage and the total quantity of desalinated water (m<sup>3</sup>) obtained in the plant.

In Chart 13 is summarized some of the researches and their main results described in this topic covering MED desalination installation.

**CHART 13 – Summary of some studies about MED installation**

Researchers	Systems analyzed	Main results
Christ <i>et al.</i> (2014)	It was investigated how a MED installation that uses sensible low grade waste heat as energy source can have its potable H <sub>2</sub> O production rate increased by means of an optimization process.	The amount of desalinated water obtained can increase around 40% depending on the temperature (50-75 °C) of the heat source and the number of desalination effects (3 to 8) in the installation.
Rahimi <i>et al.</i> (2014)	A new design of a low temperature (~75 °C) MED facility was assessed. This new configuration can have its potable water production rates enhanced by coupling it to a multi-stage flashing chamber in which steam free of salts boils from saline water.	This new configuration can produce about 50% more desalinated water than the classic optimized MED installations with low increasing in pumping power consumption in addition to a reduction of 6% in capital cost.
Rahimi <i>et al.</i> (2015)	The researchers assessed the classic multi-effect distillation technology in addition to its boosted (B-MED) and flash (F-MED) versions. All these system can operate using low grade sensible heat.	B-MED and F-MED plants have capital costs inferior to the regular one while their operating costs are near to the classic MED.
Christ <i>et al.</i> (2015b)	The classic MED and its boosted version (B-MED) were compared.	B-MED version has capacity to yield around 25% more fresh water combined with a production cost (near around 1.4 US\$/m <sup>3</sup> in 2015) inferior to the convention MED design.

Source: the author.

## 2.7 Basic aspects and literature review about Engineering Equation Solver (EES) software

The Engineering Equation Solver (EES) software (KLEIN, 2019) is the tool chosen to perform the work because it has friendly interface to implement and solve mathematical formulas. Besides that, EES has a wide library of thermodynamic properties related to many common substances like water, helium and ammonia. Additionally, the software enables the implementation of other physical properties or substances when they are not available in it. EES software is used in different current research areas such as air conditioning in the works of Kalbasi *et al.* (2020) and Alhendal *et al.* (2020); power plants in the papers published by Ahmad *et al.* (2020) and Maali and Khir (2020); refrigeration systems analyzed by Jain *et al.* (2021) and Bellos *et al.* (2021); and also H<sub>2</sub> production methods evaluated by Oruc and Dincer (2021) and Qureshy and Dincer (2021) and water desalination studied by Musharavati *et al.* (2021) and Elbassoussi *et al.* (2021).

In Figure 19 adapted from Klein and Nelis (2011) is exemplified how thermodynamic property enthalpy is obtained in this tool starting from the operational conditions of pressure and temperature at the inlet and outlet of an ammonia compressor. Then, it is calculated the output power of this control volume assuming steady state conditions. The general interface of EES software is similar to those ones of many common programming languages, for instance, C, C++, FORTRAN, Matlab and others. The software uses the Newton's method to numerically solve mathematical equations, including those ones presented during methodology section.

**FIGURE 19 – EES software example**

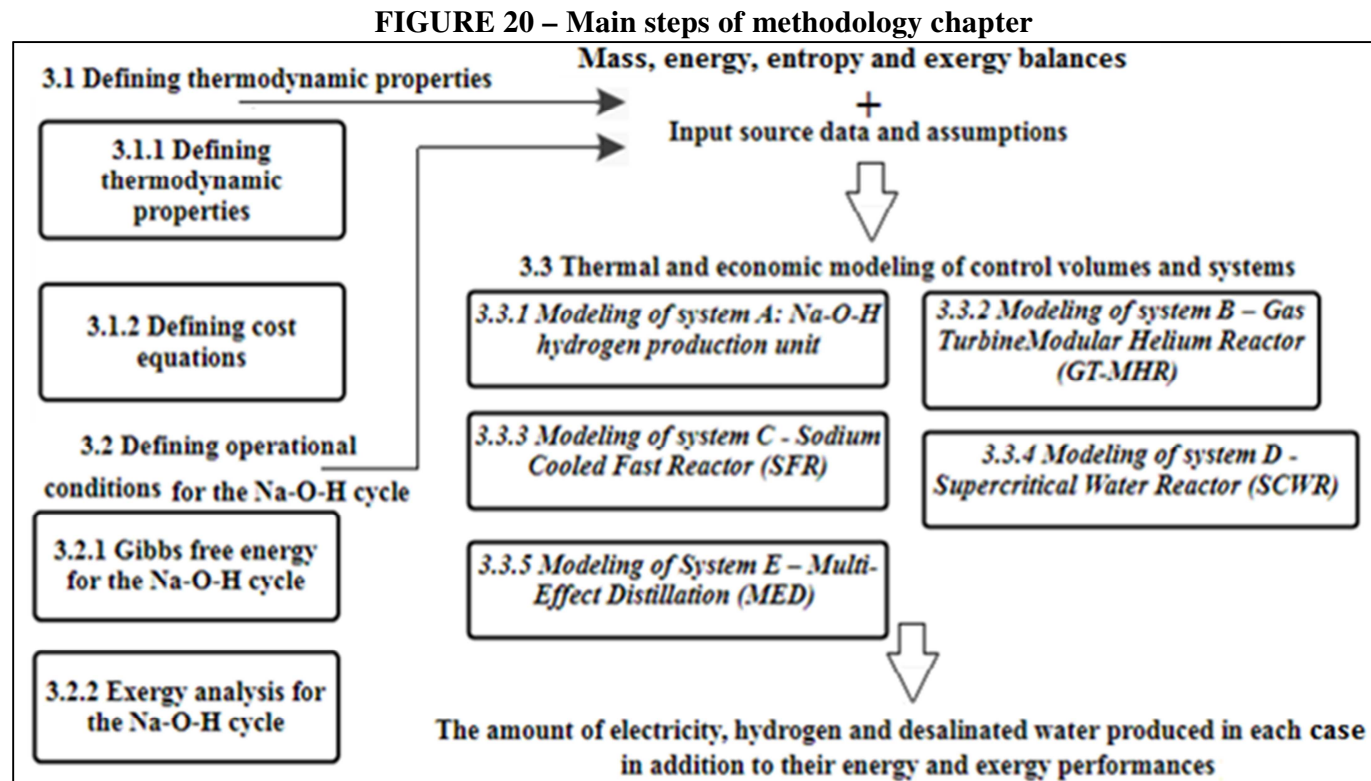
Units conversion to SI	
T[1]=converttemp(C,K,-32 [C])	"inlet temperature to compressor 1"
P[1]=0.90 [bar]*convert(bar,Pa)	"inlet pressure to compressor 1"
m_dot[1]=2.5 [kg/min]*convert(kg/min,kg/s)	"mass flow rate of ammonia entering compressor 1"
P[2]=750 [kPa]*convert(kPa,Pa)	"exit pressure of compressor 1"
T[2]=converttemp(C,K,75 [C])	"exit temperature of compressor 1"
Defining thermodynamic properties at inlet [1] and outlet [2] of the control volume	
h[1]=enthalpy(Ammonia,T=T[1],P=P[1])	"specific enthalpy of ammonia entering compressor 1"
v[1]=volume(Ammonia,T=T[1],P=P[1])	"specific volume of ammonia entering compressor 1"
Phase\$[1]=Phase\$(Ammonia,T=T[1],P=P[1])	"phase at state 1"
h[2]=enthalpy(Ammonia,T=T[2],P=P[2])	"specific enthalpy of ammonia leaving compressor 1"
v[2]=volume(Ammonia,T=T[2],P=P[2])	"specific volume of ammonia leaving compressor 1"
Phase\$[2]=Phase\$(Ammonia,T=T[2],P=P[2])	"phase at state 2"
Mass balance	
m_dot[1]=m_dot[2]	"mass balance on compressor 1"
Energy balance	
W_dot_c_1+m_dot[1]*h[1]=m_dot[2]*h[2]	"energy balance on compressor 1"

Source: adapted from Klein and Nellis (2011).

### 3 METHODOLOGY TO EVALUATE THE TRIGENERATION CASES

The steps of methodology needed to accomplish the first main aim defined in section 1.1 are schematized in Figure 20 and described throughout chapter 3. So, the methodology is employed to evaluate three trigeneration cases previously defined. They are:

- Case 1: Na-O-H hydrogen production unit + GT-MHR power plant + MED facility (Systems A + B + E);
- Case 2: Na-O-H hydrogen production unit + SFR power plant + MED facility (Systems A + C + E);
- Case 3: Na-O-H hydrogen production unit + SCWR power plant + MED facility (Systems A + D + E).



Source: the author.

Beyond the steps exhibited in Figure 20, the limitations and assumptions related to the modeling procedure performed in section 3.3 are commented in item 3.4.

### 3.1 Defining thermodynamic properties for the chemicals of the Na-O-H cycle

The first step of chapter 3 is the definition of enthalpy and entropy properties to evaluate the Na-O-H cycle in items 3.2 and 3.3.1. Thermodynamic properties needed to assess NPP's and MED technologies are provided in section 3.3 during their own specific modeling.

The total enthalpy ( $\bar{h}$ ) for any chemical substance is composed by two parts, standard enthalpy of formation ( $\bar{h}_f^0$ ) and sensible enthalpy difference ( $\Delta\bar{h}$ ) as shown in Equation (45) considering molar terms.

$$\bar{h} = \bar{h}_f^0 + \Delta\bar{h} \quad (45)$$

Çengel and Boules (2002) define enthalpy of formation as “the enthalpy of a substance at a specified state due to its chemical composition”. When the substance is at the standard reference state defined by  $T^0 = 25 \text{ }^\circ\text{C}$  and  $p^0 = 1 \text{ bar}$ , enthalpy of formation is referred as standard enthalpy of formation and the total enthalpy just becomes  $\bar{h}_f^0$  ( $\bar{h} = \bar{h}_f^0$ ) because  $\Delta\bar{h}$  is equal zero in such circumstances. The sensible enthalpy difference is the gap between the sensible enthalpy when the chemical is at any temperature and the sensible enthalpy at the standard temperature.

Usually, the values of  $\bar{h}_f^0$  for the most common substances are accessible in thermodynamic property tables like in Lide (2004) and they are enough to set enthalpy when chemicals are at the reference state. However, in situations in which matters are out of the standard condition, it is necessary to prescribe the sensible enthalpy difference at a specified temperature. This can be done in different ways such as using thermodynamic property tables or mathematical correlations like Equation (46) from the National Institute of Standards and Technology (NIST, 2018) which determines  $\Delta\bar{h}$  as an explicit function of temperature together with specific coefficients (A, B, C,

D, E and F) for each distinct chemical substance that are obtained from experimental analysis or numerical studies.

$$\Delta \bar{h} = A \left( \frac{T}{1000} \right) + \frac{B}{2} \left( \frac{T}{1000} \right)^2 + \frac{C}{3} \left( \frac{T}{1000} \right)^3 + \frac{D}{4} \left( \frac{T}{1000} \right)^4 - E \left( \frac{1000}{T} \right) + F - H \quad (46)$$

Then, the total enthalpy of a material is written as:

$$\bar{h} = \bar{h}_f^0 + A \left( \frac{T}{1000} \right) + \frac{B}{2} \left( \frac{T}{1000} \right)^2 + \frac{C}{3} \left( \frac{T}{1000} \right)^3 + \frac{D}{4} \left( \frac{T}{1000} \right)^4 - E \left( \frac{1000}{T} \right) + F - H \quad (47)$$

In a close way as enthalpy, thermodynamic property entropy is too determined according to an explicit function of temperature and also pressure like in Equation (48) adapted from Oliveira (2012) and NIST (2018) where; R is the universal gas constant equal to 8.31 J/mole·K; p is the partial pressure of the gaseous substance and p<sup>0</sup> is the standard pressure. Generally, solids and liquids do not have their enthalpy and entropy influenced by p. Still, gases have their entropy influenced by T and p while their enthalpy is only affected by T.

$$\bar{s} = A \cdot \ln \left( \frac{T}{1000} \right) + B \left( \frac{T}{1000} \right) + \frac{C}{2} \left( \frac{T}{1000} \right)^2 + \frac{D}{3} \left( \frac{T}{1000} \right)^3 - \frac{E}{2} \left( \frac{1000}{T} \right)^2 + G - R \cdot \ln \frac{p}{p^0} \quad (48)$$

Moreover, both enthalpy and entropy are estimated using specific heat at constant pressure ( $\bar{C}_p$ ), another thermodynamic property that depends on T as shown in Equation (49) from NIST (2018).  $\bar{C}_p$  represents the capacity of a substance to vary its temperature due to gain or loss heat.

$$\bar{C}_p = A + B \left( \frac{T}{1000} \right) + C \left( \frac{T}{1000} \right)^2 + D \left( \frac{T}{1000} \right)^3 + E \left( \frac{1000}{T} \right)^2 \quad (49)$$

In the specific cases of liquids and solids whose specific heat only depend on temperature, Equations (47) and (48) for the total enthalpy and entropy are approximated to Equations (50) and (51) presented by Çengel and Boules (2002) using an average Cp value.

$$\bar{h} = \bar{h}_f^0 + C_{p_{avg}}(T - T^0) \quad (50)$$

$$\bar{s} = \bar{s}^0 + C_{p_{avg}} \ln\left(\frac{T}{T^0}\right) \quad (51)$$

Coefficients A, B, C, D, E, F, G and H in Equations (47), (48) and (49) have different values for distinct substances. In Table 1 adapted from NIST (2018) are exhibit such coefficients for each one of the chemicals in the Na-O-H cycle. They give enthalpy in kJ/mol, entropy in J/mol·K and specific heat in J/mol·K in Equations (47), (48) and (49). Additionally to Table 1, Table 2 based on Fink (1995), Lide (2004) and NIST (2018) provides values of enthalpy of formation, entropy and specific heat at standard condition plus the molecular weight for the subjects in the Na-O-H trial needed to build up the thesis. In Equations (45) to (51), temperature (T) must be provided in K.

**TABLE 1 – Coefficients in Eq. (46) to (49) for the chemicals in the Na-O-H cycle**

Chemical	A	B	C	D	E	F	G	H
NaOH(s)	419.48	-1717.75	2953.57	-1597.22	-6.04	-517.86	933.07	-425.93
Na(l)	40.25	-28.23	20.69	-3.64	-0.08	-8.78	113.66	2.40
Na <sub>2</sub> O(s)	25.57	177.71	-166.33	57.61	2	-423.01	88.5	-417.98
H <sub>2</sub> (g)	33.06	-11.36	11.43	-2.77	-0.15	-9.98	172.70	0
Na <sub>2</sub> O <sub>2</sub> (s)	63.90	131.77	-123.32	50.70	-0.38	-538.43	135.69	-513.20
Na(g)	20.80	0.28	-0.39	0.12	-0.009	101.04	178.70	107.29
H <sub>2</sub> O(l)	-203.60	1523.29	-3196.41	2474.45	3.85	-256.54	-488.71	-285.83
O <sub>2</sub> (g)	31.32	-20.23	57.86	-36.50	-0.007	-8.90	246.79	0

Source: adapted from NIST (2018).

**TABLE 2 – Data at standard state for the chemicals in the Na-O-H cycle**

Chemical	Molecular weight [g/mol]	Enthalpy of formation $h_f^0(25\text{ }^\circ\text{C})$ [kJ/mol]	Standard entropy $s^0(25\text{ }^\circ\text{C})$ [Jmol <sup>-1</sup> K <sup>-1</sup> ]	Specific heat $C_p^0(25\text{ }^\circ\text{C})$ [Jmol <sup>-1</sup> K <sup>-1</sup> ]
NaOH	39.99	-425.93	64.46	59.45
Na(l)	22.98	2.41	57.86	28.23
Na <sub>2</sub> O(s)	61.97	-417.98	75.04	69.1
H <sub>2</sub> (g)	2.01	0	130.68	28.88
Na <sub>2</sub> O <sub>2</sub> (s)	77.97	-513.21	94.78	89.2
Na(g)	22.98	107.5	153.65	20.8
H <sub>2</sub> O(l)	18.01	-285.83	69.95	75.3
O <sub>2</sub> (g)	31.99	0	205.15	29.4

Source: adapted from Fink (1995), Lide (2004) and NIST (2018).



### 3.2 Determining operational conditions for the Na-O-H cycle

At this time are defined the specific operational conditions in which the reactions of the Na-O-H cycle, Equations (18), (19) and (20), are carried out in a H<sub>2</sub> production plant during the trigeneration process modeled in section 3.3. It is done through a  $\Delta G$  study followed by an exergy analysis performed respectively in sections 3.2.1 and 3.2.2 for those three reactions. This approach is realized to overcome the lack of experimental data details beyond the one provided by Miyaoka *et al.* (2012) covering the sodium-oxygen-hydrogen thermochemical process.

#### 3.2.1 Gibbs free energy analysis for the Na-O-H cycle

The theoretical ranges of operational conditions in which the chemical reactions of the Na-O-H cycle are able to proceed are investigated over a Gibbs free energy analysis initiated in item 2.4.4.

Each reaction of the Na-O-H cycle is modeled by first calculating its enthalpy change ( $\Delta H$ ) consonant Equation (34) plus entropy change ( $\Delta S$ ) based on Equation (37) to finally determine their Gibbs free energy starting from Equation (39). Thermodynamic properties enthalpy and entropy needed to calculate  $\Delta H$  and  $\Delta S$  are obtained through Equations (47) and (48) plus information in Tables 1 and 2 from item 3.1.1. All these equations and data together with the conditions of  $p$  and  $T$  (K) in which every reaction is analyzed are implemented in EES software (KLEIN, 2019) following the steps formulated here. Then, the final values of  $\Delta G$  together with  $\Delta H$  and  $\Delta S$  for every reaction are discussed in specific topics of results section in Chapter 4.

##### (i) Modeling chemical reaction 1: hydrogen production step – Equation (18)

Equation (18) is thermodynamic modeled according to Equations (52), (53) and (54) considering specific ranges of operational conditions of  $T$  ( $100\text{ }^\circ\text{C} < T_1 < 300\text{ }^\circ\text{C}$ ) and  $p$  ( $0 < p_1 < 1\text{ bar}$ ) for reaction 1 together with the number of moles ( $N$ ) in products and reactants of it.

$$\Delta H_1 = (N \cdot \bar{h})_{\text{Na}_2\text{O(s)}} + (N \cdot \bar{h})_{\text{H}_2(\text{g})} - (N \cdot \bar{h})_{\text{NaOH(s)}} - (N \cdot \bar{h})_{\text{Na(l)}} \quad (52)$$

$$\Delta S_1 = (N \cdot \bar{s})_{\text{Na}_2\text{O(s)}} + (N \cdot \bar{s})_{\text{H}_2(\text{g})} - (N \cdot \bar{s})_{\text{NaOH(s)}} - (N \cdot \bar{s})_{\text{Na(l)}} \quad (53)$$

$$\Delta G_1 = \Delta H_1 - T_1 \cdot \Delta S_1 \quad (54)$$

Reaction 1 must be carried out considering  $T_1$  between 100 °C and 300 °C to prevent liquid Na to become solid one and solid NaOH to get liquid one because Na(s) has fusion point close to 98 °C while NaOH(s) melts around 300 °C (NIST, 2018). If this reaction is not performed with solid NaOH and liquid Na, it could take place the formation of other products instead  $H_2$  in Equation (18), as explained by Marques *et al.* (2018a) based on Xu *et al.* (2006). On the other hand, it will be verified how partial p of  $H_2$  ( $p_1$ ), the only gaseous product, impacts  $\Delta G_1$ .

(ii) Modeling chemical reaction 2: metal separation step – Equation (19)

Equation (19) is evaluated using Equations (55) to (57) considering specific ranges of operational conditions of T (25 °C <  $T_2$  < 700 °C) and p (0 <  $p_2$  < 1 bar) for reaction 2 together with the number of moles (N) in products and reactants of it.

$$\Delta H_2 = (N \cdot \bar{h})_{Na_2O_s(s)} + (N \cdot \bar{h})_{Na(g)} - (N \cdot \bar{h})_{Na_2O(s)} \quad (55)$$

$$\Delta S_2 = (N \cdot \bar{s})_{Na_2O_s(s)} + (N \cdot \bar{s})_{Na(g)} - (N \cdot \bar{s})_{Na_2O(s)} \quad (56)$$

$$\Delta G_2 = \Delta H_2 - T_2 \cdot \Delta S_2 \quad (57)$$

Reaction 2 is evaluated considering a temperature ranging from 25 °C to 700 °C to establish if this process can occur at low temperatures or about 400-500 °C, the condition previously studied by Miyaoka *et al.* (2012), or just above it. Pressure variation only affects thermodynamic properties of Na(g) and it will understand how  $p_2$  affects  $\Delta G_2$ .

(iii) Modeling chemical reaction 3: hydrolysis step – Equation (20)

Equation (20) is assessed according to Equations (58), (59) and (60) considering specific ranges of operational conditions of T (25 °C <  $T_3$  < 200 °C) and p (0 <  $p_3$  < 1 bar) for reaction 3 together with the number of moles (N) in products and reactants of it.

$$\Delta H_3 = (N \cdot \bar{h})_{NaOH(s)} + (N \cdot \bar{h})_{O_2(g)} - (N \cdot \bar{h})_{Na_2O_2(s)} - (N \cdot \bar{h})_{H_2O(l)} \quad (58)$$

$$\Delta S_3 = (N \cdot \bar{s})_{NaOH(s)} + (N \cdot \bar{s})_{O_2(g)} - (N \cdot \bar{s})_{Na_2O_2(s)} - (N \cdot \bar{s})_{H_2O(l)} \quad (59)$$

$$\Delta G_3 = \Delta H_3 - T_3 \cdot \Delta S_3 \quad (60)$$

Reaction 3 is studied considering a temperature gap from 25 °C to 200 °C to determine if it is able to proceed at temperatures below 100 °C or above it, because such value was the only one experimentally evaluated by Miyaoka *et al.* (2012). Pressure ranging from 0 to 1 bar only affects thermodynamic properties of O<sub>2</sub>(g). Additionally, it shows how this variable influences ΔG<sub>3</sub>.

### 3.2.2 Exergy analysis for the Na-O-H cycle

In this part of the work is fulfilled an exergy analysis to establish which of the operational conditions found in item 3.2.1 provides the maximum exergy efficiency or the minimum exergy destroyed for the three chemical reactions of the Na-O-H cycle. In this way, the trigeneration cases and the hydrogen production unit based on this thermochemical process are evaluated after choosing the specific conditions of p and T that provides the better exergy aspects to convert reactants into products in each of those reactions. It guarantees focus to the study and discard operational conditions that do not provide high thermal performance for the system. Because of this, a parametric study relating the thermal performance of the hydrogen plant in function of all the possible values of p and T for the three reactions of the Na-O-H cycle is not performed.

#### (i) Determining the total specific exergy for the chemicals of the Na-O-H cycle

The physical exergy for each chemical of the Na-O-H cycle are presented in Equations (61) to (78) starting from Equation (27). Enthalpy and entropy for all the chemicals are obtained according to Equations (47) and (48) with information from Tables 1 and 2.

$$\bar{e}_{\text{ph\_NaOH(s)}} = (\bar{h} - \bar{h}_0)_{\text{NaOH(s)}} - T_0 \cdot (\bar{s} - \bar{s}_0)_{\text{NaOH(s)}} \quad (61)$$

$$\bar{e}_{\text{ph\_Na(l)}} = (\bar{h} - \bar{h}_0)_{\text{Na(l)}} - T_0 \cdot (\bar{s} - \bar{s}_0)_{\text{Na(l)}} \quad (62)$$

$$\bar{e}_{\text{ph\_Na}_2\text{O(s)}} = (\bar{h} - \bar{h}_0)_{\text{Na}_2\text{O(s)}} - T_0 \cdot (\bar{s} - \bar{s}_0)_{\text{Na}_2\text{O(s)}} \quad (63)$$

$$\bar{e}_{\text{ph\_H}_2\text{(g)}} = (\bar{h} - \bar{h}_0)_{\text{H}_2\text{(g)}} - T_0 \cdot (\bar{s} - \bar{s}_0)_{\text{H}_2\text{(g)}} \quad (64)$$

$$\bar{e}_{\text{ph\_Na}_2\text{O}_2\text{(s)}} = (\bar{h} - \bar{h}_0)_{\text{Na}_2\text{O}_2\text{(s)}} - T_0 \cdot (\bar{s} - \bar{s}_0)_{\text{Na}_2\text{O}_2\text{(s)}} \quad (65)$$

$$\bar{e}_{\text{ph\_Na(g)}} = (\bar{h} - \bar{h}_0)_{\text{Na(g)}} - T_0 \cdot (\bar{s} - \bar{s}_0)_{\text{Na(g)}} \quad (66)$$

$$\bar{e}_{\text{ph\_H}_2\text{O}(l)} = (\bar{h} - \bar{h}_0)_{\text{H}_2\text{O}(l)} - T_0 \cdot (\bar{s} - \bar{s}_0)_{\text{H}_2\text{O}(l)} \quad (67)$$

$$\bar{e}_{\text{ph\_O}_2(g)} = (\bar{h} - \bar{h}_0)_{\text{O}_2(g)} - T_0 \cdot (\bar{s} - \bar{s}_0)_{\text{O}_2(g)} \quad (68)$$

Then, the total exergy for each one of those substances are estimated based on Equations (69) to (76) as in Equation (28) considering the standard values of chemical exergy presented in Table 3 adapted from Morris and Szargut (1986) in addition to Rivero and Garfias (2006) plus Marques *et al.* (2020). All the exergy analysis were developed always considering constant values of standard chemical exergy at 25 °C and 101.325 kPa (~1 bar), similar to the modeling process proposed by Al-Zareer *et al.* (2017a), Al-Zareer *et al.* (2017b) and Balta *et al.* (2012).

$$\bar{e}_{\text{NaOH}(s)} = \bar{e}_{\text{ch\_NaOH}(s)} + \bar{e}_{\text{ph\_NaOH}(s)} \quad (69)$$

$$\bar{e}_{\text{Na}(l)} = \bar{e}_{\text{ch\_Na}(l)} + \bar{e}_{\text{ph\_Na}(l)} \quad (70)$$

$$\bar{e}_{\text{Na}_2\text{O}(s)} = \bar{e}_{\text{ch\_Na}_2\text{O}(s)} + \bar{e}_{\text{ph\_Na}_2\text{O}(s)} \quad (71)$$

$$\bar{e}_{\text{H}_2(g)} = \bar{e}_{\text{ch\_H}_2(g)} + \bar{e}_{\text{ph\_H}_2(g)} \quad (72)$$

$$\bar{e}_{\text{Na}_2\text{O}_2(s)} = \bar{e}_{\text{ch\_Na}_2\text{O}_2(s)} + \bar{e}_{\text{ph\_Na}_2\text{O}_2(s)} \quad (73)$$

$$\bar{e}_{\text{Na}(g)} = \bar{e}_{\text{ch\_Na}(g)} + \bar{e}_{\text{ph\_Na}(g)} \quad (74)$$

$$\bar{e}_{\text{H}_2\text{O}(l)} = \bar{e}_{\text{ch\_H}_2\text{O}(l)} + \bar{e}_{\text{ph\_H}_2\text{O}(l)} \quad (75)$$

$$\bar{e}_{\text{O}_2(g)} = \bar{e}_{\text{ch\_O}_2(g)} + \bar{e}_{\text{ph\_O}_2(g)} \quad (76)$$

**TABLE 3 – Standard chemical exergy for the substances in the Na-O-H cycle**

Chemical	Standard chemical exergy $\bar{e}_{\text{ch}}^0 = \bar{e}_{\text{ch}}(25\text{ °C}, 101.325\text{ kPa})$ [kJ/mol]	Standard chemical exergy $e_{\text{ch}}^0 = e_{\text{ch}}(25\text{ °C}, 101.325\text{ kPa})$ [kJ/kg]
NaOH(s)	74.91	14912
Na(l)	342.72	18729
Na <sub>2</sub> O(s)	296.2	4779
H <sub>2</sub> (g)	236.09	117457
Na <sub>2</sub> O <sub>2</sub> (s)	174.3	7702
Na(g)	177.1	2232
H <sub>2</sub> O(l)	0.90	50
O <sub>2</sub> (g)	3.97	124

Source: adapted from Morris and Szargut (1986), Rivero and Garfias (2006) and Marques *et al.* (2020a).

(ii) Exergy destroyed and exergy efficiency for the chemical reactions of the Na-O-H cycle

The exergy efficiency and exergy destroyed for the three chemical reactions of the Na-O-H trial are determined after implementing in the EES software (KLEIN, 2019) the equations and steps related to the exergy analysis of chemical process introduced in section 2.5.8. It results in Equations (77) to (85) exhibited below. The total exergy ( $\bar{e}$ ) of all chemicals analyzed were obtained from Equations (69) to (76) from the last subsection while the conditions of p and T in which each reaction is assessed were already provided in section 3.2.1.

(ii.a) Exergy analysis for chemical reaction 1: hydrogen production step – Equation (18)

$$E_{D_1} = T_0 S_{G_1} = T_0 \Delta S_1 \quad (77)$$

$$E_{P_1} = (N \cdot \bar{e})_{Na_2O(s)} + (N \cdot \bar{e})_{H_2(g)} \quad (78)$$

$$\varepsilon_1 = 1 - \frac{E_{D_1}}{E_{P_1} + E_{D_1}} \quad (79)$$

(ii.b) Exergy analysis for chemical reaction 2: metal separation step – Equation (19)

$$E_{D_2} = T_0 S_{G_2} \quad (80)$$

$$E_{R_2} = (N \cdot \bar{e})_{Na_2O(s)} \quad (81)$$

$$\varepsilon_2 = 1 - \frac{E_{D_2}}{E_{R_2}} \quad (82)$$

(ii.c) Exergy analysis for chemical reaction 3: hydrolysis step – Equation (20)

$$E_{D_3} = T_0 S_{G_3} \quad (83)$$

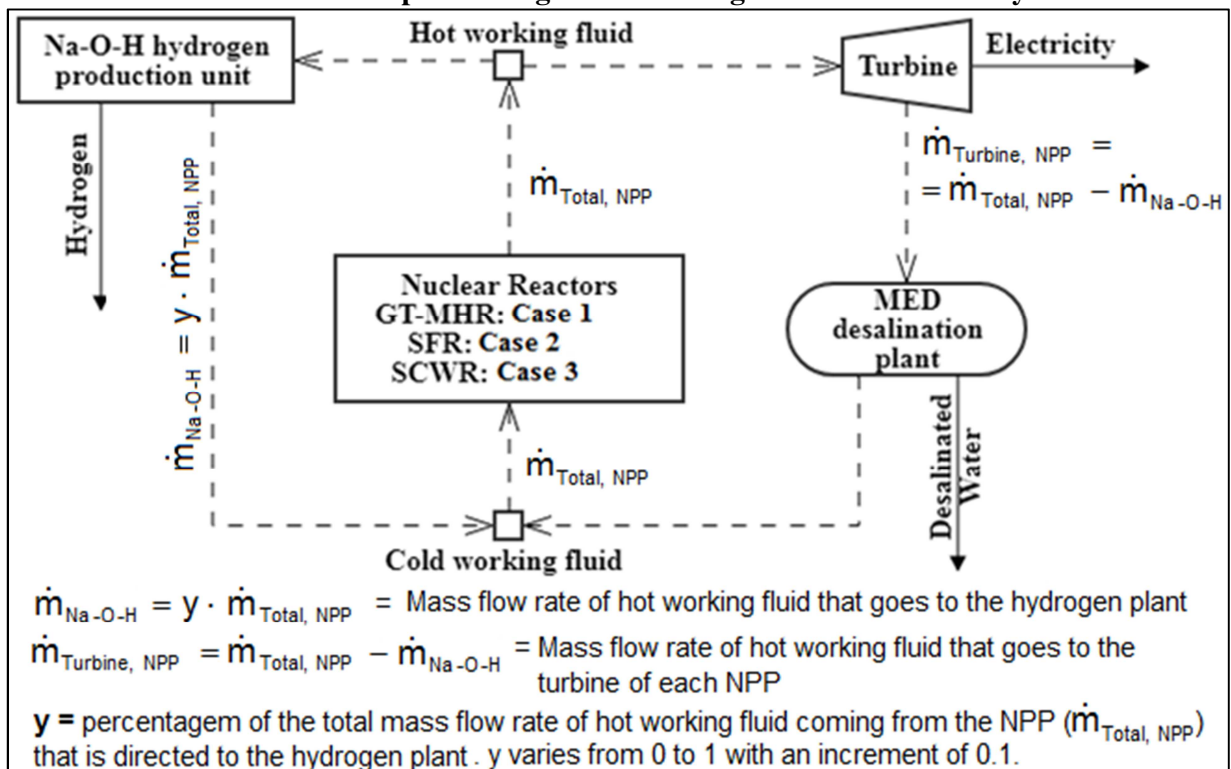
$$E_{P_3} = (N \cdot \bar{e})_{NaOH(s)} + (N \cdot \bar{e})_{O_2(g)} \quad (84)$$

$$\varepsilon_3 = 1 - \frac{E_{D_3}}{E_{P_3} + E_{D_3}} \quad (85)$$

### 3.3 Thermodynamic modeling of control volumes and systems

Figure 21 drafts how the control volumes and systems that compose each trigeneration case defined in item 1.2 are bounded to produce hydrogen, electricity and desalinated water. As noted in such figure, a hot working fluid comes from a nuclear reactor and then it is divided into two flow streams. One of them is directed to produce H<sub>2</sub> in the Na-O-H hydrogen production unit. The other generates electricity in a turbine of each nuclear power plant plus fresh water in a MED desalination installation. After performing those processes, the two flow streams, now cold ones, return to nuclear reactor to remove heat from it in order to begin the cyclic thermodynamic process again. The working fluid can be helium, steam or supercritical water, depending on the case and the kind of NPP analyzed.

**FIGURE 21 – Simplified diagram of the trigeneration cases analyzed**



Source: the author.

Each system and their constituent control volumes are analyzed and modeled over section 3.3 according to the following sequence composed by steps (i), (ii) and (iii) explained posteriorly. Each technology is modeled alone but considering the influence of other systems on it. For

example, the Na-O-H hydrogen production facility is evaluated considering the heat provided from three different NPP's as boundary conditions. In the same way, the MED plant is analyzed by replacing the condenser or cooler of different NPP's to harvest their rejected heat that act as the driven force to the desalination system.

*(i) System description:* every system is described considering their control volumes and thermodynamic cycles.

*(ii) Thermal model:* a thermal model is developed considering mass, energy and exergy balances for all systems and their control volumes using the thermodynamic fundamentals and equations introduced in sections 2.5.1 to 2.5.8. It is done to evaluate their thermal aspects like work consumed, heat exchanged, energy and exergy efficiencies, in addition to the amount of H<sub>2</sub>, electricity and H<sub>2</sub>O obtained in each trigeneration situation.

*(iii) Boundary conditions and input source data:* through this topic are provided the input source data, for instance, temperature, pressure, mass flow rate and other information necessary to model each system under attention according to phase (ii) described previously.

So, steps (ii) and (iii) are applied to systems A to E pending subsections 3.3.1 to 3.3.5. All equations presented in section 3.3 are implemented in EES software. Finally, in item 3.4 are written the simplifications and limitations related to this modeling approach that can interfere on the results of the thesis lodged in Chapter 4 related to the trigeneration cases under attention.

The amount of H<sub>2</sub>, electricity and desalinated water produced are obtained considering “y” variable that represents the mass flow rate percentage (fraction) of working fluid coming from one of the considered nuclear reactors (GT-MHR or SCWR or SFR) that is directed to the Na-O-H plant as illustrated in Figure 21. The variable y linearly varies according to constant gaps from 0 to 1 (y = 0, 0.1, 0.2, 0.3, 0.4, 0.5, 0.6, 0.7, 0.8, 0.9 and 1). When y = 0, all the coolant mass flow rate coming from each nuclear reactor is directed to the turbine to produce electricity and desalinated water. There is no H<sub>2</sub> production in such case because none working fluid goes to the Na-O-H plant. When y = 1, only hydrogen is gotten because all the thermal power released by the nuclear reactors goes to the Na-O-H plant and not to nuclear power cycles and MED installation.

### ***3.3.1 Modeling of system A – Na-O-H hydrogen production unit***

In this section is proposed, described and modeled a hydrogen production facility based on the Na-O-H cycle, which is responsible to provide H<sub>2</sub> in the trigeneration cases assessed.

#### ***(i) System description***

A theoretical hydrogen production unit based on the Na-O-H thermochemical water splitting cycle is exhibit in Figure 22. In it, solid sodium hydroxide is milled (points A.1 and A.14) and then mixed with liquid sodium (point A.2) to form a mixture of NaOH(s) and Na(l) (point A.3). Both substances only react in chemical reactor 1 because it has the specific conditions of p and T needed to start and sustain the reaction. Finally, in chemical chamber 1, Na(l) reacts with NaOH(s) to produce H<sub>2</sub>(g) (point A.4) plus Na<sub>2</sub>O(s) (point A.5), as in Equation (18), due to the heat supplied from a NPP which can be GT-MHR, SFR or SCWR through points A.16 and A.17.

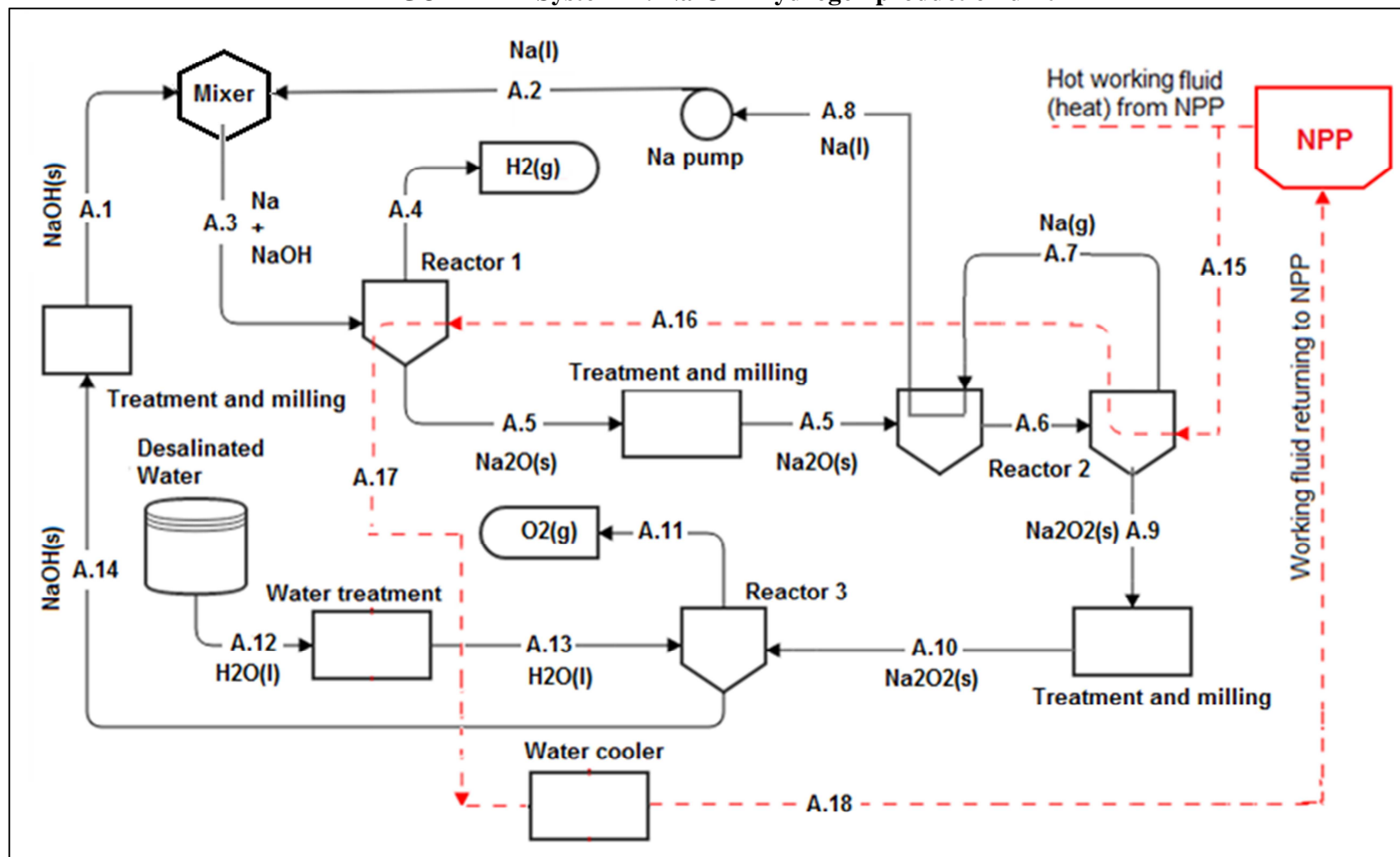
In the next step, solid sodium oxide (Na<sub>2</sub>O) is milled and goes to reactor 2 (points A.5 and A.6) where it is thermally decomposed into sodium vapor (point A.7) and sodium peroxide (point A.9), following the stoichiometric proportion of Equation (19), by thermal energy released from the coolant coming from the NPP (points A.15 and A.16). Then, sodium vapor is condensed into liquid by releasing heat to chemical chamber 2 (points A.7 and A.8) to reduce the global energy consumption in this chemical reactor.

On the other hand, sodium peroxide is milled (points A.9 and A.10) and reacts with water (point A.13) provided by the MED desalination unit (point A.12) in reactor 3, forming oxygen (point A.11) and sodium hydroxide (point A.14) as suggested by Equation (20). Then, the coolant returns to each NPP after releasing heat in a cooler (point A.17 and A.18) to reduce its temperatures in order to achieve the limits of T required at the inlet of each nuclear power plant.

The coolant from each NPP first supplies heat to chemical reactor 2 because it or Equation (19) has more  $\Delta H$  and needs higher temperature limits than Equation (18) that occur in reactor 1. All milling processes are applied to reduce the size of reactants and consequently facilitate chemical reactions proceeding. The amount of H<sub>2</sub> is influenced by each NPP in addition to the amount of working fluid from such systems that is directed to the hydrogen unit.



FIGURE 22 – System A: Na-O-H hydrogen production unit



Source: the author.

*(ii) Thermal model*

The relation between H<sub>2</sub> mass flow rate and the mass flow rate of the other chemicals is shown in Chart 14 considering stoichiometric proportions from Equations (18), (19) and (20) in addition to the molecular weight of each substance in Table 2.

**CHART 14 – Mass flow rate relations for the chemicals in the Na-O-H production unit**

$\dot{m}_{\text{NaOH}} = 40\dot{m}_{\text{H}_2}$	$\dot{m}_{\text{Na}} = 23\dot{m}_{\text{H}_2}$	$\dot{m}_{\text{Na}_2\text{O}} = 62\dot{m}_{\text{H}_2}$
$\dot{m}_{\text{Na}_2\text{O}_2} = 39\dot{m}_{\text{H}_2}$	$\dot{m}_{\text{H}_2\text{O}} = 9\dot{m}_{\text{H}_2}$	$\dot{m}_{\text{O}_2} = 8\dot{m}_{\text{H}_2}$

Source: the author.

All the mass, energy and exergy balances for each device in the GT-MHR system are in Charts 15, 16 and 17.

**CHART 15 – Mass balances for the control volumes in the Na-O-H production unit**

Device	Mass balance [kg/s]
Chemical Reactor 1	$\dot{m}_{A.3} = \dot{m}_{A.4} + \dot{m}_{A.5}$ and $\dot{m}_{A.16} = \dot{m}_{A.17}$
Chemical Reactor 2	$\dot{m}_{A.5} = \dot{m}_{A.6} = \dot{m}_{A.7} + \dot{m}_{A.9}$ and $\dot{m}_{A.15} = \dot{m}_{A.16}$
Chemical Reactor 3	$\dot{m}_{A.10} + \dot{m}_{A.13} = \dot{m}_{A.11} + \dot{m}_{A.14}$
Na Pump	$\dot{m}_{A.2} = \dot{m}_{A.8}$
Water cooler	$\dot{m}_{A.17} = \dot{m}_{A.18}$

Source: the author.

**CHART 16 – Energy balances for the control volumes in the Na-O-H production unit**

Device	Energy balance [MW]
Chemical Reactor 1	$\dot{Q}_{\text{Reactor},1} = \dot{m}_{A.4}h_{A.4} + \dot{m}_{A.5}h_{A.5} - \dot{m}_{A.3}h_{A.3} = \dot{m}_{A.16}h_{A.16} - \dot{m}_{A.17}h_{A.17}$
Chemical Reactor 2	$\dot{Q}_{\text{Reactor},2} = \dot{m}_{A.7}h_{A.7} + \dot{m}_{A.9}h_{A.9} - \dot{m}_{A.6}h_{A.6} = \dot{m}_{A.15}h_{A.15} - \dot{m}_{A.16}h_{A.16}$
Chemical Reactor 3	$\dot{Q}_{\text{Reactor},3} = (\dot{m}_{A.11}h_{A.11} + \dot{m}_{A.14}h_{A.14}) - (\dot{m}_{A.13}h_{A.13} + \dot{m}_{A.10}h_{A.10})$
Na Pump	$\dot{W}_{\text{Na,p}} = \dot{m}_{A.2}(h_{A.2} - h_{A.8})$
Water cooler	$\dot{Q}_{\text{Water cooler}} = \dot{m}_{A.17}h_{A.17} - \dot{m}_{A.18}h_{A.18}$
Na-O-H	$\eta_{\text{Na-O-H}} = \dot{m}_{A.4}h_{A.4} / (\dot{Q}_{\text{Reactor},1} + \dot{Q}_{\text{Reactor},2} + \dot{Q}_{\text{Reactor},3})$

Source: the author.

The energy efficiency of the Na-O-H plant in Chart 16 was defined here as the ratio between the potential thermal energy released during hydrogen burning due to its calorific power and the net heat required by the chemical reaction of system A.

**CHART 17 – Exergy balances for the control volumes in the Na-O-H production unit**

Device	Exergy destroyed [MW]	Exergy efficiency [-]
Chemical Reactor 1	$\dot{E}_{D,Reactor\_1} = (\dot{E}_{A.3} + \dot{E}_{A.16}) - (\dot{E}_{A.4} + \dot{E}_{A.5})$	$\epsilon_{Reactor\_1} = \frac{\dot{E}_{A.4} - \dot{E}_{A.3}}{\dot{E}_{A.16} - \dot{E}_{A.17}}$
Chemical Reactor 2	$\dot{E}_{D,Reactor\_2} = (\dot{E}_{A.15} + \dot{E}_{A.6}) - (\dot{E}_{A.7} + \dot{E}_{A.9} + \dot{E}_{A.16})$	$\epsilon_{Reactor\_2} = \frac{\dot{E}_{A.7} + \dot{E}_{A.9} - \dot{E}_{A.6}}{\dot{E}_{A.15} - \dot{E}_{A.16}}$
Chemical Reactor 3	$\dot{E}_{D,Reactor\_3} = (\dot{E}_{A.10} + \dot{E}_{A.13}) - (\dot{E}_{A.11} + \dot{E}_{A.14})$	$\epsilon_{Reactor\_3} = \frac{\dot{E}_{A.11} + \dot{E}_{A.14}}{\dot{E}_{A.10} + \dot{E}_{A.13}}$
Na pump	$\dot{E}_{D,Na\ pump} = \dot{E}_{A.8} + \dot{W}_{Na\ pump} - \dot{E}_{A.2}$	$\epsilon_{Na\ pump} = \frac{\dot{E}_{A.2} - \dot{E}_{A.8}}{\dot{W}_{Na\ pump}}$
Water Cooler	$\dot{E}_{D,Water\ cooler} = (\dot{E}_{A.19} + \dot{E}_{A.17}) - (\dot{E}_{A.20} + \dot{E}_{A.18})$	$\epsilon_{Water\ cooler} = \frac{\dot{E}_{A.20} - \dot{E}_{A.19}}{\dot{E}_{A.17} - \dot{E}_{A.18}}$
Na-O-H	$\dot{E}_{D,Na-O-H} = \sum_{Na-O-H} \dot{E}_{D, devices}$	$\epsilon_{Na-O-H} = 1 - \frac{\dot{E}_{D,Na-O-H}}{\dot{E}_{A.15} - \dot{E}_{A.17}}$

Source: the author.

*(iii) Boundary conditions and input source data*

The values of enthalpy and entropy needed to model the Na-O-H facility are obtained through Equations (47) and (48) plus information from Tables 1 and 2 in subsection 3.1.1. Additionally, the values of specific chemical exergy of every substance necessary to set the exergy in each point of the system according to Equation (28) are presented in Table 3. The conditions of p and T in which each chemical reaction of the sodium-oxygen-hydrogen cycle is performed during the trigeneration cases are provided now. They are:

- Reaction 1 – hydrogen production step – Equation (18):  $T_1 = 100\text{ °C}$  and  $p_1 = 1\text{ bar}$
- Reaction 2 – metal separation step – Equation (19):  $T_2 = 450\text{ °C}$  and  $p_2 = 0\text{ bar}$  (vacuum)
- Reaction 3 – hydrolysis step – Equation (20):  $T_3 = 25\text{ °C}$  and  $p_3 = 1\text{ bar}$

Such values of p and T were obtained after performing a Gibbs free energy analysis followed by an exergy analysis of those reactions explained in sections 3.2.1 and 3.2.2. The results related to those two analyses are reported in chapter 4, but the conditions of pressure and temperature found in them were presented in this topic in advance.

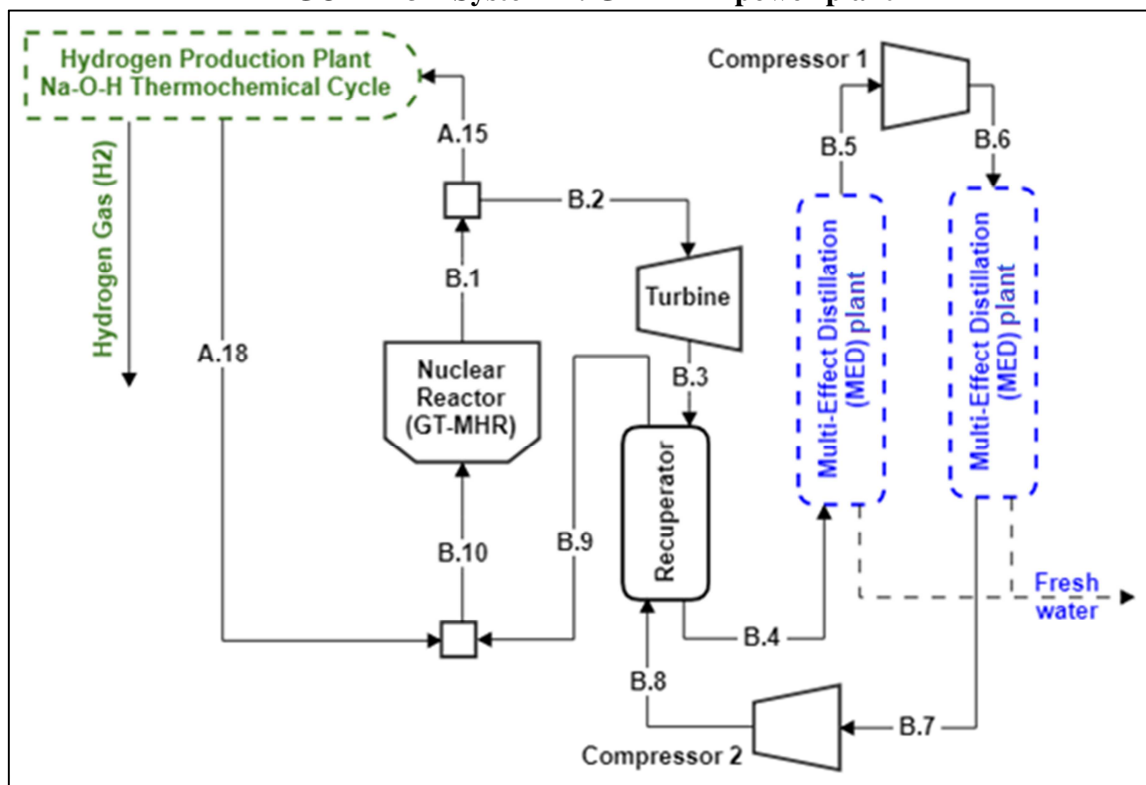
### 3.3.2 Modeling of system B – GT-MHR power plant

The Gas Turbine Modular Helium Reactor (GT-MHR) chosen as one possible heat source to the trigeneration case of electricity, H<sub>2</sub> and fresh water is studied according to steps (i), (ii) and (iii).

#### (i) System description

The GT-MHR analyzed is presented in Figure 23. It is based on a Brayton power cycle. In a first moment, helium coolant at low temperature (point B.10) removes heat from reactor core. After leaving it, He at high temperature (point B.1) is separated into two streams, one to the hydrogen unit through point A.15 and another to gas turbine (point B.2) to produce electricity. After leaving turbine (point B.3), the coolant flows inside recuperator (points B.3 and B.4), a heat exchanger whose function is to preheat the coolant before it reaches reactor core.

**FIGURE 23 – System B: GT-MHR power plant**



Source: the author.

Then, helium releases heat in the MED installation through points B.4 and B.5 in Figure 23. After that, He is compressed in two stages with intermediate cooling in another MED plant (points B.5, B.6, B.7 and B.8), it is heated in recuperator (points B.8 and B.9) and then mixed with helium leaving the hydrogen unit through point A.18 to return to reactor core (point B.10) in order to begin the cyclic thermodynamic process again. The amount of helium coolant that flows to the hydrogen production facility through point A.15 impacts the final amount of electricity, hydrogen and fresh water secured.

*(ii) Thermal model*

All the mass, energy and exergy balances for each device in the GT-MHR system are presented in Charts 18, 19 and 20. The term  $y$  in Chart 18 represents the percentage (fraction) of helium coolant coming from the nuclear reactor that is directed to the Na-O-H installation. It varies from 0 to 1 with an increment of 0.1.

**CHART 18 – Mass balances for the control volumes in the GT-MHR power plant**

Device	Mass balance [kg/s]
Nuclear Reactor	$\dot{m}_{B.10} = \dot{m}_{B.1} = \dot{m}_{A.15} + \dot{m}_{B.2}$ ; $\dot{m}_{B.10} = \dot{m}_{A.18} + \dot{m}_{B.9}$ ; $\dot{m}_{A.15} = y * \dot{m}_{B.1}$
Turbine	$\dot{m}_{B.2} = \dot{m}_{B.3}$
Recuperator	$\dot{m}_{B.3} = \dot{m}_{B.4}$ and $\dot{m}_{B.8} = \dot{m}_{B.9}$
Compressor 1	$\dot{m}_{B.5} = \dot{m}_{B.6}$
Compressor 2	$\dot{m}_{B.7} = \dot{m}_{B.8}$

Source: the author.

**CHART 19 – Energy balances for the control volumes in the GT-MHR power plant**

Device	Energy balance [MW]
Nuclear Reactor	$\dot{Q}_{GT-MHR} = \dot{m}_{B.1} h_{B.1} - \dot{m}_{B.10} h_{B.10}$
Turbine	$\dot{W}_{Turbine} = \dot{m}_{B.2} h_{B.2} - \dot{m}_{B.3} h_{B.3}$
Recuperator	$\dot{Q}_{Recuperator} = \dot{m}_{B.3} h_{B.3} - \dot{m}_{B.4} h_{B.4} = \dot{m}_{B.9} h_{B.9} - \dot{m}_{B.8} h_{B.8}$
Compressor 1	$\dot{W}_{compressor1} = \dot{m}_{B.6} h_{B.6} - \dot{m}_{B.5} h_{B.5}$
Compressor 2	$\dot{W}_{compressor2} = \dot{m}_{B.8} h_{B.8} - \dot{m}_{B.7} h_{B.7}$
GT-MHR	$\eta_{GT-MHR} = (\dot{W}_{Turbine} - \dot{W}_{compressor1} - \dot{W}_{compressor2}) / \dot{Q}_{GT-MHR}$

Source: the author.

**CHART 20 – Exergy balances for the control volumes in the GT-MHR power plant**

Device	Exergy destroyed [MW]	Exergy efficiency
Nuclear Reactor	$\dot{E}_{D, \text{Reactor}} = \left( \frac{T_0}{\bar{T}_{\text{He}}} - \frac{T_0}{T_{\text{Nuclear fuel}}} \right) \cdot \dot{Q}_{\text{GT-MHR}}$	$\epsilon_{\text{Reactor}} = \frac{\dot{E}_{B.1} - \dot{E}_{B.10}}{\left( 1 - \frac{T_0}{T_{\text{Nuclear fuel}}} \right) \cdot \dot{Q}_{\text{GT-MHR}}}$
Turbine	$\dot{E}_{D, \text{Turbine}} = \dot{E}_{B.2} - \dot{E}_{B.3} - \dot{W}_{\text{Turbine}}$	$\epsilon_{\text{Turbine}} = \frac{\dot{W}_{\text{Turbine}}}{\dot{E}_{B.2} - \dot{E}_{B.3}}$
Recuperator	$\dot{E}_{D, \text{Recuperator}} = \dot{E}_{B.3} + \dot{E}_{B.8} - \dot{E}_{B.4} - \dot{E}_{B.9}$	$\epsilon_{\text{Recuperator}} = \frac{\dot{E}_{B.3} - \dot{E}_{B.4}}{\dot{E}_{B.9} - \dot{E}_{B.8}}$
Compressor 1	$\dot{E}_{D, \text{Compressor1}} = \dot{E}_{B.5} + \dot{W}_{\text{Compressor1}} - \dot{E}_{B.6}$	$\epsilon_{\text{Compressor1}} = \frac{\dot{E}_{B.6} - \dot{E}_{B.5}}{\dot{W}_{\text{Compressor1}}}$
Compressor 2	$\dot{E}_{D, \text{Compressor2}} = \dot{E}_{B.7} + \dot{W}_{\text{Compressor2}} - \dot{E}_{B.8}$	$\epsilon_{\text{Compressor2}} = \frac{\dot{E}_{B.8} - \dot{E}_{B.7}}{\dot{W}_{\text{Compressor2}}}$
GT-MHR	$\dot{E}_{D, \text{GT-MHR}} = \sum_{\text{GT-MHR}} \dot{E}_{D, \text{devices}}$	$\epsilon_{\text{GT-MHR}} = 1 - \frac{\dot{E}_{D, \text{GT-MHR}}}{\left( 1 - \frac{T_0}{T_{\text{Nuclear fuel}}} \right) \cdot \dot{Q}_{\text{GT-MHR}}}$

Observation:  $\bar{T}_{\text{He}}$  is calculated considering the mean values of T at the inlet and outlet of the nuclear reactor.

Source: the author.

### (iii) Boundary conditions and input source data

In Table 4, adapted from Mohammadkhani *et al.* (2014) plus Zare *et al.* (2013), the values of T and p for helium in every state were acquired from these two studies while the values of h and s related to these points were get from EES software after providing to it those values of p and T. These p and T values from Table 4 represent usual operational conditions for a GT-MHR. It was considered that He coolant leaves each MED plant at 30 °C (points B.5 and B.7) without pressure drop. He coolant returns from the H<sub>2</sub> production unit at the same condition as point B.9 in order to not interfere on the standard original outlet condition designed for the GT-MHR. The total mass flow rate of helium is 470.2 kg/s, what provides a power of 1000 MW<sub>th</sub> from reactor core with the conditions of enthalpy in Table 4 at the inlet and outlet of it. The nuclear fuel can operate near 1200 °C (SUKHAREV and FOMICHENKO, 2014). Depending on y variation, from 0 to 1, part of this He mass flow rate (470.2 kg/s) goes to the Na-O-H plant to produce H<sub>2</sub> or to the turbine of GT-MHR to generated electricity and then desalinated H<sub>2</sub>O in the MED installation.

**TABLE 4 – Thermodynamic properties of helium in the GT-MHR power plant**

State n° [i]	Type of Fluid	Pressure p [kPa]	Temperature T [°C]	Enthalpy h [kJ/kg]	Entropy s [kJkg <sup>-1</sup> K <sup>-1</sup> ]
B.1	Helium	7930	850.0	5861	25.81
A.15	Helium	7930	850.0	5861	25.81
B.2	Helium	7930	850.0	5861	25.81
B.3	Helium	2630	475.4	3901	26.00
B.4	Helium	2580	158.1	2253	23.17
B.5	Helium	2580	30.0	1588	21.34
B.6	Helium	4423	112.5	2022	21.57
B.7	Helium	4423	30.0	1594	20.22
B.8	Helium	8110	112.5	2034	20.35
B.9	Helium	8030	440.1	3734	23.43
A.18	Helium	8030	440.1	3734	23.43
B.10	Helium	8030	440.1	3734	23.43

Source: adapted from Mohammadkhani *et al.* (2014) plus Zare *et al.* (2013).

### 3.3.3 Modeling of system C – SFR power plant

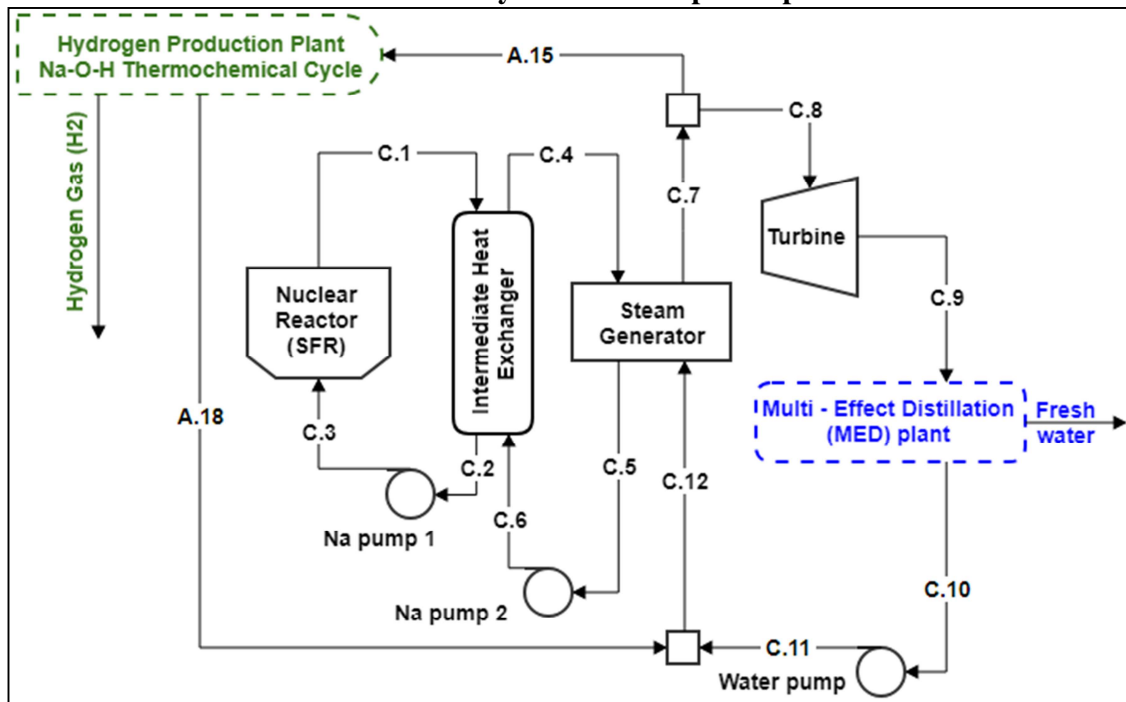
In this part of the development is modeled the Sodium Cooled Fast Reactor (SFR) selected to provided heat to both Na-O-H hydrogen production unit and MED desalination plant.

#### *(i) System description*

The Sodium Cooled Fast Reactor (SFR) system studied is presented in Figure 24. It is composed by two sodium circuits or loops plus an energy conversion system based on a steam Rankine power cycle, where steam produced in it is used to produce H<sub>2</sub>, electricity and desalinated H<sub>2</sub>O.

In sodium first loop (points C.1, C.2 and C.3), liquid Na removes heat from nuclear reactor and then transfer this energy to liquid Na in the second loop (points C.4, C.5 and C.6) through an intermediate heat exchanger (IHE). After that, Na in the second loop boils water in a steam generator (points C.12 and C.7). The steam produced is divided into two flow streams; the first one to the hydrogen plant (point A.15) and the other to a steam turbine (point C.8) to generate electricity. Steam is then condensed into liquid water through points C.9 and C.10 by releasing heat to the MED desalination plant in order to produce fresh water. After that, water is pumped (points C.10 and C.11) and mixed with the stream coming from the Na-O-H plant (points C.11 and A.18) to return to nuclear reactor trough point C.12. The percentage of steam from SFR that is directed to the Na-O-H facility will influence the making of H<sub>2</sub>, electricity and fresh H<sub>2</sub>O.

FIGURE 24 – System C: SFR power plant



Source: the author.

*(ii) Thermal model*

In Charts 21, 22 and 23 are presented the mass, energy, entropy and exergy balances for each device in the SFR system. In Chart 21,  $y$  represents the percentage (fraction) of steam coming from the steam generator that is directed to the Na-O-H installation.  $Y$  varies from 0 to 1 with an increment of 0.1.

**CHART 21 – Mass balances for the control volumes in the SFR power plant**

Device	Mass balance [kg/s]
Nuclear Reactor (NR)	$\dot{m}_{C.1} = \dot{m}_{C.3}$
Na Pump 1	$\dot{m}_{C.2} = \dot{m}_{C.3}$
Na Pump 2	$\dot{m}_{C.5} = \dot{m}_{C.6}$
Intermediate Heat Exchanger (IHE)	$\dot{m}_{C.1} = \dot{m}_{C.2}$ and $\dot{m}_{C.4} = \dot{m}_{C.6}$
Steam Generator (SG)	$\dot{m}_{C.4} = \dot{m}_{C.5}$ ; $\dot{m}_{C.7} = \dot{m}_{C.12}$ ; $\dot{m}_{A.15} = y * \dot{m}_{C.7}$ and $\dot{m}_{C.7} = \dot{m}_{A.15} + \dot{m}_{C.8}$
Steam Turbine (ST)	$\dot{m}_{C.8} = \dot{m}_{C.9}$
Water Pump	$\dot{m}_{C.10} = \dot{m}_{C.11}$

Source: the author.



**CHART 22 – Energy balances for the control volumes in the SFR power plant**

Device	Energy balance [MW]
Nuclear Reactor (NR)	$\dot{Q}_{\text{SFR}} = \dot{m}_{\text{C},1}(h_{\text{C},1} - h_{\text{C},3})$
Na Pump 1	$\dot{W}_{\text{Na Pump 1}} = \dot{m}_{\text{C},3}(h_{\text{C},3} - h_{\text{C},2})$
Na Pump 2	$\dot{W}_{\text{Na Pump 2}} = \dot{m}_{\text{C},3}(h_{\text{C},3} - h_{\text{C},2})$
Intermediate Heat Exchanger (IHE)	$\dot{Q}_{\text{IHE}} = \dot{m}_{\text{C},1}(h_{\text{C},1} - h_{\text{C},2}) = \dot{m}_{\text{C},4}(h_{\text{C},4} - h_{\text{C},6})$
Steam Generator (SG)	$\dot{Q}_{\text{SG}} = \dot{m}_{\text{C},4}(h_{\text{C},5} - h_{\text{C},4}) = \dot{m}_{\text{C},7}(h_{\text{C},7} - h_{\text{C},12})$
Steam Turbine (ST)	$\dot{W}_{\text{Turbine}} = \dot{m}_{\text{C},8}(h_{\text{C},8} - h_{\text{C},9})$
Water Pump	$\dot{W}_{\text{Water Pump}} = \dot{m}_{\text{C},3}(h_{\text{C},3} - h_{\text{C},2})$
SFR	$\eta_{\text{SFR}} = (\dot{W}_{\text{Turbine}} - \dot{W}_{\text{Water Pump}}) / \dot{Q}_{\text{SFR}}$

Source: the author.

**CHART 23 – Exergy balances for the control volumes in the SFR power plant**

Component	Exergy destroyed [MW]	Exergy efficiency
Nuclear Reactor (NR)	$\dot{E}_{\text{D, Reactor}} = \left( \frac{T_0}{\bar{T}_{\text{Na}}} - \frac{T_0}{T_{\text{Nuclear fuel}}} \right) \cdot \dot{Q}_{\text{SFR}}$	$\epsilon_{\text{Reactor}} = \frac{\dot{E}_{\text{C},1} - \dot{E}_{\text{C},3}}{\left( 1 - \frac{T_0}{T_{\text{Nuclear fuel}}} \right) \cdot \dot{Q}_{\text{SFR}}}$
Na Pump 1	$\dot{E}_{\text{D, Na Pump 1}} = \dot{E}_{\text{C},2} + \dot{W}_{\text{Na Pump 1}} - \dot{E}_{\text{C},3}$	$\epsilon_{\text{Na Pump 1}} = \frac{\dot{E}_{\text{C},2} - \dot{E}_{\text{C},3}}{\dot{W}_{\text{Na Pump 1}}}$
Na Pump 2	$\dot{E}_{\text{D, Na Pump 2}} = \dot{E}_{\text{C},5} + \dot{W}_{\text{Na Pump 2}} - \dot{E}_{\text{C},6}$	$\epsilon_{\text{Na Pump 2}} = \frac{\dot{E}_{\text{C},5} - \dot{E}_{\text{C},6}}{\dot{W}_{\text{Na Pump 2}}}$
IHE	$\dot{E}_{\text{D, IHE}} = (\dot{E}_{\text{C},1} + \dot{E}_{\text{C},6}) - (\dot{E}_{\text{C},2} + \dot{E}_{\text{C},4})$	$\epsilon_{\text{IHE}} = \frac{\dot{E}_{\text{C},4} - \dot{E}_{\text{C},6}}{\dot{E}_{\text{C},1} - \dot{E}_{\text{C},2}}$
Steam Generator (SG)	$\dot{E}_{\text{D, SG}} = (\dot{E}_{\text{C},12} + \dot{E}_{\text{C},4}) - (\dot{E}_{\text{C},5} + \dot{E}_{\text{C},7})$	$\epsilon_{\text{IHE}} = \frac{\dot{E}_{\text{C},7} - \dot{E}_{\text{C},12}}{\dot{E}_{\text{C},4} - \dot{E}_{\text{C},5}}$
Steam Turbine (ST)	$\dot{E}_{\text{D, Turbine}} = \dot{E}_{\text{C},8} - \dot{E}_{\text{C},9} - \dot{W}_{\text{Turbine}}$	$\epsilon_{\text{Turbine}} = \frac{\dot{W}_{\text{Turbine}}}{\dot{E}_{\text{C},8} - \dot{E}_{\text{C},9}}$
Water Pump	$\dot{E}_{\text{D, Water Pump}} = \dot{E}_{\text{C},10} + \dot{W}_{\text{Water Pump}} - \dot{E}_{\text{C},11}$	$\epsilon_{\text{Water Pump}} = \frac{\dot{E}_{\text{C},10} - \dot{E}_{\text{C},11}}{\dot{W}_{\text{Water Pump}}}$
SFR	$\dot{E}_{\text{D, SFR}} = \sum_{\text{SFR}} \dot{E}_{\text{D, devices}}$	$\epsilon_{\text{SFR}} = 1 - \dot{E}_{\text{D, SFR}} / \left( \left( 1 - \frac{T_0}{T_{\text{Nuclear fuel}}} \right) \cdot \dot{Q}_{\text{SFR}} \right)$

Observation:  $\bar{T}_{\text{Na}}$  is calculated considering the mean values of T at the inlet and outlet of the nuclear reactor.

Source: the author.

(iii) Boundary conditions and input source data

The values of p and T in Table 5 (adapted from KHALID et al., 2016) were obtained from such research while the values of h and s of each state were acquired from EES software with the respective values of p and T. These p and T values from Table 5 represent usual operational conditions for a SFR. Considering the values of h in Table 5 plus 1000 MW thermal released by the nuclear reactor, the mass flow rate of sodium in first and second loops are respectively equal to 5667 kg/s and 4614 kg/s while, causing a mass flow rate of steam in the tertiary circuit equal to 335.4 kg/s. This steam mass flow rate is divided between the Na-O-H plant and the SFR energy conversion system considering y variation from 0 to 1. The nuclear fuel is able to supply heat at 1000 K (DI MAIO *et al.*, 2014). Steam enters the MED installation at 65 °C with quality (x) = 0.7 and leaves it at 65 °C with quality (x) = 0 without pressure drop.

**TABLE 5 - Thermodynamic properties of Na and water/steam in the SFR power plant**

State n° [i]	Type of Fluid	Pressure p [kPa]	Temperature T [°C]	Enthalpy h [kJ/kg]	Entropy s [kJkg <sup>-1</sup> K <sup>-1</sup> ]
C.1	Liquid sodium	900	550.00	599.8	1.0730
C.2	Liquid sodium	880	410.00	421.9	0.8352
C.3	Liquid sodium	900	411.00	423.3	0.8371
C.4	Liquid sodium	1000	527.00	571.0	1.0390
C.5	Liquid sodium	980	355.00	351.2	0.7253
C.6	Liquid sodium	1000	356.00	352.5	0.7273
C.7	Superheated steam	17000	510.00	3312	6.3010
A.15	Superheated steam	17000	510.00	3312	6.3010
C.8	Superheated steam	17000	510.00	3312	6.3010
C.9	Steam/Water	25	65.00	2102	6.3040
C.10	Saturated liquid water	25	65.00	272.0	0.8935
C.11	Compressed liquid water	17000	67.00	290.3	0.8964
A.18	Compressed liquid water	17000	67.00	290.3	0.8964
C.12	Compressed liquid water	17000	67.00	290.3	0.8964

Source: adapted from Khalid *et al.* (2016).

**3.3.4 Modeling of system D - SCWR power plant**

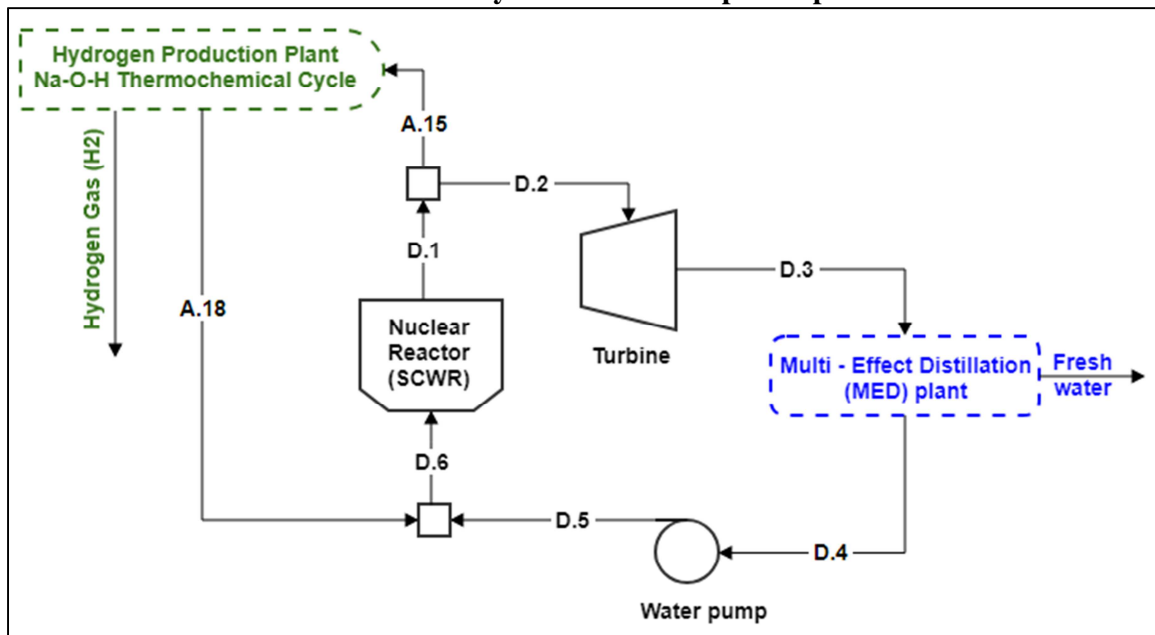
The Supercritical Water Reactor (SCWR) selected to supply thermal energy to the Na-O-H hydrogen production unit and to the multi-effect distillation plant is modeled at this moment.

(i) System description

SCWR analyzed is presented in Figure 25. It produces supercritical water (point D.1) at high pressure and high temperature from pressurized liquid water (point D.6) by removing heat

released during fission reaction inside nuclear reactor core. The total mass flow rate of supercritical water is divided into two flow streams; one directed to the Na-O-H hydrogen production plant (point A.15) and another to the electricity conversion system and then MED desalination plant through point D.2. In this way, the amount of  $H_2$ , electricity and  $H_2O$  depend on how the mass flow rate of supercritical water is divided between points A.15 and D.2.

**FIGURE 25 – System D: SCWR power plant**



Source: the author.

The stream of supercritical water that goes to the hydrogen unit supplies thermal energy to the chemical reactions of the Na-O-H cycle. After that, this stream returns to the SCWR system through point A.18 to be mixed with point D.5 in order to allow again the heat removal process in reactor core to produce water at supercritical condition. At the same time, the other stream, point D.2, passes through a turbine to produce electricity and turns into point D.3, characterized as steam at low pressure and temperature. After that, steam is condensed into liquid water and then pumped through points D.4 and D.5 to be mixed with the stream coming from point A.18, at the same thermodynamic condition as point D.5, to return to nuclear reactor core. Steam condensation is performed in a MED installation, where the heat released during such process is reused to produce fresh water instead wasting such energy to the environment in a usual condenser.

*(ii) Thermal model*

The mass, energy, entropy and exergy balances related to SCWR system and its devices can be seen in Charts 24, 25 and 26. In Chart 24,  $y$  represents the percentage of supercritical water coming from the nuclear reactor that is directed to the Na-O-H installation.  $y$  varies from 0 to 1 It varies from 0 to 1 with an increment of 0.1.

**CHART 24 – Mass balances for the control volumes in the SCWR power plant**

Device	Mass balance [kg/s]
Nuclear Reactor (NR)	$\dot{m}_{D,1} = \dot{m}_{D,6}$ ; $\dot{m}_{D,6} = \dot{m}_{A,18} + \dot{m}_{D,5}$ and $\dot{m}_{A,15} = y * \dot{m}_{D,1}$
Steam Turbine (ST)	$\dot{m}_{D,2} = \dot{m}_{D,3}$
MED plant	$\dot{m}_{D,3} = \dot{m}_{D,4}$
Water pump	$\dot{m}_{D,4} = \dot{m}_{D,5}$

Source: the author.

**CHART 25 – Energy balances for the control volumes in the SCWR power plant**

Device	Energy balance [MW]
Nuclear Reactor	$\dot{Q}_{SCWR} = \dot{m}_{D,1}h_{D,1} - \dot{m}_{D,6}h_{D,6}$
Steam Turbine	$\dot{W}_{Turbine} = \dot{m}_{D,2}h_{D,2} - \dot{m}_{D,3}h_{D,3}$
Water pump	$\dot{W}_{Pump} = \dot{m}_{D,5}h_{D,5} - \dot{m}_{D,4}h_{D,4}$
SCWR	$\eta_{SCWR} = (\dot{W}_{Turbine} - \dot{W}_{Pump}) / \dot{Q}_{SCWR}$

Source: the author.

**CHART 26 – Exergy balances for the control volumes in the SCWR power plant**

Device	Exergy destroyed [MW]	Exergy efficiency
Nuclear Reactor	$\dot{E}_{D,Reactor} = \left( \frac{T_0}{\bar{T}_{H_2O}} - \frac{T_0}{T_{Nuclear\ fuel}} \right) \cdot \dot{Q}_{SCWR}$	$\epsilon_{Reactor} = \frac{\dot{E}_{D,1} - \dot{E}_{D,6}}{\left( 1 - \frac{T_0}{T_{Nuclear\ fuel}} \right) \cdot \dot{Q}_{SCWR}}$
Steam Turbine	$\dot{E}_{D,Turbine} = \dot{E}_{D,2} - \dot{E}_{D,3} - \dot{W}_{Turbine}$	$\epsilon_{Turbine} = \frac{\dot{W}_{Turbine}}{\dot{E}_{D,2} - \dot{E}_{D,3}}$
Water pump	$\dot{E}_{D,Pump} = \dot{E}_{D,4} + \dot{W}_{Pump} - \dot{E}_{D,5}$	$\epsilon_{Pump} = \frac{\dot{E}_{D,4} - \dot{E}_{D,5}}{\dot{W}_{Pump}}$
SCWR	$\dot{E}_{D,SCWR} = \sum_{SCWR} \dot{E}_D$	$\epsilon_{SCWR} = 1 - \frac{\dot{E}_{D,SCWR}}{\left( 1 - \frac{T_0}{T_{Nuclear\ fuel}} \right) \cdot \dot{Q}_{SCWR}}$

Observation:  $\bar{T}_{H_2O}$  is calculated considering the mean values of  $T$  at the inlet and outlet of the nuclear reactor.

Source: the author.

(iii) Considerations and input source data

The thermodynamic properties  $h$  and  $s$  of each point of the SCWR NPP are presented in Table 6 adapted from Schulenberg *et al.* (2014) and Su *et al.* (2014) after implementing in EES software the conditions of  $p$  and  $T$  related to the SCWR also in Table 6. These  $p$  and  $T$  values from Table 6 are usual operational conditions for a SCWR. Considering such values of  $h$  in addition to a 1000 MW thermal released from the nuclear reactor causes a mass flow rate of supercritical water equal to 349.1 kg/s. The nuclear fuel can reach  $T$  close to 1000 K as reported in the researches of Guzonas and Novotny (2014) and also of Moghrabi and Novog (2018). Steam enters the MED plant at 65 °C with quality  $(x) = 0.75$  and leaves it at 65 °C with quality  $(x) = 0$ .

**TABLE 6 - Thermodynamic properties of water/steam in the SCWR power plant**

State n° [i]	Type of Fluid	Pressure $p$ [kPa]	Temperature $T$ [°C]	Enthalpy $h$ [kJ/kg]	Entropy $s$ [kJkg <sup>-1</sup> K <sup>-1</sup> ]
D.1	Supercritical water	25000	520	3236	6.054
A.15	Supercritical water	25000	520	3236	6.054
D.2	Supercritical water	25000	520	3236	6.054
D.3	Steam/Water	25	65	2031	6.096
D.4	Saturated liquid water	25	65	272.1	0.8935
D.5	Compressed liquid water	25000	67	301	0.9041
A.18	Compressed liquid water	25000	67	301	0.9041
D.6	Compressed liquid water	25000	67	301	0.9041

Source: adapted from Schulenberg *et al.* (2014) and Su *et al.* (2014).

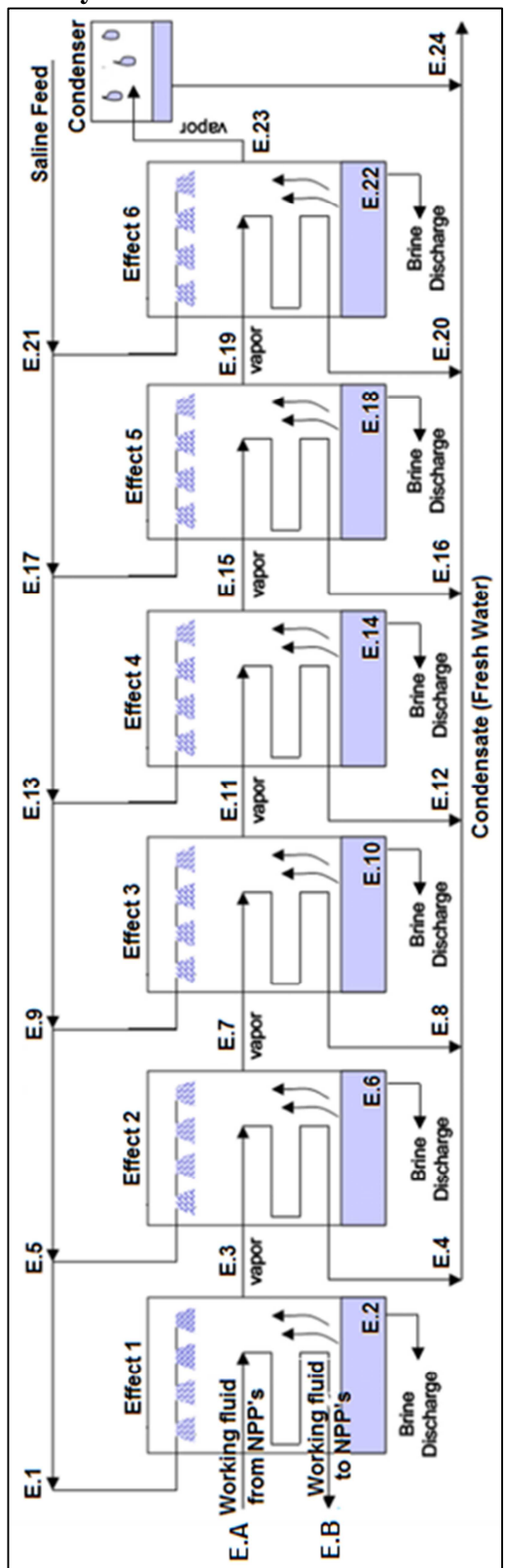
**3.3.5 Modeling of system E – MED desalination plant**

The MED desalination system under attention is assessed according to steps (i), (ii) and (iii).

(i) System description

In Figure 26 adapted from Islam *et al.* (2018) is shown the multi-effect distillation facility studied in this work. It follows the physical principles described in section 2.3 covering a traditional MED system. This technology is composed by six effects plus a MED condenser (points E.1 to E.24) to cool water steam formed in the last desalination stage. The heat that usually is rejected to the environment through the condenser or cooler of three NPP's (GT-MHR, SFR and SCWR) is recovered in the first effect of this desalination system; it acts as the driven force for this process. It was proposed a 6-effect MED facility because most of the heat sources employed in the work are at 65 °C. In this way, a typical 4 °C difference between each desalination effect implies on a temperature close to 40 °C in the last desalination effect. Such temperature is the limit to avoid water condensation at very low pressures as it will be discussed later during results section.

FIGURE 26 – System E: six-effect MED desalination plant



Source: adapted from Islam et al. 2018.

*(ii) Thermal model*

In Charts 27, 28 and 29 are presented the mass, energy and exergy balances for each of the six effects that compose the MED plant in Figure 25. In relation to the mass balances, they are accomplished pondering three different ones; one general covering all the solutions flowing through the effect represented by Equation (89); another comprehending the mass of salt in each point of every effect as in Equation (90), considering salt concentration (b) in all states; one more to the mass of steam produced in an effect that is condensed into fresh water in a next effect as in Equation (91). The energy balances in Chart 28 represents the amount of heat supplied to each effect to allow the thermal distillation. The specific properties enthalpy and entropy at each state are determined in EES software with the values of temperature, salt concentration and the physical state of water (quality) for every point of the desalination facility.

$$\dot{m}_{\text{Sea water}} = \dot{m}_{\text{Brine}} + \dot{m}_{\text{Fresh water}} \quad (89)$$

$$b_{\text{Sea water}} \dot{m}_{\text{Sea water}} = b_{\text{Brine}} \dot{m}_{\text{Brine}} + b_{\text{Fresh Water}} \dot{m}_{\text{Fresh water}} \quad (90)$$

$$\dot{m}_{\text{Steam}} = \dot{m}_{\text{Fresh water}} \quad (91)$$

**CHART 27 – Mass balances for each effect in the MED desalination plant**

Effect	General [kg/s]	Salt [kg/s]	Steam/Water [kg/s]
1	$\dot{m}_{E.1} = \dot{m}_{E.2} + \dot{m}_{E.3}$	$b_{E.1} \dot{m}_{E.1} = b_{E.2} \dot{m}_{E.2} + b_{E.3} \dot{m}_{E.3}$	$\dot{m}_{E.3} = \dot{m}_{E.4}$
2	$\dot{m}_{E.5} = \dot{m}_{E.6} + \dot{m}_{E.7}$	$b_{E.5} \dot{m}_{E.5} = b_{E.6} \dot{m}_{E.6} + b_{E.7} \dot{m}_{E.7}$	$\dot{m}_{E.7} = \dot{m}_{E.8}$
3	$\dot{m}_{E.9} = \dot{m}_{E.10} + \dot{m}_{E.11}$	$b_{E.9} \dot{m}_{E.9} = b_{E.10} \dot{m}_{E.10} + b_{E.11} \dot{m}_{E.11}$	$\dot{m}_{E.11} = \dot{m}_{E.12}$
4	$\dot{m}_{E.13} = \dot{m}_{E.14} + \dot{m}_{E.15}$	$b_{E.13} \dot{m}_{E.13} = b_{E.14} \dot{m}_{E.14} + b_{E.15} \dot{m}_{E.15}$	$\dot{m}_{E.15} = \dot{m}_{E.16}$
5	$\dot{m}_{E.17} = \dot{m}_{E.18} + \dot{m}_{E.19}$	$b_{E.17} \dot{m}_{E.17} = b_{E.18} \dot{m}_{E.18} + b_{E.19} \dot{m}_{E.19}$	$\dot{m}_{E.19} = \dot{m}_{E.20}$
6	$\dot{m}_{E.21} = \dot{m}_{E.22} + \dot{m}_{E.23}$	$b_{E.21} \dot{m}_{E.21} = b_{E.22} \dot{m}_{E.22} + b_{E.23} \dot{m}_{E.23}$	$\dot{m}_{E.23} = \dot{m}_{E.24}$
Condenser	-	-	$\dot{m}_{E.23} = \dot{m}_{E.24}$
MED Plant	$R = \dot{m}_{\text{Freshwater}} / \dot{m}_{\text{Seawater}}$ $\dot{m}_{\text{Total,Seawater}} = \dot{m}_{E.1} + \dot{m}_{E.5} + \dot{m}_{E.9} + \dot{m}_{E.13} + \dot{m}_{E.17} + \dot{m}_{E.21}$ $\dot{m}_{\text{Total,Brine}} = \dot{m}_{E.2} + \dot{m}_{E.6} + \dot{m}_{E.10} + \dot{m}_{E.14} + \dot{m}_{E.18} + \dot{m}_{E.22}$ $\dot{m}_{\text{Total,Fresh water}} = \dot{m}_{E.4} + \dot{m}_{E.8} + \dot{m}_{E.12} + \dot{m}_{E.16} + \dot{m}_{E.20} + \dot{m}_{E.24}$		

Source: the author.

Recovery factor (R) in Chart 27 is the ratio between the total amount of potable water produced and the mass flow rate of sea water that enters the system.

**CHART 28 – Energy balances for each effect in the MED desalination plant**

Effect	Energy Balances [MW]
1	$\dot{Q}_1 = \dot{Q}_{NPP} = \dot{m}_{E,A} h_{E,A} - \dot{m}_{E,B} h_{E,B} = \dot{m}_{E,2} h_{E,2} + \dot{m}_{E,3} h_{E,3} - \dot{m}_{E,1} h_{E,1}$
2	$\dot{Q}_2 = \dot{m}_{E,3} (h_{E,3} - h_{E,4}) = \dot{m}_{E,6} h_{E,6} + \dot{m}_{E,7} h_{E,7} - \dot{m}_{E,5} h_{E,5}$
3	$\dot{Q}_3 = \dot{m}_{E,7} (h_{E,7} - h_{E,8}) = \dot{m}_{E,10} h_{E,10} + \dot{m}_{E,11} h_{E,11} - \dot{m}_{E,9} h_{E,9}$
4	$\dot{Q}_4 = \dot{m}_{E,11} (h_{E,11} - h_{E,12}) = \dot{m}_{E,14} h_{E,14} + \dot{m}_{E,15} h_{E,15} - \dot{m}_{E,13} h_{E,13}$
5	$\dot{Q}_5 = \dot{m}_{E,15} (h_{E,15} - h_{E,16}) = \dot{m}_{E,18} h_{E,18} + \dot{m}_{E,19} h_{E,19} - \dot{m}_{E,17} h_{E,17}$
6	$\dot{Q}_6 = \dot{m}_{E,19} (h_{E,19} - h_{E,20}) = \dot{m}_{E,22} h_{E,22} + \dot{m}_{E,23} h_{E,23} - \dot{m}_{E,21} h_{E,21}$
MED Condenser	$\dot{Q}_{MED, Condenser} = \dot{m}_{E,23} (h_{E,23} - h_{E,24})$

Source: the author.

**CHART 29 – Exergy balances for each effect in the MED desalination plant**

Effect	Exergy destroyed [MW]	Exergy efficiency
1	$\dot{E}_{D,1} = (\dot{E}_{E,A} + \dot{E}_{E,1}) - (\dot{E}_{E,B} + \dot{E}_{E,2} + \dot{E}_{E,3})$	$\epsilon_1 = \frac{\dot{E}_{E,2} + \dot{E}_{E,3} - \dot{E}_{E,1}}{\dot{E}_{E,A} - \dot{E}_{E,B}}$
2	$\dot{E}_{D,2} = (\dot{E}_{E,3} + \dot{E}_{E,5}) - (\dot{E}_{E,4} + \dot{E}_{E,6} + \dot{E}_{E,7})$	$\epsilon_2 = \frac{\dot{E}_{E,6} + \dot{E}_{E,7} - \dot{E}_{E,5}}{\dot{E}_{E,3} - \dot{E}_{E,4}}$
3	$\dot{E}_{D,3} = (\dot{E}_{E,7} + \dot{E}_{E,9}) - (\dot{E}_{E,8} + \dot{E}_{E,10} + \dot{E}_{E,11})$	$\epsilon_3 = \frac{\dot{E}_{E,10} + \dot{E}_{E,11} - \dot{E}_{E,9}}{\dot{E}_{E,7} - \dot{E}_{E,8}}$
4	$\dot{E}_{D,4} = (\dot{E}_{E,11} + \dot{E}_{E,13}) - (\dot{E}_{E,12} + \dot{E}_{E,14} + \dot{E}_{E,15})$	$\epsilon_4 = \frac{\dot{E}_{E,14} + \dot{E}_{E,15} - \dot{E}_{E,13}}{\dot{E}_{E,11} - \dot{E}_{E,12}}$
5	$\dot{E}_{D,5} = (\dot{E}_{E,15} + \dot{E}_{E,17}) - (\dot{E}_{E,16} + \dot{E}_{E,18} + \dot{E}_{E,19})$	$\epsilon_5 = \frac{\dot{E}_{E,18} + \dot{E}_{E,19} - \dot{E}_{E,17}}{\dot{E}_{E,15} - \dot{E}_{E,16}}$
6	$\dot{E}_{D,6} = (\dot{E}_{E,19} + \dot{E}_{E,21}) - (\dot{E}_{E,20} + \dot{E}_{E,22} + \dot{E}_{E,23})$	$\epsilon_6 = \frac{\dot{E}_{E,22} + \dot{E}_{E,23} - \dot{E}_{E,21}}{\dot{E}_{E,19} - \dot{E}_{E,20}}$
MED condenser	$\dot{E}_{D, MED\ cond} = \dot{E}_{E,23} - \dot{E}_{E,24}$	$\epsilon_{MED\_Cond} = \frac{\dot{E}_{E,24}}{\dot{E}_{E,23}}$
MED plant	$\dot{E}_{D, MED\ plant} = \sum \dot{E}_{D, MED}$	$\epsilon_{MED\_Plant} = 1 - \frac{\dot{E}_{D, MED\_Plant}}{\dot{E}_A - \dot{E}_B}$

Source: the author.



(iii) Boundary conditions and input source data

The system is evaluated considering the following conditions:

- Points E.1, E.5, E.9, E.13, E.17 and E.21 represent saline water entering the system at 25 °C with  $b_{\text{saline water}} = 3,5\% = 35.000 \text{ ppm}$ .
- Points E.2, E.6, E.10, E.14, E.18 and E.22 correspond to brine leaving the installation with  $b_{\text{Brine}} = 5\% = 50.000 \text{ ppm}$ .
- Points E.3, E.7, E.11, E.15, E.19 and E.23 are saturated steam, that will be condensed into fresh water, exiting each effect at  $x = 1$  with  $b_{\text{Steam}} = b_{\text{Fresh water}} = 0,0240\% = 240 \text{ ppm}$ .
- Points E.4, E.8, E.12, E.16, E.20 and E.24 represent condensed or desalinated water produced in each effect.
- Temperature difference in each effect equal to 4 °C.
- Conditions of each source entering and leaving the desalination plant:
  - GT-MHR – MED plant 1: helium coolant entering the first effect at around 135 °C and leaving it at 30 °C. He pressure remains constant and equal to 2580 kPa.
  - GT-MHR – MED plant 2: helium coolant entering the effect at around 135 °C and leaving it at 30 °C. He pressure remains constant and equal to 4423 kPa.
  - SFR: steam at 65 °C with  $x = 0.70$  enters the system and leaves it at 65 °C with  $x = 0$ .
  - SCWR: steam at 65 °C with  $x = 0.75$  enters the system and leaves it at 65 °C with  $x = 0$ .

### 3.4 Model limitations, simplifications and assumptions

Along this section are presented the limitations, simplifications or assumptions related to the modeling process described in section 3.3 that may affect the results lodged in chapter 4.

(i) Simplifications related to the three chemical reactions of the Na-O-H thermochemical cycle

- Every chemical reaction that composes the Na-O-H system stoichiometric proceeds under well-defined molar quantities defined in section 2.1.3. There are no products or reactants in molar excess. Reactants completely turn into products, that is, reactions have yield of 100%. In practical experiments, reactants may exist in molar excess to facilitate reaction proceeding which may have yield inferior to 100%.

- Each one of those chemical reactions only happens under constant specific conditions of pressure and temperature inside a chemical reactor.
- All the chemical substances in the sodium-oxygen-hydrogen cycle are totally recycled without loss of material, except water which is the source of hydrogen.
- The milling, mixer and pumping processes in the Na-O-H installation introduced in section 3.3.1 are evaluated only considering mass conservation.
- All the results presented over chapter 4, especially those ones discussed in subsections 4.2 to 4.7, directly related to the Na-O-H cycle, are based on a theoretical analysis performed in sections 3.1 and 3.2. In this way, the values of  $p$  and  $T$  discussed for each chemical reaction of this thermochemical system are theoretical and maximized ones, due to all the assumptions made to develop the work, and they can change in experimental situations.

(ii) Considerations about thermodynamic properties and source data

Thermodynamic properties enthalpy ( $h$ ), entropy ( $s$ ) and specific heat ( $C_p$ ) employed in this work come from different sources like data available on NIST (2018) and other references. In this way, the theoretical values of such properties could present some deviation when compared to experimental measures or different theoretical references. Additionally, such properties also can present little divergence when they are compared using different source data like thermodynamic properties tables or EES software internal library because each reference adopts a specific method to order those thermodynamic variables. In this way, calculations which depend on those thermodynamic properties like entropy generation, exergy destroyed or energy exchanged may have small fluctuation due to the source data considered.

Additionally, all the exergy analysis were developed always considering constant values of standard chemical exergy at 25 °C and 101.325 kPa (- 1 bar) for all the substances analyzed in the work, similar to the approach performed in the thermodynamic modeling proposed in the works of Al-Zareer *et al.* (2017a), Al-Zareer *et al.* (2017b) and Balta *et al.* (2012). In this way, possible influences of  $p$  and  $T$  on chemical exergy of substances were neglected due to the complexity related to this subject and also to the lack of information available in literature to deal with chemical exergy out of the standard condition.

*(iii) Assumptions covering control volumes*

- All components and their respective systems operate under steady state conditions. It is disregarded the start up or shut down related to them.
- They were neglected heat and pressure losses inside components in each system.
- They are disregarded heat and pressure losses between components. So, the modeling process does not take account components linking devices such as pipes.
- It was considered an increase of about 1-2°C in water pumping process to guarantee compressed liquid water at pump outlets in EES modeling.
- It was omitted some devices, including the safety ones like valves, need to operate any actual system. In this way, the systems described in section 3.3 are only simplifications or even a first approach of actual plants, but with the main devices of interest for this work.
- Potential and kinetic exergy and energies are not evaluated in the work because variations in systems velocity and height are neglected to facilitate its development.

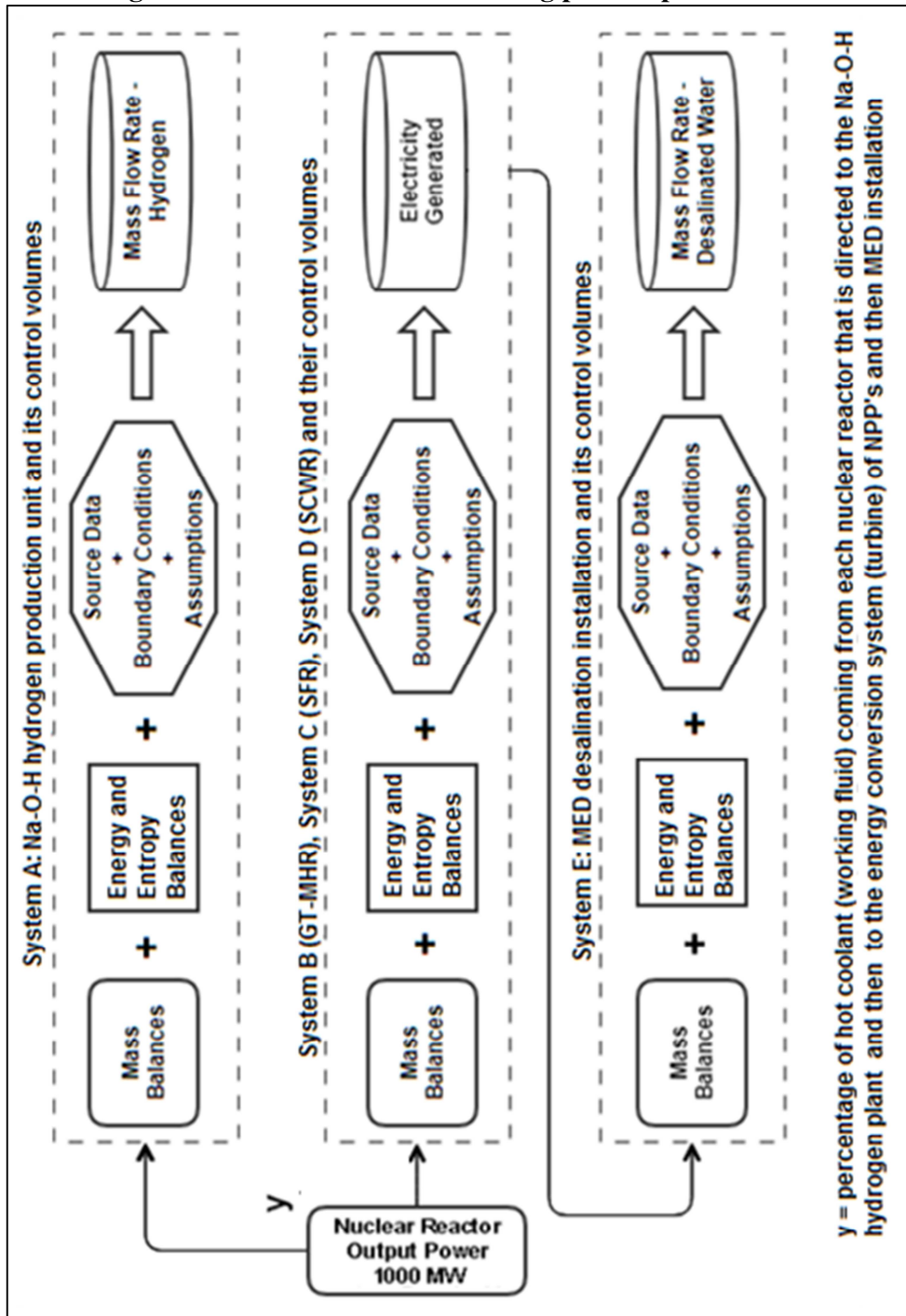
**3.5 Simulations in EES software of the trigeneration cases: flowchart, inputs and outputs**

At this point of the work are implemented in EES software, the mass, energy, entropy and exergy balances combined with specific boundary conditions plus assumptions related to systems A, B, C, D and E, described over chapter 3, in order to estimate the amount of H<sub>2</sub>, electricity and desalinated H<sub>2</sub>O obtained in the trigeneration cases proposed. The amount of these three goods produced are evaluated considering “y” variable that represents the mass flow rate percentage of working fluid (thermal energy) coming from the nuclear reactor of GT-MHR, SFR or SCWR that is directed to the Na-O-H production plant or to the energy conversion system of each NPP and then MED installation as suggested by Figure 21. All equations presented in chapter 3 are implemented according to the algorithm flowchart in Figure 27. After this procedure, they are being obtained the following outputs (results) related to the trigeneration cases under study that are presented and discussed in specific sections of chapter 4 as anticipated at this moment:

- 4.1) Verifying input source data: before discussing the main results found in the work, they are explained how results validation phase is performed.

- 4.2) Enthalpy change ( $\Delta H$ ) analysis for the Na-O-H cycle: in this section are analyzed enthalpy change for each chemical step of the sodium-oxygen-hydrogen process.
- 4.3) Entropy change ( $\Delta S$ ) analysis for the Na-O-H cycle:  $\Delta S$  for each one of the three chemical reactions of the sodium-oxygen-hydrogen are commented in such topic.
- 4.4) Gibbs free energy ( $\Delta G$ ) analysis for the Na-O-H cycle: similar to items 4.2 and 4.3, but now focusing on  $\Delta G$  for every chemical step of the thermochemical cycle studied.
- 4.5) Exergy analysis for the Na-O-H cycle: it is close to the study carried out in the last topic, but at this time an exergy analysis of its reactions are presented.
- 4.6) Thermal aspects of electricity generation in each trigeneration case: it covers the amount of electricity generated in all cases (GT-MHR, SFR and SCWR) in addition to their energy and exergy efficiencies.
- 4.7) Thermal aspects of hydrogen production in each trigeneration case: it is presented the exergy and energy efficiencies of the Na-O-H plant considering all the 3 cases analyzed in addition to the  $H_2$  mass flow rate obtained in each one of them.
- 4.8) Thermal aspects of desalinated water production in each trigeneration case: desalinated  $H_2O$  quantity distilled in the MED installation in every case plus their specific energy consumption and exergy efficiency are commented.

FIGURE 27 – Algorithm flowchart of the modeling process performed in EES software



Source: the author.

Chart 30 summarizes the input and output variables related to the systems evaluated while Figure 28 exhibits a print screen from EES software to show some of the results related to SCWR power plant when the thermal energy released by it is only used to produce electricity.

**CHART 30 – Summary of the input and output variables**

System analyzed	Input Variables	Intermediate variables	Output variables
NPP (GT-MHR, SFR and SCWR)	Operational conditions of p [kPa] and T [°C] for every point of each NPP. The nuclear reactor of all NPP provides an output power of 1000 MW.	Thermodynamic properties h [kJ/kg] and s [kJ/kg*K] for every point of each NPP.	Mass flow rate [kg/s] of working fluid from each NPP; The amount of electricity generated [kW] and exergy destroyed [kW]; energy and exergy efficiencies in every NPP.
Na-O-H hydrogen production system	1) Operational conditions of p [bar] and T [K] for every chemical reaction of the Na-O-H cycle. 2) standard chemical exergy [kJ/kg] for all the chemicals in the cycle. 3) Amount of hot working fluid coming from every NPP at p [bar] and T [°C] that goes to the H <sub>2</sub> plant (y).	1) Thermodynamic properties h [kJ/kg] and s [kJ/kg*K] for each chemical substance (products and reactants) in the Na-O-H cycle and 2) physical exergy for every substance.	1) Enthalpy change, entropy change and Gibbs free energy for the three chemical steps of the Na-O-H cycle. 2) Exergy destroyed [kJ] and exergy efficiency for every chemical reaction. 3) Mass flow rate of H <sub>2</sub> considering the working fluid from each NPP.
MED desalination installation	1) Amount of working fluid coming from every NPP at p [bar] and T [°C] that goes to the MED unit. 2) Operational conditions of p and T and salt concentration of sea water, brine and steam in each effect of the MED system.	Thermodynamic properties h [kJ/kg] and s [kJ/kg*K] for each point of the MED installation.	1) The amount of desalinated water produced [kg/s] considering the working fluid of each NPP. 2) The exergy destroyed [kW] in the installation in every case.

Source: the author.

**FIGURE 28 – EES software results for SCWR nuclear power plant**

Unit Settings: SI C kPa kJ mass deg			
$\Delta E = 301,3$ [MW]	$\epsilon_{\text{pump}} = 0,8912$	$\epsilon_{\text{reactor}} = 0,6798$	$\epsilon_{\text{SFR}} = 0,5722$
$E_{A,18} = 0$ [MW]	$E_{D,1} = 489,5$ [MW]	$E_{D,2} = 489,5$ [MW]	$E_{D,3} = 74,67$ [MW]
$E_{d,\text{MED}} = 71,16$ [MW]	$E_{d,\text{pump}} = 1,073$ [MW]	$E_{d,\text{reactor}} = 228$ [MW]	$E_{d,\text{SFR}} = 304,5$ [MW]
$E_{\text{out,SCWR}} = 410,6$ [MW]	$h_0 = 104,8$ [kJ/kg]	$h_{A,15} = 3236$ [kJ/kg]	$h_{A,18} = 301$ [kJ/kg]
$h_{D,4} = 272,1$ [kJ/kg]	$h_{D,5} = 301$ [kJ/kg]	$h_{D,6} = 301$ [kJ/kg]	$\dot{m}_{A,15} = 0$ [kg/s]
$\dot{m}_{D,3} = 340,7$ [kg/s]	$\dot{m}_{D,4} = 340,7$ [kg/s]	$\dot{m}_{D,5} = 340,7$ [kg/s]	$\dot{m}_{D,6} = 340,7$ [kg/s]
$P_{D,1} = 25000$ [kPa]	$P_{D,2} = 25000$ [kPa]	$P_{D,3} = 25,02$ [kPa]	$P_{D,4} = 25,02$ [kPa]
$\dot{Q}_{\text{reactor}} = 1000$ [MW]	$s_0 = 0,3669$ [kJ/(kg*K)]	$s_{A,15} = 6,054$ [kJ/(kg*K)]	$s_{A,18} = 0,9041$ [kJ/(kg*K)]
$s_{D,4} = 0,8935$ [kJ/(kg*K)]	$s_{D,5} = 0,9041$ [kJ/(kg*K)]	$s_{D,6} = 0,9041$ [kJ/(kg*K)]	$S_{G,\text{pump}} = 0,003599$ [MW/K]
$T_{A,15} = 520$ [C]	$T_{A,18} = 67$ [C]	$\bar{T} = 566,5$ [K]	$T_{D,1} = 520$ [C]
$T_{D,5} = 67$ [C]	$T_{D,6} = 67$ [C]	$T_{\text{fuel}} = 1000$ [K]	$\dot{W}_{\text{pump}} = 9,856$ [MW]
$x_{A,18} = -100$	$x_{D,1} = 100$	$x_{D,2} = 100$	$x_{D,3} = 0,75$
$\epsilon_{\text{turbine}} = 0,9898$	$\eta_{\text{SCWR}} = 0,4007$	$E_{A,15} = 0$ [MW]	
$E_{D,4} = 3,514$ [MW]	$E_{D,5} = 12,3$ [MW]	$E_{D,6} = 12,3$ [MW]	
$E_{d,\text{turbine}} = 4,251$ [MW]	$E_{\text{in,fuel}} = 702$ [MW]	$E_{\text{in,SCWR}} = 711,9$ [MW]	
$h_{D,1} = 3236$ [kJ/kg]	$h_{D,2} = 3236$ [kJ/kg]	$h_{D,3} = 2031$ [kJ/kg]	
$\dot{m}_{A,18} = 0$ [kg/s]	$\dot{m}_{D,1} = 340,7$ [kg/s]	$\dot{m}_{D,2} = 340,7$ [kg/s]	
$P_0 = 100$ [kPa]	$P_{A,15} = 25000$ [kPa]	$P_{A,18} = 25000$ [kPa]	
$P_{D,5} = 25000$ [kPa]	$P_{D,6} = 25000$ [kPa]	$\dot{Q}_{\text{MED}} = 599,3$ [MW]	
$s_{D,1} = 6,054$ [kJ/(kg*K)]	$s_{D,2} = 6,054$ [kJ/(kg*K)]	$s_{D,3} = 6,096$ [kJ/(kg*K)]	
$S_{G,\text{reactor}} = 1,754$ [MW/K]	$S_{G,\text{turbine}} = 0,01426$ [MW/K]	$T_0 = 298$ [K]	
$T_{D,2} = 520$ [C]	$T_{D,3} = 65$ [C]	$T_{D,4} = 65$ [C]	
$\dot{W}_{\text{turbine}} = 410,6$ [MW]		$x_{A,15} = 100$	
$x_{D,4} = 0$	$x_{D,5} = -100$	$x_{D,6} = -100$	
No unit problems were detected.			
Calculation time = 78 ms			

Source: the author.

## 4 RESULTS AND DISCUSSIONS ABOUT THE TRIGENERATION CASES

In this chapter are discussed the main results obtained after implementing in EES software all equations with their respective source data presented along chapter 3. All outcomes are in accordance to the first main aim defined in section 1.1.

### 4.1 Verifying input source data

During the first portion of results section is verified if the main source data employed to develop the work was well-implemented. In Table 7 are exhibited the calculated values of enthalpy, entropy and specific heat for each substance of the Na-O-H cycle starting from Equations (40), (41) and (42) together with information from Table 1 considering standard conditions of p and T.

**TABLE 7 – Calculated thermodynamic properties for the Na-O-H cycle**

Chemical	Enthalpy of formation $\bar{h}^0_f$ (25 °C) [kJ/mol]	Entropy $\bar{s}^0$ (25 °C) [Jmol <sup>-1</sup> K <sup>-1</sup> ]	Specific heat $\bar{C}_p^0$ (25 °C) [Jmol <sup>-1</sup> K <sup>-1</sup> ]
NaOH	-425.92	64.45	59.48
Na(l)	2.41	57.86	32.68
Na <sub>2</sub> O(s)	-418.20	74.48	69.92
H <sub>2</sub> (g)	-0.03	130.63	28.93
Na <sub>2</sub> O <sub>2</sub> (s)	-513.33	94.71	89.28
Na(g)	108.65	153.64	20.76
H <sub>2</sub> O(l)	-285.87	69.94	75.32
O <sub>2</sub> (g)	-0.01	205.15	29.37

Source: the author.

These calculated values are close to the tabulated ones for these same chemicals which are in Table 2. This verification ensures reliability for many of the results discussed in the following topics of chapter 4, especially for those ones presented in items 4.4 and 4.5 associated with the Gibbs free energy and exergy analyses which were performed in subsections 3.2.1 and 3.2.2 about the sodium-oxygen-hydrogen procedure. As a result of it, every aspect of this thermochemical cycle that depends on its thermodynamic properties is also checked, including its enthalpy and entropy changes commented in subsection 4.2 and 4.3.



The validity of other key input source data like thermodynamic properties in Tables 4, 5 and 6 related to each NPP combined with the thermal modeling proposed in section 3.3 are clarified in other topics of this chapter. Advancing that the thermodynamic results related to each system or cases analyzed match possible and expected physical behaviors as it will be addressed later.

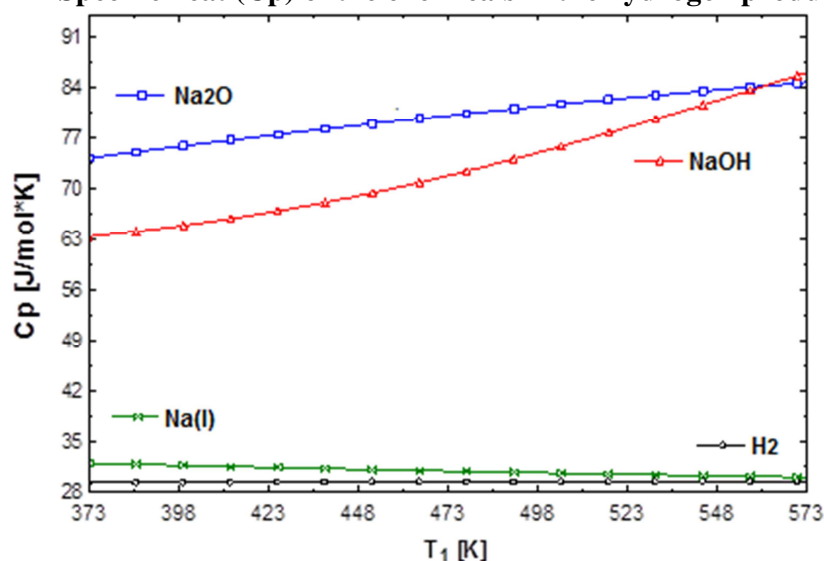
#### 4.2 Enthalpy change analysis for the Na-O-H cycle

The enthalpy change combined with specific heat results for every chemical reaction of the sodium-oxygen-hydrogen cycle are discussed in subtopics (i), (ii) and (iii) of this section through Graphs 7 to 12 after implementing in EES software Equations (52), (55) and (58) from item 3.2.1 in addition to Equation (50) for all the chemicals in the Na-O-H system.

##### (i) Analysis of the hydrogen production step – reaction 1: Equation (18)

Graph 7 shows the specific heat as a function of  $T_1$  (temperature of the hydrogen production step) for  $\text{Na}_2\text{O}$ ,  $\text{H}_2$ ,  $\text{NaOH}$ , and  $\text{Na}$ . According to this diagram, the specific heat of  $\text{NaOH}$  increases sharply from 63 J/mol·K to 87 J/mol·K when  $T_1$  varies from 373 K (100 °C) to 573 K (200 °C). Considering this same temperature range,  $\text{Na}_2\text{O}$  (s),  $\text{Na(l)}$  and  $\text{H}_2$  respectively have an almost constant specific heat of 78 J/mol·K, 33 J/mol·K and 30 J/mol·K. Such behavior can be one of the possible explanations for the results exhibited in Graph 8.

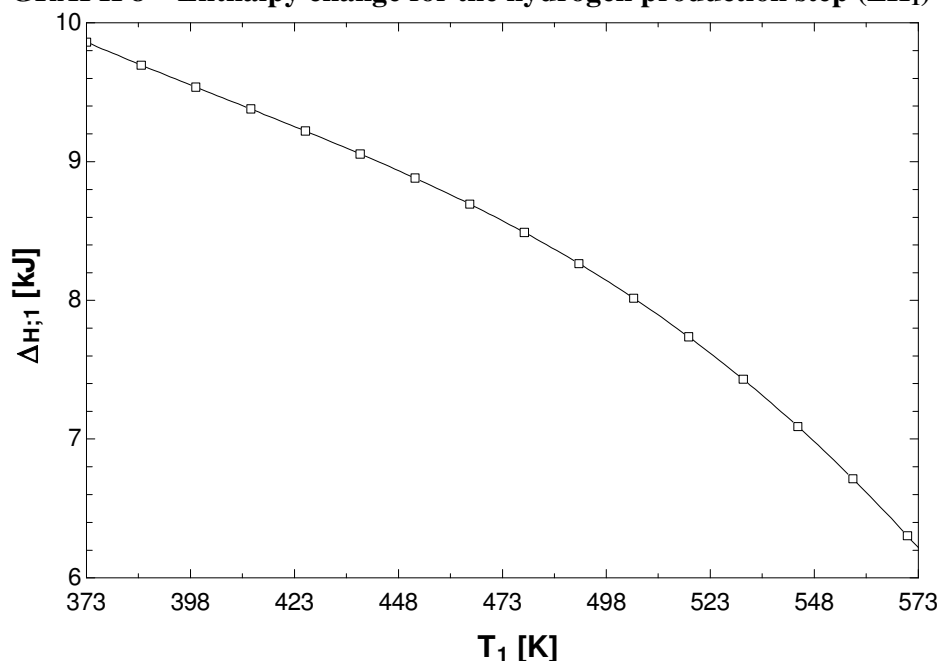
**GRAPH 7 – Specific heat ( $C_p$ ) of the chemicals in the hydrogen production step**



Source: the author.

Graph 8 presents enthalpy change for the hydrogen production step ( $\Delta H_1$ ). As it can be observed,  $\Delta H_1$  reduces from 9.5 kJ to 6.5 kJ when  $T_1$  grows from 373 K to 573 K. As explained before, specific heat of NaOH increases sharply while the  $C_p$  of  $\text{Na}_2\text{O}$ , Na and  $\text{H}_2$  remain almost constant. This fact contributes to the total enthalpy of NaOH, as suggested by Equation (50), and consequently, the total enthalpy of reactants increases while enthalpy of products tend to stay constant because their  $C_p$  has low variation. Therefore,  $\Delta H_1$  calculated from Equation (52) declines as in Graph 8.

**GRAPH 8 – Enthalpy change for the hydrogen production step ( $\Delta H_1$ )**



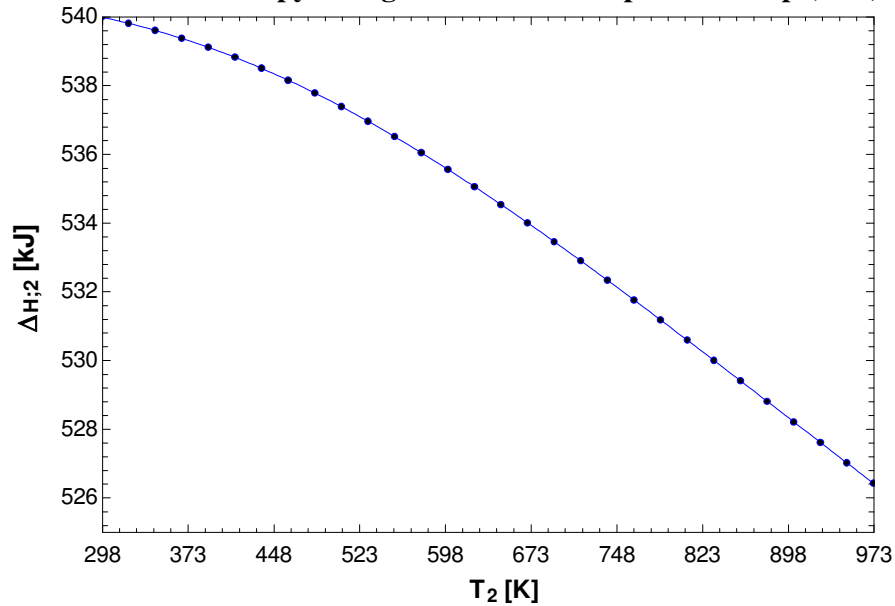
Source: the author.

*(ii) Analysis of the metal separation step – reaction 2: Equation (19)*

The results of chemical reaction 2 (metal separation process) are presented in Graphs 9 and 10 related to  $\text{Na}_2\text{O}$  (reactant) and  $\text{Na(g)}$  plus  $\text{Na}_2\text{O}_2$  (products) of reaction. According to Graph 9, enthalpy change for reaction 2 is always endothermic ( $\Delta H_2 > 0$ ) for any temperature condition.  $\Delta H_2$  varies from 540 to 526 kJ when reaction temperature ( $T_2$ ) rises from 298 K (25 °C) to 973 K (700 °C). It can be explained according to the following reasons. First, the specific heat of  $\text{Na}_2\text{O}_2$  increases from 90 to 110 J/mol·K while  $C_p$  of  $\text{Na(g)}$  keeps a constant value around 20 J/mol·K in the interval 298 K to 973 K as presented in Graph 10. Considering this same gap of  $T_2$ , specific

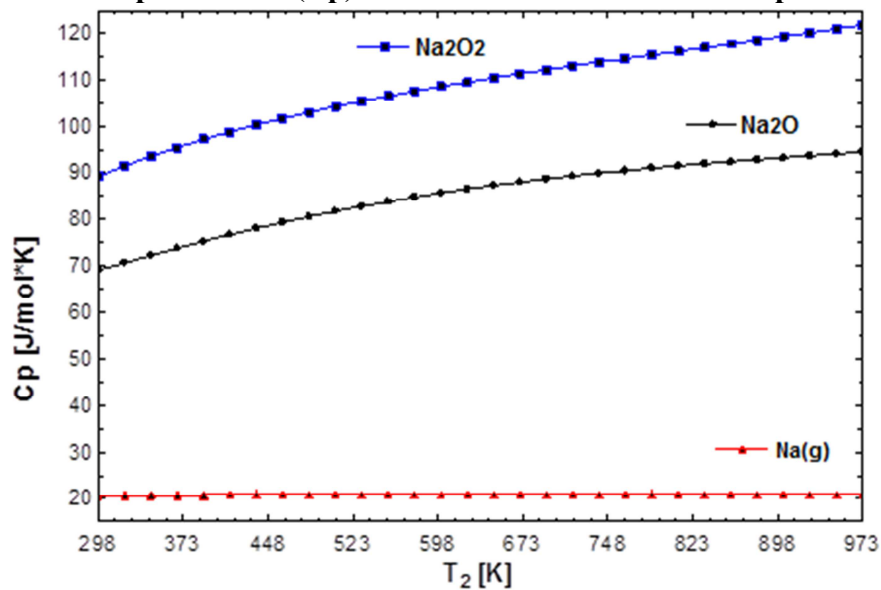
heat of  $\text{Na}_2\text{O}$  rises from 70 to 90  $\text{J/mol}\cdot\text{K}$ . Second, based on information from Table 2, the combined standard enthalpy of formation of products is higher than reactants, considering the stoichiometric proportion of this reaction. These two aspects contribute to the total enthalpy of products overcome the enthalpy of reactants as suggested by Equation (50). In this way,  $\Delta H_2$  determined by Equation (55) is always positive.

**GRAPH 9 – Enthalpy change for the metal separation step ( $\Delta H_2$ )**



Source: the author.

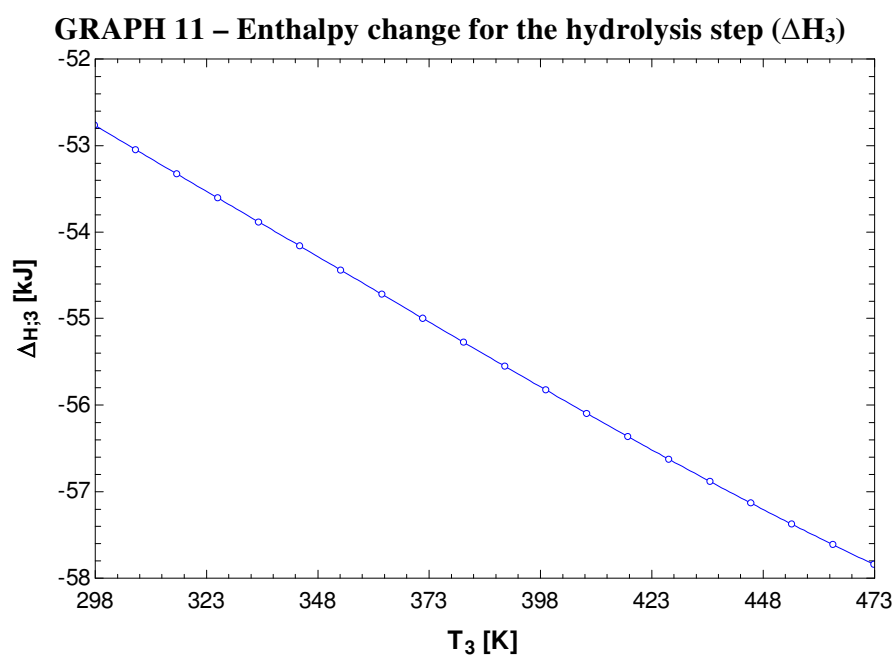
**GRAPH 10 – Specific heat ( $C_p$ ) of the chemicals in the metal separation step**



Source: the author.

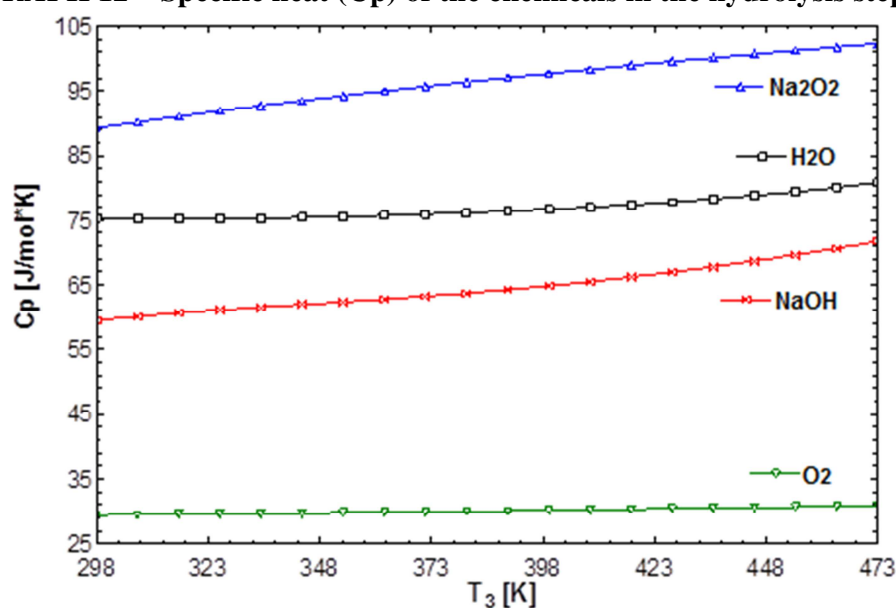
(iii) Analysis of the hydrolysis step – reaction 3: Equation (20)

The results for the chemical reaction 3 or hydrolysis process are shown in Graphs 11 and 12 related to the substances  $\text{Na}_2\text{O}_2$ ,  $\text{H}_2\text{O}$ ,  $\text{NaOH}$  and  $\text{O}_2$ . Graph 11 represents the enthalpy change for the hydrolysis step ( $\Delta H_3$ ) as a function of its temperature ( $T_3$ ).  $\Delta H_3$  decreases from -53 to -58 kJ when  $T_3$  rises from 298 K (25 °C) to 473 K (200 °C). In this way, the reaction is always exothermic for any  $T_3$  and the amount of heat released from it increases, that is, the reaction becomes more exothermic due to the increase in the temperature. This fact can be understood due to two complementary aspects.



Source: the author.

First, considering stoichiometric proportions,  $\text{H}_2\text{O}$  plus  $\text{Na}_2\text{O}_2$  (reactants) have greater standard enthalpy of formation than  $\text{NaOH}$  plus  $\text{O}_2$  (products), as can be verified in Table 2, resulting in an exothermic condition. Second, reactants have higher specific heat than products for any temperature as shown in Graph 12. These two aspects combined, like in Equation (50), make  $\text{H}_2\text{O}$  and  $\text{Na}_2\text{O}_2$  have total enthalpy superior to  $\text{NaOH}$  and  $\text{O}_2$ , resulting in a negative enthalpy change in Equation (58). So, the hydrolysis step is expected to be exothermic, what is in accordance with results in Graph 11.

**GRAPH 12 – Specific heat (Cp) of the chemicals in the hydrolysis step**

Source: the author.

### 4.3 Entropy change analysis for the Na-O-H cycle

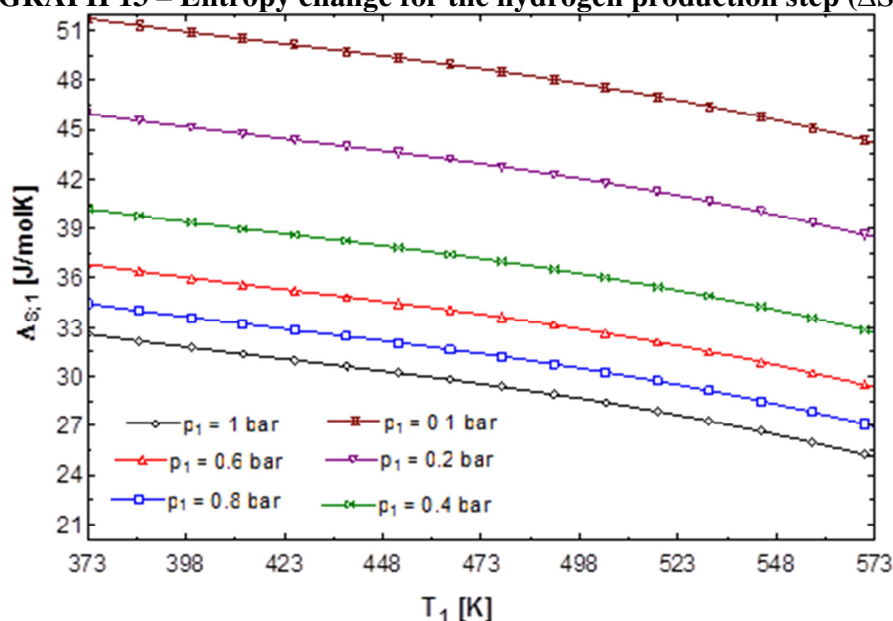
The results of entropy change for all the three chemical steps of the Na-O-H cycle are discussed in subtopics (i), (ii) and (iii) of this section through Graphs 13, 14 and 15 after implementing in EES software Equations (53), (56) and (59) from item 3.2.1.

#### (i) Analysis of the hydrogen production step – reaction 1: Equation (18)

Entropy change for the hydrogen production step ( $\Delta S_1$ ) is exhibited in Graph 13 and follows a similar interpretation as that one provided in topic 4.2 covering  $\Delta H_1$  and specific heat for reaction 1. As a general characteristic, Graph 13 shows that  $\Delta S_1$  decreases when reaction temperature increases from 373 K to 573 K. When  $T_1$  rises, the specific heat of NaOH increases sharply while the values of  $C_p$  for  $H_2$ ,  $Na_2O$  and  $Na(l)$  remain almost constant (Graph 7). Additionally, considering stoichiometric proportions, products ( $H_2$  plus  $Na_2O$ ) have standard entropy superior to reactants ( $NaOH$  plus  $Na$ ) according to Table 2, making entropy change of reaction positive based on Equation (53). However, the final value of  $\Delta S_1$  lowers because the total entropy of products remains almost constant due to their few specific heat change while the total entropy of reactants grows due to enhance their specific heat as suggested by Equation (51). For the specific case when  $p_1 = 1$  bar,  $\Delta S_1$  varies from 32 to 26 J/K.

The effect of pressure on entropy change is also presented in Graph 13. As a general trend, reducing  $p_1$  causes increase in  $\Delta S_1$ . Analyzing Equation (48), it perceives that when  $p_1 < p^0$  (standard condition), considering a specific value of  $T_1$ , the overall value of  $\Delta S_1$  rises, what explain the results presented in Graph 13. This reduction in  $p_1$  only affects gaseous products, in such reaction  $H_2$ . Consequently,  $\Delta S$  for reaction 1 calculated using Equation (53) also increases. For a preset value of  $T_1 = 373$  K,  $\Delta S_1$  rises from 33 to 51 J/K when  $p_1$  reduces from 1 to 0.1 bar.

**GRAPH 13 – Entropy change for the hydrogen production step ( $\Delta S_1$ )**

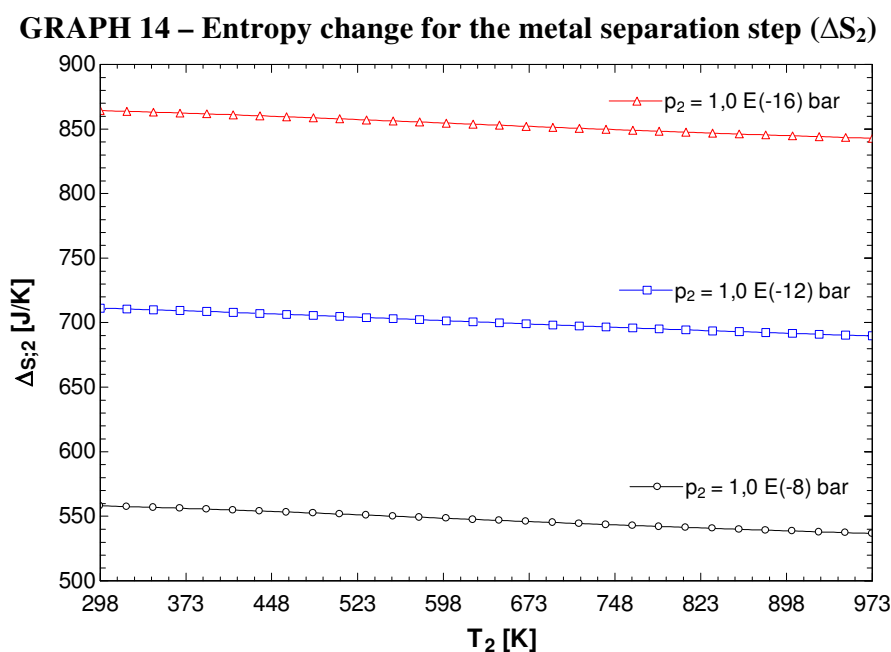


Source: the author.

(ii) Analysis of the metal separation step – reaction 2: Equation (19)

Graph 14 introduces the influence of  $T_2$  and  $p_2$  on entropy change of the metal separation step ( $\Delta S_2$ ). The influence of  $T_2$  on  $\Delta S_2$  follows an explanation close to that one for enthalpy change and specific heat for this same chemical reaction in section 4.2. According to such discussion, the overall specific heat of products increases due to enhancing their temperature and they are higher than the specific heat of reactant which reduces by increasing  $T_2$ . Additionally, considering information from Table 2, products have superior standard entropy to reactants. These two aspects combined make the total entropy of products be greater than reactants as suggested by Equation (51). In this way, entropy change for the metal separation step from Equation (56) is always positive. For the preset value of  $p_2 = 10^{-12}$  bar,  $\Delta S_2$  varies from 710 to 700 J/K.

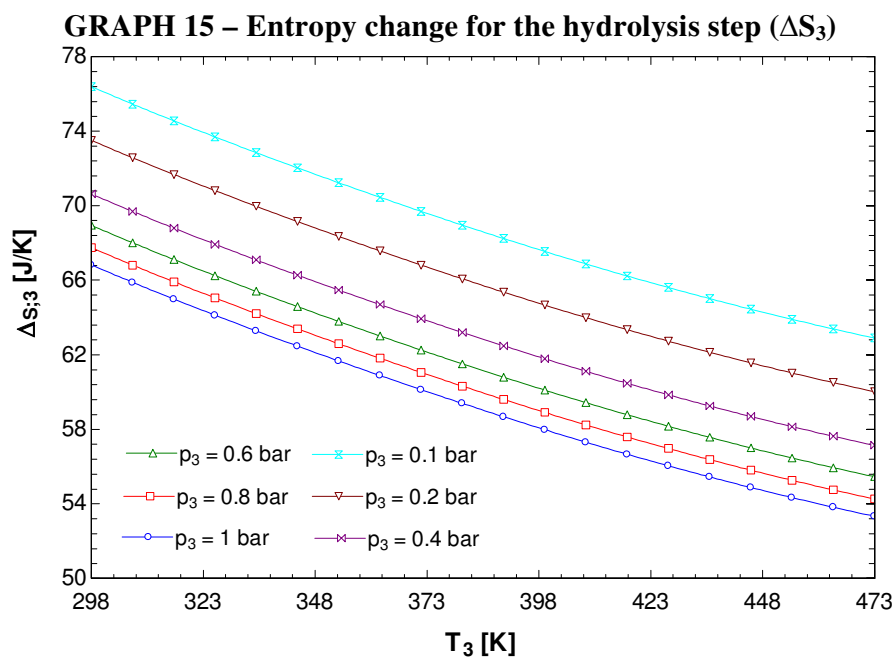
On the other way, the influence of  $p_2$  on entropy change can be explained from Equation (48). According to it, a reduction on  $p_2$  for a value lower than  $p^0$  (standard condition) increases the value of entropy, what is in accordance with Graph 14. For the specific case when  $T_2 = 973$  K,  $\Delta S_2$  grows from 550 to 850 J/K when  $p_2$  diminishes from  $10^{-8}$  to  $10^{-16}$  bar, approaching to a theoretical vacuum situation.



Source: the author.

(iii) Analysis of the hydrolysis step – reaction 3: Equation (20)

Additionally, in Graph 15 is possible to verify the entropy change for the hydrolysis step ( $\Delta S_3$ ) as a function of  $T_3$  and  $p_3$ . As an overall behavior,  $\Delta S_3$  always declines when  $T_3$  grows for a preset value of  $p_3$ . The effect of temperature on entropy change also can be explained according to the specific heat for each one of the chemicals involved in the reaction (Graph 12), similarly as well as for the explanation covering enthalpy change (Graph 11) but now considering standard entropy instead of standard enthalpy of formation. Then, the entropy of reactants tends to enhance more than products according to Equation (51) because reactants ( $\text{Na}_2\text{O}_2$  and  $\text{H}_2\text{O}$ ) have superior  $C_p$  with strong growth of it compared to products ( $\text{NaOH}$  and  $\text{O}_2$ ). That diminishes the entropy change of reaction although products have combined superior standard entropy to reactants based on information from Table 2.



Source: the author.

In a complementary manner,  $\Delta S_3$  in Graph 15 always decreases when its pressure increases for a constant temperature. Analyzing Equation (48), it is possible to verify that reducing  $p_3$  to a value lower than the standard one ( $p_0$ ), considering a specific value of  $T_3$ , the overall entropy grows, what explain the results presented over Graph 15. This reduction in  $p_3$  only affects gaseous products, in such case oxygen gas ( $O_2$ ). For the specific case when  $p_3 = 1$  bar,  $\Delta S_3$  varies from 67 to 54 J/K when  $T_3$  rises from 298 to 473 K. On the other hand, for the preset value  $T_3 = 298$  K, entropy change decreases from 77 to 67 J/K when  $p_3$  increases from 0.1 to 1 bar.

#### 4.4 Gibbs free energy analysis for the Na-O-H cycle

In this part of results chapter are argued about the theoretical conditions of  $p$  and  $T$  in which the three reactions of the Na-O-H cycle are able to proceed in accordance with the  $\Delta G$  study proposed in section 3.2.1.

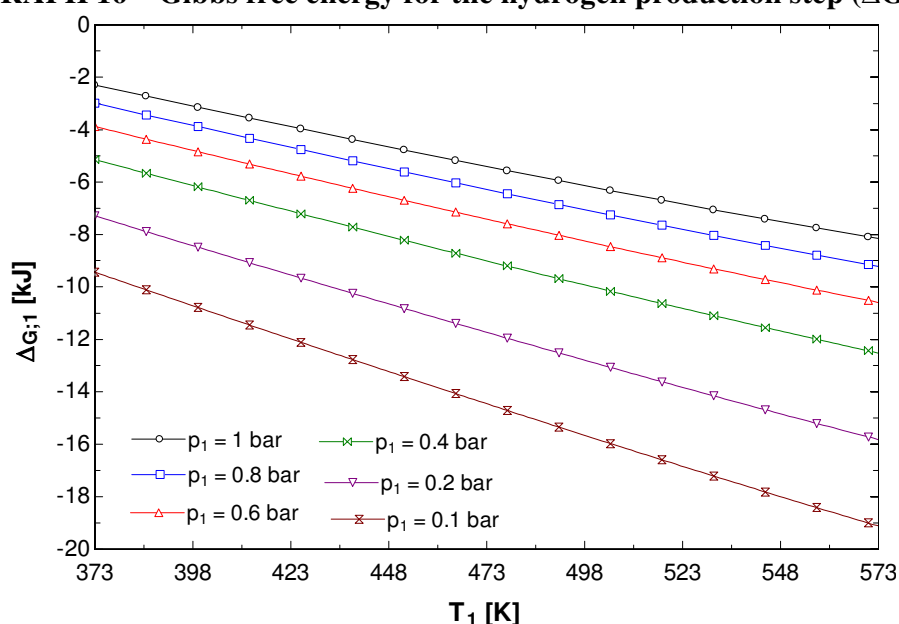
##### (i) Analysis of the hydrogen production step – reaction 1: Equation (18)

Graph 16 shows the values of Gibbs free energy for the hydrogen production step ( $\Delta G_1$ ) considering its pressure and temperature. According to it,  $\Delta G_1$  is always negative for  $T_1$  between 373 K and 573 K and  $p_1$  between 0.1 and 1 bar. This means reaction 1 has potential to proceed considering the analyzed range of conditions. In this way,  $\Delta G_1$  decreases as  $T_1$  increases for a



preset value of  $p_1$ ; and it reduces when  $p_1$  rises for a constant temperature value. In the specific case when  $p_1 = 1$  bar,  $\Delta G_1$  reduces from -2.1 to -7.1 kJ when  $T_1$  varies from 373 to 573 K. Additionally,  $\Delta G_1$  drops from -2.1 to -9 kJ when  $p_1$  decreases from 1 to 0.1 bar at 373 K. The effect of pressure on  $\Delta G_1$  can be explained through Chatelier's principle or the Equilibrium Law (CASTELLAN, 1983). When pressure decreases,  $H_2$  releasing in Equation (18) is facilitated because the chemical equilibrium is dislocated favoring the formation of gaseous products, making it easy the overall reaction progressing, what impacts on reducing its Gibbs free energy.

**GRAPH 16 – Gibbs free energy for the hydrogen production step ( $\Delta G_1$ )**

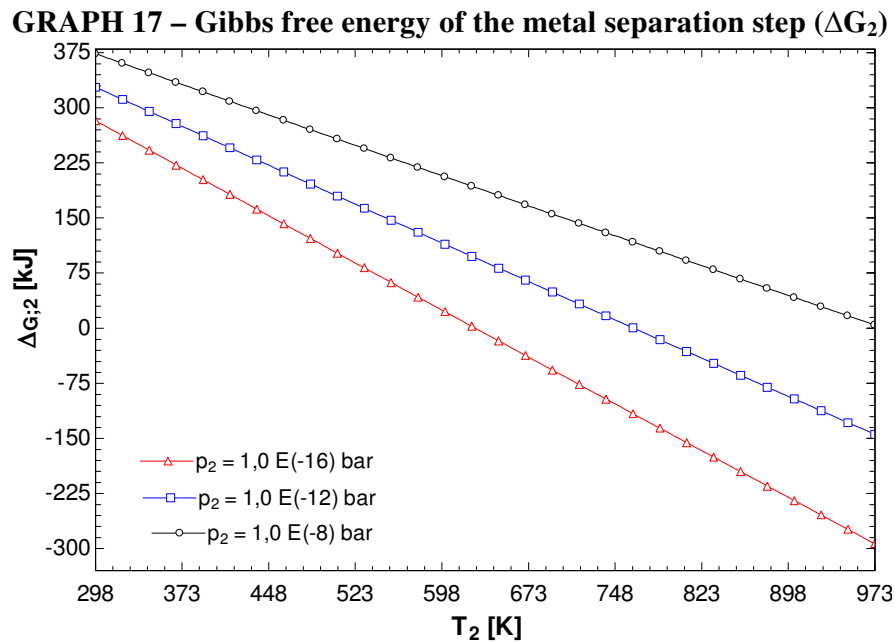


Source: the author.

When Miyaoka *et al.* (2012) experimentally carried out the hydrogen releasing phase under 1 bar argon atmosphere at 573 and 623 K, they concluded such phase had low yielding. It could happen because this reaction was not carried out considering a low pressure atmosphere, what facilitates reaction proceeding as the explanation given in the last paragraph. So, based on the results presented in Graph 16, Equation (18) could be theoretically performed at 373 K (100 °C) under 1 bar instead of fulfilling it at 573-623 K. This outputs agrees with information from Miyaoka *et al.* (2012) that suggested reaction 1 has theoretical equilibrium temperature around 305 K (32 °C), when  $p_1 = 1$  bar, making  $\Delta G$  null at such condition.

*(ii) Analysis of the metal separation step – reaction 2: Equation (19)*

Related to the Gibbs free energy of the metal separation step ( $\Delta G_2$ ), it is always positive when  $p_2$  varies from 1 to 0.1 bar despite  $T_2$  values. This function represented by Equation (57) just become negative, can proceed under very low pressures or vacuum when the increase in entropy change ( $\Delta S_2$ ) overcomes the high enthalpy change of reaction ( $\Delta H_2$ ) making  $\Delta G_2 < 0$ . Due to this fact, results presented in Graph 17 only were showed considering very low values of  $p_2$ . Table 8 adapted from Tilford (1992) shows a wide pressure ranges covering different vacuum states.



Source: the author.

**TABLE 8 – Pressure ranges for vacuum conditions**

Condition	Pressure range	
	Pa	bar
Very high pressure	$10^8 - 10^{11}$	$10^3 - 10^6$
High pressure	$10^5 - 10^8$	$10^0 - 10^3$
Atmospheric	$10^2 - 10^5$	$10^{-3} - 10^0$
Low vacuum	$10^{-1} - 10^2$	$10^{-6} - 10^{-3}$
High vacuum	$10^{-4} - 10^{-1}$	$10^{-9} - 10^{-6}$
Very high vacuum	$10^{-7} - 10^{-4}$	$10^{-12} - 10^{-9}$
Ultra high vacuum	$10^{-10} - 10^{-7}$	$10^{-15} - 10^{-12}$

Source: adapted from Tilford (1992).

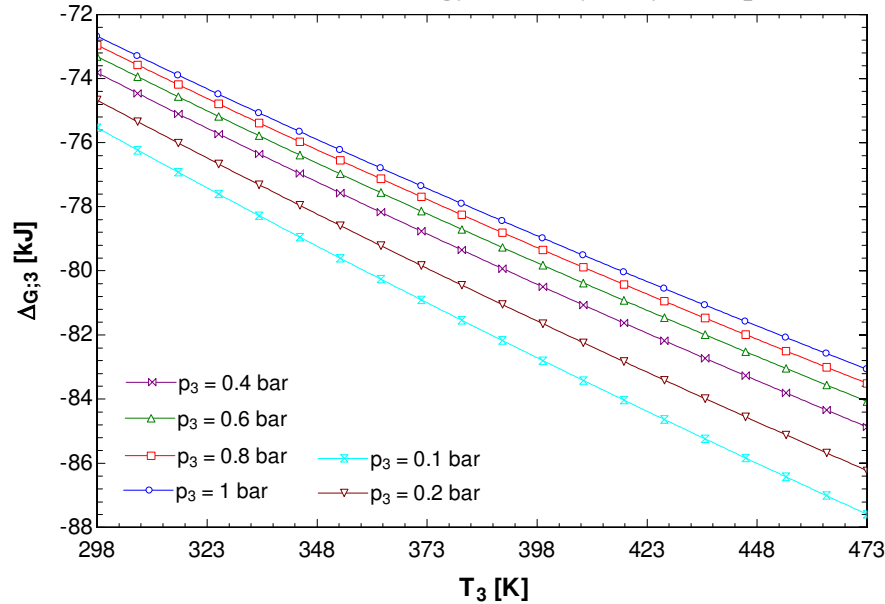
When  $p_2 = 10^{-8}$  bar, a high vacuum condition, the reaction is able to occur for  $T_2$  higher than 970 K (697 °C). However, for  $p_2 = 10^{-12}$  bar, a very high vacuum, metal separation phase can prosecute at around 740 K (467 °C) or beyond. The results in Graph 17 agree with experimental analysis fulfilled by Miyaoka *et al.* (2012), indicating that Equation (19) may happen only under a vacuum or low pressure atmosphere for temperatures around 773 K. For  $p_2$  lower than  $10^{-12}$  bar, the reaction has potential to ensue at  $T_2$  below 723 K. However, reducing the operational pressure of a system until very low values it is a challenging task in practical situations, what could restrict its application to small and medium scale processes as noted by Marques *et al.* (2018a). The Na-O-H cycle is a pure thermochemical method, only demands heat; then, a possible way to overcome such problem might be operating the system at high temperatures, probably superior to 1000 °C, to enable  $p_2$  near 1 bar and thus facilitating its befall from the pressure view point. If the metal separation step is accomplished under atmospheric pressure, such high temperature requirement could be reduced if a proper catalyst were employed.

(iii) Analysis of the hydrolysis step – reaction 3: Equation (20)

Finally, Graph 18 presents the values of Gibbs free energy for reaction 3 ( $\Delta G_3$ ) as a function of  $p_3$  and  $T_3$ . According to it,  $\Delta G_3$  is always negative for  $T_3$  between 298 K and 473 K and  $p_3$  between 1 and 0.1 bar. This means hydrolysis step has potential to occur considering the evaluated conditions. In this way,  $\Delta G_3$  reduces by increasing  $T_3$ , for a well-defined pressure state, and it reduces when  $p_3$  rises for a constant temperature value. In the specific case when  $p_3 = 1$  bar,  $\Delta G_3$  declines from -72 to -81 kJ when  $T_3$  varies from 298 to 473 K. On the other hand,  $\Delta G_3$  diminishes from about -72 to -76 kJ when  $p_3$  decreases from 1 to 0.1 bar at 298 K.

So, complementing the experimental analysis realized by the researchers (MIYAOKA *et al.*, 2012), it concludes chemical reaction 3 has the possibility to occur considering the temperature range 25-200 °C for a pressure gap between 0.1 and 1 bar. In this way, this reaction can progress at low temperatures, like 25 °C, instead the 100 °C suggested by those authors (MIYAOKA *et al.*, 2012) under 1 bar atmosphere.

Finally, the specific requirements of pressure and temperature in which each one of the chemical reactions of the Na-O-H cycle are performed in the hydrogen production unit are defined after the exergy analysis carried out in section 3.2.2 which outcomes are presented in the following topic.

**GRAPH 18 – Gibbs free energy of the hydrolysis step ( $\Delta G_3$ )**

Source: the author.

#### 4.5 Exergy analysis for the Na-O-H cycle

The results attached to the exergy analysis of the chemical reactions that compose the sodium-oxygen-hydrogen method are interpreted from now on. Such discussion is complemented with information in Table 9 that covers the specific values of chemical, physical and total exergy for every substance in this chemical process. The physical exergy of every substance and consequently their total exergy have little deviation considering the analyzed conditions of pressure and temperature defined in section 3.2.2 in which each reaction is assessed.

**TABLE 9 – Chemical, physical and total exergy for the substances in the Na-O-H cycle**

Chemical	Standard chemical exergy $\bar{e}_{ch}^0$ (25 °C; 101.325 kPa) [kJ/mol]	Physical exergy $\bar{e}_{ph}^0$ [kJ/mol]	Total exergy $\bar{e}$ [kJ/mol]
NaOH(s)	74.91	2.11	77.01
Na(l)	342.72	1.35	344.05
Na(g)	177.1	-98.32 <sup>1</sup>	78.78
Na <sub>2</sub> O(s)	296.2	3.45	299.65
H <sub>2</sub> (g)	236.09	1.25	237.34
Na <sub>2</sub> O <sub>2</sub> (s)	174.3	1.75	176.05
H <sub>2</sub> O(l)	0.90	1.45	2.35
O <sub>2</sub> (g)	3.97	0.61	4.58

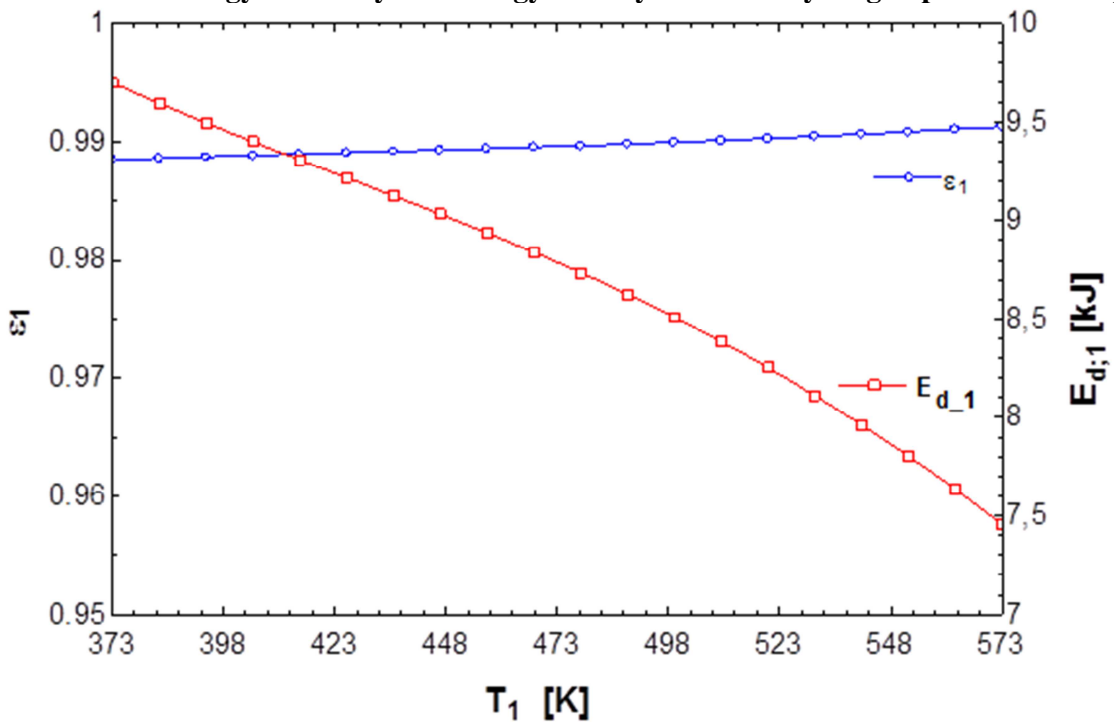
1- Calculated at vacuum condition considering the exergy balances from Equations (80), (81) and (82).

Source: the author.

*(i) Analyzing chemical reaction 1 – hydrogen production step: Equation (18)*

The overall exergy efficiency of reaction 1 and the total amount of exergy destroyed in it, considering a temperature interval from 373 K to 573 K is presented in Graph 19. The exergy efficiency of the hydrogen production step vary little and remains almost constant at about 98% (0.98), while its exergy destroyed diminishes from 9.5 kJ to 7.5 kJ. Such high value of exergy efficiency plus the low value of exergy destruction ensue because exergy of reactants, sodium hydroxide and liquid sodium, are used to produce Na<sub>2</sub>O together with H<sub>2</sub>; this last one is a fuel with high chemical exergy content (RIVERO and GARFIAS, 2006). The reduction in  $p_1$  has very little impact on the results shown in Graph 19.

**GRAPH 19 – Exergy efficiency and exergy destroyed for the hydrogen production step**

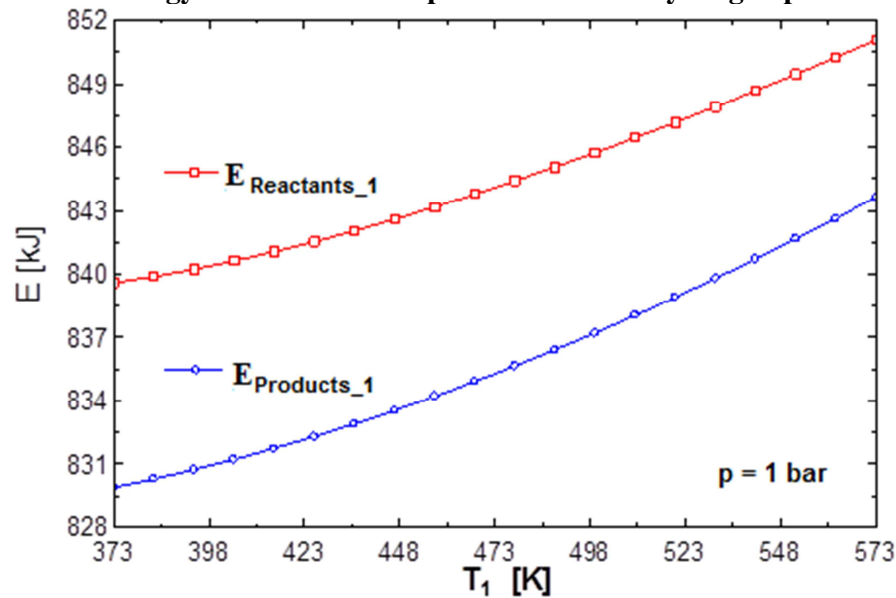


Source: the author.

Providing support information to Graph 19, Graph 20 shows the final values of exergy of products and reactants for reaction 1. As it is possible to verify, exergy of reactants increases from 839 kJ to 850 kJ while exergy of products increases from 830 kJ to 843 kJ, what impacts on a variation of 7.5 kJ to 9.5 kJ of exergy destroyed in Graph 19.

According to Graphs 19 and 20, the minimum amount of exergy destroyed (7.5 kJ) and exergy efficiency (98%) for the hydrogen releasing step happen at 573 K (300 °C). However, such process could be more easily performed if it is carried out at 373 K (100 °C) that allows using a low temperature heat source but destroying a little more exergy, a net value of 9 kJ, but keeping exergy efficiency around 96%.

**GRAPH 20 – Exergy of reactants and products for the hydrogen production step**

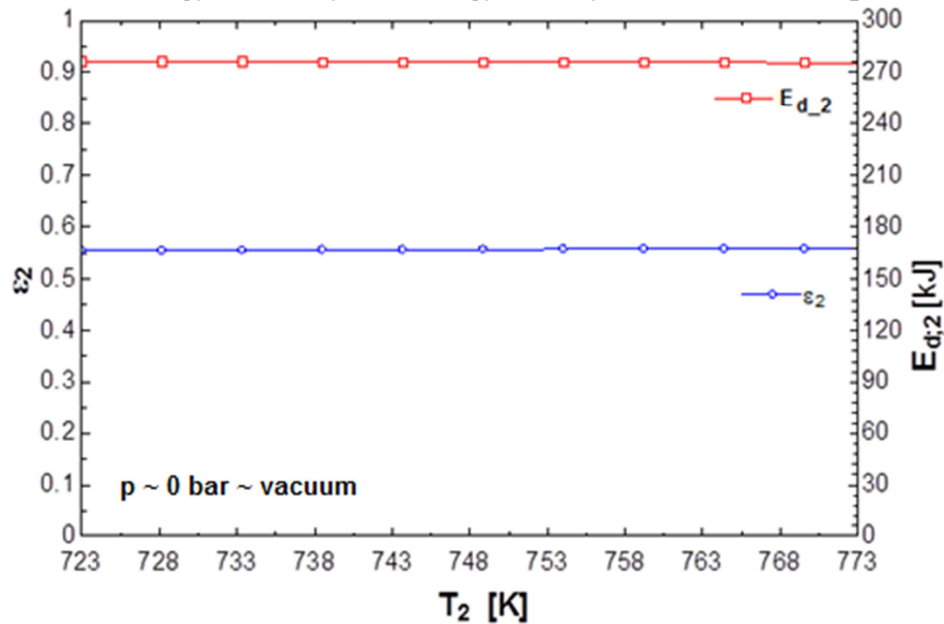


Source: the author.

(ii) Analyzing chemical reaction 2 – metal separation step: Equation (19)

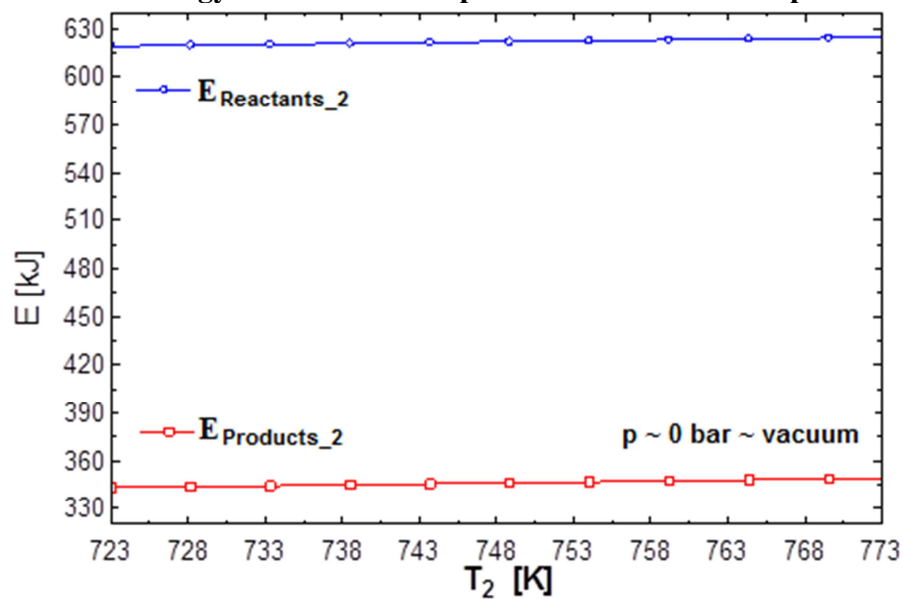
Based on Graph 21, reaction 2 has exergy efficiency around 0.56 (56%) related to an exergy destroyed of 280 kJ considering a temperature range from 723 K to 773 K. Such values of exergy destroyed and exergy efficiency were found considering that this reaction is ensued at vacuum as suggested by Miyaoka *et al.* (2012) and Marques *et al.* (2019).

The adverse conditions of pressure (extremely low) and temperature (relatively high) in which the reaction must take place are directly related to the chemicals involved in it, like the metal oxide  $\text{Na}_2\text{O}$  that is a very stable substance with low Gibbs free energy equal to -375.5 kJ/mol (LIDE, 2004), what difficult its proceeding and contribute to generate a large amount of entropy in the process, around 850 J/K, as noted in the thermodynamic analysis covering the Na-O-H cycle (MARQUES *et al.*, 2019). This conjecture is a possible explanation to the high exergy destroyed plus the low exergy efficiency of reaction 2.

**GRAPH 21 – Exergy efficiency and exergy destroyed for the metal separation step**

Source: the author.

Complementing information from Graph 21, Graph 22 exhibits the values of exergy of products and reactants for the metal separation step. In it, reactants have exergy equal to 620 kJ while products have exergy about 340 kJ, resulting in 280 kJ of exergy destroyed as argued in the last paragraph. The almost constant values of the variables in Graphs 21 and 22 are function of the almost constant total exergy of the chemical substances of reaction 2 shown in Table 9.

**GRAPH 22 – Exergy of reactants and products for the metal separation step**

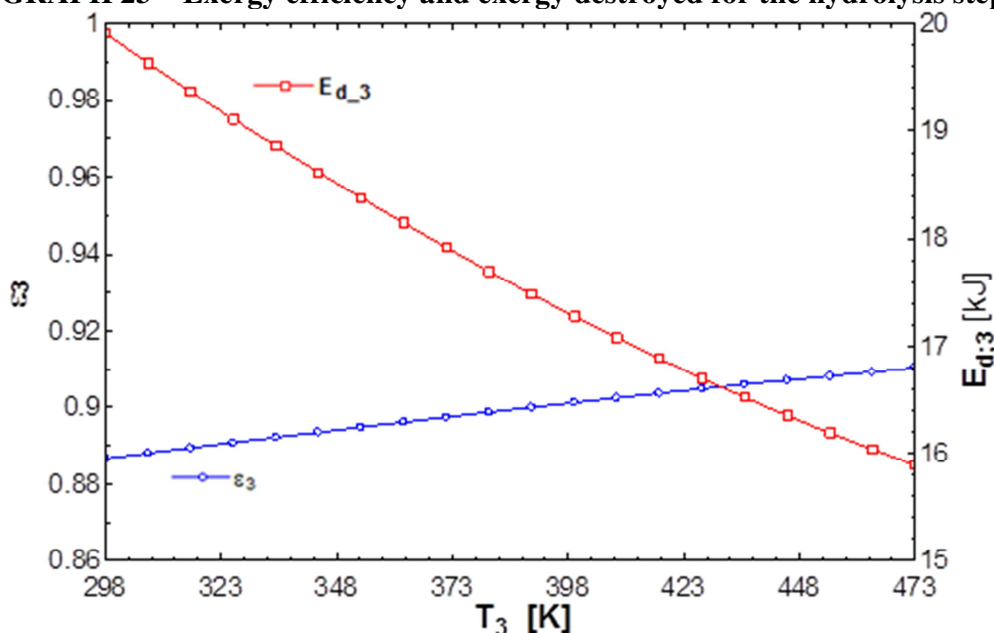
Source: the author.

After analyzing the results in Graphs 21 and 22, it is perceptible that reaction 2 have almost exergy destroyed (280 kJ) and exergy efficiency (56%) when its temperature ranges from 723 K (450 °C) to 773 K (500 °C) under vacuum pressure. So, the metal separation step should be carried out at 450 °C rather than 500 °C to facilitate the use of a low temperature heat source because there is no perceptible change in its exergy performance in function of its temperature.

(iii) Analyzing chemical reaction 3 – hydrolysis step: Equation (20)

The values of exergy destroyed and exergy efficiency for the hydrolysis step are presented in Graph 23. After analyzing this diagram, it concludes that reaction 3 has exergy efficiency varying from 0.89 (89%) to 0.91 (91%) allied to an exergy destroyed varying from 20 kJ to 16 kJ when  $T_3$  enhance from 298 K to 473 K. Such high exergy efficiency and low exergy destroyed, when compared to the values from reaction 2, is explained due to the relatively easy proceeding of reaction 3, in function of the thermodynamic behavior and characteristics of the chemicals involved in the process, verified by a Gibbs free energy analysis proposed by Marques *et al.* (2019) in addition to the experimental study carried out by Miyaoka *et al.* (2012).

**GRAPH 23 – Exergy efficiency and exergy destroyed for the hydrolysis step**



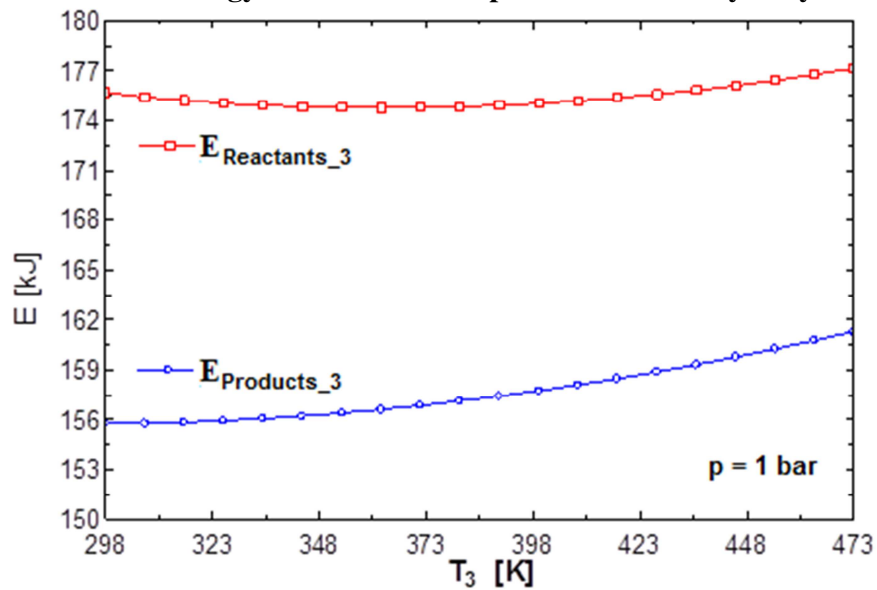
Source: the author.

Yet, in Graph 24 is introduced the exergy of products and reactants for reaction 3. In the case of reactants, their exergy remains almost constant at around 175 kJ while exergy of products shows



a little increasing from 156 kJ to 161 kJ under a temperature interval from 298 K to 473 K. It results in an exergy destroyed of 4 kJ, what could explain the values of exergy destroyed shown in Graph 23. The little variation of exergy of products happens thanks to the little increasing in the total exergy of NaOH and O<sub>2</sub> as data provided in Table 9.

**GRAPH 24 – Exergy of reactants and products for the hydrolysis step**



Source: the author.

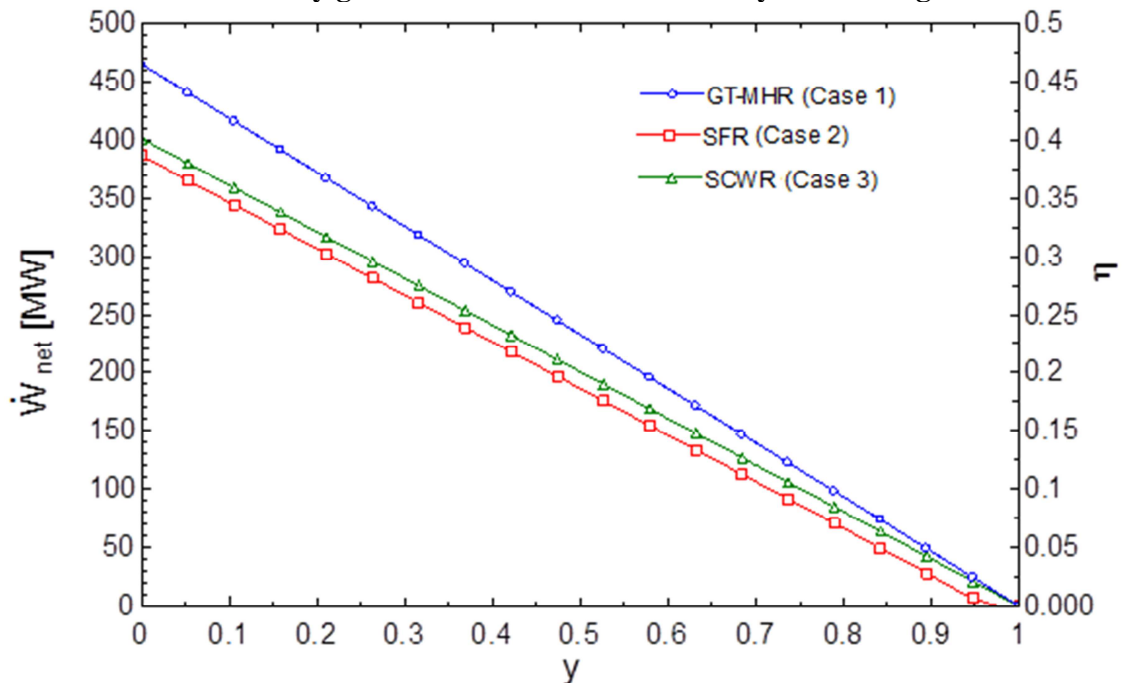
Finally, the outputs in Graphs 23 and 24 show that reaction 3 have the maximum exergy efficiency (87%) and the minimum exergy destroyed (16 kJ) at 473 K (200 °C) under 1 bar. However, the reaction should be fulfilled at 298 K (25 °C), even destroying a little more exergy (20 kJ) to avoid the use of any heat source.

So, after performing this exergy analysis for the Na-O-H cycle, the trigeneration process of hydrogen, electricity and desalinated water are evaluated and discussed in the next sections considering that reaction 1 happens at 100 °C and 1 bar, reaction 2 proceeds at 450 °C under vacuum; reaction 3 is accomplished at 25 °C and 1 bar. The specific vacuum level or low pressure necessary to proceed reaction 2 was not measured or specified by Miyaoka *et al.* (2012) while the values (10<sup>-8</sup> bar, 10<sup>-12</sup> bar and 10<sup>-16</sup> bar) exhibited in Graph 17 are just a theoretical or mathematical one from solving Equation (57) for the metal separation step when  $\Delta G_2 = 0$ , and they not represent the exact actual pressure value required to accomplish Equation (19) in experimental situations.

#### 4.6 Thermal aspects of electricity generation in each trigeration case

In Graph 25 is exhibited the amount of net electricity ( $\dot{W}_{net}$ ) generated in cases 1, 2 and 3 in function of the mass flow rate of hot working fluid coming from every type of nuclear reactor that is directed to the hydrogen production unit ( $y$ ) or to the energy conversion system of each NPP (GT-MHR, SFR and SCWR). Additionally, this same diagram reveals the thermal efficiency ( $\eta$ ) of all nuclear power plants regarding  $y$  variation.

**GRAPH 25 – Electricity generated and thermal efficiency in each trigeration case**



Source: the author.

Based on information from Graph 25, it is possible to observe that GT-MHR (case 1) produces the highest amount of electrical power in function of  $y$  when compared to SFR (case 2) and SCWR (case 3), always considering 1000 MW<sub>th</sub> released from all nuclear reactors. In the case of GT-MHR, its maximum output electrical power is about 460 MW when  $y = 0$ , decreasing linearly until 0 MW when  $y$  reaches the value 1. In the events of cases 2 and 3, electricity production reaches respectively, 400 MW and 390 MW. Both variables linearly diminish until 0 while  $y$  increases from 0 to 1. For all cases, when  $y = 1$ , the total mass flow rate of working fluid from all nuclear reactors is directed to the H<sub>2</sub> production facility, making it impossible to produce

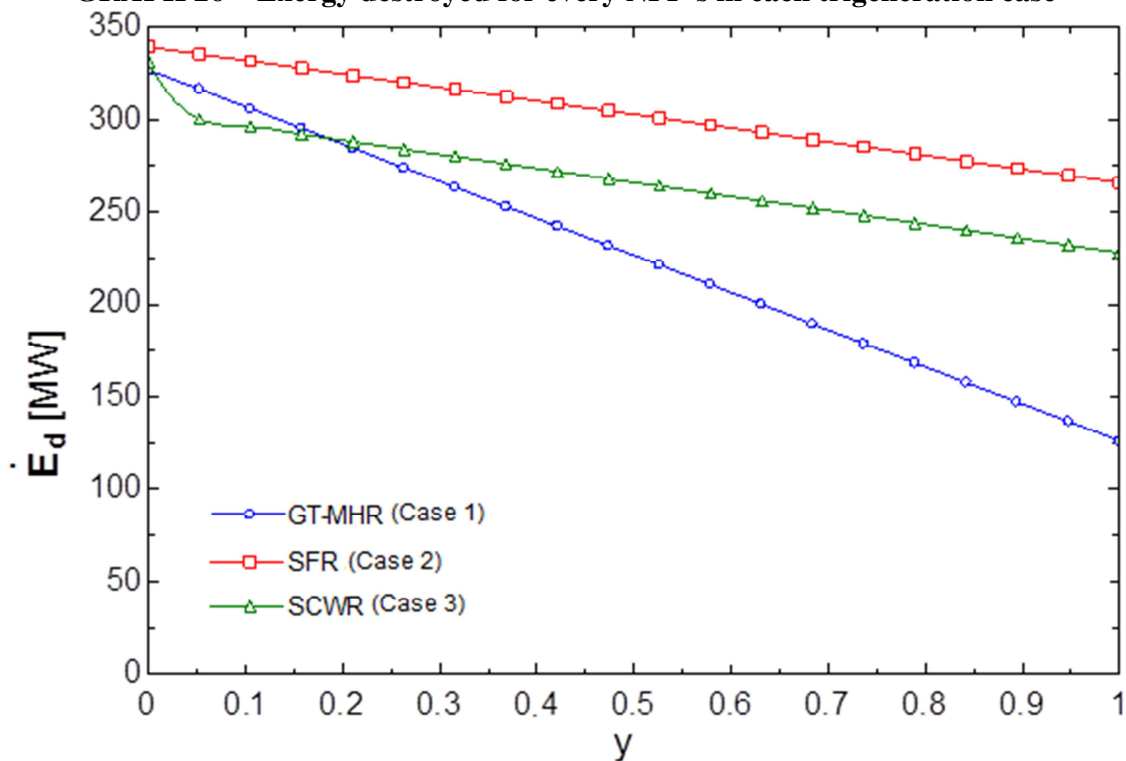
electricity, but only  $H_2$ . In contrast, when  $y = 0$ , only electrical work is gotten because none working fluid goes to the Na-O-H installation.

Still related to the last Graph,  $\eta$  of every NPP linearly decreases from an uppermost value up to 0 for the range  $0 < y < 1$ . It happens because the thermal power released by each nuclear reactor remains constant and equal to 1000 MW while the net power generated in each scenario lowers until 0 due to directing the mass flow rate of working fluid to produce  $H_2$  in the Na-O-H plant instead of electricity. GT-MHR has the highest values of  $\eta$  whose maximum value is 46% (0.46), followed by SCWR with utmost thermal efficiency close to 40% (0.40) while SFR is the less efficient with  $\eta = 38\%$  (0.38). These values of thermal efficiency agree with expected ones for such technologies as it can be verified in specific studies covering GEN-IV nuclear technologies like the one published by Poullikkas (2013) or those ones provided in section 2.3.

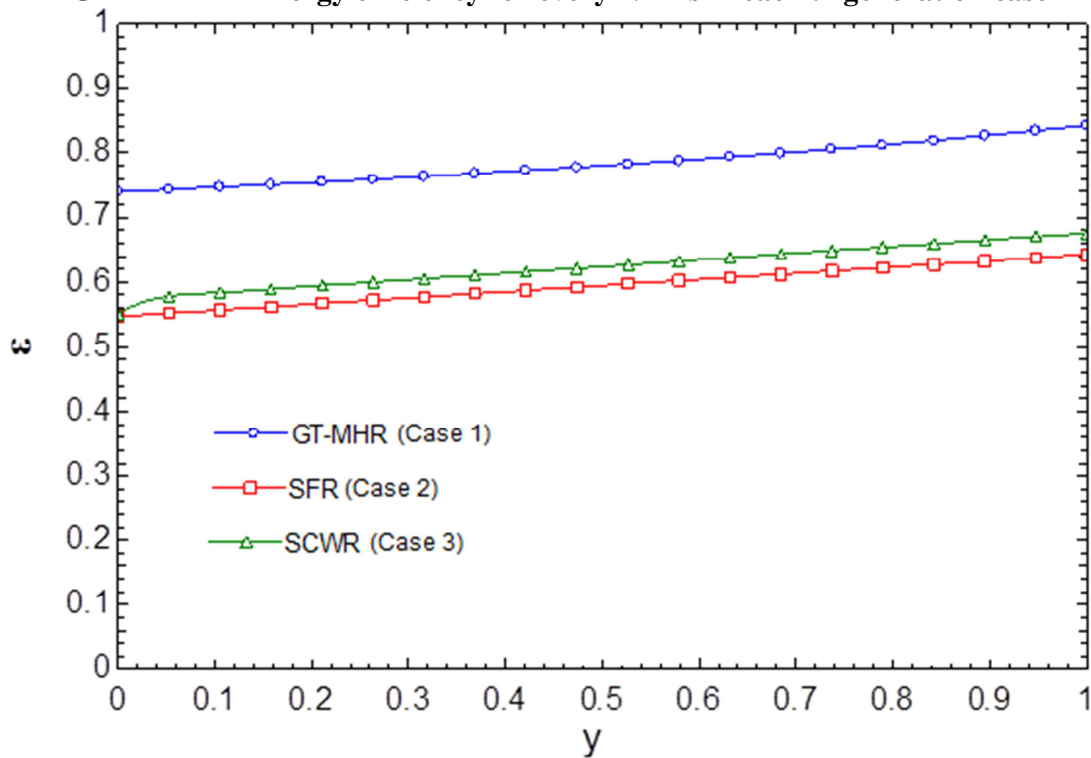
The higher amounts of electricity generated and thermal efficiency related to the GT-MHR system compared to the other two nuclear power cycles is basic due to the highest temperature achieved by helium coolant (850 °C) in contrast to the about 500 °C reached by steam or supercritical water in the cases of SFR and SCWR. This behavior is in accordance to the second law of thermodynamics that affirms the thermal efficiency of any thermal power plant enhances or is proportional to its temperature (ÇENGEL and BOULES, 2002).

Following the same line of approach proposed by Marques *et al.* (2018b), the thermal efficiency of SFR and SCWR could be a little higher, about 3%, if steam after leaving turbine was not condensed at 65 °C aiming the desalination process, but near at the 40 °C usually adopted in the steam Rankine power cycles (CARLSON *et al.*, 2019 and HABIBI *et al.*, 2019). This temperature represents the thermodynamic limit to condense water steam in order to avoid extremely low pressures or even vacuum inside condenser that can compromise its structural integrity. This physical behavior of water is represented in many thermodynamic diagrams, for instance, the ones available on The American Society of Heating, Refrigerating and Air-Conditioning Engineers (ASHRAE, 2017).

Continuing the analysis of each trigeneration case, in Graphs 26 and 27 are presented the values of exergy destroyed and exergy efficiency in each NPP as function of  $y$ .

**GRAPH 26 – Exergy destroyed for every NPP's in each trigeneration case**

Source: the author.

**GRAPH 27 – Exergy efficiency for every NPP's in each trigeneration case**

Source: the author.

Based on the last two graphs, it is verified that GT-MHR has the lowest values of exergy destroyed ( $125 \text{ MW} < E_D < 330 \text{ MW}$ ) and consequently it has the highest values of exergy efficiency ( $0.72 < \varepsilon < 0.82$ ). In contrast, SFR presents the highest exergy destroyed ( $280 \text{ MW} < E_D < 330 \text{ MW}$ ), what impacts on the less values of exergy efficiency ( $0.58 < \varepsilon < 0.63$ ). SCWR presents an intermediate behavior between GTMHR and SFR, but much more close to SCWR, presenting an exergy destruction varying from 270 MW to 330 MW with exergy efficiency ranging from 0.59 to 0.64. Such values of exergy efficiency are similar to other types of thermal power plants in development like the innovative solar tower proposed by Yilmaz *et al.* (2019b), which have exergy efficiency close to 58% or the hybrid biogas-geothermal power cycle evaluated by Rostamzadeh *et al.* (2018) whose exergy efficiency lies about 70%. The exergy destruction in all scenarios reduces in function of  $y$  because the working fluid is directed to the Na-O-H plant and not to the NPP's.

Generally, the exergy destroyed and exergy efficiency for the systems SCWR and SFR have potential to improvements if some technics to enhance the overall thermal efficiency of steam Rankine cycles were adopted like regeneration or reheating (ÇENGEL and BOULES, 2002). However, if such modifications were considered during system modeling in section 3.3, the complexity and consequently the analysis of such systems will be hampered because their number of components would increase. Still, even if those changes were adopted, SCWR and SFR probably will not be able to achieve the same standards of thermal efficiency as in GT-MHR because this last one works with helium at higher temperatures ( $850 \text{ }^\circ\text{C}$ ) than the other two facilities whose water working fluid operates at  $500\text{-}550 \text{ }^\circ\text{C}$ . This approach or the inclusion of regeneration or reheating are not necessary because the main aim of this thesis is to provide a first view on thermal aspects of systems under development, including GEN-IV technologies whose operation are expected to begin only beyond 2030.

Complementing the last paragraph, the quantity of electrical work, thermal efficiency, exergy destroyed and exergy efficiency observed are optimized. This is because during the modeling process of all NPP's, described in section 3.3, some considerations and assumptions related to them were made such as neglecting possible heat and pressure losses in all control volumes that impact on their final performance. Besides that, the systems analyzed and exhibited in Figures 23,

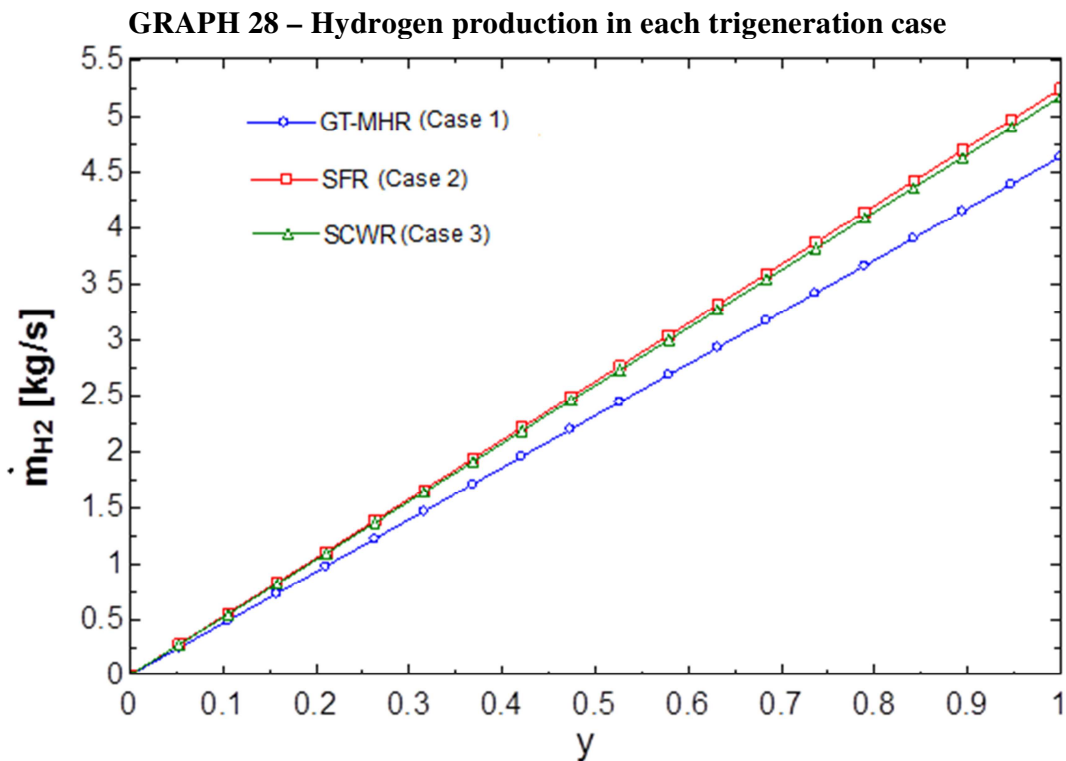
24 and 25 correspond to basic configurations or simplifications of actual power cycles with the minimum number of basic components necessary to their operation. In this way, some key devices essential to operate that kind of installation, for instance, valves, pipes, safety devices and others were not considered in the analysis. This same line of thinking also covers the Na-O-H hydrogen production unit and the MED desalination plant assessed. Additionally, the thermal analysis of each individual control volumes of every NPP is not performed in this section because the scope of the research is to evaluate the overall thermodynamic aspects of thermal power cycles in a trigeneration process of hydrogen, desalinated water and electricity and not the behavior of each device of every power plant. So, considering everything commented in this part of results chapter, it is possible to conclude that GT-MHR has the best thermal performance to produce electricity when compared to SFR and SCWR. However, in practical operations may happen deviations in the theoretical values of thermal efficiency of these three technologies in function of the simplifications and assumptions needed to develop the research, what could change the behavior related to electricity generation results discussed through section 4.6.

#### **4.7 Thermal aspects of hydrogen production in each trigeneration case**

In Graph 28 is presented the mass flow rate of H<sub>2</sub> obtained in the Na-O-H plant as function of the percentage of hot working fluid (y) coming from each nuclear power plant (cases 1, 2 and 3) that is directed to this H<sub>2</sub> production facility as schematized in Figure 21.

According to this diagram, SFR (case 2) and SCWR (case 3) are able to produce almost the same H<sub>2</sub> quantity, varying from 0 to 5.2 kg/s when y varies from 0 to 1. At the same time, GT-MHR (case 1) makes 0 to 4.5 kg/s of hydrogen considering the same gap for y, what represents a value 10% inferior when compared to the other two nuclear power plants. This fact is explained through the working fluid employed in each scenario. Despite He coolant in the GT-MHR has higher temperature (850 °C) than water/steam coolant in the systems SFR and SCWR (500-550 °C), H<sub>2</sub>O has higher standard specific heat (33.6 J/mol·K) than helium (20.8 J/mol·K) (LIDE, 2004). Consequently, water can release more heat to promote a same temperature reduction when compared to helium. In this way, supercritical water and steam are able to supply superior amount of heat to helium even having inferior temperature.

In comparison, relatively well-developed thermochemical water splitting cycles with a lot of information available, such as the four-step and the five-step variations of the Cu-Cl cycle studied by Al-Zareer *et al.* (2017a) and Al-Zareer *et al.* (2017b), which are apt to yield respectively 2 kg/s and 3.56 kg/s of H<sub>2</sub> together with some amount of electrical power starting from a SCWR with an thermal output energy of 2450 MW. Then, the Na-O-H cycle coupled to GEN-IV technologies can match in the future, though more research and development, the same standards as other promising thermochemical processes. The values of H<sub>2</sub> obtained in Graph 28 are theoretical and maximized ones in function of all assumptions and simplifications considered in section 3.4 to develop the work; in practical situations such amounts probably will decrease.



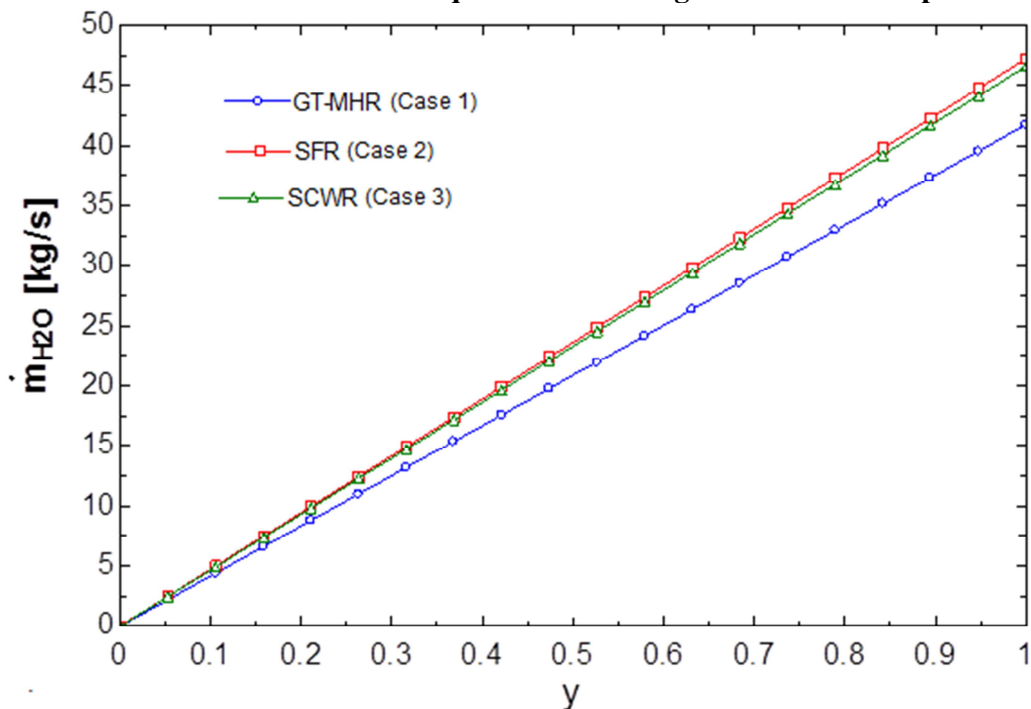
Source: the author.

Complementing the discussion introduced in the last two paragraphs, some of the largest H<sub>2</sub> production installations based on methane steam reforming, the main H<sub>2</sub> production method currently, produces 20-30 ton/h (5.5-8 kg/s) of this gas (TECHNIPFMC, 2018). The maximum amount of H<sub>2</sub> obtained from the 1000 MW GEN-IV systems analyzed in the thesis, 5 kg/s or 18 ton/h, have potential to compete with the largest hydrogen production facilities worldwide if the sodium-oxygen-hydrogen thermochemical procedure become a mature technology in the future.

The Na-O-H system, as any thermochemical water splitting method of H<sub>2</sub> production, demands a certain deal of water. The total quantity of H<sub>2</sub>O consumed in this cycle depends on the amount of H<sub>2</sub> yield that is associated to the stoichiometric proportions of the chemical reactions of the cycle represented by Equations (18), (19) and (20). So, complementing Graph 28, in Graph 29 is introduced the total mass flow rate of water needed in each case to make H<sub>2</sub> in function of  $y$ .

As the amount of water required in each case is proportional to the quantity of H<sub>2</sub> produced, the overall behavior of water mass flow rate in Graph 29 follows a similar pattern to that one previously described in Graph 28. After checking Graph 29, it is verified that cases 2 and 3 require 0 to 47 kg/s of H<sub>2</sub>O when  $y$  increases from 0 to 1. In relation to the case 1, the quantity of water demanded increases from 0 to 40 kg/s for the interval  $0 < y < 1$ . As it is being commented in the next section, the deal of desalinated water produced in each trigeneration case is enough to attend the water demand in the Na-O-H hydrogen production installation.

**GRAPH 29 – Amount of water required in each trigeneration case to produce H<sub>2</sub>**



Source: the author.

Besides H<sub>2</sub>O, a thermochemical cycle necessary requires other chemical compounds. In this way, in Table 10 are presented the mass flow rate of each chemical in the Na-O-H cycle needed to



produce 1 and 5 kg/s of H<sub>2</sub>. The values presented in this table are regardless cases 1, 2 or 3 and only depends on the stoichiometric molar proportions from Equations (18), (19) and (20) converted into mass flow rate in Chart 14.

**TABLE 10 – Mass flow rate for every chemical in the Na-O-H cycle in function of H<sub>2</sub>**

$\dot{m}_{\text{H}_2}$	$\dot{m}_{\text{Na}}$	$\dot{m}_{\text{NaOH}}$	$\dot{m}_{\text{Na}_2\text{O}}$	$\dot{m}_{\text{Na}_2\text{O}_2}$	$\dot{m}_{\text{H}_2\text{O}}$	$\dot{m}_{\text{O}_2}$
[kg/s]	[kg/s]	[kg/s]	[kg/s]	[kg/s]	[kg/s]	[kg/s]
1	23	40	63	32	9	8
5	115	200	315	160	45	40

Source: the author.

In relation to the energy aspects of the Na-O-H system, after analyzing the production of each 1 kg/s of H<sub>2</sub> with Equations (18) to (20), it is noticeable that chemical reactor 1 demands 5 MW, chemical reactor 2 requests 163 MW while chemical reactor 3 releases 26.5 MW. Because of this, reaction 1 (H<sub>2</sub> production step) and reaction 2 (metal separation phase) are endothermic while reaction 3 (hydrolysis step) is exothermic. This behavior does not depend on the case under attention, but only relies on the  $\Delta H$  of reactions suggested by Equations (18), (19) and (20).

Considering that hydrogen has a mean enthalpy of combustion close to 286 kJ/mol or 143000 kJ/kg (OLIVEIRA, 2012), a mass flow rate of 1 kg/s of H<sub>2</sub> implies on a potential thermal energy of 143 MW. Regarding this thermal potential energy of H<sub>2</sub> and the net heat value required by the system through chemical reactors 1 (5 MW) and 2 (163 MW) explained in the last paragraph, it infers that the sodium-oxygen-hydrogen production unit has energy efficiency around 80%, considering the ratio between the energy released by 1 mol of H<sub>2</sub> (143 MW) and the total energy demanded by chemical chambers 1 and 2 (168 MW) to produce such amount of hydrogen gas.

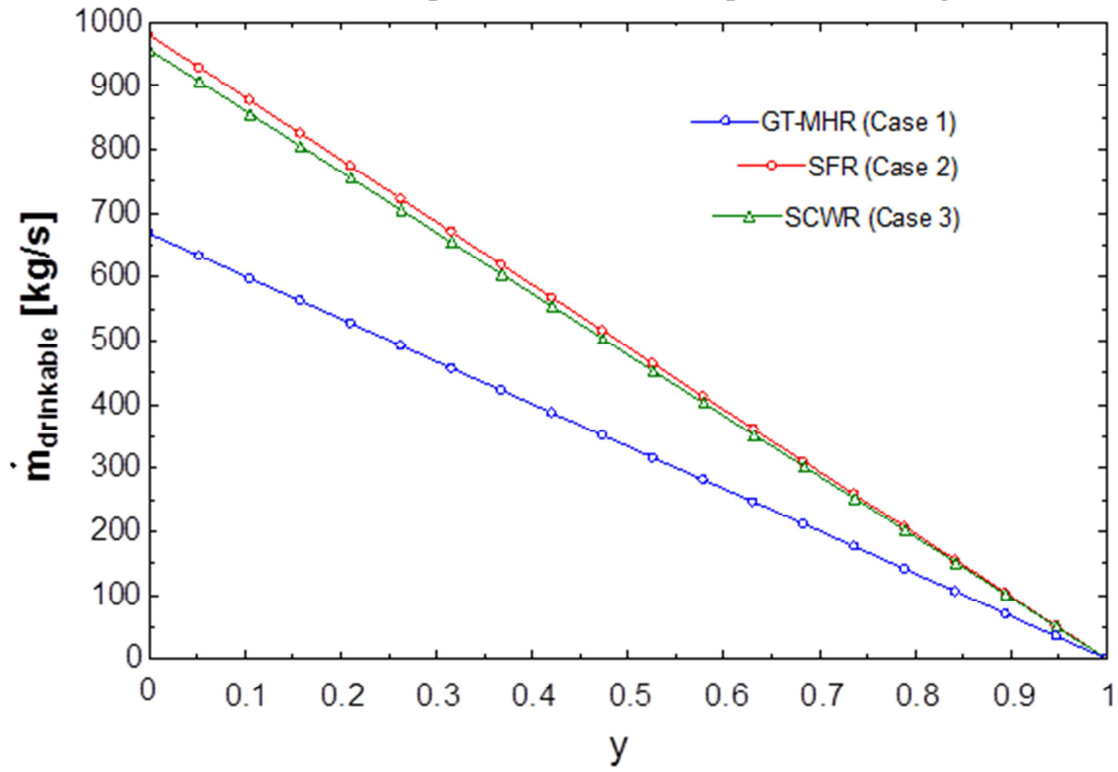
In relation to chemical reactor 2, just looking to the stoichiometric of Equation (19), it would demand a total quantity of 265 MW aiming the making of 1 kg/s of H<sub>2</sub>, resulting in energy efficiency about 50% instead of the 80% commented in the last paragraph. However, from this total of 265 MW, 102 MW (38%) is provided by condensing sodium gas formed in reactor 2 to attempt chemical chamber 1 itself that needs liquid sodium as exhibited in Figure 22 and Equation (18). The remaining 163 MW introduced in the penultimate paragraph are supplied by the working fluid coming from each NPP. This approach enhances the overall thermal performance of the Na-O-H unit due to the need of less thermal energy from nuclear reactors.

Finally, after evaluating the exergy aspects of the Na-O-H cycle associated with the exergy analyses performed for its reactions in sections 3.2.2 and 4.5 in addition to the H<sub>2</sub> plant in Chart 17, it observes that for each 1kg/s of H<sub>2</sub> produced: chemical reactor 1 has exergy efficiency of 96% and exergy destroyed of 4.5 MW; chemical chamber 2 destroys 100 MW and has exergy efficiency of 58%; chemical reactor 3 has exergy efficiency of 87% and destroys 9 MW of exergy. These values are weakly dependent on the scenarios evaluated and they are mainly flagged by the thermodynamic behavior described in sections 4.2 to 4.5 related to the reactions of the Na-O-H cycle and not by the heat source that drives the process. Additionally, the Na-O-H cycle has a theoretical overall exergy efficiency of 80% and destroys 113.5 MW to produce 1 kg/s of H<sub>2</sub>. This relatively high value of exergy efficiency for the Na-O-H cycle, and also to other thermochemical routes, can be explained because the energy provided to the system is used to produce H<sub>2</sub>, a substance with relatively high chemical exergy (236 kJ/mol). The values of exergy and energy efficiencies for the Na-O-H cycle probably will decrease in practical situations.

In a complementary manner, relatively well-known thermochemical cycles under research and development, for example, variations of the Cu-Cl system assessed by Ishaq and Dincer (2019) have energy and exergy efficiencies around 40% and 70% while the Mg-Cl process evaluated by Balta *et al.* (2012) has energy and exergy efficiencies near 63% and 34%, respectively.

#### **4.8 Thermal aspects of desalinated water production in each trigeneration case**

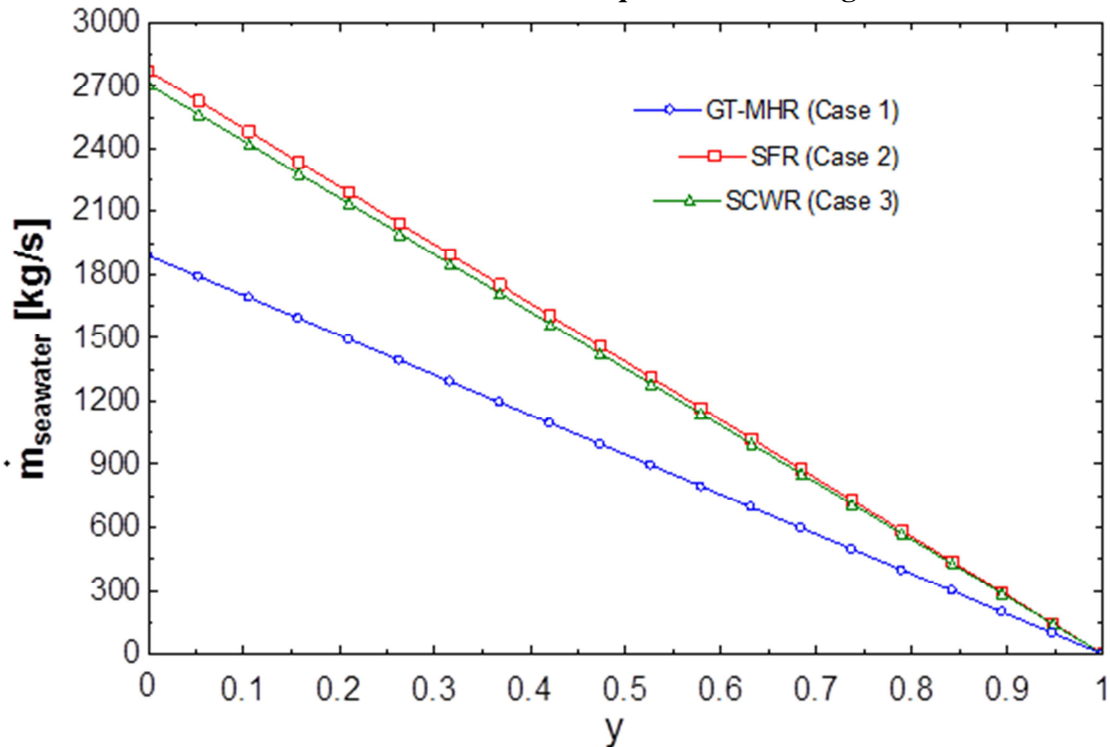
The mass flow rate of desalinated water produced in every trigeneration case is exhibited in Graph 30. As it can be checked in such diagram, SFR and SCWR, cases 2 and 3, make 0 to 980 kg/s (0.98 m<sup>3</sup>/s or 84,670 m<sup>3</sup>/day) of drinkable H<sub>2</sub>O when  $y$  varies from 0 to 1. Considering this same interval for  $y$ , GT-MHR (case 3) makes up to 670 kg/s (0.67 m<sup>3</sup>/s or 59,610 m<sup>3</sup>/day) of fresh one. All this water quantity have possibility to enhancements, around 50%, if some variations of the MED system were adopted like those ones already exemplified over section 2.6 that were proposed by Wang *et al.* (2011), Christ *et al.* (2015b) or Dastgerdi *et al.* (2016). In comparison, the largest MED desalination plant in the world, Marafiq IWPP built in Saudi Arabia, has a production capacity around 800,000 m<sup>3</sup>/day (PINTO and MARQUES, 2017). Al-Mutaz and Wazeer (2015) relate that this installation has 27 desalination units, each one composed by 8 effects, against the 6-effect single unit MED evaluated in the work.

**GRAPH 30 – Desalinated water produced in the MED plant in each trigeration case**

Source: the author.

For all situations, the recovery rate of pure water from saline one is 0.35, a typical value for a MED installation, what is in agreement with some already validated researches like the one carried out by Dastgerdi *et al.* (2016). The quantity of sea water requested in each scenario to produce potable H<sub>2</sub>O in Graph 30 is exhibited in Graph 31.

Comparing information from Graphs 29 and 30, it is noticeable that the amount of potable H<sub>2</sub>O distilled in all cases is more than enough to attend water demand in the Na-O-H hydrogen production facility. In this way, the remaining water excess could be used in essential human activities like agriculture and drinking. In this last situation, considering that each person demands around 110 liters of water per day (0.0013 kg/s), considering all their needs like washing and just not drinking, as recommend United Nations (UOL, 2015), the excess of H<sub>2</sub>O, near 950 kg/s when  $y = 1$ , is enough to provided water to about 730 mil people in cases 2 and 3 or 537 mil people in the event of case 1 due to a H<sub>2</sub>O surplus near 700 kg/s. SFR and SCWR have potential to produce more H<sub>2</sub>O because their working fluids are able to provide further energy as explanation given at the end of section 4.6.

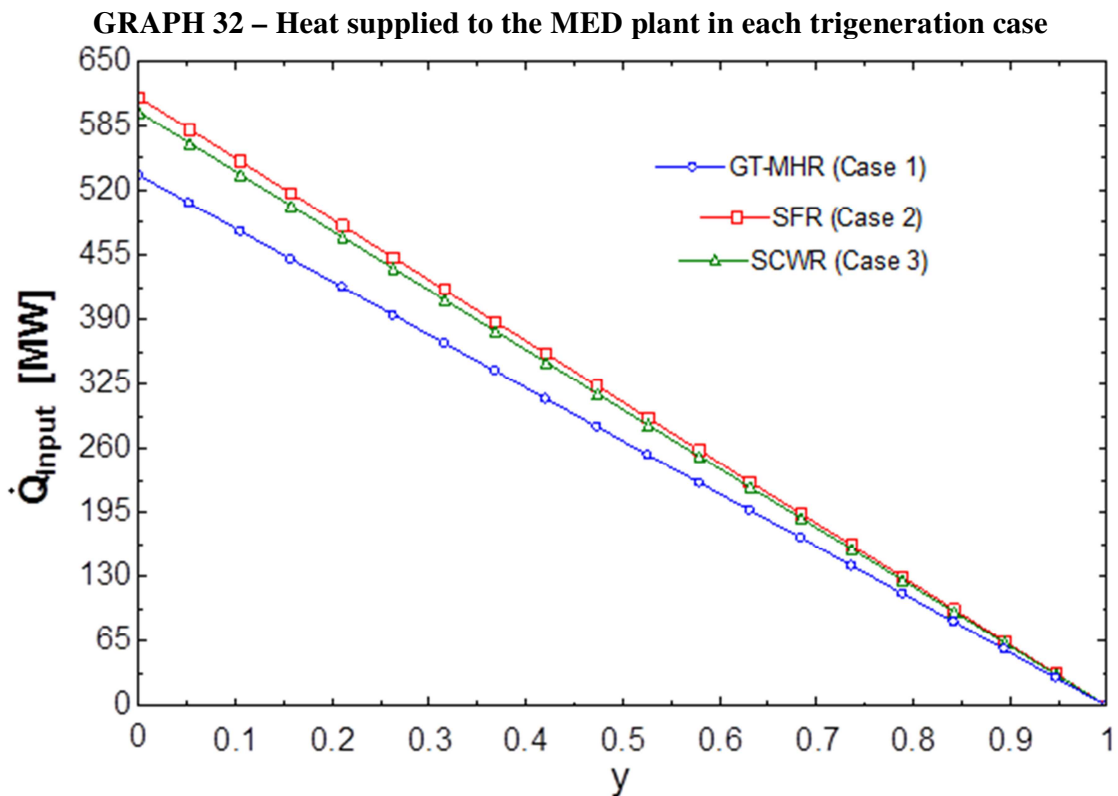
**GRAPH 31 – Sea water mass flow rate required in each trigeneration case**

Source: the author.

The overall heat released by each condenser (in the cases of SFR and SCWR) or coolers (in the instance of GT-MHR) to the MED plant in function of  $y$  is presented in Graph 32. This energy is the driven force for this kind of desalination technology. In the matter of GT-MHR, it releases around 550 MW when  $y = 0$  while SFR and SCWR provide near to 600 MW. These amounts of heat linearly diminish until 0 when  $y$  increases till 1, due to using the working fluid from nuclear reactors only to produce  $H_2$  in the Na-O-H plant and not electricity and desalinated water in the NPP's.

Following same lines of thinking from the last two paragraphs, source data provided by IEA (2018) accounts that 26700 TWh/year (3.048 TW) of electrical power were generated worldwide in 2018. From this total, 74% were secured from coal, gas, oil and nuclear. Usually, this kind of resources produce electricity through some energy conversion system like a Brayton or a steam Rankine power cycles. Considering an averaged estimated efficiency value near 40% for all these technologies and the total amount of electricity generated by them, it would be rejected close to 3.31 TW to the environment through their coolers or condensers. If all this quantity of waste heat

could be recovered in a MED installation like that one in Figure 26, it would be produced about  $4.96 \times 10^6$  kg/s of desalinated  $H_2O$ . This quantity has potential to attend the necessities of around 4.0 billion people. In this way, a potential solution to the present and future lack of potable  $H_2O$  in the world already exist, being necessary to find the better way to take advantage of it, considering that most of thermal power plants were not designed to operate together with a MED unit.



Source: the author.

Considering the values of drinkable water made in Graph 30 and the total energy supplied to the systems in Graph 32, it concludes that the MED facility analyzed has a specific thermal energy consumption of  $0.6 \text{ MW}/(\text{kg/s of } H_2O)$ , equivalent to  $166 \text{ kWh}/\text{m}^3$ . This value is similar to the  $0.67 \text{ MW}/(\text{kg/s of } H_2O)$  found in the paper of Dastgerdi *et al.* (2016) when they provide  $5.42 \text{ MW}$  to distill  $8 \text{ kg/s}$  of drinkable  $H_2O$ . The quantity of  $166 \text{ kWh}/\text{m}^3$  computed in the present research is far above when compared to the mean typical thermal energy consumption which varies from  $6$  to  $16 \text{ kWh}/\text{m}^3$  in the event of the traditional MED plants around the world reported in the studies of Eltawil *et al.* (2009) and Youssef *et al.* (2014). Such energy requirement is

mainly flagged by the Marafiq IWPP, the largest multi-effect distillation installation worldwide. The superior energy consumption to produce potable water in the MED system assessed in the present research when compared to the conventional multi-effect distillation plants is explained below mainly due to two aspects related to the classical MED facilities exemplified by the Marafiq IWPP.

First matter, this installation is a hybrid power-desalination plant that operates according to a power blocks of gas-fired turbines (AL-SUBAIE, 2007) based on a Brayton cycle which usually has thermal efficiency and also operational temperature higher than the Rankine power cycles (ÇENGEL and BOULES, 2002). This last one covers SFR and SCWR nuclear power plants. The upper temperature limit makes possible to increase the net amount of fresh water produced in addition to enhance the number of desalination effects in the system, as discussed in section 2.4, raising the final amount of drinkable H<sub>2</sub>O obtained in it.

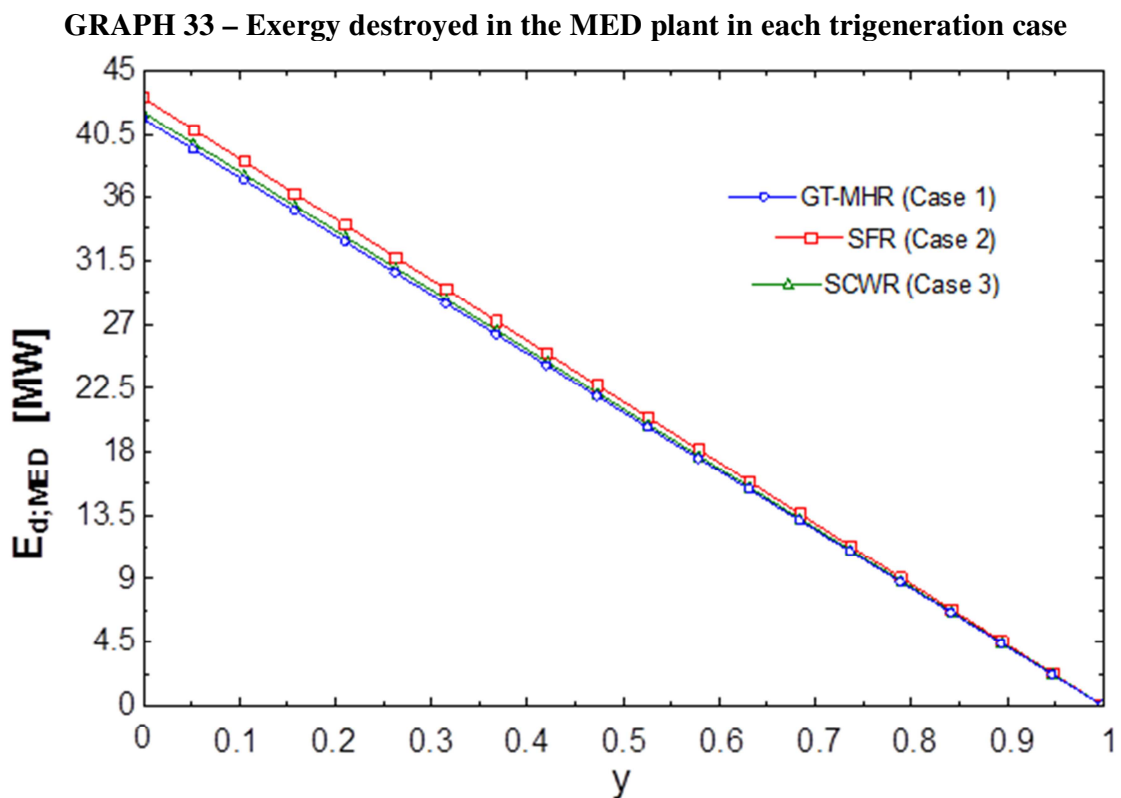
This last fact is sustained after analyzing the results and conclusions reported in the paper of Christ *et al.* (2015a), where such authors concluded that the production rate of desalinated water can increase about seven times if the temperature limits related to the heat sources enhance from 65 °C to 95 °C. If this approach were considered during system modeling, especially for SFR and SCWR, the global fresh water production rate would have potential to increase around seven times due to the possibility to rise the number of desalination effects in the system, but keeping a much closer level of energy released by the working fluid to the MED system considering this gap of temperature because the enthalpy of vaporization are almost the same at 65 °C or 95 °C for the particular case of water, as can be checked in thermodynamic property tables from Moran *et al.* (2011). However, this measure reduces the thermal efficiency of those NPP's.

Second fact, Marafiq IWPP uses a TVC (thermal vapor compression) technology capable to recover low grade steam to further increase the production rate of H<sub>2</sub>O and the overall thermal efficiency of the installation. The adoption of TVC is becoming a common practice to raise the efficiency of thermal systems like power plants and also desalination installations as Al-Mutaz and Wazeer (2014) beyond Chen *et al.* (2019) relate in their studies. These two aspects combined contribute to increase the overall water quantity yield in the Marafiq IWPP, but consuming a

relatively low amount of energy, impacting on the low energy consumption in MW by each  $\text{m}^3$  gained in this installation.

Despite presenting high energy consumption when compared to conventional MED plants, the trigeneration cases proposed in this ongoing research employ waste heat sources that would be rejected to the environment anyway. This kind of energy have low temperature and consequently low potential to produce work or other useful effect, because they have low exergy content, what also justifies their low yield when compared to other MED installation that uses heat source at relatively high exergy content like the Marafiq IWPP desalination installation. Despite this drawback, the amount of desalinated water produced in the proposed trigeneration cases is adequate to attempt the water demand of many people.

Finally, the exergy destroyed in the MED plant are shown in Graph 33.



Source: the author.

Consonant this last picture, the maximum exergy destroyed for all scenarios is 42 MW when  $y = 0$ . Then, it linearly diminishes until 0 when  $y$  increases until 1. All cases present similar values of exergy destroyed because in all of them the MED plant operates at much close operational condition, including a 4 °C temperature difference between each effect. With the quantities of exergy added to the system through its first effect, in addition to the total exergy destroyed in the installation, both in function of  $y$ , it concludes that this MED plant has an overall exergy efficiency close to 57% despite the case under attention.

After everything discussed in this topic, it was concluded that SFR and SCWR are better options to produce desalinated water than GT-MHR because they attain more H<sub>2</sub>O than the last one but keeping the same standards of exergy destroyed. However, in practical operations may happen deviations in the theoretical values of desalinated water production in function of the simplifications and assumptions necessary to develop the thesis related to the systems GEN-IV and MED, what could change the behavior related to the results discussed through section 4.7.

#### **4.9 The best option to trigenerate H<sub>2</sub>, electricity and desalinated water**

Consonant with the results discussed in sections 4.6, 4.7 and 4.8, the trigeneration process evaluated has potential to produce around 5 kg/s of hydrogen, 400 MW of electricity and 800 kg/s of desalinated H<sub>2</sub>O. Such values can have little variation depending on the GEN-IV considered as the energy source as can be seen in Graphs 25, 28 and 30. These are theoretical and maximized values in function of all the simplifications and assumptions made to model all the trigeneration cases. Because of this, it is expected that the values found in the research related to the production of electricity, H<sub>2</sub> and fresh water decrease in practical situations.

SCWR and SFR were considered the best options to produce those three goods because they have potential to produce H<sub>2</sub> and electricity in similar quantities to GT-MHR, but they have potential to produce more fresh water than GT-MHR. However, SCWR is considered the best trigeneration case even when compared to SFR because SCWR is a simplified Rankine cycle, what naturally demands fewer components in the system in comparison to SFR that have a full Rankine cycle in addition to two sodium loops, as can be verified in Figures 8 and 9. Such characteristic tends to facilitate an actual operation of SCWR.



## 5 THERMODYNAMIC STUDY ABOUT VARIATIONS OF THE Na-O-H CYCLE

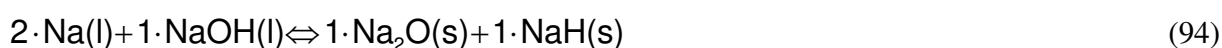
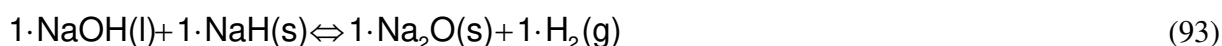
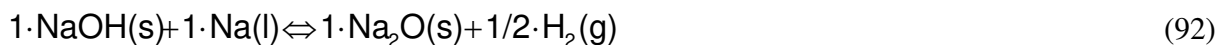
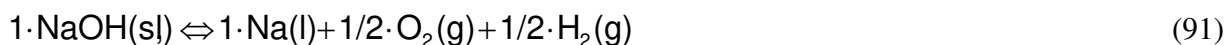
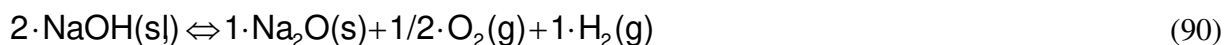
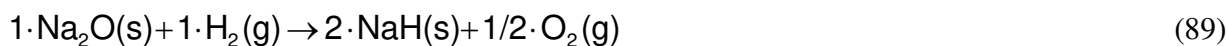
Aiming to increase the thermal performance of the Na-O-H cycle, the second main goal of this work is to analyze different variations (a, b, c, d and e) of such system to determine if one of them has better thermal aspects compared to its traditional form, variation (a), first proposed by Miyaoka *et al.* (2012) and previously discussed in subsection 2.2.4. This aim is accomplished by comparing the enthalpy ( $\Delta H$ ), entropy ( $\Delta S$ ) and Gibbs free energy ( $\Delta G$ ) changes plus energy efficiency ( $\eta$ ) for all variations of the Na-O-H trial, considering standard conditions of pressure and temperature for all the chemical reactions involved in all forms of such method. All configurations studied are obtained from the ternary system Na-NaOH-Na<sub>2</sub>O-NaH explained in section 5.1.

### 5.1 The reciprocal ternary system Na-NaOH-Na<sub>2</sub>O-NaH and its chemical reactions

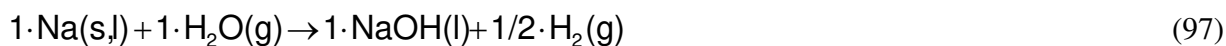
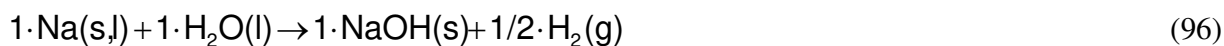
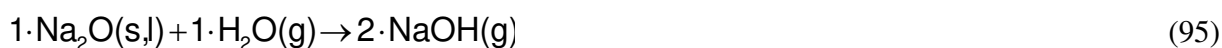
In a simple way, the reciprocal ternary system Na-NaOH-Na<sub>2</sub>O-NaH is a combination or mixture of specific chemical substances that can coexist together at certain conditions of pressure and temperature beyond the composition of the chemicals involved in the process. The substances usually related to this ternary system are: Na (sodium metal); NaOH (sodium hydroxide); NaH (sodium hydride); Na<sub>2</sub>O (sodium or disodium oxide) and also Na<sub>2</sub>O<sub>2</sub> (sodium or disodium peroxide) in some cases.

Some possible chemical reactions related to the ternary system Na-NaOH-Na<sub>2</sub>O-NaH are now presented. These equations mainly can be found in the paper published by Gnanasekaran (1999) and also in other references such as Ivanovskii and Kozlov (1964), Addison *et al.* (1965), Newman and Smith (1974), Veleckis and Leibowitz (1987), Xu *et al.* (2006), Borgstedt (2012), Draley and Weeks (2013) plus Mao *et al.* (2015) that also studied this ternary system. Such chemical transformations are grouped into Equations (86) to (94).





Other chemical reactions associated with the Na-NaOH-Na<sub>2</sub>O-NaH system are in Equations (95), (96), (97) and (98) adapted from Newman and Smith (1974).



Later in section 5.3, all the reactions presented in this topic are combined to build some chemical cyclic processes mainly based on the substances Na, NaOH, Na<sub>2</sub>O and NaH, thus making the Na-O-H (sodium-hydrogen-oxygen) thermochemical water splitting cycle of hydrogen production together with some of its possible variations.

## 5.2 Generic thermochemical water splitting cycle

In general, a thermochemical water splitting cycle consists of a bunch of cyclic chemical reactions able to produce both H<sub>2</sub> and O<sub>2</sub> gases from cracking H<sub>2</sub>O molecules. A generic thermochemical cycle is exemplified using Equations (99), (100) and (101).





Following this example and using a combination of chemical reactions (86) to (98) introduced in section 5.1 from the reciprocal ternary system Na-NaOH-Na<sub>2</sub>O-NaH, it is possible to arrange different configurations of the sodium-oxygen-hydrogen method as shown in section 5.3. In the specific case of such cycle of H<sub>2</sub> making, the generic substances A, B, C, D e E in reactions (99), (100) and (101) are replaced by substances composed by the elements Na, O and H like NaH, Na<sub>2</sub>O and NaOH.

The thermochemical trials presented in next section are evaluated and compared according to changes in their enthalpy, entropy and Gibbs free energy in addition to energy efficiency for chemical reactions at standard conditions of p and T, in order to determine which configuration of the Na-O-H cycle has the better thermodynamic aspects to produce 1 mol of hydrogen gas.

### 5.3 Thermodynamic modeling of variations of the Na-O-H cycle

In subtopics 5.3.1 to 5.3.6 of this section are introduced different modes, variations (a) to (e), of the sodium-oxygen-hydrogen thermochemical water splitting cycle based on Equations (86) to (98) lodged over section 5.1. All forms of the Na-O-H procedure are assessed considering the following steps:

- Presentation of the chemical reactions involved in each cycle mode together with their reactants and products, always aiming the production of 1 mole of H<sub>2</sub> for all Na-O-H method variations: (Na-O-H)<sub>a</sub>, (Na-O-H)<sub>b</sub>, (Na-O-H)<sub>c</sub>, (Na-O-H)<sub>d</sub>, and (Na-O-H)<sub>e</sub>;
- Application of enthalpy, entropy and Gibbs free energy changes for every reaction that compose each cycle variation as previously done in subsection 3.2.1;
- Application of these same physical principles together with energy efficiency calculation for all the thermochemical trials like in Equations (35) and (36).
- All chemical reactions and cycles are evaluated under standard conditions of pressure ( $p^0 = 1 \text{ bar}$ ) and temperature ( $T^0 = 25 \text{ }^\circ\text{C}$ ). So, they are used standard molar enthalpy of formation ( $\bar{h}_f^0$ ) and standard molar entropy ( $\bar{s}^0$ ) from Table 11 (NIST, 2018 and LIDE,

2004) combined with Table 2 to perform all the calculations in section 5.4 which results are noted in section 5.5.

- As all the chemical reactions evaluated in this chapter are under standard conditions, the entropy generation ( $S_G$ ) becomes into the entropy change ( $\Delta S$ ) because there is no heat exchanged ( $Q = 0$ ). It happens because the reactions were analyzed considering that products and reactants are at the same standard temperature (25 °C).

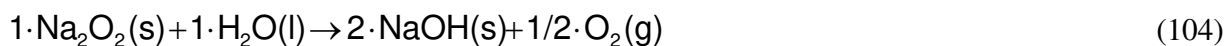
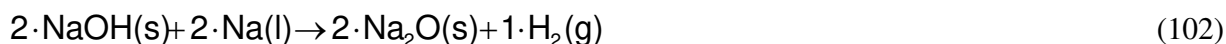
**Table 11 - Standards enthalpy of formation and entropy for Na compounds**

Chemicals	$\bar{h}_f^0$ [kJ/mol]	$\bar{S}^0$ [J/mol*K]
Na (s)	0	51.46
Na (l)	2.41	57.86
Na (g)	107.30	153.65
NaOH (s)	-425.93	64.46
NaOH (l)	-416.88	75.91
NaOH (g)	-197.76	228.47
NaH (s)	-56.44	40.03
Na <sub>2</sub> O (s)	-417.98	75.04
Na <sub>2</sub> O <sub>2</sub> (s)	-513.21	94.78

Source: NIST (2018) and Lide (2004).

### 5.3.1 Modeling Na-O-H cycle – variation (a) – (Na-O-H)<sub>a</sub>

Variation (a) is composed by three chemical steps represented by Equations (102), (103) and (104). It is the classic form of the Na-O-H process first proposed by Miyaoka *et al.* (2012).



Additionally, the condensation of Na(g) from Equation (103) to be used as Na(l) in Equation (102) could be represented by Equation (105) as a physical change and not as a chemical step. Variation (a) and its reactions are modeled through Equations (106) to (119).



(i) Modeling hydrogen production step – Reaction 1 – Eq. (102)

Reaction 1 of variation (a) of the Na-O-H cycle is modeled according to Equations (106) to (108).

$$\Delta H^0_{a.1} = (\mathbf{N} \cdot \bar{h}_f^0)_{\text{Na}_2\text{O}(s)} + (\mathbf{N} \cdot \bar{h}_f^0)_{\text{H}_2(g)} - (\mathbf{N} \cdot \bar{h}_f^0)_{\text{NaOH}(s)} - (\mathbf{N} \cdot \bar{h}_f^0)_{\text{Na}(l)} \quad (106)$$

$$\Delta S^0_{a.1} = (\mathbf{N} \cdot \bar{s}^0)_{\text{Na}_2\text{O}(s)} + (\mathbf{N} \cdot \bar{s}^0)_{\text{H}_2(g)} - (\mathbf{N} \cdot \bar{s}^0)_{\text{NaOH}(s)} - (\mathbf{N} \cdot \bar{s}^0)_{\text{Na}(l)} \quad (107)$$

$$\Delta G^0_{a.1} = \Delta H^0_{a.1} - T^0 \cdot \Delta S^0_{a.1} \quad (108)$$

(ii) Modeling metal separation step – Reaction 2 – Eq. (103)

Reaction 2 of (Na-O-H)<sub>a</sub> is evaluated using Equations (109) to (111).

$$\Delta H^0_{a.2} = (\mathbf{N} \cdot \bar{h}_f^0)_{\text{Na}_2\text{O}_s(s)} + (\mathbf{N} \cdot \bar{h}_f^0)_{\text{Na}(g)} - (\mathbf{N} \cdot \bar{h}_f^0)_{\text{Na}_2\text{O}(s)} \quad (109)$$

$$\Delta S^0_{a.2} = (\mathbf{N} \cdot \bar{s}^0)_{\text{Na}_2\text{O}_s(s)} + (\mathbf{N} \cdot \bar{s}^0)_{\text{Na}(g)} - (\mathbf{N} \cdot \bar{s}^0)_{\text{Na}_2\text{O}(s)} \quad (110)$$

$$\Delta G^0_{a.2} = \Delta H^0_{a.2} - T^0 \cdot \Delta S^0_{a.2} \quad (111)$$

(iii) Modeling hydrolysis step – Reaction 3 – Eq. (104)

Equations (112) to (114) are applied to assessed reaction 3 of variation (a) of the sodium-oxygen-hydrogen cycle.

$$\Delta H^0_{a.3} = (\mathbf{N} \cdot \bar{h}_f^0)_{\text{NaOH}(s)} + (\mathbf{N} \cdot \bar{h}_f^0)_{\text{O}_2(g)} - (\mathbf{N} \cdot \bar{h}_f^0)_{\text{Na}_2\text{O}_2(s)} - (\mathbf{N} \cdot \bar{h}_f^0)_{\text{H}_2\text{O}(l)} \quad (112)$$

$$\Delta S^0_{a.3} = (\mathbf{N} \cdot \bar{s}^0)_{\text{NaOH}(s)} + (\mathbf{N} \cdot \bar{s}^0)_{\text{O}_2(g)} - (\mathbf{N} \cdot \bar{s}^0)_{\text{Na}_2\text{O}_2(s)} - (\mathbf{N} \cdot \bar{s}^0)_{\text{H}_2\text{O}(l)} \quad (113)$$

$$\Delta G^0_{a.3} = \Delta H^0_{a.3} - T^0 \cdot \Delta S^0_{a.3} \quad (114)$$

(iv) Modeling sodium condensation phase – Eq. (105)

Sodium condensation is analyzed using Equation (115).

$$\Delta H^0_{a.4} = (\mathbf{N} \cdot \bar{h}_f^0)_{\text{Na}(l)} - (\mathbf{N} \cdot \bar{h}_f^0)_{\text{Na}(g)} \quad (115)$$

(v) Modeling Na-O-H cycle – variation (a)

Equations (116) to (119) are applied to evaluate the thermodynamic aspects of (Na-O-H)<sub>a</sub>.

$$\Delta H^0_a = \Delta H^0_{a.1} + \Delta H^0_{a.2} + \Delta H^0_{a.3} + \Delta H^0_{a.4} \quad (116)$$

$$\Delta S^0_a = \Delta S^0_{a.1} + \Delta S^0_{a.2} + \Delta S^0_{a.3} \quad (117)$$

$$\Delta G^0_a = \Delta G^0_{a.1} + \Delta G^0_{a.2} + \Delta G^0_{a.3} \quad (118)$$

$$\eta_a = \frac{(\Delta H_{\text{combustion}})_{\text{H}_2(\text{g})}}{\Delta H^0_a} \quad (119)$$

**5.3.2 Modeling Na-O-H cycle – variation (b) – (Na-O-H)<sub>b</sub>**

Equations (120), (121) and (122) constitute variation (b) of the Na-O-H thermochemical trial. This form and its reactions are studied according to Equations (123) to (135).



(i) Modeling sodium hydroxide decomposition step – Reaction 1 – Eq. (120)

Reaction 1 of variation (b) of the Na-O-H cycle is modeled according to Equations (123) to (125).

$$\Delta H^0_{b.1} = (\mathbf{N} \cdot \bar{h}_f^0)_{\text{NaH}(\text{s})} + (\mathbf{N} \cdot \bar{h}_f^0)_{\text{O}_2(\text{g})} - (\mathbf{N} \cdot \bar{h}_f^0)_{\text{NaOH}(\text{s})} \quad (123)$$

$$\Delta S^0_{b.1} = (\mathbf{N} \cdot \bar{s}^0)_{\text{NaH}(\text{s})} + (\mathbf{N} \cdot \bar{s}^0)_{\text{O}_2(\text{g})} - (\mathbf{N} \cdot \bar{s}^0)_{\text{NaOH}(\text{s})} \quad (124)$$

$$\Delta G^0_{b.1} = \Delta H^0_{b.1} - T^0 \cdot \Delta S^0_{b.1} \quad (125)$$

(ii) Modeling sodium hydride decomposition (hydrogen releasing) step – Reaction 2 – Eq. (121)

Reaction 2 of (Na-O-H)<sub>b</sub> is evaluated using Equations (126) to (128).

$$\Delta H_{b,2}^0 = (\mathbf{N} \cdot \bar{h}_f^0)_{\text{Na(l)}} + (\mathbf{N} \cdot \bar{h}_f^0)_{\text{H}_2(\text{g})} - (\mathbf{N} \cdot \bar{h}_f^0)_{\text{NaH(s)}} \quad (126)$$

$$\Delta S_{b,2}^0 = (\mathbf{N} \cdot \bar{s}^0)_{\text{Na(l)}} + (\mathbf{N} \cdot \bar{s}^0)_{\text{H}_2(\text{g})} - (\mathbf{N} \cdot \bar{s}^0)_{\text{NaH(s)}} \quad (127)$$

$$\Delta G_{b,2}^0 = \Delta H_{b,2}^0 - T^0 \cdot \Delta S_{b,2}^0 \quad (128)$$

(iii) Modeling hydrolysis (hydrogen releasing) step – Reaction 3 – Eq. (122)

Equations (129) to (131) are applied to assessed reaction 3 of variation (b) of the sodium-oxygen-hydrogen cycle.

$$\Delta H_{b,3}^0 = (\mathbf{N} \cdot \bar{h}_f^0)_{\text{NaOH(s)}} + (\mathbf{N} \cdot \bar{h}_f^0)_{\text{H}_2(\text{g})} - (\mathbf{N} \cdot \bar{h}_f^0)_{\text{Na(l)}} - (\mathbf{N} \cdot \bar{h}_f^0)_{\text{H}_2\text{O(l)}} \quad (129)$$

$$\Delta S_{b,3}^0 = (\mathbf{N} \cdot \bar{s}^0)_{\text{NaOH(s)}} + (\mathbf{N} \cdot \bar{s}^0)_{\text{H}_2(\text{g})} - (\mathbf{N} \cdot \bar{s}^0)_{\text{Na(l)}} - (\mathbf{N} \cdot \bar{s}^0)_{\text{H}_2\text{O(l)}} \quad (130)$$

$$\Delta G_{b,3}^0 = \Delta H_{b,3}^0 - T^0 \cdot \Delta S_{b,3}^0 \quad (131)$$

(iv) Modeling Na-O-H cycle – variation (b)

Equations (132) to (135) are applied to evaluate the thermodynamic aspects of (Na-O-H)<sub>b</sub>.

$$\Delta H_b^0 = \Delta H_{b,1}^0 + \Delta H_{b,2}^0 + \Delta H_{b,3}^0 \quad (132)$$

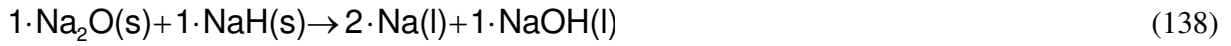
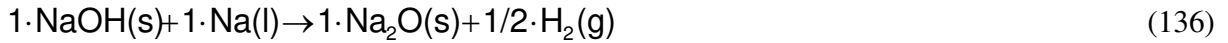
$$\Delta S_b^0 = \Delta S_{b,1}^0 + \Delta S_{b,2}^0 + \Delta S_{b,3}^0 \quad (133)$$

$$\Delta G_b^0 = \Delta G_{b,1}^0 + \Delta G_{b,2}^0 + \Delta G_{b,3}^0 \quad (134)$$

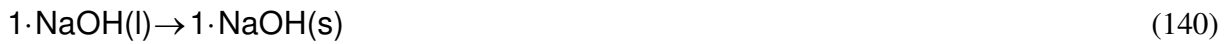
$$\eta_b = \frac{(\Delta H_{\text{combustion}})_{\text{H}_2(\text{g})}}{\Delta H_b^0} \quad (135)$$

**5.3.3 Modeling Na-O-H cycle – variation (c) – (Na-O-H)<sub>c</sub>**

Na-O-H thermochemical procedure variation (c) is represented by Equations (136), (137), (138) and (139).



Additionally, the solidification of NaOH(l) from Equation (138) to be used as NaOH(s) in Equation (136) or Equation (138) could be represented by Equation (140) as a physical change and not as a chemical process. Such cycle and its chemical reactions are evaluated following the steps described by Equations (141) to (157).



(i) Modeling hydrogen production step – Reaction 1 – Eq. (136)

Reaction 1 of variation (c) of the Na-O-H cycle is modeled according to Equations (141) to (143).

$$\Delta H^0_{c.1} = (\mathbf{N} \cdot \bar{h}_f^0)_{\text{Na}_2\text{O(s)}} + (\mathbf{N} \cdot \bar{h}_f^0)_{\text{H}_2\text{(g)}} - (\mathbf{N} \cdot \bar{h}_f^0)_{\text{NaOH(s)}} - (\mathbf{N} \cdot \bar{h}_f^0)_{\text{Na(l)}} \quad (141)$$

$$\Delta S^0_{c.1} = (\mathbf{N} \cdot \bar{s}^0)_{\text{Na}_2\text{O(s)}} + (\mathbf{N} \cdot \bar{s}^0)_{\text{H}_2\text{(g)}} - (\mathbf{N} \cdot \bar{s}^0)_{\text{NaOH(s)}} - (\mathbf{N} \cdot \bar{s}^0)_{\text{Na(l)}} \quad (142)$$

$$\Delta G^0_{c.1} = \Delta H^0_{c.1} - T^0 \cdot \Delta S^0_{c.1} \quad (143)$$

(ii) Modeling sodium hydroxide decomposition step – Reaction 2 – Eq. (137)

Reaction 2 of (Na-O-H)<sub>c</sub> is evaluated using Equations (144) to (146).

$$\Delta H^0_{c.2} = (\mathbf{N} \cdot \bar{h}_f^0)_{\text{NaH(s)}} + (\mathbf{N} \cdot \bar{h}_f^0)_{\text{O}_2\text{(g)}} - (\mathbf{N} \cdot \bar{h}_f^0)_{\text{NaOH(s)}} \quad (144)$$

$$\Delta S^0_{c.2} = (\mathbf{N} \cdot \bar{s}^0)_{\text{NaH(s)}} + (\mathbf{N} \cdot \bar{s}^0)_{\text{O}_2\text{(g)}} - (\mathbf{N} \cdot \bar{s}^0)_{\text{NaOH(s)}} \quad (145)$$

$$\Delta G^0_{c.2} = \Delta H^0_{c.2} - T^0 \cdot \Delta S^0_{c.2} \quad (146)$$

(iii) Modeling metal separation step – Reaction 3 – Eq. (138)



Equations (147), (148) and (149) are applied to assessed reaction 3 of variation (c) of the sodium-oxygen-hydrogen cycle.

$$\Delta H^0_{c.3} = (\mathbf{N} \cdot \bar{h}_f^0)_{\text{Na(l)}} + (\mathbf{N} \cdot \bar{h}_f^0)_{\text{NaOH(l)}} - (\mathbf{N} \cdot \bar{h}_f^0)_{\text{Na}_2\text{O(s)}} - (\mathbf{N} \cdot \bar{h}_f^0)_{\text{NaH(s)}} \quad (147)$$

$$\Delta S^0_{c.3} = (\mathbf{N} \cdot \bar{s}^0)_{\text{Na(l)}} + (\mathbf{N} \cdot \bar{s}^0)_{\text{NaOH(l)}} - (\mathbf{N} \cdot \bar{s}^0)_{\text{Na}_2\text{O(s)}} - (\mathbf{N} \cdot \bar{s}^0)_{\text{NaH(s)}} \quad (148)$$

$$\Delta G^0_{c.3} = \Delta H^0_{c.3} - T^0 \cdot \Delta S^0_{c.3} \quad (149)$$

(iv) Modeling hydrolysis (hydrogen releasing) step – Reaction 4 – Eq. (139)

Equations (150), (151) and (152) are applied to assessed reaction 4 of variation (c) of the Na-O-H thermochemical procedure.

$$\Delta H^0_{c.4} = (\mathbf{N} \cdot \bar{h}_f^0)_{\text{NaOH(s)}} + (\mathbf{N} \cdot \bar{h}_f^0)_{\text{H}_2\text{(g)}} - (\mathbf{N} \cdot \bar{h}_f^0)_{\text{Na(l)}} - (\mathbf{N} \cdot \bar{h}_f^0)_{\text{H}_2\text{O(l)}} \quad (150)$$

$$\Delta S^0_{c.4} = (\mathbf{N} \cdot \bar{s}^0)_{\text{NaOH(s)}} + (\mathbf{N} \cdot \bar{s}^0)_{\text{H}_2\text{(g)}} - (\mathbf{N} \cdot \bar{s}^0)_{\text{Na(l)}} - (\mathbf{N} \cdot \bar{s}^0)_{\text{H}_2\text{O(l)}} \quad (151)$$

$$\Delta G^0_{c.4} = \Delta H^0_{c.4} - T^0 \cdot \Delta S^0_{c.4} \quad (152)$$

(v) Modeling sodium hydroxide solidification phase – Eq. (140)

Sodium hydroxide solidification is analyzed using Equation (153).

$$\Delta H^0_{c.5} = (\mathbf{N} \cdot \bar{h}_f^0)_{\text{NaOH(s)}} - (\mathbf{N} \cdot \bar{h}_f^0)_{\text{NaOH(l)}} \quad (153)$$

(vi) Modeling Na-O-H cycle – variation (c)

Equations (154) to (157) are applied to evaluate the thermodynamic aspects of (Na-O-H)<sub>c</sub>.

$$\Delta H^0_c = \Delta H^0_{c.1} + \Delta H^0_{c.2} + \Delta H^0_{c.3} + \Delta H^0_{c.4} + \Delta H^0_{c.5} \quad (154)$$

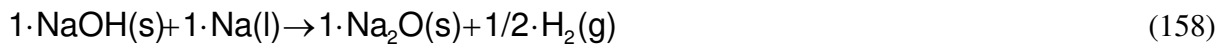
$$\Delta S^0_c = \Delta S^0_{c.1} + \Delta S^0_{c.2} + \Delta S^0_{c.3} + \Delta S^0_{c.4} \quad (155)$$

$$\Delta G^0_c = \Delta G^0_{c.1} + \Delta G^0_{c.2} + \Delta G^0_{c.3} + \Delta G^0_{c.4} \quad (156)$$

$$\eta_c = \frac{(\Delta H_{\text{combustion}})_{\text{H}_2(\text{g})}}{\Delta H_c^0} \quad (157)$$

### 5.3.4 Modeling Na-O-H cycle – variation (d) – (Na-O-H)<sub>d</sub>

Variation (d) is composed by Equations (158), (159) and (160). Such mode and its reactions are modeled in accordance with Equations (161) to (173).



#### (i) Modeling hydrogen production step – Reaction 1 – Eq. (158)

Reaction 1 of variation (d) of the Na-O-H cycle is modeled according to Equations (161) to (163).

$$\Delta H_{\text{d},1}^0 = (\mathbf{N} \cdot \bar{h}_f^0)_{\text{Na}_2\text{O}(\text{s})} + (\mathbf{N} \cdot \bar{h}_f^0)_{\text{H}_2(\text{g})} - (\mathbf{N} \cdot \bar{h}_f^0)_{\text{NaOH}(\text{s})} - (\mathbf{N} \cdot \bar{h}_f^0)_{\text{Na}(\text{l})} \quad (161)$$

$$\Delta S_{\text{d},1}^0 = (\mathbf{N} \cdot \bar{s}^0)_{\text{Na}_2\text{O}(\text{s})} + (\mathbf{N} \cdot \bar{s}^0)_{\text{H}_2(\text{g})} - (\mathbf{N} \cdot \bar{s}^0)_{\text{NaOH}(\text{s})} - (\mathbf{N} \cdot \bar{s}^0)_{\text{Na}(\text{l})} \quad (162)$$

$$\Delta G_{\text{d},1}^0 = \Delta H_{\text{d},1}^0 - T^0 \cdot \Delta S_{\text{d},1}^0 \quad (163)$$

#### (ii) Modeling metal separation step – Reaction 2 – Eq. (159)

Reaction 2 of (Na-O-H)<sub>d</sub> is evaluated using Equations (164) to (166).

$$\Delta H_{\text{d},2}^0 = (\mathbf{N} \cdot \bar{h}_f^0)_{\text{Na}(\text{l})} + (\mathbf{N} \cdot \bar{h}_f^0)_{\text{O}_2(\text{g})} - (\mathbf{N} \cdot \bar{h}_f^0)_{\text{Na}_2\text{O}(\text{s})} \quad (164)$$

$$\Delta S_{\text{d},2}^0 = (\mathbf{N} \cdot \bar{s}^0)_{\text{Na}(\text{l})} + (\mathbf{N} \cdot \bar{s}^0)_{\text{O}_2(\text{g})} - (\mathbf{N} \cdot \bar{s}^0)_{\text{Na}_2\text{O}(\text{s})} \quad (165)$$

$$\Delta G_{\text{d},2}^0 = \Delta H_{\text{d},2}^0 - T^0 \cdot \Delta S_{\text{d},2}^0 \quad (166)$$

#### (iii) Modeling hydrolysis (hydrogen releasing) step – Reaction 3 – Eq. (160)

Equations (167), (168) and (169) are applied to assessed reaction 3 of variation (c) of the sodium-oxygen-hydrogen cycle.

$$\Delta H^0_{d.3} = (\mathbf{N} \cdot \bar{h}_f^0)_{\text{NaOH(s)}} + (\mathbf{N} \cdot \bar{h}_f^0)_{\text{H}_2(\text{g})} - (\mathbf{N} \cdot \bar{h}_f^0)_{\text{Na(l)}} - (\mathbf{N} \cdot \bar{h}_f^0)_{\text{H}_2\text{O(l)}} \quad (167)$$

$$\Delta S^0_{d.3} = (\mathbf{N} \cdot \bar{s}^0)_{\text{NaOH(s)}} + (\mathbf{N} \cdot \bar{s}^0)_{\text{H}_2(\text{g})} - (\mathbf{N} \cdot \bar{s}^0)_{\text{Na(l)}} - (\mathbf{N} \cdot \bar{s}^0)_{\text{H}_2\text{O(l)}} \quad (168)$$

$$\Delta G^0_{d.3} = \Delta H^0_{b.3} - T^0 \cdot \Delta S^0_{b.3} \quad (169)$$

(iv) Modeling Na-O-H cycle – variation (d)

Equations (170) to (173) are applied to evaluate the thermodynamic aspects of (Na-O-H)<sub>d</sub>.

$$\Delta H^0_d = \Delta H^0_{d.1} + \Delta H^0_{d.2} + \Delta H^0_{d.3} \quad (170)$$

$$\Delta S^0_d = \Delta S^0_{d.1} + \Delta S^0_{d.2} + \Delta S^0_{d.3} \quad (171)$$

$$\Delta G^0_d = \Delta G^0_{d.1} + \Delta G^0_{d.2} + \Delta G^0_{d.3} \quad (172)$$

$$\eta_d = \frac{(\Delta H_{\text{combustion}})_{\text{H}_2(\text{g})}}{\Delta H^0_d} \quad (173)$$

**5.3.5 Modeling Na-O-H cycle – variation (e) – (Na-O-H)<sub>e</sub>**

Na-O-H method variation (e) is represented by Equations (174) and (175). Such cycle and its chemical reactions are evaluated following the steps described by Equations (176) to (185).



(i) Modeling sodium hydroxide decomposition step – Reaction 1 – Eq. (174)

Reaction 1 of variation (e) of the Na-O-H cycle is modeled according to Equations (176) to (178).

$$\Delta H^0_{e.1} = (\mathbf{N} \cdot \bar{h}_f^0)_{\text{NaH(s)}} + (\mathbf{N} \cdot \bar{h}_f^0)_{\text{O}_2(\text{g})} - (\mathbf{N} \cdot \bar{h}_f^0)_{\text{NaOH(s)}} \quad (176)$$

$$\Delta S^0_{e.1} = (\mathbf{N} \cdot \bar{s}^0)_{\text{NaH(s)}} + (\mathbf{N} \cdot \bar{s}^0)_{\text{O}_2(\text{g})} - (\mathbf{N} \cdot \bar{s}^0)_{\text{NaOH(s)}} \quad (177)$$

$$\Delta G^0_{e.1} = \Delta H^0_{b.1} - T^0 \cdot \Delta S^0_{b.1} \quad (178)$$

(ii) Modeling hydrolysis (hydrogen releasing) step – Reaction 2 – Eq. (175)

Reaction 2 of (Na-O-H)<sub>e</sub> is evaluated using Equations (179) to (181).

$$\Delta H^0_{e.2} = (\mathbf{N} \cdot \bar{h}_f^0)_{\text{NaOH(s)}} + (\mathbf{N} \cdot \bar{h}_f^0)_{\text{H}_2(\text{g})} - (\mathbf{N} \cdot \bar{h}_f^0)_{\text{NaH(s)}} - (\mathbf{N} \cdot \bar{h}_f^0)_{\text{H}_2\text{O(l)}} \quad (179)$$

$$\Delta S^0_{e.2} = (\mathbf{N} \cdot \bar{s}^0)_{\text{NaOH(s)}} + (\mathbf{N} \cdot \bar{s}^0)_{\text{H}_2(\text{g})} - (\mathbf{N} \cdot \bar{s}^0)_{\text{NaH(s)}} - (\mathbf{N} \cdot \bar{s}^0)_{\text{H}_2\text{O(l)}} \quad (180)$$

$$\Delta G^0_{e.2} = \Delta H^0_{b.3} - T^0 \cdot \Delta S^0_{b.3} \quad (181)$$

(iii) Modeling Na-O-H cycle – variation (e)

Equations (182) to (185) are applied to evaluate the thermodynamic aspects of (Na-O-H)<sub>a</sub>.

$$\Delta H^0_e = \Delta H^0_{e.1} + \Delta H^0_{e.2} \quad (182)$$

$$\Delta S^0_e = \Delta S^0_{e.1} + \Delta S^0_{e.2} \quad (183)$$

$$\Delta G^0_e = \Delta G^0_{e.1} + \Delta G^0_{e.2} \quad (184)$$

$$\eta_e = \frac{(\Delta H_{\text{combustion}})_{\text{H}_2(\text{g})}}{\Delta H^0_e} \quad (185)$$

#### 5.4 Analyzing the results of all variations of the Na-O-H thermochemical cycle

In this part of chapter 5 are presented the results obtained for each variation of the Na-O-H cycle after implementing Equations (102) to (185) with source data from Table 11. Additionally, in Tables 12 to 16 (subsections 5.4.1 to 5.4.6), beyond the values of entropy change ( $\Delta S$ ) and Gibbs free energy ( $\Delta G$ ) for each cycle variation in addition to its chemical reactions, they are also presented a maximum value (max) plus an minimum one (min) for both enthalpy change ( $\Delta H_{\max}$  and  $\Delta H_{\min}$ ) and thermal efficiency ( $\eta_{\max}$  and  $\eta_{\min}$ ) for all variations under attention. In subsection 5.4.7 are performed comparisons among all Na-O-H trial configurations in order to determine which one of them is the best choice to produce 1 mol of  $H_2$ , considering their thermal characteristics ( $\Delta H$ ,  $\Delta S$ ,  $\Delta G$  and  $\eta$ ).

The variable  $\Delta H_{\min}$  related to a cycle variation considers the sum of its endothermic and/or exothermic reactions as in Equation (35). All cycle variations have  $\Delta H_{\min}$  equal to 285.83 kJ that is the minimum theoretical enthalpy change required to split liquid water into  $H_2$  and  $O_2$  gases as in Equation (10). This fact ensures that all equations exhibited in section 5.3 were well implemented, what validates the results presented over section 5.4. On the other hand, the variable  $\Delta H_{\max}$  for a cycle variation only considers the sum of its endothermic reactions as in Equation (35). It does not have a maximum or minimum limit like  $\Delta H_{\min}$ .

Still related to the results discussed in sections 5.4.1 to 5.4.6, the variable  $\eta_{\min}$  for a cycle variation only considers the sum of its endothermic reactions as in Equation (35) to determine cycle thermal efficiency in Equation (36). A maximum enthalpy change reduces system efficiency. It does not have a minimum or maximum limit as  $\eta_{\max}$ . Additionally, the variable  $\eta_{\max}$  for a cycle variation considers the sum of all its endothermic and exothermic reactions as in Equation (35) to determine cycle efficiency in Equation (36). A minimum enthalpy change maximizes system efficiency. Due to it, all cycle variations have a maximum theoretical thermal efficiency equal to 100 % because in such case, each cycle demands the minimum amount of enthalpy change ( $\Delta H_{\min} = 285.83$  kJ) that is equal to the energy released during  $H_2$  combustion ( $\Delta H_{\text{combustion}} = 285.83$  kJ).

This distinction was done because in practical situations could be unfeasible, depending on their operational conditions, to recover the heat released by the exothermic chemical reactions of a thermochemical system. This fact impacts on the final quantities of enthalpy change and thermal efficiency for the cycle because the heat recovered from exothermic processes could be used to reduce the overall enthalpy change or energy required by the cycle, what influences on its thermal performance as suggested by Equation (36). The minimum value of  $\Delta H$  and the maximum one for  $\eta$  validates the results exhibited over section 5.4 because all variations of the Na-O-H method have  $\eta_{\max} = 100\%$  and  $\Delta H_{\min} = 285.83$  kJ, which are the thermodynamic limits for those variables in a direct thermal decomposition of water (thermolysis) like in Equation (10), as explanation given later in chapter 6.

#### 5.4.1 Analyzing variation (a) of the Na-O-H cycle

In Table 12 are exhibited the values of enthalpy ( $\Delta H_{a,i}^0$ ), entropy ( $\Delta S_{a,i}^0$ ) and Gibbs free energy ( $\Delta G_{a,i}^0$ ) changes plus energy efficiency ( $\eta_a$ ) for the three chemical steps plus Na condensation phase of the Na-O-H trial variation (a) when using Equations (106) to (119) together with source data from Table 11.

Variables	Reaction 1 Eq. (102)	Reaction 2 Eq. (103)	Reaction 3 Eq. (104)	Condensation Eq. (105)	Cycle variation (a)
$\Delta H_{a,i}^0$ [kJ]	11.08	537.35	-52.82	-209.78	548.43 <sup>1</sup> to 285.83 <sup>2</sup>
$\Delta S_{a,i}^0$ [J/K]	36.12	252.00	66.77	-	354.89
$\Delta G_{a,i}^0$ [kJ]	0.31	462.25	-72.71	-	389.85
$\eta_a$ [%]	-	-	-	-	52.11 <sup>1</sup> to 100 <sup>2</sup>

1-Whitout recovering the energy released from Equations (104) and (105) - ( $\Delta H_{\max}$  and  $\eta_{\min}$ ).

2-Recovering the energy released from Equations (104) and (105) - ( $\Delta H_{\min}$  and  $\eta_{\max}$ ).

**Source: the author.**

According to Table 12, step 1, step 2, step 3 and Na condensation phase have respectively  $\Delta H_{a,i}^0$  equal to 11.08 kJ, 537.35 kJ, -52.82 kJ and -209.78 kJ, resulting in a net enthalpy change varying from 548.43 to 285.83 kJ and consequently, energy efficiency ranging from 52.11 % to 100 %. Additionally, (Na-O-H)<sub>a</sub> has a total entropy change about 354.89 J/K because steps 1, 2 and 3 have  $\Delta S_{a,i}^0$  respectively equal to 36.12 J/K, 252.00 J/K, 66.77 J/K. Finally, (Na-O-H)<sub>a</sub> has a net  $\Delta G_a^0 = 389.85$  kJ determined by the sum of the Gibbs free energy of each reaction ( $\Delta G_{a,1}^0 = 0.31$  kJ,  $\Delta G_{a,2}^0 = 462.25$  kJ and  $\Delta G_{a,3}^0 = -72.71$  kJ). This efficiency value is close to that one found out

in previous researches (MIYAOKA *et al.*, 2012 and MARQUES *et al.*, 2019), indicating that the equations introduced in section 5.3 were well implemented, validating then part of the results gotten in this chapter.

#### 5.4.2 Analyzing variation (b) of the Na-O-H cycle

The variables  $\Delta H_{b,i}^0$ ,  $\Delta S_{b,i}^0$  and  $\Delta G_{b,i}^0$  for the three chemical reactions, Equations (120), (121) and (122), of the Na-O-H cycle variation (b) are shown in Table 13 after applying Equations (123) to (125) combined with thermodynamic data from Table 11. Farther, in Table 13, it is possible to see the net values of such variables for the cycle itself together with its energy efficiency. Then, based on the quantities of enthalpy, entropy and Gibbs free energy for each reaction, the overall values of such variables for variation (b) are:  $428.34 \text{ kJ} < \Delta H_b^0 < 285.83 \text{ kJ}$ ,  $\Delta S_b^0 = 163.31 \text{ J/K}$ ,  $\Delta G_b^0 = 237.16 \text{ kJ}$  and  $66.72 \% < \eta_b < 100 \%$ .

**Table 13 -  $\Delta H_{b,i}^0$ ,  $\Delta S_{b,i}^0$ ,  $G_{b,i}^0$  and  $\eta_b$  for (Na-O-H)<sub>b</sub> and its chemical reactions**

Variables	Reaction 1 Eq. (120)	Reaction 2 Eq. (121)	Reaction 3 Eq. (122)	Cycle variation (b)
$\Delta H_{b,i}^0$ [kJ]	369.49	58.85	-142.51	$428.34^1$ to $285.83^2$
$\Delta S_{b,i}^0$ [J/K]	78.15	83.17	1.99	163.31
$\Delta G_{b,i}^0$ [kJ]	346.20	34.06	-143.10	237.16
$\eta_b$ [%]	-	-	-	$66.72^1$ to $100^2$

1-Whitout recovering the energy released from Equation (122) - ( $\Delta H_{\max}$  and  $\eta_{\min}$ ).

2-Recovering the energy released from Equation (122) - ( $\Delta H_{\min}$  and  $\eta_{\max}$ ).

Source: the author.

#### 5.4.3 Analyzing variation (c) of the Na-O-H cycle

The results related to the Na-O-H method variation (c) and its four chemical steps plus a NaOH solidification phase are presented in Table 14 after implementing Equations (141) to (157) with information from Table 11. As it can be seen in Table 14, variation (c) has: enthalpy change varying from 437.91 kJ to 294.88 kJ, entropy change about 174.76 J/K, Gibbs free energy around 242.80 kJ and energy efficiency ( $\eta_c$ ) ranging from 65.34 % to 100 %. Such net amounts are consequence from the following results related to all the reactions, Equations (136), (137), (138), (139) and (140) in this variation of the Na-O-H cycle; step 1:  $\Delta H_{c,1}^0 = 5.54 \text{ kJ}$ ,  $\Delta S_{c,1}^0 = 18.06 \text{ J/K}$ ,  $\Delta G_{c,1}^0 = 0.15 \text{ kJ}$ ; step 2:  $\Delta H_{c,2}^0 = 62.36 \text{ kJ}$ ,  $\Delta S_{c,2}^0 = 76.56 \text{ J/K}$ ,  $\Delta G_{c,2}^0 = 39.54 \text{ kJ}$ ; step 3:  $\Delta H_{c,3}^0 =$

369.49 kJ,  $\Delta S^0_{c,3} = 78.15$  J/K,  $\Delta G^0_{c,3} = 346.20$  kJ; step 4:  $\Delta H^0_{c,4} = -142.51$  kJ,  $\Delta S^0_{c,4} = 1.99$  J/K,  $\Delta G^0_{c,4} = -143.10$  kJ; NaOH solidification phase:  $\Delta H^0_{c,5} = -9.05$  kJ.

**Table 14 -  $\Delta H^0_{c,i}$ ,  $\Delta S^0_{c,i}$ ,  $\Delta G^0_{c,i}$  and  $\eta_c$  for (Na-O-H)<sub>c</sub> and its chemical reactions**

Variables	Reaction 1 Eq. (136)	Reaction 2 Eq. (137)	Reaction 3 Eq. (138)	Reaction 4 Eq. (139)	Solidification Eq. (140)	Cycle variation (c)
$\Delta H^0_{c,i}$ [kJ]	5.54	369.49	62.36	-142.51	-9.05	437.39 <sup>1</sup> to 285.83 <sup>2</sup>
$\Delta S^0_{c,i}$ [J/K]	18.06	78.15	76.56	1.99	-	174.76
$\Delta G^0_{c,i}$ [kJ]	0.15	346.20	39.54	-143.10	-	242.80
$\eta_c$ [%]	-	-	-	-	-	65.34 <sup>1</sup> to 100 <sup>2</sup>

1-Whitout recovering the energy released from Equations (139) and (140) - ( $\Delta H_{\max}$  and  $\eta_{\min}$ ).

2-Recovering the energy released from Equations (139) and (140) - ( $\Delta H_{\min}$  and  $\eta_{\max}$ ).

**Source: the author.**

#### 5.4.4 Analyzing variation (d) of the Na-O-H cycle

In Table 15 are shown the values of enthalpy, entropy and Gibbs free energy changes plus energy efficiency for the three chemical reactions of the Na-O-H thermochemical procedure variation (d) when using Equations (161) to (173) together with source data from Table 11. According to it, reactions 1, 2 and 3, Equations (158), (159) and (160), have respectively  $\Delta H^0_{d,i}$  equal to 5.54 kJ, 422.80 kJ and -142.51 kJ, resulting in a net enthalpy change varying from 428.34 kJ to 285.83 kJ plus energy efficiency ranging from 66.72% to 100 %. Additionally, considering the values of  $\Delta S^0_{d,i}$  in Table 5, (Na-O-H)<sub>d</sub> has a total entropy change of 163.31 J/K because reactions 1, 2 and 3 have  $\Delta S^0_{d,i}$  respectively equal to 18.06 J/K, 143.26 J/K, 1.99 J/K. In relation to the Gibbs free energy change of variation (d), it has a net  $\Delta G^0_d = 237.16$  kJ determined by the sum of the Gibbs free energy of each reaction ( $\Delta G^0_{d,1} = 0.15$  kJ,  $\Delta G^0_{d,2} = 380.11$  kJ and  $\Delta G^0_{d,3} = -143.10$  kJ).

**Table 15 -  $\Delta H^0_{d,i}$ ,  $\Delta S^0_{d,i}$ ,  $\Delta G^0_{d,i}$  and  $\eta_d$  for (Na-O-H)<sub>d</sub> and its chemical reactions**

Variables	Reaction 1 Eq. (158)	Reaction 2 Eq. (159)	Reaction 3 Eq. (160)	Cycle variation (d)
$\Delta H^0_{d,i}$ [kJ]	5.54	422.80	-142.51	428.34 <sup>1</sup> to 285.83 <sup>2</sup>
$\Delta S^0_{d,i}$ [J/K]	18.06	143.26	1.99	163.31
$\Delta G^0_{d,i}$ [kJ]	0.15	380.11	-143.10	237.16
$\eta_d$ [%]	-	-	-	66.72 <sup>1</sup> to 100 <sup>2</sup>

1-Whitout recovering the energy released from Equation (160) - ( $\Delta H_{\max}$  and  $\eta_{\min}$ ).

2-Recovering the energy released from Equation (160) - ( $\Delta H_{\min}$  and  $\eta_{\max}$ ).

**Source: the author.**



### 5.4.5 Analyzing variation (e) of the Na-O-H cycle

The results related to the Na-O-H process variation (e) and its two chemical reactions are in Table 16 after implementing Equations (176) to (185) plus information from Table 11. As it can be seen, variation (e) has:  $\Delta H_e^0 =$  varying from 369.49 kJ to 285.83 kJ,  $\Delta S_e^0 = 163.31$  J/K,  $\Delta G_e^0 = 237.16$  kJ. The superior and inferior values for  $\Delta H_e^0$  impact on a cycle thermal efficiency which varies from 77.35 % to 100 %. These overall values are consequence from the following results related to all the chemical steps, Equations (174) and (175), of this Na-O-H cycle mode; step 1:  $\Delta H_{e,1}^0 = 369.49$  kJ,  $\Delta S_{e,1}^0 = 78.15$  J/K,  $\Delta G_{e,1}^0 = 346.20$  kJ; step 2:  $\Delta H_{e,2}^0 = -83.86$  kJ,  $\Delta S_{e,2}^0 = 85.16$  J/K,  $\Delta G_{e,2}^0 = -109.03$  kJ.

**Table 16 -  $\Delta H_{e,i}^0$ ,  $\Delta S_{e,i}^0$ ,  $\Delta G_{e,i}^0$ , and  $\eta_e$  for (Na-O-H)<sub>e</sub> and its chemical reactions**

Variables	Reaction 1 Eq. (174)	Reaction 2 Eq. (175)	Cycle variation (e)
$\Delta H_{e,i}^0$ [kJ]	369.49	-83.66	369.49 <sup>1</sup> to 285.83 <sup>2</sup>
$\Delta S_{e,i}^0$ [J/K]	78.15	85.16	163.31
$\Delta G_{e,i}^0$ [kJ]	346.20	-109.03	237.16
$\eta_e$ [%]	-	-	77.35 <sup>1</sup> to 100 <sup>2</sup>

1-Whitout recovering the energy released from Equation (175) - ( $\Delta H_{\max}$  and  $\eta_{\min}$ ).

2-Recovering the energy released from Equation (175) - ( $\Delta H_{\min}$  and  $\eta_{\max}$ ).

Source: the author.

### 5.4.6 Comparing all variations of the Na-O-H cycle

In this topic is made a comparison among all the five variations of the Na-O-H cycle presented in chapter 5 in order to determine which one of them has the better thermal aspects ( $\Delta H$ ,  $\Delta S$ ,  $\Delta G$  and  $\eta$ ) to produce 1 mol of hydrogen gas.

According to Table 17, (Na-O-H)<sub>e</sub> has the better minimum thermal efficiency (77.35%) in function of having the less inferior enthalpy change (369.49 kJ). Variation (e), together with variations (b) and (d), also have the inferior values of entropy (163.31 J/K) and Gibbs free energy (237.16 kJ) changes. Additionally, (Na-O-H)<sub>e</sub> is only composed by 2-chemical steps and none physical phase change, making it the simplest Na-O-H cycle variation from the theoretical practical implementation viewpoint. Because of these facts, it was classified as the 1<sup>o</sup> position in Table 17. In function of all these results, (Na-O-H)<sub>e</sub> have potential to be the better option aiming an practical implementation of this cycle in the future.

(Na-O-H)<sub>b</sub> and (Na-O-H)<sub>d</sub> were classified as the 2°/3° better options. Both have  $\Delta H = 428.34$  kJ,  $\Delta S = 163.31$  J/K,  $\Delta G = 237.16$  kJ and  $\eta = 66.72$  %. Both (b) and (d) Na-O-H cycle variations have 3-chemical steps and none physical phase. Then, (Na-O-H)<sub>c</sub> was classified as the 4° better option because its values for enthalpy, entropy and Gibbs free energy changes plus energy efficiency are respectively equal to 437.91 kJ, 174.76 J/K, 242.80 kJ and 65.34%. Additionally, it is composed by 4-chemical steps plus 1-physical change.

**Table 17 -  $\Delta H_i^0$ ,  $\Delta S_i^0$ ,  $\Delta G_i^0$  and  $\eta_i$  for all variations of the Na-O-H cycle**

Variables	Cycle variation (a)	Cycle variation (b)	Cycle variation (c)	Cycle variation (d)	Cycle variation (e)
$\Delta H_i^0$ [kJ]	548.43 <sup>1</sup>	428.34 <sup>1</sup>	437.39 <sup>1</sup>	428.34 <sup>1</sup>	369.49 <sup>1</sup>
$\Delta S_i^0$ [J/K]	354.89	163.31	174.76	163.31	163.31
$\Delta G_i^0$ [kJ]	389.85	237.16	242.80	237.16	237.16
$\eta_i$ [%]	52.11 <sup>2</sup>	66.72 <sup>2</sup>	65.34 <sup>2</sup>	66.72 <sup>2</sup>	77.35 <sup>2</sup>
Chemical steps	3	3	4	3	2
Physical change steps	1	0	1	0	0
Classification	5°	2°/3°	4°	2°/3°	1°

1-It is the maximum enthalpy change for each cycle. All variations have min enthalpy change equal to 285.83 kJ.

2- It is the minimum thermal efficiency for each cycle. All variations have max energy efficiency equal to 100%.

**Source: the author.**

Finally, according to results discussed in subsections 5.4 to 5.4.6 and resumed in Table 17, it concludes the (Na-O-H)<sub>a</sub> cycle has the inferior overall theoretical thermodynamic performance when compared to the other four variations of the Na-O-H cycle. It has  $\Delta H = 548.43$  kJ,  $\Delta S = 354.89$  J/K,  $\Delta G = 389.85$  kJ and  $\eta = 52.11$  %.

Then, after the thermodynamic comparative study performed over chapter 5, it infers that there are other configurations of the Na-O-H system that provide better thermal aspects when compared to its traditional approach. In this way, variations (b, c, d and e), specially (e), of the Na-O-H trial have potential to operate at temperatures inferior to 400-500°C and pressure above vacuum (very low) related to variation (a), what implies on a less challenge practical implementation of this cycle in the future and better thermodynamic results related to it in comparison to those ones already commented in chapter 4 and also papers (like Marques *et al.*, 2020a and Marques *et al.*, 2020b) about the (Na-O-H)<sub>a</sub>. However, the exact values of p and T out of standard conditions that guarantee possible occurrence for the other cycle variations ( $\Delta G < 0$ ) needed to be figure out through more specific future researches, including Gibbs free energy, reaction kinetics and experimental ones.

## 6 THERMODYNAMIC LIMITS FOR THERMOCHEMICAL CYCLES

Finally, in the third aim of this research are established the thermodynamic limits (the minimum requirements of enthalpy, entropy and Gibbs free energy changes plus the maximum energy efficiency) for thermochemical water splitting cycles of hydrogen production. It is done after comparing and analyzing the values of  $\Delta H$ ,  $\Delta S$ ,  $\Delta G$  and  $\eta$  among different thermochemical cycles (Li-O-H, K-O-H, Rb-O-H, Cs-O-H and also Na-O-H) regarding all their respective variations and the direct thermal decomposition of water (thermolysis process). These additional four cycles are analogous to the Na-O-H one and its various modes proposed in chapter 5, but they have compounds based on chemical elements of the Group 1A of the periodic table like lithium (Li), potassium (K), rubidium (Rb) and cesium (Cs) instead of sodium (Na). This final aim is realized in chapter 6 considering standard conditions of temperature and pressure for all systems under attention, combined with many of the concepts introduced in section 5.4. Water thermolysis was chosen as the standard reference to carry out such comparison because it is a direct thermal way to decompose  $H_2O$  molecules to get  $H_2$ ; in contrast, thermochemical cycles are an indirect way to achieve the same goal. Therefore, this chapter is developed taking into consideration the following steps:

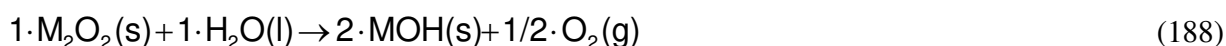
- Generalization of the Na-O-H cycle and its five variations into the generic M-O-H system in section 6.1. M represents metal elements (Li, K, Rb and Cs) of the Group 1A of the periodic table.
- Presentation in subsections 6.1.1 to 6.1.4 of the cycles Li-O-H (lithium-oxygen-hydrogen), K-O-H (potassium-oxygen-hydrogen), Rb-O-H (rubidium-oxygen-hydrogen) and Cs-O-H (cesium-oxygen-hydrogen) in accordance with all modes of the M-O-H procedure.
- Thermodynamic modeling for the systems Li-O-H, K-O-H, Rb-O-H and Cs-O-S based on the methodology described over section 5.3 for all variations of the Na-O-H method. It is performed during section 6.2.
- In section 6.4 are presented, compared and analyzed the values of  $\Delta H$ ,  $\Delta S$ ,  $\Delta G$  and  $\eta$  among the systems under study and water thermolysis in order to establish the thermodynamic limits for thermochemical water splitting trials of hydrogen making.

## 6.1 Generic metal-oxygen-hydrogen (M-O-H) cycle and its variations

The generic M-O-H cycle and its five modes, Equations (186) to (202), result when Na in all variations of the Na-O-H trial introduced in section 5.3 are replaced by the ordinary element M. It represents all metals of the Group 1A of the periodic table, in such case, Li, K, Rb and Cs, except Fr that is not assessed in the thesis due to the lack of thermodynamic data about it. These four elements combined with the M-O-H system are used to create the cycles Li-O-H, K-O-H, Rb-O-H and Cs-O-H which are structurally similar to the Na-O-H one, but having other chemical elements from the Group 1A instead of Na. Some of these processes are actual ones while others are hypothetical ones as it is explained in the next subsections of this chapter.

### (i) Generic M-O-H cycle – variation (a) – (M-O-H)<sub>a</sub>

Variation (a) of the M-O-H cycle is composed by Equations (186) to (189).



### (ii) Generic M-O-H cycle – variation (b) – (M-O-H)<sub>b</sub>

Equations (190), (191) and (192) represent variation (b) of the M-O-H cycle.



### (iii) Generic M-O-H cycle – variation (c) – (M-O-H)<sub>c</sub>

Variation (c) of the M-O-H cycle is composed by Equations (193), (194), (195), (196) and (197).



(iv) Generic M-O-H cycle – variation (d) – (M-O-H)<sub>d</sub>

Equations (198), (199) and (200) represent variation (d) of the generic M-O-H cycle.



(v) Generic M-O-H cycle – variation (e) – (M-O-H)<sub>e</sub>

Variation (e) of the M-O-H cycle is composed by Equations (201) and (202).



### **6.1.1 Lithium-oxygen-hydrogen (Li-O-H) cycle and its variations**

If lithium substitutes the generic metal element M in Equations (186) to (202) associated with the M-O-H cycle and its variations, the result is the lithium-oxygen-hydrogen (Li-O-H) system and its five modes. Nakamura *et al.* (2013) proposed three chemical reactions, through an experimental study, that constitute variation (a) of the Li-O-H cycle like Miyaoka *et al.* (2012) did for the Na-O-H system. Additionally, Nakamura *et al.* (2013) present other chemical reactions that can be used to build other variations of the Li-O-H system.

### ***6.1.2 Potassium-oxygen-hydrogen (K-O-H) cycle and its variations***

The potassium-oxygen-hydrogen (K-O-H) cycle and its five modes are analogous to the M-O-H system in Equations (186) to (202), but adding K element instead of the M one. Variation (a) of the K-O-H cycle is referenced in the works of Yalçın (1989) and Abanades *et al.* (2006) while Natola and Touzain (1970) present a phase diagram considering a chemical reaction involving the substances K, K<sub>2</sub>O and K<sub>2</sub>O<sub>2</sub>.

### ***6.1.3 Rubidium-oxygen-hydrogen (Rb-O-H) cycle and its variations***

All forms of the rubidium-oxygen-hydrogen (Rb-O-H) process are obtained when the ordinary element M is supplanted by rubidium one in Equations (186) to (202) from subsection 6.1.1. They were not found in the literature studies covering the chemical steps of the Rb-O-H cycle. So, in a first moment, such system is just a hypothetical method analogous to the Na-O-H one and its variations.

### ***6.1.4 Cesium-oxygen-hydrogen (Cs-O-H) cycle and its variations***

All five variations of the cesium-oxygen-hydrogen (Cs-O-H) cycle are built when cesium (Cs) is put on place of the metal element M in Equations (186) to (202) related to M-O-H system. Badawi *et al.* (2012) show some of the possible chemical steps involved in the Cs-O-H cycle while Guéneau and Flèche (2015) exhibit calculated phase diagrams covering some chemical reactions of the cycle. Additionally, both works present a variety of thermodynamic information about the chemical substances of the Cs-O-H system.

## **6.2 Thermodynamic modeling of the cycles Li-O-H, K-O-H, Rb-O-H and Cs-O-H**

The thermodynamic modeling of the five variations of the Na-O-H cycle presented over section 5.3 are reused at this point of chapter 6 in order to model five variations of the cycles Li-O-H, K-O-H, Rb-O-H and Cs-O-H. So, the chemical element Na in all equations in section 5.3 is displaced by the metal elements Li, K, Rb and Cs. This approach avoids the repetition of many

equations that would be used to determine the same parameters ( $\Delta H$ ,  $\Delta S$ ,  $\Delta G$  and  $\eta$ ) for similar structural chemical steps that differ from each other due to their basic chemical elements in function of the trial under analysis (Na-O-H, Li-O-H, K-O-H, Rb-O-H or Cs-O-H).

Still, information contained in Tables 18, 19, 20 and 21 adapted from NIST (2018) are used with Equations (102) to (185) to determine the enthalpy change ( $\Delta H$ ), entropy change ( $\Delta S$ ), Gibbs free energy change ( $\Delta G$ ) and energy efficiency ( $\eta$ ) for every cycle variation (a, b, c, d and e) and their respective chemical reactions for the systems Li-O-H, K-O-H, Rb-O-h and Cs-O-H. It is the same methodology applied for the Na-O-H process in subsections 5.3.1 to 5.3.5, but replacing the element Na by Li, K, Rb and Cs in the case of each specific cycle.

**TABLE 18 - Standards enthalpy of formation and entropy for Li compounds**

Chemicals	$\bar{h}_f^0$ [kJ/mol]	$\bar{S}^0$ [J/mol*K]
Li (s)	0	29.09
Li (l)	2.38	33.94
Li (g)	159.30	138.78
LiOH (s)	-484.93	42.81
LiOH (l)	-474.42	47.97
LiOH (g)	-234.30	210.67
LiH (s)	-90.5	20.03
Li <sub>2</sub> O (s)	-598.73	37.85
Li <sub>2</sub> O <sub>2</sub> (s)	-634.3	58.52

Source: adapted from NIST(2018) and Lide (2004).

**TABLE 19 - Standards enthalpy of formation and entropy for K compounds**

Chemicals	$\bar{h}_f^0$ [kJ/mol]	$\bar{S}^0$ [J/mol*K]
K (s)	0	64.83
K (l)	2.27	71.40
K (g)	89.00	160.34
KOH (s)	-424.72	78.90
KOH (l)	-412.71	96.62
KOH (g)	-232.63	236.41
KH (s)	-57.82	50.18
K <sub>2</sub> O (s)	-363.17	94.03
K <sub>2</sub> O <sub>2</sub> (s)	-494.1	102.10

Source: adapted from NIST(2018) and Lide (2004).

**TABLE 20 - Standards enthalpy of formation and entropy for Rb compounds**

Chemicals	$\bar{h}_f^0$ [kJ/mol]	$\bar{S}^0$ [J/mol*K]
Rb (s)	0	76.78
Rb (l)	2.18	83.76
Rb (g)	80.90	170.09
RbOH (s)	-418.78	94.42
RbOH (l)	-402.44	175.84
RbOH (g)	-238.02	248.81
RbH (s)	-52.30	59.00
Rb <sub>2</sub> O (s)	-339.00	126.00
Rb <sub>2</sub> O <sub>2</sub> (s)	-452.00	160.00

Source: adapted from NIST(2018) and Lide (2004).

**TABLE 21 - Standards enthalpy of formation and entropy for Cs compounds**

Chemicals	$\bar{h}_f^0$ [kJ/mol]	$\bar{S}^0$ [J/mol*K]
Cs(s)	0	85.15
Cs(l)	2.09	92.70
Cs(g)	76.50	175.60
CsOH(s)	-416.73	98.74
CsOH(l)	-405.97	118.51
CsOH(g)	-259.41	254.81
CsH(s)	-54.00	67.00
Cs <sub>2</sub> O(s)	-345.80	146.9
Cs <sub>2</sub> O <sub>2</sub> (s)	-390.00	215.4

Source: adapted from NIST(2018) and Lide (2004).

### 6.3 Modeling thermal decomposition of water (thermolysis)

In this section is determined the values of  $\Delta H$ ,  $\Delta S$ ,  $\Delta G$  and  $\eta$  for the thermal decomposition of liquid water, Equation (203), at standard condition through Equations (204) to (207). These results combined with those ones discussed in topic 6.4 for all variations of the cycles Li-O-H, K-O-H, Rb-O-H, Cs-O-H and also Na-O-H will help to define the maximum thermodynamic efficiency for thermochemical water splitting cycles of hydrogen production.



*(i) Modeling water thermal decomposition – Eq. (203)*

Water thermolysis from Equation (15) is assessed according to Equations (204) to (207).



$$\Delta H^0_{\text{H}_2\text{O}} = (\mathbf{N} \cdot \bar{h}_f^0)_{\text{O}_2(\text{g})} + (\mathbf{N} \cdot \bar{h}_f^0)_{\text{H}_2(\text{g})} - (\mathbf{N} \cdot \bar{h}_f^0)_{\text{H}_2\text{O}(\text{l})} \quad (204)$$

$$\Delta S^0_{\text{H}_2\text{O}} = (\mathbf{N} \cdot \bar{s}^0)_{\text{O}_2(\text{g})} + (\mathbf{N} \cdot \bar{s}^0)_{\text{H}_2(\text{g})} - (\mathbf{N} \cdot \bar{s}^0)_{\text{H}_2\text{O}(\text{l})} \quad (205)$$

$$\Delta G^0_{\text{H}_2\text{O}} = \Delta H^0_{\text{H}_2\text{O}} - T^0 \cdot \Delta S^0_{\text{H}_2\text{O}} \quad (206)$$

$$\eta_{\text{H}_2\text{O}} = \frac{(\Delta H_{\text{combustion}})_{\text{H}_2(\text{g})}}{\Delta H^0_{\text{H}_2\text{O}}} \quad (207)$$

#### 6.4 Results for the cycles Li-O-H, K-O-H, Rb-O-H and water thermolysis

In Tables 22, 23, 24 and 25 are exhibited the amounts of  $\Delta H$ ,  $\Delta S$ ,  $\Delta G$  and  $\eta$  for every variation of the cycles Li-O-H, K-O-H, Rb-O-H and Cs-O-H after implementing Equations (102) to (185) with information from Tables 18, 19, 20 and 21 for each respective procedure, as explained in section 6.2. However, the values of enthalpy, entropy and Gibbs free energy changes for each individual chemical reaction of every method variation can be checked in Tables 26 to 45 that are placed in the Appendix section. In section 6.4 only are discussed the overall amounts of such variables for cycle variations and not for their individual chemical steps. Through this section, the quantities of  $\Delta H$ ,  $\Delta S$ ,  $\Delta G$  and  $\eta$  for water thermolysis are also commented in order to achieve the last main aim of the thesis.

In general, the same kind of discussion performed over section 5.4 for the results related to every configuration of the Na-O-H trial could be done here but that is not the case. Instead of that, some concepts introduced in section 5.4 such as the differentiation between the minimum ( $\Delta H_{\text{min}}$ ) and the maximum ( $\Delta H_{\text{max}}$ ) enthalpy changes and between the minimum ( $\eta_{\text{min}}$ ) and the maximum ( $\eta_{\text{max}}$ ) energy efficiency for thermochemical cycles are needed to discuss and understand the results presented in this section.

##### 6.4.1 Results for the Li-O-H cycle and its variations

Table 22 presents the values of  $\Delta H_{\max}$ ,  $\Delta S$ ,  $\Delta G$  and  $\eta_{\min}$  for every variation of the lithium-oxygen-hydrogen cycle obtained after implementing all equations from subsections 5.3.1 to 5.3.5 and replacing the element Na by Li with thermodynamic data for lithium compounds in Table 18.

**TABLE 22 -  $\Delta H_i^0$ ,  $\Delta S_i^0$ ,  $\Delta G_i^0$  and  $\eta_i$  for all Li-O-H cycle variations**

Variables	Cycle variation (a)	Cycle variation (b)	Cycle variation (c)	Cycle variation (d)	Cycle variation (e)
$\Delta H_i^0$ [kJ]	649.40 <sup>1</sup>	487.31 <sup>1</sup>	614.00 <sup>1</sup>	603.49 <sup>1</sup>	394.43 <sup>1</sup>
$\Delta S_i^0$ [J/K]	372.99	163.31	168.47	163.31	163.31
$\Delta G_i^0$ [kJ]	488.52	237.16	246.13	237.16	237.22
$\eta_i$ [%]	44.01 <sup>2</sup>	58.65 <sup>2</sup>	46.55 <sup>2</sup>	47.36 <sup>2</sup>	72.46 <sup>2</sup>

1-It is the maximum enthalpy change for each cycle. All variations have a min enthalpy change equal to 285.83 kJ.

2- It is the minimum thermal efficiency for each cycle. All variations have max thermal efficiency equal 100%.

Observation: Table 22 is obtained from Tables 26 to 30 in Appendix chapter.

**Source: the author.**

#### 6.4.2 Results for the K-O-H cycle and its variations

The results of enthalpy, entropy, Gibbs free energy and energy efficiency for all the five variations of the K-O-H trial evaluated in the work are exhibited in Table 23 after implementing Equations (102) to (185) and replacing the element Na by K together with data from Table 19 for potassium compounds.

**TABLE 23 -  $\Delta H_i^0$ ,  $\Delta S_i^0$ ,  $\Delta G_i^0$  and  $\eta_i$  for all K-O-H cycle variations**

Variables	Cycle variation (a)	Cycle variation (b)	Cycle variation (c)	Cycle variation (d)	Cycle variation (e)
$\Delta H_i^0$ [kJ]	528.80 <sup>1</sup>	426.99 <sup>1</sup>	439.00 <sup>1</sup>	426.99 <sup>1</sup>	366.90 <sup>1</sup>
$\Delta S_i^0$ [J/K]	341.19	163.31	181.03	163.31	163.31
$\Delta G_i^0$ [kJ]	357.61	237.16	243.89	237.16	237.16
$\eta_i$ [%]	54.05 <sup>2</sup>	66.94 <sup>2</sup>	65.10 <sup>2</sup>	66.94 <sup>2</sup>	77.90 <sup>2</sup>

1-It is the maximum enthalpy change for each cycle. All variations have a min enthalpy change equal to 285.83 kJ.

2- It is the minimum thermal efficiency for each cycle. All variations have max thermal efficiency equal 100%.

Observation: Table 23 is obtained from Tables 31 to 35 in Appendix chapter.

**Source: the author.**

#### 6.4.3 Results for the Rb-O-H cycle and its variations

Table 24 presents the values of  $\Delta H_{\max}$ ,  $\Delta S$ ,  $\Delta G$  and  $\eta_{\min}$  for every variation of the rubidium-oxygen-hydrogen cycle obtained after implementing all equations from sections 5.3.1 to 5.3.5 and replacing the element Na by Rb with thermodynamic data for rubidium compounds in Table 20.

**TABLE 24 -  $\Delta H_i^0$ ,  $\Delta S_i^0$ ,  $\Delta G_i^0$  and  $\eta_i$  for all Rb-O-H cycle variations**

Variables	Cycle variation (a)	Cycle variation (b)	Cycle variation (c)	Cycle variation (d)	Cycle variation (e)
$\Delta H_i^0$ [kJ]	543.01 <sup>1</sup>	420.96 <sup>1</sup>	443.86 <sup>1</sup>	420.96 <sup>1</sup>	366.48 <sup>1</sup>
$\Delta S_i^0$ [J/K]	335.97	163.31	220.00	163.31	163.31
$\Delta G_i^0$ [kJ]	343.15	237.16	236.79	237.16	237.16
$\eta_i$ [%]	52.63 <sup>2</sup>	67.89 <sup>2</sup>	64.39 <sup>2</sup>	67.89 <sup>2</sup>	77.99 <sup>2</sup>

1-It is the maximum enthalpy change for each cycle. All variations have a min enthalpy change equal to 285.83 kJ.

2- It is the minimum thermal efficiency for each cycle. All variations have max thermal efficiency equal 100%.

Observation: Table 24 is obtained from Tables 36 to 40 in Appendix chapter.

**Source: the author.**

#### 6.4.4 Results for the Cs-O-H cycle and its variations

The results of enthalpy, entropy, Gibbs free energy and energy efficiency for all five variations of the K-O-H cycle evaluated in the work are exhibited in Table 25 after implementing Equations (102) to (185) and replacing the element Na by Cs together with source data from Table 21 for cesium compounds.

**TABLE 25 -  $\Delta H_i^0$ ,  $\Delta S_i^0$ ,  $\Delta G_i^0$  and  $\eta_i$  for all Cs-O-H cycle variations**

Variables	Cycle variation (a)	Cycle variation (b)	Cycle variation (c)	Cycle variation (d)	Cycle variation (e)
$\Delta H_i^0$ [kJ]	592.28 <sup>1</sup>	418.82 <sup>1</sup>	431.57 <sup>1</sup>	418.82 <sup>1</sup>	362.73 <sup>1</sup>
$\Delta S_i^0$ [J/K]	329.11	163.31	183.08	163.31	163.31
$\Delta G_i^0$ [kJ]	336.57	237.16	242.03	237.16	237.16
$\eta_i$ [%]	48.25 <sup>2</sup>	68.24 <sup>2</sup>	66.23 <sup>2</sup>	68.24 <sup>2</sup>	78.79 <sup>2</sup>

1-It is the maximum enthalpy change for each cycle. All variations have a min enthalpy change equal to 285.83 kJ.

2- It is the minimum thermal efficiency for each cycle. All variations have max thermal efficiency equal 100%.

Observation: Table 25 is obtained from Tables 41 to 45 in Appendix chapter.

**Source: the author.**

#### 6.4.5 Comparing the results of the thermochemical cycles and water thermolysis

Water thermolysis at standard conditions has:  $\Delta H^0 = 285.83$  kJ,  $\Delta S^0 = 163.31$  J/K,  $\Delta G^0 = 237.15$  kJ and  $\eta^0 = 100\%$ . Such amounts were found by implementing Equations (204) to (207) with information from Table 11 for Equation (203). Additionally, after analyzing Tables 22 to 25 for the procedures Li-O-H, K-O-H, Rb-O-H and Cs-O-H in addition to Table 17 for the Na-O-H cycle and its many configurations, it is perceptible that:

- The minimum enthalpy change ( $\Delta H_{\min}$ ) for all thermochemical cycles considered, despite their variations, are equal to 285.83 kJ. This quantity is the same one required to direct crack water molecules into oxygen and hydrogen gas in the thermolysis process.
- The minimum amount of entropy change ( $\Delta S$ ) for variations (b), (d) and (e) of the cycles under attention are near to 163.31 J/K, the same amount for the thermolysis system. Variations (a) and (c) of any kind of cycle have  $\Delta S$  superior to 163.31 J/K.
- The minimum Gibbs free energy change ( $\Delta G$ ) for variations (b), (d) and (e) of any cycle assessed are about 237.16 kJ, the almost same value found during the modeling of water thermolysis reaction. Variations (a) and (c) of all cycles have  $\Delta G$  superior to 237.16 J/K.
- The maximum energy efficiency ( $\eta_{\max}$ ) for all the cycles evaluated, despite their variations, are equal to 100%, when the cycle demands the minimum amount of enthalpy change ( $\Delta H_{\min} = 285.83$  kJ) to occur as in the thermolysis process which has  $\eta_{\max}$  equal to 100% under standard conditions.
- Variations (b), (d) and (e) of the cycles analyzed, despite the metal under consideration (Na, Li, K, Rb or Cs), have the same overall values of  $\Delta H_{\min}$  about 285.83 kJ,  $\Delta S$  equal to 163.31 J/K,  $\Delta G$  near 237.15 kJ and  $\eta_{\max}$  equal to 100% as those ones for water thermolysis, as it can be seen in Tables 22 to 25. It happens because all those cycles represent indirect ways to reach water thermolysis; the net reaction of variations (b), (d) and (e) are simply water thermolysis, where  $H_2O$  turns into  $O_2$  and  $H_2$ , as can be observed in section 6.1. Variations (b), (d) and (e) only have chemical steps and none physical change. On the other hand, variations (a) and (c) have values of  $\Delta H_{\min}$ ,  $\Delta S$ ,  $\Delta G$  and  $\eta_{\max}$  different from water thermolysis because their net reaction are not just water thermolysis, this two variations also have a physical phase change like a metal condensation step in Equation (189) for variation (a) that will change the net values of  $\Delta H_{\min}$ ,  $\Delta S$ ,  $\Delta G$  and  $\eta_{\max}$ , making them different from water thermolysis and also from variations (b), (d) and (e).

So, accounting standard conditions of  $p$  and  $T$ , the cycles assessed in chapter 6 in addition to the Na-O-H one studied in chapter 5, all they have their minimum  $\Delta H$ ,  $\Delta S$  and  $\Delta G$  respectively equal to 285.83 kJ, 163.31 J/K and 237.15 kJ in addition to a maximum  $\eta = 100$  %, which are quantities similar to those ones for water thermolysis. Such behavior is not a coincidence and it

happens because this last one is a possible direct way to thermally decompose  $\text{H}_2\text{O}$  molecules into  $\text{O}_2$  and  $\text{H}_2$ . In this manner, it can be understood as the theoretical and ideal thermodynamic limit or reference (the minimum enthalpy, entropy and Gibbs free energy changes plus the maximum energy efficiency) for thermal water splitting process. On the other hand, thermochemical water splitting trials represents indirect way to achieve the same finality, what naturally increases the requirements of enthalpy and entropy in comparison to thermolysis due to increasing the number of chemical reactions and physical state change steps in some cases. However, actual thermochemical cycles are able to allow their proceeding because their chemical reactions decrease the overall Gibbs free energy to split water ( $\Delta G$  inferior to 0 for actual situations), allowing relatively low operational temperatures in the range of 500 °C for some cycles (Mg-Cl and Cu-Cl) when compared to the conventional  $\text{H}_2\text{O}$  thermolysis (2200 °C or above).

### **6.5 Thermodynamic limits for thermochemical cycles operating at standard conditions**

After comparing, analyzing and discussing the quantities of enthalpy change, entropy change, Gibbs free energy change and energy efficiency among the cycles under attention (Li-O-H, K-O-H, Rb-O-H, Cs-O-H and also the Na-O-H) and the thermolysis process in the last section, they are introduced the thermodynamic limits (the minimum requirements of  $\Delta H$ ,  $\Delta S$  and  $\Delta G$  plus the maximum  $\eta$ ) for thermochemical water splitting cycles of hydrogen production. Such concepts are generalized and extrapolated for any thermochemical process operating at standard conditions of  $p$  and  $T$  from the results related to the cycles studied in chapter 5 and 6 of this thesis.

So, all thermochemical water splitting cycles of hydrogen production operating at standard conditions of  $p$  (1 bar) and  $T$  (25 °C), aiming to produce 1 mol of  $\text{H}_2$ , have: enthalpy change superior to 285.83 kJ; entropy change superior to 163.31 J/K; Gibbs free energy change superior to 237.15 kJ and also energy efficiency inferior to 100%. It means that the energy needed by a thermochemical cycle to produce 1 mol of hydrogen gas is superior to the potential energy recovered by burning 1 mol of  $\text{H}_2$ .

## 6.6 Thermodynamic limits for thermochemical cycles operating at actual conditions

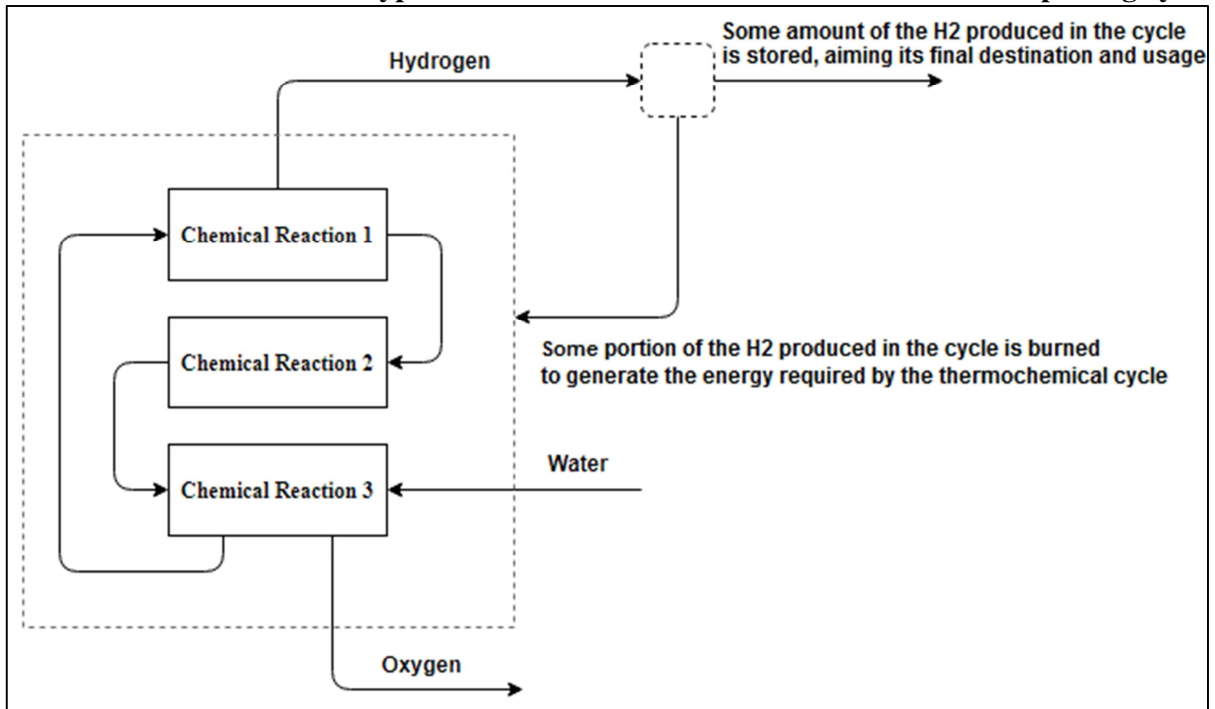
In practical situations, thermochemical water splitting cycle operates out of standard conditions of pressure and temperature for at least one or even all of its chemical steps in order to enable system occurrence, which is the decreasing of its Gibbs free energy until 0 or below it. Then, considering the mean values of  $\Delta H \sim 500$  kJ,  $\Delta S \sim 1000$  J/K,  $\Delta G \sim -70$  kJ and  $\eta = 50\%$  discussed in sections 4.2, 4.3 and 4.4 for the Na-O-H cycle operating at 100 °C (1 bar), 450 °C (0 bar) and 25 °C (1 bar) for its respective three steps, the statements introduced in the last section can be extrapolated for thermochemical cycles operating at actual conditions instead of standard ones.

Then, all thermochemical water splitting cycles of H<sub>2</sub> production operating at actual conditions, aiming to produce 1 mol of H<sub>2</sub>, have: enthalpy change superior to 285.83 kJ; entropy change superior to 163.31 J/K; Gibbs free energy change superior to 237.15 kJ and also energy efficiency inferior to 100%. It means that the energy needed by a thermochemical cycle to produce 1 mol of hydrogen gas is superior to the potential energy recovered by burning 1 mol of H<sub>2</sub>.

## 6.7 Impossibility of a self-sustainable thermochemical water splitting cycle of H<sub>2</sub> production

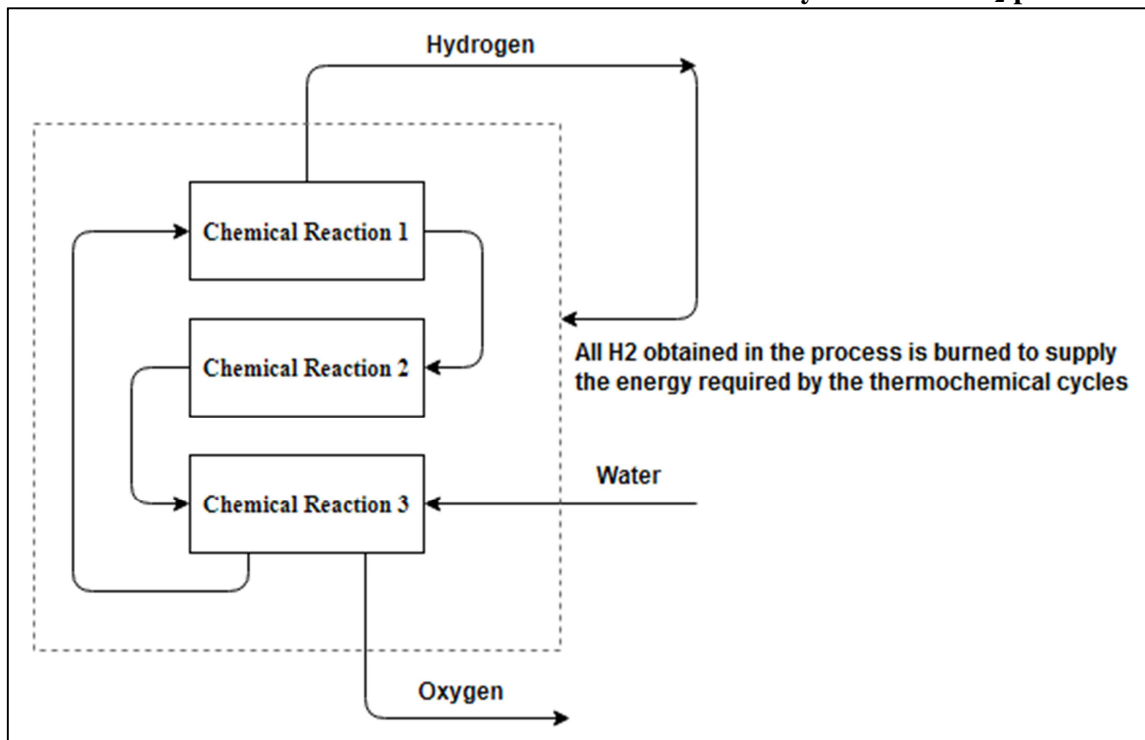
A hypothetical self-sustainable thermochemical water splitting trial of hydrogen production is a thermochemical cycle whose enthalpy requirement ( $\Delta H_{\text{auto sustainable}} < 285.83$  kJ) to generate 1 mol of H<sub>2</sub> would be inferior to the thermal energy released by the combustion of 1 mol of H<sub>2</sub> ( $\Delta H_{\text{combustion}} = 285.83$  kJ). In this way, some portion of the H<sub>2</sub> obtained in the process could be burned to supply the thermal energy demanded by the cycle, avoiding the use of any external heat source. A hypothetical self-sustainable 3-step thermochemical cycle is schematized in Figure 29. However, such concept is not possible because as said before, ideal and actual thermochemical cycles always demand enthalpy change superior to the energy released during H<sub>2</sub> combustion (285.83 kJ). In the best case, if a thermochemical cycle would have energy efficiency equal to 100%, the cycle would demand exactly 285.83 kJ to occur. In this way, the burning of all H<sub>2</sub> gotten in the process could be used to supply exactly the amount of energy required by it, but there would not be net H<sub>2</sub> made in the cycle because all of them would be applied to generate the heat requirement instead being stored after its making as suggested in Figure 30. Finally, Figure 31 represents actual thermochemical methods which necessarily demand external heat sources.

**FIGURE 29 – Scheme of a hypothetic self-sustainable thermochemical water splitting cycle**

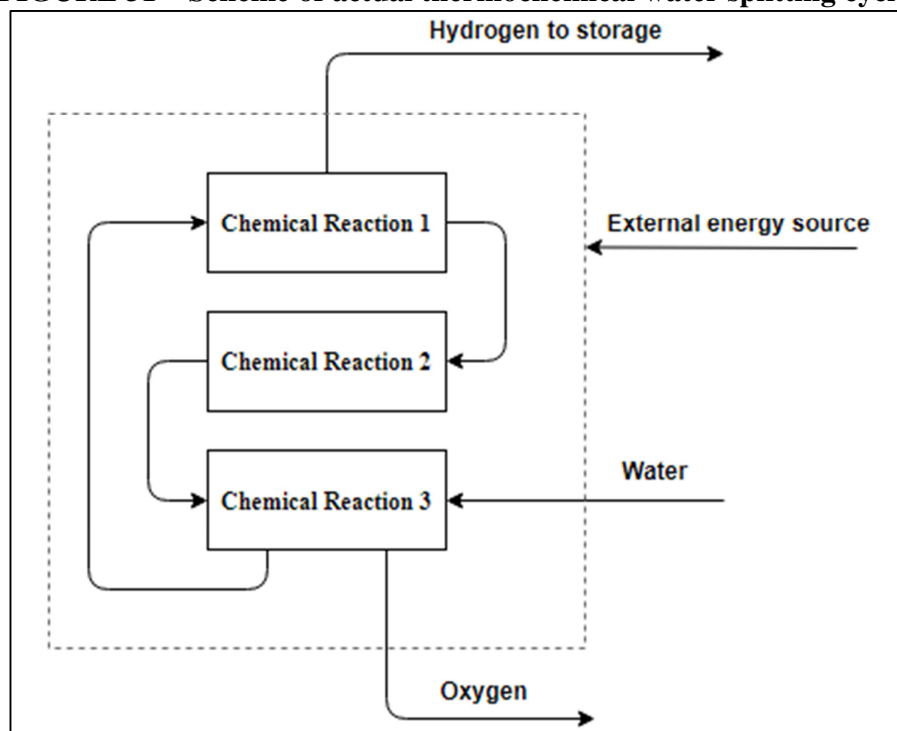


Source: the author.

**FIGURE 30 – Scheme of a self-sustainable thermochemical cycle without H<sub>2</sub> production**



Source: the author.

**FIGURE 31 – Scheme of actual thermochemical water splitting cycles**

Source: the author.



## 7 FINAL CONCLUSIONS

H<sub>2</sub> production based on the techniques Na-O-H thermochemical cycle through the heat supplied by a GEN-IV nuclear reactor coupled to a MED desalination unit allows the attaining of electricity, H<sub>2</sub> and H<sub>2</sub>O. These three products express key goods presently, what justifies the development of a thesis covering this trigeneration process, a task never done before which guarantees novelty for a research covering it. So, it becomes necessary to figure out if this new trigeneration process, considering its possible cases, has satisfactory thermal aspects aiming an actual implementation of it in the future.

The first main aim of this thesis was to evaluate the thermal performance of three trigeneration cases of electricity, hydrogen and desalinated water. H<sub>2</sub> comes from a hydrogen production unit based on the Na-O-H thermochemical water splitting cycle whose required heat is provided by three different 1000 MW<sub>th</sub> nuclear power plants (GT-MHR, SFR and SCWR), what distinguish every case. Fresh water is secured in a MED desalination facility that replaces the condensers or coolers in each NPP. It was considered a 1000 MW<sub>th</sub> for each NPP because this amount of heat is a common standard reference value for this kind of technology and study. Such aim is developed by implementing mass, energy, entropy, exergy and cost balances in the Engineering Equation Solver (EES) software to determine the amount of H<sub>2</sub>, electricity and desalinated H<sub>2</sub>O acquired. Consonant with results, this trigeneration process has potential to produce around 5 kg/s of hydrogen, 400 MW of electricity and 800 kg/s of desalinated H<sub>2</sub>O. Such values can have little variation depending on the GEN-IV considered as the energy source. These are theoretical and maximized values in function of all the simplifications and assumptions made to model all the trigeneration cases. Because of this, it is expected that the values found in the research decrease in practical situations.

SCWR and SFR were considered the best options to produce those three goods because they have potential to produce H<sub>2</sub> and electricity in similar quantities to GT-MHR, but they have potential to produce more fresh water than GT-MHR. However, SCWR is considered the best trigeneration case even when compared to SFR because SCWR is a simplified Rankine cycle, what naturally

demands fewer components in the system in comparison to SFR that have a full Rankine cycle in addition to two sodium loops. Such characteristic tends to facilitate an actual operation of SCWR.

All the results found in the first main aim can be extrapolated to estimate the potential to trigenerate electricity,  $H_2$  and desalinated water for the other GEN-IV reactors (GFR, LFR, MSR and VHTR) that were not evaluated in the work in function of available data and also to avoid the repetition of results. This last fact happens because some of these systems have operational thermodynamic conditions close to those ones already analyzed. For example, GT-MHR and VHTR work with helium coolant at around 800-900 °C what would implies on similar results for VHTR like the ones exhibited over section 4.6, 4.7 and 4.8 for GT-MHR.

The second main goal of this work was to analyze different variations (a, b, c, d and e) of the Na-O-H system to determine if one of them has better thermal aspects when compared to the traditional form of this cycle, variation (a), initially proposed by Miyaoka *et al.* (2012). Then, after the thermodynamic comparative study performed over chapter 5, it infers that there are other configurations of the sodium-oxygen-hydrogen system that could provide better thermal aspects when compared to its traditional approach, especially variation (e), a two-step process. It implies on a less challenge practical implementation of this cycle in the future and better thermodynamic results related to it in comparison to those ones already commented in chapter 4 about variation (a) of the sodium-oxygen-hydrogen procedure. Additionally, under standard conditions of pressure and temperature, variation (e) has theoretical energy efficiency near 77% while variation (a) has theoretical thermal efficiency around 52%.

Finally, in the third aim of this research were established the thermodynamic limits (the minimum requirements of enthalpy, entropy and Gibbs free energy changes plus the maximum energy efficiency) for thermochemical water splitting cycles of hydrogen production after analyzing and comparing the values of  $\Delta H$ ,  $\Delta S$ ,  $\Delta G$  and  $\eta$  among different thermochemical cycles (Li-O-H, K-O-H, Rb-O-H and Cs-O-H) with their respective variations and the direct thermal decomposition of water (thermolysis). According to the main founding, all thermochemical water splitting cycles of hydrogen production cycles must have  $\Delta H$  superior to 285.83 kJ to produce 1 mol of  $H_2$ . As consequence, it is impossible to build a self-sustainable closed thermochemical trial.

Then, after everything discussed through this research thesis, it concludes the trigeneration process of hydrogen, water and electricity based on the processes Na-O-H thermochemical cycles, GEN-IV nuclear reactors and MED desalination installation have potential to attempt the demand for such goods if they become mature technologies in the future through more research and development, specially the sodium-oxygen-hydrogen cycle .

The results presented and discussed over chapters 4, 5 and 6 were obtained considering many approximations and simplifications presented in section 3.4 in order to allow and facilitated the development of the research. Among the assumptions made they were neglected potential and kinetic energy in thermodynamic calculations (enthalpy and entropy changes in addition to energy and exergy balances) and tabulated constant values of standard chemical exergy. Pressure and heat losses in the systems under attention were not considered because the plants and installations analyzed are theoretical and simplified ones of technologies that still are under development or even do not have an actual design. Additionally, all chemical reactions and processes were modeled considering that they have yield equal to 100% combined with perfect stoichiometric proportion without molar excess of products or reactants. In function of all the simplifications performed, the values of pressure and temperature and the thermodynamic properties related to them (enthalpy, entropy and others) could have different values if were analyzed actual installations instead of theoretical and simplified ones. It would influence the final values of some variables calculated in the research such as thermal efficiency and the amount of hydrogen, electricity and desalinated water produced. However, despite all the simplifications made and their influence on the final results, it was possible to estimate the potential of the trigeneration cases proposed in the main aim of the thesis.

### **7.1 Suggestions for future researches**

- Determine which cycle (Li-O-H, Na-O-H, K-O-H, Rb-O-H, Cs-O-H) have the better “chemistry aspects” by using the 12 green chemistry principles such as waste prevention, design for degradation, design for energy efficiency, availability and so on. After the analysis, cycles that not have potential to be in accordance with the majority of the 12 principles should not be evaluated following the next suggestions for future researches.

- Gibbs free energy analysis combined with exergy analysis to evaluate possible theoretical operational conditions for the processes Li-O-H, K-O-H, Rb-O-H and Cs-O-H.
- Kinetic studies to evaluate reaction rates of the chemical steps in the systems Li-O-H, Na-O-H, K-O-H, Rb-O-H and Cs-O-H in order to determine which ones have the highest reaction rates, which facilitates their practical implementation; the faster reaction rate, the more chances of practical implementation it will have.
- Experimental analysis of each individual chemical reaction for every variation (a, b, c, d and e) of the cycles Li-O-H, Na-O-H, K-O-H, Rb-O-H and Cs-O-H. It is done to determine actual operational conditions of p and T for every chemical step and also to measure their actual reaction rates.
- Assembly of an experimental small scale plant for each cycle (Li-O-H, Na-O-H, K-O-H, Rb-O-H and Cs-O-H) in order to assess their behavior aiming a practical implementation of such systems in the future.
- Vacuum pump tests to determine the vacuum levels required to proceed chemical reaction 2 (metal separation step) in variation (a) of the cycles Li-O-H, Na-O-H, K-O-H, Rb-O-H and Cs-O-H. This research suggestion also can be applied to other variations (b, c, d and e) of such systems when one of their chemical steps must be performed in vacuum or very low pressure conditions.
- Evaluation and design of an experimental apparatus to evaluate the safety of chemical reaction 1 (hydrogen production step) due to the presence of alkali metals (Li, Na, K, Rb and Cs) that may leak and react with water and even air causing explosion.

## REFERENCES

ABANADES, A.; RUBBIA, C.; SALMIERI, D. Thermal cracking of methane into hydrogen for a CO<sub>2</sub>-free utilization of natural gas. **International Journal of Hydrogen Energy**, v. 38, n. 20, p. 8491-8496, 2013.

ABANADES, Stéphane et al. Screening of water-splitting thermochemical cycles potentially attractive for hydrogen production by concentrated solar energy. **Energy**, v. 31, n. 14, p. 2805-2822, 2006.

ABBAS, Hazzim F.; DAUD, WMA Wan. Hydrogen production by methane decomposition: a review. **International Journal of Hydrogen Energy**, v. 35, n. 3, p. 1160-1190, 2010.

ABDELKAREEM, Mohammad Ali et al. Recent progress in the use of renewable energy sources to power water desalination plants. **Desalination**, v. 435, p. 97-113, 2018.

ABRAM, Tim; ION, Sue. Generation-IV nuclear power: A review of the state of the science. **Energy Policy**, v. 36, n. 12, p. 4323-4330, 2008.

ACAR, Canan; DINCER, Ibrahim; NATERER, Greg F. Review of photocatalytic water-splitting methods for sustainable hydrogen production. **International Journal of Energy Research**, v. 40, n. 11, p. 1449-1473, 2016.

ADDISON, C. C.; PULHAM, R. J.; ROY, R. J. 19. Liquid metals. Part X. Solutions of hydrogen in liquid sodium. **Journal of the Chemical Society (Resumed)**, p. 116-121, 1965.

AHMAD, Adnan Darwish et al. Power boosting of a combined cycle power plant in Jordan: An integration of hybrid inlet cooling & solar systems. **Energy Conversion and Management**, v. 214, p. 112894, 2020.

AHN, Yoonhan; LEE, Jeong Ik. Study of various Brayton cycle designs for small modular sodium-cooled fast reactor. **Nuclear Engineering and Design**, v. 276, p. 128-141, 2014.

ALHENDAL, Yousuf et al. Thermal performance analysis of low-GWP refrigerants in automotive air-conditioning system. **Advances in Materials Science and Engineering**, v. 2020, 2020.

ALKAISI, Ahmed; MOSSAD, Ruth; SHARIFIAN-BARFOROUSH, Ahmad. A review of the water desalination systems integrated with renewable energy. **Energy Procedia**, v. 110, p. 268-274, 2017.

AL-HAMADI, Fatima I. et al. Analysis of OECD/NEA medium 1000 MWth sodium-cooled fast reactor using the Monte Carlo serpent code and ENDF/B-VIII. 0 nuclear data library. **Nuclear Science and Techniques**, v. 31, n. 12, p. 1-11, 2020.

AL-MUTAZ, Ibrahim S.; WAZEER, Irfan. Current status and future directions of MED-TVC desalination technology. **Desalination and Water Treatment**, v. 55, n. 1, p. 1-9, 2015.

AL-MUTAZ, Ibrahim S.; WAZEER, Irfan. Development of a steady-state mathematical model for MEE-TVC desalination plants. **Desalination**, v. 351, p. 9-18, 2014.

AL-SUBAIE, Khalid Z. Precise way to select a desalination technology. **Desalination**, v. 206, n. 1-3, p. 29-35, 2007.

AL-ZAREER, Maan; DINCER, Ibrahim; ROSEN, Marc A. Development and assessment of a novel integrated nuclear plant for electricity and hydrogen production. **Energy Conversion and Management**, v. 134, p. 221-234, 2017a.

AL-ZAREER, Maan; DINCER, Ibrahim; ROSEN, Marc A. Performance analysis of a supercritical water-cooled nuclear reactor integrated with a combined cycle, a Cu-Cl

thermochemical cycle and a hydrogen compression system. **Applied Energy**, v. 195, p. 646-658, 2017b.

AMAN, Delvin et al. Comparing nickel and cobalt perovskites for steam reforming of glycerol. **Molecular Catalysis**, v. 452, p. 60-67, 2018.

AMERICAN SOCIETY OF HEATING, REFRIGERATING AND AIR-CONDITIONING ENGINEERS (ASHRAE). **Handbook Fundamentals**. 2017.

AMIN, Ashraf M.; CROISET, Eric; EPLING, William. Review of methane catalytic cracking for hydrogen production. **International Journal of Hydrogen Energy**, v. 36, n. 4, p. 2904-2935, 2011.

ANIS, Shaheen Fatima; HASHAIKEH, Raed; HILAL, Nidal. Reverse osmosis pretreatment technologies and future trends: A comprehensive review. **Desalination**, v. 452, p. 159-195, 2019.

ANSARIFAR, H.; SHAMS, M. Numerical simulation of hydrogen production by gasification of large biomass particles in high temperature fluidized bed reactor. **International Journal of Hydrogen Energy**, v. 43, n. 10, p. 5314-5330, 2018.

AOTO, Kazumi et al. A summary of sodium-cooled fast reactor development. **Progress in Nuclear Energy**, v. 77, p. 247-265, 2014.

AYDIN, Ebubekir Siddik; YUCEL, Ozgun; SADIKOGLU, Hasan. Numerical and experimental investigation of hydrogen-rich syngas production via biomass gasification. **International Journal of Hydrogen Energy**, v. 43, n. 2, p. 1105-1115, 2018.

BADAWI, Michael et al. Molecular structures and thermodynamic properties of 12 gaseous cesium-containing species of nuclear safety interest: Cs<sub>2</sub>, CsH, CsO, Cs<sub>2</sub>O, CsX, and Cs<sub>2</sub>X<sub>2</sub> (X= OH, Cl, Br, and I). **Journal of Nuclear Materials**, v. 420, n. 1-3, p. 452-462, 2012.

BALTA, M. Tolga; DINCER, Ibrahim; HEPBASLI, Arif. Energy and exergy analyses of magnesium-chlorine (Mg-Cl) thermochemical cycle. **International Journal of Hydrogen Energy**, v. 37, n. 6, p. 4855-4862, 2012.

BALTA, M. Tolga; DINCER, Ibrahim; HEPBASLI, Arif. Thermodynamic assessment of geothermal energy use in hydrogen production. **International Journal of Hydrogen Energy**, v. 34, n. 7, p. 2925-2939, 2009.

BAYKARA, S. Z. Experimental solar water thermolysis. **International Journal of Hydrogen Energy**, v. 29, n. 14, p. 1459-1469, 2004.

BELLOS, Evangelos; CHATZOVOULOS, Ion; TZIVANIDIS, Christos. Yearly investigation of a solar-driven absorption refrigeration system with ammonia-water absorption pair. **Thermal Science and Engineering Progress**, p. 100885, 2021.

BETELIN, V. B. et al. Mathematical simulation of hydrogen–oxygen combustion in rocket engines using LOGOS code. **Acta Astronautica**, v. 96, p. 53-64, 2014.

BIANCHI, Fosco et al. Regional and world level scenarios for sodium fast reactor deployment. **Nuclear Engineering and Design**, v. 241, n. 4, p. 1145-1151, 2011.

BICER, Yusuf et al. Comparative life cycle assessment of various ammonia production methods. **Journal of Cleaner Production**, v. 135, p. 1379-1395, 2016.

BLÄSING, Marc; MÜLLER, Michael. Co-gasification of waste wood with coal: Release of condensable and non-condensable inorganic gas species. **International Journal of Hydrogen Energy**, v. 43, n. 1, p. 435-441, 2018.

BÖLÜKDEMİR, M. H.; KOÇ, H.; ESER, E. Calculation of thermophysical properties of copper compounds in CuCl production cycle. **Journal of Physics and Chemistry of Solids**, v. 112, p. 258-261, 2018.



BORGNAKKE, Claus; SONNTAG, Richard E. **Fundamentals of thermodynamics**: John Wiley & Sons, Inc, 2009.

BORGSTEDT, Hans Ulrich. **Material behavior and physical chemistry in liquid metal systems**. Springer Science & Business Media, 2012.

BRITISH PETROLEUM COMPANY (BPC). **BP Statistical Review of World Energy**. British Petroleum Company, 67<sup>th</sup> edition, 2018.

BROGIOLI, Dorian; LA MANTIA, Fabio; YIP, Ngai Yin. Thermodynamic analysis and energy efficiency of thermal desalination processes. **Desalination**, v. 428, p. 29-39, 2018.

BURN, Stewart et al. Desalination techniques—A review of the opportunities for desalination in agriculture. **Desalination**, v. 364, p. 2-16, 2015.

CARLSON, Fletcher et al. Model of the impact of use of thermal energy storage on operation of a nuclear power plant Rankine cycle. **Energy Conversion and Management**, v. 181, p. 36-47, 2019.

CASTELLAN, Gilbert W. **Physical Chemistry: Third Edition**. Addison-Wesley Publishing Company, 1983.

ÇELİK, Dicle; YILDIZ, Meltem. Investigation of hydrogen production methods in accordance with green chemistry principles. **International Journal of Hydrogen Energy**, v. 42, n. 36, p. 23395-23401, 2017.

ÇENGEL, Yunus A.; BOLES, Michael A. **Thermodynamics: an engineering approach**. 2002.

CHAICHI, A.; SADRNEZHAAD, S. K.; MALEKJAFARIAN, M. Synthesis and characterization of supportless Ni-Pd-CNT nanocatalyst for hydrogen production via steam reforming of methane. **International Journal of Hydrogen Energy**, v. 43, n. 3, p. 1319-1336, 2018.

CHAKIK, Fatima Ezzahra; KADDAMI, Mohammed; MIKOU, Mohammed. Effect of operating parameters on hydrogen production by electrolysis of water. **International Journal of Hydrogen Energy**, v. 42, n. 40, p. 25550-25557, 2017.

CHEN, Jing et al. CFD investigation on thermal-hydraulic behaviors of a wire-wrapped fuel subassembly for sodium-cooled fast reactor. **Annals of Nuclear Energy**, v. 113, p. 256-269, 2018.

CHEN, Q. et al. Energy, exergy and economic analysis of a hybrid spray-assisted low-temperature desalination/thermal vapor compression system. **Energy**, v. 166, p. 871-885, 2019.

CHRIST, Alexander; REGENAUER-LIEB, Klaus; CHUA, Hui Tong. Application of the Boosted MED process for low-grade heat sources—a pilot plant. **Desalination**, v. 366, p. 47-58, 2015a.

CHRIST, Alexander; REGENAUER-LIEB, Klaus; CHUA, Hui Tong. Boosted Multi-Effect Distillation for sensible low-grade heat sources: A comparison with feed pre-heating Multi-Effect Distillation. **Desalination**, v. 366, p. 32-46, 2015b.

CHRIST, Alexander; REGENAUER-LIEB, Klaus; CHUA, Hui Tong. Thermodynamic optimisation of multi effect distillation driven by sensible heat sources. **Desalination**, v. 336, p. 160-167, 2014.

CORUMLU, Vahit; OZSOY, Ahmet; OZTURK, Murat. Thermodynamic studies of a novel heat pipe evacuated tube solar collectors based integrated process for hydrogen production. **International Journal of Hydrogen Energy**, v. 43, n. 2, p. 1060-1070, 2018.

DA SILVA, Aline Lima; DE FRAGA MALFATTI, Celia; MÜLLER, Iduvirges Lourdes. Thermodynamic analysis of ethanol steam reforming using Gibbs energy minimization method: a detailed study of the conditions of carbon deposition. **International Journal of Hydrogen Energy**, v. 34, n. 10, p. 4321-4330, 2009.

DASTGERDI, Hamid Rezvani; WHITTAKER, Peter B.; CHUA, Hui Tong. New MED based desalination process for low grade waste heat. **Desalination**, v. 395, p. 57-71, 2016.

DEMIDOV, D. V.; MISHIN, I. V.; MIKHAILOV, M. N. Gibbs free energy minimization as a way to optimize the combined steam and carbon dioxide reforming of methane. **International Journal of Hydrogen Energy**, v. 36, n. 10, p. 5941-5950, 2011.

DEYAB, M. A. Enhancement of corrosion resistance in MSF desalination plants during acid cleaning operation by cationic surfactant. **Desalination**, v. 456, p. 32-37, 2019.

DI MAIO, Damiano Vitale et al. An alternative solution for heavy liquid metal cooled reactors fuel assemblies. **Nuclear Engineering and Design**, v. 278, p. 503-514, 2014.

DIMITRIOU, Pavlos et al. Combustion and emission characteristics of a hydrogen-diesel dual-fuel engine. **International Journal of Hydrogen Energy**, 2018.

DINCER, Ibrahim. Green methods for hydrogen production. **International Journal of Hydrogen Energy**, v. 37, n. 2, p. 1954-1971, 2012.

DOBÓ, Zsolt; PALOTÁS, Árpád Bence. Impact of the current fluctuation on the efficiency of Alkaline Water Electrolysis. **International Journal of Hydrogen Energy**, v. 42, n. 9, p. 5649-5656, 2017.

DRALEY, Joseph E.; Weeks, J. R. **Corrosion by liquid metals**. Springer Science & Business Media, 2013.

DUFOUR, Javier et al. Life cycle assessment of alternatives for hydrogen production from renewable and fossil sources. **International Journal of Hydrogen Energy**, v. 37, n. 2, p. 1173-1183, 2012.

DUMAN, Gozde; YANIK, Jale. Two-step steam pyrolysis of biomass for hydrogen production. **International Journal of Hydrogen Energy**, v. 42, n. 27, p. 17000-17008, 2017.

ECONOMIC AND SOCIAL COMMISSION FOR WESTERN ASIA (ESCWA). **ESCWA Water Development Report 3: Role of Desalination in Addressing Water Scarcity**. United Nations, 2009.

ELBASSOUSSI, Muhammad H.; ANTAR, M. A.; ZUBAIR, Syed M. Hybridization of a triple-effect absorption heat pump with a humidification-dehumidification desalination unit: Thermodynamic and economic investigation. **Energy Conversion and Management**, v. 233, p. 113879, 2021.

ELTAWIL, Mohamed A.; ZHENGMING, Zhao; YUAN, Liqiang. A review of renewable energy technologies integrated with desalination systems. **Renewable and Sustainable Energy Reviews**, v. 13, n. 9, p. 2245-2262, 2009.

FINK, J. K.; LEIBOWITZ, L. **Thermodynamic and transport properties of sodium liquid and vapor**. Argonne National Lab., 1995.

FORSBERG, Charles W. Hydrogen, nuclear energy, and the advanced high-temperature reactor. **International Journal of Hydrogen Energy**, v. 28, n. 10, p. 1073-1081, 2003.

FREITAS, Antonio CD; GUIRARDELLO, Reginaldo. Comparison of several glycerol reforming methods for hydrogen and syngas production using Gibbs energy minimization. **International Journal of Hydrogen Energy**, v. 39, n. 31, p. 17969-17984, 2014.

GABRIEL, Kamiel; FINNEY, Leonard; DOLLOSO, Patrick. Preliminary results of the integrated hydrolysis reactor in the Cu-Cl hydrogen production cycle. **International Journal of Hydrogen Energy**, 2019.

GABRIEL, Kerron J.; LINKE, Patrick; EL-HALWAGI, Mahmoud M. Optimization of multi-effect distillation process using a linear enthalpy model. **Desalination**, v. 365, p. 261-276, 2015.

GHARAGHEIZI, Farhad et al. A group contribution method for determination of the standard molar chemical exergy of organic compounds. **Energy**, v. 70, p. 288-297, 2014.

GHOSH, Devleena. "We don't want to eat coal": Development and its Discontents in a Chhattisgarh district in India. **Energy Policy**, v. 99, p. 252-260, 2016.

GILLIS, Ryan J.; AL-ALI, Khalid; GREEN, William H. Thermochemical production of hydrogen from hydrogen sulfide with iodine thermochemical cycles. **International Journal of Hydrogen Energy**, v. 43, n. 29, p. 12939-12947, 2018.

GNANASEKARAN, T. Thermochemistry of binary Na–NaH and ternary Na–O–H systems and the kinetics of reaction of hydrogen/water with liquid sodium—a review. **Journal of Nuclear Materials**, v. 274, n. 3, p. 252-272, 1999.

GONDAL, Irfan Ahmad; MASOOD, Syed Athar; KHAN, Rafiullah. Green hydrogen production potential for developing a hydrogen economy in Pakistan. **International Journal of Hydrogen Energy**, v. 43, n. 12, p. 6011-6039, 2018.

GOODARZI, Sina et al. Techno-economic evaluation of a multi effect distillation system driven by low-temperature waste heat from exhaust flue gases. **Desalination**, v. 460, p. 64-80, 2019.

GUDE, Veera Gnaneswar. Desalination and sustainability—an appraisal and current perspective. **Water research**, v. 89, p. 87-106, 2016.

GUÉNEAU, C.; FLÈCHE, J.-L. Thermodynamic assessment of the cesium–oxygen system by coupling density functional theory and CALPHAD approaches. **Calphad**, v. 49, p. 67-78, 2015.

GUZONAS, D.; NOVOTNY, R. Supercritical water-cooled reactor materials—Summary of research and open issues. **Progress in Nuclear Energy**, v. 77, p. 361-372, 2014.

HABIBI, Hamed et al. Thermo-economic performance comparison of two configurations of combined steam and organic Rankine cycle with steam Rankine cycle driven by Al<sub>2</sub>O<sub>3</sub>-therminol VP-1 based PTSC. **Solar Energy**, v. 180, p. 116-132, 2019.

HASELI, Y. Criteria for chemical equilibrium with application to methane steam reforming. **International Journal of Hydrogen Energy**, 2019.

HE, Zhenyu et al. Membrane-assisted propane partial oxidation for solid oxide fuel cell applications. **Journal of Power Sources**, v. 392, p. 200-205, 2018.

HILLERT, Mats; SELLEBY, Malin. Methods for storage of Gibbs energy data of substances. **Calphad**, v. 53, p. 146-150, 2016.

HIRAYAMA, Makoto et al. Comparative risk study of hydrogen and gasoline dispensers for vehicles. **International Journal of Hydrogen Energy**, 2018.

HOGNON, Céline et al. Hydrogen production by catalytic partial oxidation of propane over CeO<sub>2</sub>. **Chemical Engineering Science**, v. 181, p. 46-57, 2018.

HOLLADAY, Jamie D. et al. An overview of hydrogen production technologies. **Catalysis today**, v. 139, n. 4, p. 244-260, 2009.

INTERNATIONAL ENERGY AGENCY (IEA). Global Energy & CO<sub>2</sub> Status Report. **Electricity**. Available at: [www.iea.org/geco/electricity](http://www.iea.org/geco/electricity). 2018.

INTERNATIONAL ENERGY AGENCY (IEA). Hydrogen production and storage—R&D priorities and gaps. **International Energy Agency-Hydrogen Co-Ordination Group-Hydrogen Implementing Agreement**, 2006.

INTERNATIONAL RENEWABLE ENERGY AGENCY (IRENA). **Hydrogen from Renewable Power Technology Outlook for the Energy Transition**. 2018.

ISHAQ, H.; DINCER, I. A comparative evaluation of three CuCl cycles for hydrogen production. **International Journal of Hydrogen Energy**, 2019.

ISHAQ, H.; DINCER, I.; NATERER, G. F. Exergy analysis of waste heat recovery from furnace cement slag for clean hydrogen production. **Energy**, 2019.

ISHAQ, H.; DINCER, I.; NATERER, G. F. Industrial heat recovery from a steel furnace for the cogeneration of electricity and hydrogen with the copper-chlorine cycle. **Energy conversion and management**, v. 171, p. 384-397, 2018.

ISLAM, M. S. et al. Desalination technologies for developing countries: A review. **Journal of Scientific Research**, v. 10, n. 1, p. 77-97, 2018.

IVANOVSKII, N. N.; KOZLOV, F. A. Thermodynamic calculation of the reaction between sodium and water for a sodium-water type steam heater. **Soviet Atomic Energy**, v. 17, n. 5, p. 1155-1158, 1964.

JAIN, Vaibhav; SINGHAL, Ashu; JOSHI, Harsh. Exergy Analysis of Novel Combined Absorption Refrigeration System. In: **Advances in Electromechanical Technologies**. Springer, Singapore, 2021. p. 47-59.

JEONG, Woo Seok; JEONG, Yong Hoon. Performance of supercritical Brayton cycle using CO<sub>2</sub>-based binary mixture at varying critical points for SFR applications. **Nuclear Engineering and Design**, v. 262, p. 12-20, 2013.

Ji, Hyunjin et al. Hydrogen production from steam reforming using an indirect heating method. **International Journal of Hydrogen Energy**, v. 43, n. 7, p. 3655-3663, 2018.

JOSHI, Anand S.; DINCER, Ibrahim; REDDY, Bale V. Exergetic assessment of solar hydrogen production methods. **International Journal of Hydrogen Energy**, v. 35, n. 10, p. 4901-4908, 2010.

KALBASI, Rasool; RUHANI, Behrooz; ROSTAMI, Sara. Energetic analysis of an air handling unit combined with enthalpy air-to-air heat exchanger. **Journal of Thermal Analysis and Calorimetry**, v. 139, n. 4, p. 2881-2890, 2020.

KAMINSKI, Wladyslaw; MARSZALEK, Joanna; TOMCZAK, Elwira. Water desalination by pervaporation–Comparison of energy consumption. **Desalination**, v. 433, p. 89-93, 2018.

KASAHARA, S. et al. Current R&D status of thermochemical water splitting iodine-sulfur process in Japan Atomic Energy Agency. **International Journal of Hydrogen Energy**, v. 42, n. 19, p. 13477-13485, 2017.

KELLY, John E. Generation IV International Forum: A decade of progress through international cooperation. **Progress in Nuclear Energy**, v. 77, p. 240-246, 2014.

KHALID, Farrukh; DINCER, Ibrahim; ROSEN, Marc A. Comparative assessment of CANDU 6 and Sodium-cooled Fast Reactors for nuclear desalination. **Desalination**, v. 379, p. 182-192, 2016.

KIM, T. K. et al. Core design studies for a 1000 MWth advanced burner reactor. **Annals of Nuclear Energy**, v. 36, n. 3, p. 331-336, 2009.

KLEIN, S. & NELLIS G. **Thermodynamics**. New York: Cambridge. 2011.

KLEIN, S.A. **EES – Engineering Equation Solver**, Version 10.439, Year: 2019. F-Chart Software, <http://fchartsoftware.com>. Available at Federal University of Minas Gerais (UFMG).

LIDE, David R. (Ed.). **CRC handbook of chemistry and physics**. CRC press, 2004.



LIKKASIT, Chonnawee et al. Solar-aided hydrogen production methods for the integration of renewable energies into oil & gas industries. **Energy Conversion and Management**, v. 168, p. 395-406, 2018.

LIM, Dong-Won; LEE, Jae-Han; KIM, Sung-Kyun. Four-bar linkage modeling and kinematics analysis of an in-vessel transfer system for Prototype Gen-IV Sodium-cooled Fast Reactor. **Annals of Nuclear Energy**, v. 113, p. 493-505, 2018.

LOCATELLI, Giorgio; MANCINI, Mauro; TODESCHINI, Nicola. Generation IV nuclear reactors: Current status and future prospects. **Energy Policy**, v. 61, p. 1503-1520, 2013.

LUO, Wenhua; HU, Wangyu. Gibbs free energy, surface stress and melting point of nanoparticle. **Physica B: Condensed Matter**, v. 425, p. 90-94, 2013.

MAALI, Rafika; KHIR, Tahar. Performance analysis of different orc power plant configurations using solar and geothermal heat sources. **International Journal of Green Energy**, v. 17, n. 6, p. 349-362, 2020.

MABROUK, A. A. et al. Impacts of tube bundle arrangement and feed flow pattern on the scale formation in large capacity MED desalination plants. **Desalination**, v. 357, p. 275-285, 2015.

MAO, Jianfeng; GU, Qinfen; GREGORY, Duncan H. Revisiting the hydrogen storage behavior of the Na-OH system. **Materials**, v. 8, n. 5, p. 2191-2203, 2015.

MARQUES, João G. O.; COSTA, Antonella L.; PEREIRA, Cláudia. Gibbs free energy ( $\Delta G$ ) analysis for the NaOH (sodium-oxygen-hydrogen) thermochemical water splitting cycle. **International Journal of Hydrogen Energy**, v. 44, n. 29, p. 14536-14549, 2019.

MARQUES, João G. O.; COSTA, Antonella L.; PEREIRA, Cláudia. NaOH thermochemical water splitting cycle: A new approach in hydrogen production based on sodium cooled fast reactor. **International Journal of Hydrogen Energy**, v. 43, n. 16, p. 7738-7753, 2018a.

MARQUES, João G. O.; COSTA, Antonella L.; PEREIRA, Cláudia. Produção de água dessalinizada via processo MED (Multi-Effect Distillation) utilizando o calor rejeitado pelo condensador da usina PWR Angra 2. **Anais da Quarta Semana de Engenharia Nuclear e Ciências das Radiações – IV SENCIR**, 2018b.

MARQUES, João G. O.; COSTA, Antonella L.; PEREIRA, Cláudia. Thermodynamic study of a novel trigeneration process of hydrogen, electricity and desalinated water: The case of Na-OH thermochemical cycle, SCWR nuclear power plant and MED desalination installation. **Energy Conversion and Management**, v. 209, p. 112648, 2020b.

MARQUES, João GO; COSTA, Antonella L.; PEREIRA, Cláudia. Exergy analysis for the Na-OH (sodium-oxygen-hydrogen) thermochemical water splitting cycle. **International Journal of Hydrogen Energy**, v. 45(20), p. 11424-11437, 2020a.

MEZHER, Toufic et al. Techno-economic assessment and environmental impacts of desalination technologies. **Desalination**, v. 266, n. 1-3, p. 263-273, 2011.

MICARI, M. et al. Techno-economic assessment of multi-effect distillation process for the treatment and recycling of ion exchange resin spent brines. **Desalination**, v. 456, p. 38-52, 2019.

MILLER, Sydney; SHEMER, Hilla; SEMIAT, Raphael. Energy and environmental issues in desalination. **Desalination**, v. 366, p. 2-8, 2015.

MIYAOKA, Hiroki et al. Low-temperature water-splitting by sodium redox reaction. **International Journal of Hydrogen Energy**, v. 37, n. 23, p. 17709-17714, 2012.

MOGHRABI, A.; NOVOG, D. R. Determination of the optimal few-energy group structure for the Canadian Super Critical Water-cooled Reactor. **Annals of Nuclear Energy**, v. 115, p. 27-38, 2018.

MOHAMMADKHANI, F. et al. Exergoeconomic assessment and parametric study of a Gas Turbine-Modular Helium Reactor combined with two Organic Rankine Cycles. **Energy**, v. 65, p. 533-543, 2014.

MORAN, Michael J. et al. **Fundamentals of engineering thermodynamics**. John Wiley & Sons, 2011.

MOROSUK, Tatiana; TSATSARONIS, George. Advanced exergy-based methods used to understand and improve energy-conversion systems. **Energy**, v. 169, p. 238-246, 2019.

MORRIS, David R.; SZARGUT, Jan. Standard chemical exergy of some elements and compounds on the planet earth. **Energy**, v. 11, n. 8, p. 733-755, 1986.

MUSHARAVATI, Farayi; KHANMOHAMMADI, Shoaib; PAKSERESHT, Amirhossein. Proposed a new geothermal based poly-generation energy system including Kalina cycle, reverse osmosis desalination, electrolyzer amplified with thermoelectric: 3E analysis and optimization. **Applied Thermal Engineering**, v. 187, p. 116596, 2021.

MYLES, K. M.; CAFASSO, F. A. The reciprocal ternary system Na-NaOH-Na<sub>2</sub>O-NaH. **Journal of Nuclear Materials**, v. 67, n. 3, p. 249-253, 1977.

NAKAMURA, Naoya et al. Hydrogen production via thermochemical water-splitting by lithium redox reaction. **Journal of alloys and compounds**, v. 580, p. S410-S413, 2013.

NATIONAL INSTITUTE OF STANDARDS AND TECHNOLOGY (NIST). **Chemistry webbook: NIST standard reference database No. 69**, 2018.

NATOLA, F.; TOUZAIN, Ph. Diagramme de phases du système K-K<sub>2</sub>O et le monoxyde de potassium K<sub>2</sub>O. **Canadian Journal of Chemistry**, v. 48, n. 13, p. 1955-1958, 1970.

NERAC (Nuclear Energy Research Advisory Committee); GIF (Generation IV International Forum). A technology roadmap for generation IV nuclear energy systems. In: **The U.S DOE Nuclear Energy Research Advisory Committee and the Generation IV International Forum**. 2002.

NEWMAN, R. N.; SMITH, C. A. Sodium/water combustion and the chemistry of wastage at sodium/water leak sites. **Journal of Nuclear Materials**, v. 52, n. 2, p. 173-183, 1974.

NSW PUBLIC WORKS. **Brackish groundwater: a viable community water supply option?** Waterlines Report Series No. 66, NSW-Public-Works, 2011.

NUCLEAR ENERGY AGENCY (NEA). Technology roadmap update for Generation IV nuclear energy systems. In: **OECD Nuclear Energy Agency for the Generation IV International Forum**. 2014.

OHTA, Shigeo. Molecular hydrogen as a preventive and therapeutic medical gas: initiation, development and potential of hydrogen medicine. **Pharmacology & Therapeutics**, v. 144, n. 1, p. 1-11, 2014.

OLIVEIRA, P. P. **Fundamentos de termodinâmica aplicada**. Análise Energética e Exergética. Lidel, 2012.

OMONIYI, Oluwafemi A.; DUPONT, Valerie. Chemical looping steam reforming of acetic acid in a packed bed reactor. **Applied Catalysis B: Environmental**, v. 226, p. 258-268, 2018.

ORUC, Onur; DINCER, Ibrahim. Development and performance assessment power generating systems using clean hydrogen. **Energy**, v. 215, p. 119100, 2021.

OUAGUED, Malika; KHELLAF, Abdallah; LOUKARFI, Larbi. Performance analyses of Cu–Cl hydrogen production integrated solar parabolic trough collector system under Algerian climate. **International Journal of Hydrogen Energy**, v. 43, n. 6, p. 3451-3465, 2018.

OZBILEN, Ahmet; DINCER, Ibrahim; ROSEN, Marc A. Comparative environmental impact and efficiency assessment of selected hydrogen production methods. **Environmental Impact Assessment Review**, v. 42, p. 1-9, 2013.

OZBILEN, Ahmet; DINCER, Ibrahim; ROSEN, Marc A. Development of a four-step Cu–Cl cycle for hydrogen production–Part I: Exergoeconomic and exergoenvironmental analyses. **International Journal of Hydrogen Energy**, v. 41, n. 19, p. 7814-7825, 2016a.

OZBILEN, Ahmet; DINCER, Ibrahim; ROSEN, Marc A. Development of a four-step Cu–Cl cycle for hydrogen production–Part II: multi-objective optimization. **International Journal of Hydrogen Energy**, v. 41, n. 19, p. 7826-7834, 2016b.

OZCAN, Hasan; DINCER, Ibrahim. Comparative performance assessment of three configurations of magnesium–chlorine cycle. **International Journal of Hydrogen Energy**, v. 41, n. 2, p. 845-856, 2016c.

OZCAN, Hasan; DINCER, Ibrahim. Energy and exergy analyses of a solar driven Mg–Cl hybrid thermochemical cycle for co-production of power and hydrogen. **International Journal of Hydrogen Energy**, v. 39, n. 28, p. 15330-15341, 2014.

OZCAN, Hasan; DINCER, Ibrahim. Exergoeconomic optimization of a new four-step magnesium–chlorine cycle. **International Journal of Hydrogen Energy**, v. 42, n. 4, p. 2435-2445, 2017.

OZCAN, Hasan; DINCER, Ibrahim. Experimental investigation of an improved version of the four-step magnesium-chlorine cycle. **International Journal of Hydrogen Energy**, v. 43, n. 11, p. 5808-5819, 2018.

OZCAN, Hasan; DINCER, Ibrahim. Modeling of a new four-step magnesium–chlorine cycle with dry HCl capture for more efficient hydrogen production. **International Journal of Hydrogen Energy**, v. 41, n. 19, p. 7792-7801, 2016b.

OZCAN, Hasan; DINCER, Ibrahim. Thermodynamic modeling of a nuclear energy based integrated system for hydrogen production and liquefaction. **Computers & Chemical Engineering**, v. 90, p. 234-246, 2016a.

PATEL, C. R. P. et al. Enhanced hydrogen generation by water electrolysis employing carbon nano-structure composites. **International Journal of Hydrogen Energy**, v. 43, n. 6, p. 3180-3189, 2018.

PENG, Xiao-Long et al. Gibbs free energy of gaseous phosphorus dimer. **Chemical Engineering Science**, v. 190, p. 122-125, 2018.

PETERS, Jens F.; PETRAKOPOULOU, Fontina; DUFOUR, Javier. Exergetic analysis of a fast pyrolysis process for bio-oil production. **Fuel Processing Technology**, v. 119, p. 245-255, 2014.

PIACENTINO, Antonio. Application of advanced thermodynamics, thermoeconomics and exergy costing to a Multiple Effect Distillation plant: In-depth analysis of cost formation process. **Desalination**, v. 371, p. 88-103, 2015.

PINTO, F. Silva; MARQUES, R. Cunha. Desalination projects economic feasibility: A standardization of cost determinants. **Renewable and Sustainable Energy Reviews**, v. 78, p. 904-915, 2017.

PODILA, K.; RAO, Y. F. CFD analysis of flow and heat transfer in Canadian supercritical water reactor bundle. **Annals of Nuclear Energy**, v. 75, p. 1-10, 2015.

POULLIKKAS, Andreas. An overview of future sustainable nuclear power reactors. **International Journal of Energy & Environment**, v. 4, n. 5, 2013.

QASIM, Muhammad et al. Reverse osmosis desalination: A state-of-the-art review. **Desalination**, v. 459, p. 59-104, 2019.

QUISPE, Isabel; NAVIA, Rodrigo; KAHHAT, Ramzy. Energy potential from rice husk through direct combustion and fast pyrolysis: A review. **Waste Management**, v. 59, p. 200-210, 2017.

QURESHY, Ali MMI; DINCER, Ibrahim. Multi-Component Modeling and Simulation of a New Photoelectrochemical Reactor Design for Clean Hydrogen Production. **Energy**, p. 120196, 2021.

RAHIMI, Bijan et al. A novel process for low grade heat driven desalination. **Desalination**, v. 351, p. 202-212, 2014.

RAHIMI, Bijan et al. Thermo-economic analysis of two novel low grade sensible heat driven desalination processes. **Desalination**, v. 365, p. 316-328, 2015.

RICCA, Antonio et al. Innovative catalyst design for methane steam reforming intensification. **Fuel**, v. 198, p. 175-182, 2017.

RIVERO, R. and; GARFIAS, M. Standard chemical exergy of elements updated. **Energy**, v. 31, n. 15, p. 3310-3326, 2006.

RODRÍGUEZ, Daniel González et al. Computational model of a sulfur-iodine thermochemical water splitting system coupled to a VHTR for nuclear hydrogen production. **Energy**, v. 147, p. 1165-1176, 2018.

ROSTAMZADEH, Hadi et al. A novel multigeneration system driven by a hybrid biogas-geothermal heat source, Part I: Thermodynamic modeling. **Energy Conversion and Management**, v. 177, p. 535-562, 2018.

RUZICKOVA, M. et al. Overview and progress in the European project:“supercritical water reactor–fuel qualification test”. **Progress in Nuclear Energy**, v. 77, p. 381-389, 2014.

SAGIR, Emrah et al. Biological hydrogen production from sugar beet molasses by agar immobilized *R. capsulatus* in a panel photobioreactor. **International Journal of Hydrogen Energy**, v. 43, n. 32, p. 14987-14995, 2018.

ŞAHİN, Hacı Mehmet; EROL, Özgür; ACIR, Adem. Utilization of thorium in a gas turbine–modular helium reactor. **Energy conversion and management**, v. 63, p. 25-30, 2012.

SANUSI, Yinka S.; MOKHEIMER, Esmail MA; HABIB, Mohamed A. Thermo-economic analysis of integrated membrane-SMR ITM-oxy-combustion hydrogen and power production plant. **Applied Energy**, v. 204, p. 626-640, 2017.

SAYYAADI, Hoseyn. A conceptual design of a dual hydrogen-power generation plant based on the integration of the gas-turbine cycle and copper chlorine thermochemical plant. **International Journal of Hydrogen Energy**, v. 42, n. 48, p. 28690-28709, 2017.

SAYYAADI, Hoseyn; BOROJENI, Milad Saeedi. Conceptual design, process integration, and optimization of a solar CuCl thermochemical hydrogen production plant. **International Journal of Hydrogen Energy**, v. 42, n. 5, p. 2771-2789, 2017.

SCHMIDT, O. et al. Future cost and performance of water electrolysis: An expert elicitation study. **International Journal of Hydrogen Energy**, v. 42, n. 52, p. 30470-30492, 2017.

SCHULENBERG, Thomas; LEUNG, Laurence KH; OKA, Yoshiaki. Review of R&D for supercritical water cooled reactors. **Progress in Nuclear Energy**, v. 77, p. 282-299, 2014.

SCHULENBERG, Thomas; VISSER, Dirk C. Thermal-hydraulics and safety concepts of supercritical water cooled reactors. **Nuclear Engineering and Design**, v. 264, p. 231-237, 2013.

SENGODAN, Sivaprakash et al. Advances in reforming and partial oxidation of hydrocarbons for hydrogen production and fuel cell applications. **Renewable and Sustainable Energy Reviews**, v. 82, p. 761-780, 2018.

SHANDRO, Janis A. et al. Perspectives on community health issues and the mining boom–bust cycle. **Resources Policy**, v. 36, n. 2, p. 178-186, 2011.



SHARON, H.; REDDY, K. S. A review of solar energy driven desalination technologies. **Renewable and Sustainable Energy Reviews**, v. 41, p. 1080-1118, 2015.

SHIN, Gahui; YUN, Jinwon; YU, Sangseok. Thermal design of methane steam reformer with low-temperature non-reactive heat source for high efficiency engine-hybrid stationary fuel cell system. **International Journal of Hydrogen Energy**, v. 42, n. 21, p. 14697-14707, 2017.

SOLSVIK, Jannike; HAUG-WARBERG, Tore; JAKOBSEN, Hugo A. Implementation of chemical reaction equilibrium by Gibbs and Helmholtz energies in tubular reactor models: application to the steam–methane reforming process. **Chemical Engineering Science**, v. 140, p. 261-278, 2016.

SONG, Guohui et al. A unified correlation for estimating specific chemical exergy of solid and liquid fuels. **Energy**, v. 40, n. 1, p. 164-173, 2012.

SORGULU, F.; DINCER, I. Cost evaluation of two potential nuclear power plants for hydrogen production. **International Journal of Hydrogen Energy**, v. 43, n. 23, p. 10522-10529, 2018.

SU, Yali et al. Optimization study for thermal efficiency of supercritical water reactor nuclear power plant. **Annals of Nuclear Energy**, v. 63, p. 541-547, 2014.

SU, Yali et al. Theoretical study on the flow instability of supercritical water in the parallel channels. **Progress in Nuclear Energy**, v. 68, p. 169-176, 2013.

SUKHAREV, Yu P.; FOMICHENKO, P. A. GT-MHR project high-temperature reactor neutronic issues and ways to resolve them. **Nuclear Engineering and Design**, v. 271, p. 392-396, 2014.

TALEBBEYDOKHTI, Peyman et al. Analysis and optimization of LT-MED system powered by an innovative CSP plant. **Desalination**, v. 413, p. 223-233, 2017.

TECHNIPFMC 2018. **Hydrogen technology. Consistent market leadership.** 2018.

THABIT, Mshael S. et al. Evaluation of forward osmosis as a pretreatment process for multi stage flash seawater desalination. **Desalination**, v. 461, p. 22-29, 2019.

TILFORD, C. R. (1992). **Pressure and vacuum measurements.** Physical methods of chemistry.

TOURE, Oumar; DUSSAP, Claude-Gilles. Determination of Gibbs energies of formation in aqueous solution using chemical engineering tools. **Bioresource technology**, v. 213, p. 359-368, 2016.

TUNA, Celso Eduardo et al. Biogas steam reformer for hydrogen production: Evaluation of the reformer prototype and catalysts. **International Journal of Hydrogen Energy**, 2017.

TZANAKAKIS, V. A.; ANGELAKIS, A. N. Chemical exergy as a unified and objective indicator in the assessment and optimization of land treatment systems. **Ecological modelling**, v. 222, n. 17, p. 3082-3091, 2011.

UNITED NATIONS INTERNATIONAL CHILDREN'S EMERGENCY FUND (UNICEF). **World Health Organization, Progress on Sanitation and Drinking Water – Update and MDG Assessment**, 2015.

UNIVERSO ONLINE (UOL). **É possível viver com 110 litros de água por dia? Veja como seria a sua vida.** Available at: [www.noticias.uol.com.br/cotidiano/ultimas-noticias/2015/02/05/e-possivel-viver-com-110-litros-de-agua-por-dia-veja-como-seria-a-sua-vida.htm](http://www.noticias.uol.com.br/cotidiano/ultimas-noticias/2015/02/05/e-possivel-viver-com-110-litros-de-agua-por-dia-veja-como-seria-a-sua-vida.htm). 2015.

VAGHASIA, Rahul; JIANU, Ofelia A.; ROSEN, Marc A. Experimental study of effect of anolyte concentration and electrical potential on electrolyzer performance in thermochemical hydrogen production using the Cu-Cl cycle. **International Journal of Hydrogen Energy**, v. 43, n. 9, p. 4160-4166, 2018.

VELECKIS, E.; LEIBOWITZ, L. Phase relations for reactions of hydrogen with sodium oxide between 500 and 900 C. **Journal of Nuclear Materials**, v. 144, n. 3, p. 235-243, 1987.

VOGL, Valentin; ÅHMAN, Max; NILSSON, Lars J. Assessment of hydrogen direct reduction for fossil-free steelmaking. **Journal of Cleaner Production**, v. 203, p. 736-745, 2018.

WAJDA, Tomasz; GABRIEL, Kamiel. Thermolysis reactor scale-up for pilot scale CuCl hybrid hydrogen production. **International Journal of Hydrogen Energy**, 2018.

WANG, Xiaolin et al. Low grade heat driven multi-effect distillation technology. **International Journal of Heat and Mass Transfer**, v. 54, n. 25-26, p. 5497-5503, 2011.

WANG, Xinyu et al. Energy and exergy analysis of rice husk high-temperature pyrolysis. **International Journal of Hydrogen Energy**, v. 41, n. 46, p. 21121-21130, 2016.

WANG, Xurong; DAI, Yiping. An exergoeconomic assessment of waste heat recovery from a Gas Turbine-Modular Helium Reactor using two transcritical CO<sub>2</sub> cycles. **Energy Conversion and Management**, v. 126, p. 561-572, 2016.

WEGER, Lindsey; ABÁNADES, Alberto; BUTLER, Tim. Methane cracking as a bridge technology to the hydrogen economy. **International Journal of Hydrogen Energy**, v. 42, n. 1, p. 720-731, 2017.

WU, Wei; CHEN, Han Yu; HWANG, Jenn-Jiang. Energy analysis of a class of copper–chlorine (Cu–Cl) thermochemical cycles. **International Journal of Hydrogen Energy**, v. 42, n. 25, p. 15990-16002, 2017.

XU, Qiang et al. Reaction of hydrogen with sodium oxide: a reversible hydrogenation/dehydrogenation system. **Journal of Power Sources**, v. 155, n. 2, p. 167-171, 2006.

XU, Shaojie et al. Decomposition of hydriodic acid by electrolysis in the thermochemical water sulfur–iodine splitting cycle. **International Journal of Hydrogen Energy**, v. 43, n. 7, p. 3597-3604, 2018.

YALÇIN, S. A review of nuclear hydrogen production. **International Journal of Hydrogen Energy**, v. 14, n. 8, p. 551-561, 1989.

YAN, Xing L.; HINO, Ryutaro (Ed.). **Nuclear Hydrogen Production Handbook**. CRC Press, 2011.

YILMAZ, Fatih; OZTURK, Murat; SELBAS, Resat. Design and thermodynamic analysis of coal-gasification assisted multigeneration system with hydrogen production and liquefaction. **Energy Conversion and Management**, v. 186, p. 229-240, 2019a.

YILMAZ, Fatih; OZTURK, Murat; SELBAS, Resat. Development and performance analysis of a new solar tower and high temperature steam electrolyzer hybrid integrated plant. **International Journal of Hydrogen Energy**, 2019b.

YING, Zhi et al. Development of a novel flowsheet for sulfur–iodine cycle based on the electrochemical Bunsen reaction for hydrogen production. **International Journal of Hydrogen Energy**, v. 42, n. 43, p. 26586-26596, 2017.

YOO, Yong Hwan et al. Investigation of the threshold temperatures of sodium-carbon dioxide reaction for SFR system design. **Nuclear Engineering and Design**, v. 320, p. 235-249, 2017.

YOUSSEF, P. G.; AL-DADAH, R. K.; MAHMOUD, S. M. Comparative analysis of desalination technologies. **Energy Procedia**, v. 61, p. 2604-2607, 2014.

YUAN, Hongsheng et al. Heterogeneous bubble nucleation model on heated surface based on free energy analysis. **International Journal of Heat and Mass Transfer**, v. 122, p. 1198-1209, 2018.

YUN, Jinwon et al. Four different configurations of a 5 kW class shell-and-tube methane steam reformer with a low-temperature heat source. **International Journal of Hydrogen Energy**, v. 43, n. 9, p. 4546-4562, 2018.

ZARE, V. Exergoeconomic analysis with reliability and availability considerations of a nuclear energy-based combined cycle power plant. **Energy**, v. 96, p. 187-196, 2016.

ZARE, V.; MAHMOUDI, S. M. S. A thermodynamic comparison between organic Rankine and Kalina cycles for waste heat recovery from the Gas Turbine-Modular Helium Reactor. **Energy**, v. 79, p. 398-406, 2015.

ZARE, V.; MAHMOUDI, S. M. S.; YARI, M. An exergoeconomic investigation of waste heat recovery from the Gas Turbine-Modular Helium Reactor (GT-MHR) employing an ammonia-water power/cooling cycle. **Energy**, v. 61, p. 397-409, 2013.

ZENG, Kai; ZHANG, Dongke. Recent progress in alkaline water electrolysis for hydrogen production and applications. **Progress in Energy and Combustion Science**, v. 36, n. 3, p. 307-326, 2010.

ZHANG, Ke et al. A review of recent researches on Bunsen reaction for hydrogen production via SI water and H<sub>2</sub>S splitting cycles. **Journal of energy chemistry**, v. 33, p. 46-58, 2019.

ZHONG, Xianping et al. Analysis of wall temperature jump of China Generation IV SFR Steam Generator. **Annals of Nuclear Energy**, v. 114, p. 510-517, 2018.

ZHOU, Chenglin et al. Absorption behaviors of SO<sub>2</sub> in HI acid for the iodine-sulfur thermochemical cycle. **International Journal of Hydrogen Energy**, v. 42, n. 47, p. 28164-28170, 2017.

ZHOU, Chenglin et al. Experimental investigation of reaction kinetics of gas-liquid-solid Bunsen reaction in iodine-sulfur process. **International Journal of Hydrogen Energy**, 2019.

ZHOU, Lu; BASSET, Jean Marie. Unsupported NiPt alloy metal catalysts prepared by water-in-oil (W/O) microemulsion method for methane cracking. **Fuel**, v. 181, p. 805-810, 2016.

## APPENDIX

The thermodynamic data presented over Appendix chapter refers to the values of enthalpy, entropy and Gibbs free energy changes plus energy efficiency calculated for each reaction of every cycle under study in chapter 6 (Li-O-H, K-O-H, Rb-O-H and Cs-O-H). It was done to shorten chapter 6 and facilitate its reading, analysis and discussion by not showing intermediate information ( $\Delta H$ ,  $\Delta S$ ,  $\Delta G$  and  $\eta$ ) for every reaction of each system but only describing the overall values of such variable for the cycles as in Tables 22 to 25 in section 6.4. Additionally, a similar discussion performed in section 5.4 for all variations of the Na-O-H trial also could be done here for the other cycles, but it is not the case because there is no necessity to do it.

### Results of all chemical reactions for all variations of the Li-O-H cycle

Tables 26 to 30 are obtained after implementing Equations (102) to (185) for all variations (a, b, c, d and e) of the Li-O-H cycle described in section 6.1.1 together with thermodynamic data for Li compounds from Table 18, as explained in section 6.2. The results related to all configurations of the lithium-oxygen-hydrogen procedure in Tables 26 to 30 are combined to build Table 22 in section 6.4.

**TABLE 26 -  $\Delta H_{a,i}^0$ ,  $S_{a,i}^0$ ,  $G_{a,i}^0$  and  $\eta_a$  for (Li-O-H)<sub>a</sub> and its chemical reactions**

Variables	Reaction 1 Eq. (186)	Reaction 2 Eq. (187)	Reaction 3 Eq. (188)	Condensation Eq. (189)	Li-O-H cycle variation (a)
$\Delta H_{a,i}^0$ [kJ]	-232.36	881.76	-49.73	-313.84	649.40 <sup>1</sup> to 285.83 <sup>2</sup>
$\Delta S_{a,i}^0$ [J/K]	52.88	260.38	59.73	-	372.99
$\Delta G_{a,i}^0$ [kJ]	-248.11	804.16	-67.52	-	488.52
$\eta_a$ [%]	-	-	-	-	44.01 <sup>1</sup> to 100 <sup>2</sup>

1-Whitout recovering the energy released from Equations (188) and (189) - ( $\Delta H_{\max}$  and  $\eta_{\min}$ ).

2-Recovering the energy released from Equations (188) and (189) - ( $\Delta H_{\min}$  and  $\eta_{\max}$ ).

Source: the author.

**TABLE 27 -  $\Delta H_{b,i}^0$ ,  $\Delta S_{b,i}^0$ ,  $G_{b,i}^0$  and  $\eta_b$  for (Li-O-H)<sub>b</sub> and its chemical reactions**

Variables	Reaction 1 Eq. (190)	Reaction 2 Eq. (191)	Reaction 3 Eq. (192)	Li-O-H Cycle variation (b)
$\Delta H_{b,i}^0$ [kJ]	394.43	92.88	-201.48	487.31 <sup>1</sup> to 285.83 <sup>2</sup>
$\Delta S_{b,i}^0$ [J/K]	79.80	79.25	4.26	163.31
$\Delta G_{b,i}^0$ [kJ]	370.65	69.26	-202.79	237.16
$\eta_b$ [%]	-	-	-	58.65 <sup>1</sup> to 100 <sup>2</sup>

1-Whitout recovering the energy released from Equation (192) - ( $\Delta H_{\max}$  and  $\eta_{\min}$ ).

2-Recovering the energy released from Equation (192) - ( $\Delta H_{\min}$  and  $\eta_{\max}$ ).

Source: the author.

**TABLE 28 -  $\Delta H^0_{c,i}$ ,  $\Delta S^0_{c,i}$ ,  $\Delta G^0_{c,i}$  and  $\eta_c$  for (Li-O-H)<sub>c</sub> and its chemical reactions**

Variables	Reaction 1 Eq. (193)	Reaction 2 Eq. (194)	Reaction 3 Eq. (195)	Reaction 4 Eq. (196)	Solidification Eq. (197)	Li-O-H cycle variation (c)
$\Delta H^0_{c,i}$ [kJ]	-116.18	394.43	219.57	-201.48	-10.51	614.00 <sup>1</sup> to 285.83 <sup>2</sup>
$\Delta S^0_{c,i}$ [J/K]	26.44	79.80	57.97	4.26	-	168.47
$\Delta G^0_{c,i}$ [kJ]	-124.05	370.65	202.29	-202.74	-	246.13
$\eta_c$ [%]	-	-	-	-	-	46.55 <sup>1</sup> to 100 <sup>2</sup>

1-Whitout recovering the energy released from Equations (196) and (197) - ( $\Delta H_{\max}$  and  $\eta_{\min}$ ).

2-Recovering the energy released from Equations (196) and (197) - ( $\Delta H_{\min}$  and  $\eta_{\max}$ ).

Source: the author.

**TABLE 29 -  $\Delta H^0_{d,i}$ ,  $\Delta S^0_{d,i}$ ,  $\Delta G^0_{d,i}$  and  $\eta_d$  for (Li-O-H)<sub>d</sub> and its chemical reactions**

Variables	Reaction 1 Eq. (198)	Reaction 2 Eq. (199)	Reaction 3 Eq. (200)	Li-O-H cycle variation (d)
$\Delta H^0_{d,i}$ [kJ]	-116.18	603.49	-201.48	603.49 <sup>1</sup> to 285.83 <sup>2</sup>
$\Delta S^0_{d,i}$ [J/K]	26.44	132.61	4.26	163.31
$\Delta G^0_{d,i}$ [kJ]	-124.05	563.97	-202.74	237.16
$\eta_d$ [%]	-	-	-	47.36 <sup>1</sup> to 100 <sup>2</sup>

1-Whitout recovering the energy released from Equation (200) - ( $\Delta H_{\max}$  and  $\eta_{\min}$ ).

2-Recovering the energy released from Equation (200) - ( $\Delta H_{\min}$  and  $\eta_{\max}$ ).

Source: the author.

**TABLE 30 -  $\Delta H^0_{e,i}$ ,  $\Delta S^0_{e,i}$ ,  $\Delta G^0_{e,i}$  and  $\eta_e$  for (Li-O-H)<sub>e</sub> and its chemical reactions**

Variables	Reaction 1 Eq. (201)	Reaction 2 Eq. (202)	Li-O-H cycle variation (e)
$\Delta H^0_{e,i}$ [kJ]	394.43	-108.60	394.43 <sup>1</sup> to 285.83 <sup>2</sup>
$\Delta S^0_{e,i}$ [J/K]	79.80	83.31	163.31
$\Delta G^0_{e,i}$ [kJ]	370.65	-133.42	237.22
$\eta_e$ [%]	-	-	72.46 <sup>1</sup> to 100 <sup>2</sup>

1-Whitout recovering the energy released from Equation (202) - ( $\Delta H_{\max}$  and  $\eta_{\min}$ ).

2-Recovering the energy released from Eq. (202) - ( $\Delta H_{\min}$  and  $\eta_{\max}$ ).

Source: the author.

### Results of all chemical reactions for all variations of the K-O-H cycle

Tables 31 to 35 are obtained after implementing Equations (102) to (185) for all variations (a, b, c, d and e) of the K-O-H cycle described in section 6.1.2 together with thermodynamic data for potassium compounds from Table 19, as explained in section 6.2. The results related to all configurations of the potassium-oxygen-hydrogen procedure in Tables 31 to 35 are combined to build Table 23 in section 6.4.

**TABLE 31 -  $\Delta H_{a,i}^0$ ,  $S_{a,i}^0$ ,  $G_{a,i}^0$  and  $\eta_a$  for (K-O-H)<sub>a</sub> and its chemical reactions**

Variables	Reaction 1 Eq. (186)	Reaction 2 Eq. (187)	Reaction 3 Eq. (188)	Condensation Eq. (189)	K-O-H cycle variation (a)
$\Delta H_{a,i}^0$ [kJ]	118.56	410.24	-69.51	-173.46	528.8 <sup>1</sup> to 285.83 <sup>2</sup>
$\Delta S_{a,i}^0$ [J/K]	18.14	234.72	88.33	-	341.19
$\Delta G_{a,i}^0$ [kJ]	113.15	340.29	-95.83	-	357.61
$\eta_a$ [%]	-	-	-	-	54.05 <sup>1</sup> to 100 <sup>2</sup>

1-Whitout recovering the energy released from Equations (188) and (189) - ( $\Delta H_{\max}$  and  $\eta_{\min}$ ).

2-Recovering the energy released from Equations (188) and (189) - ( $\Delta H_{\min}$  and  $\eta_{\max}$ ).

Source: the author.

**TABLE 32 -  $\Delta H_{b,i}^0$ ,  $\Delta S_{b,i}^0$ ,  $G_{b,i}^0$  and  $\eta_b$  for (K-O-H)<sub>b</sub> and its chemical reactions**

Variables	Reaction 1 Eq. (190)	Reaction 2 Eq. (191)	Reaction 3 Eq. (192)	K-O-H cycle variation (b)
$\Delta H_{b,i}^0$ [kJ]	366.90	60.09	-141.16	426.99 <sup>1</sup> to 285.83 <sup>2</sup>
$\Delta S_{b,i}^0$ [J/K]	73.86	86.56	2.89	163.31
$\Delta G_{b,i}^0$ [kJ]	344.89	34.29	-142.02	237.16
$\eta_b$ [%]	-	-	-	66.94 <sup>1</sup> to 100 <sup>2</sup>

1-Whitout recovering the energy released from Equation (192) - ( $\Delta H_{\max}$  and  $\eta_{\min}$ ).

2-Recovering the energy released from Equation (192) - ( $\Delta H_{\min}$  and  $\eta_{\max}$ ).

Source: the author.

**TABLE 33 -  $\Delta H_{c,i}^0$ ,  $\Delta S_{c,i}^0$ ,  $\Delta G_{c,i}^0$  and  $\eta_c$  for (K-O-H)<sub>c</sub> and its chemical reactions**

Variables	Reaction 1 Eq. (193)	Reaction 2 Eq. (194)	Reaction 3 Eq. (195)	Reaction 4 Eq. (196)	Solidification Eq. (197)	K-O-H cycle variation (c)
$\Delta H_{c,i}^0$ [kJ]	59.28	366.90	12.82	-141.16	-12.01	439.00 <sup>1</sup> to 285.83 <sup>2</sup>
$\Delta S_{c,i}^0$ [J/K]	9.07	73.86	95.21	2.89	-	181.03
$\Delta G_{c,i}^0$ [kJ]	56.57	344.89	-15.55	-142.02	-	243.89
$\eta_c$ [%]	-	-	-	-	-	65.10 <sup>1</sup> to 100 <sup>2</sup>

1-Whitout recovering the energy released from Equations (196) and (197) - ( $\Delta H_{\max}$  and  $\eta_{\min}$ ).

2-Recovering the energy released from Equations (196) and (197) - ( $\Delta H_{\min}$  and  $\eta_{\max}$ ).

Source: the author.

**TABLE 34 -  $\Delta H_{d,i}^0$ ,  $\Delta S_{d,i}^0$ ,  $\Delta G_{d,i}^0$  and  $\eta_d$  for (K-O-H)<sub>d</sub> and its chemical reactions**

Variables	Reaction 1 Eq. (198)	Reaction 2 Eq. (199)	Reaction 3 Eq. (200)	K-O-H cycle variation (d)
$\Delta H_{d,i}^0$ [kJ]	59.28	367.71	-141.16	426.99 <sup>1</sup> to 285.83 <sup>2</sup>
$\Delta S_{d,i}^0$ [J/K]	9.07	151.35	2.89	163.31
$\Delta G_{d,i}^0$ [kJ]	56.57	322.60	-142.02	237.16
$\eta_d$ [%]	-	-	-	66.94 <sup>1</sup> to 100 <sup>2</sup>

1-Whitout recovering the energy released from Equation (200) - ( $\Delta H_{\max}$  and  $\eta_{\min}$ ).

2-Recovering the energy released from Equation (200) - ( $\Delta H_{\min}$  and  $\eta_{\max}$ ).

Source: the author.



**TABLE 35 -  $\Delta H_{e,i}^0$ ,  $\Delta S_{e,i}^0$ ,  $\Delta G_{e,i}^0$  and  $\eta_e$  for (K-O-H)<sub>e</sub> and its chemical reactions**

Variables	Reaction 1 Eq. (201)	Reaction 2 Eq. (202)	K-O-H cycle variation (e)
$\Delta H_{e,i}^0$ [kJ]	366.90	-81.07	366.90 <sup>1</sup> to 285.83 <sup>2</sup>
$\Delta S_{e,i}^0$ [J/K]	73.86	89.45	163.31
$\Delta G_{e,i}^0$ [kJ]	344.89	-107.71	237.16
$\eta_e$ [%]	-	-	77.90 <sup>1</sup> to 100 <sup>2</sup>

1-Whitout recovering the energy released from Equation (202) - ( $\Delta H_{\max}$  and  $\eta_{\min}$ ).

2-Recovering the energy released from Equation (202) - ( $\Delta H_{\min}$  and  $\eta_{\max}$ ).

Source: the author.

### Results of all chemical reactions for all variations of the Rb-O-H cycle

Tables 36 to 40 are obtained after implementing Equations (102) to (185) for all variations (a, b, c, d and e) of the Rb-O-H cycle described in section 6.1.3 together with thermodynamic data for rubidium compounds from Table 20, as explained in section 6.2. The results related to all configurations of the rubidium-oxygen-hydrogen procedure in Tables 36 to 40 are combined to build Table 24 in section 6.4.

**TABLE 36 -  $\Delta H_{a,i}^0$ ,  $S_{a,i}^0$ ,  $G_{a,i}^0$  and  $\eta_a$  for (Rb-O-H)<sub>a</sub> and its chemical reactions**

Variables	Reaction 1 Eq. (186)	Reaction 2 Eq. (187)	Reaction 3 Eq. (188)	Condensation Eq. (189)	Rb-O-H cycle variation (a)
$\Delta H_{a,i}^0$ [kJ]	155.21	387.80	-99.74	-157.44	543.01 <sup>1</sup> to 285.83 <sup>2</sup>
$\Delta S_{a,i}^0$ [J/K]	26.31	248.18	61.48	-	335.97
$\Delta G_{a,i}^0$ [kJ]	147.36	313.84	-118.05	-	343.15
$\eta_a$ [%]	-	-	-	-	52.63 <sup>1</sup> to 100 <sup>2</sup>

1-Whitout recovering the energy released from Equations (188) and (189) - ( $\Delta H_{\max}$  and  $\eta_{\min}$ ).

2-Recovering the energy released from Equations (188) and (189) - ( $\Delta H_{\min}$  and  $\eta_{\max}$ ).

Source: the author.

**TABLE 37 -  $\Delta H_{b,i}^0$ ,  $\Delta S_{b,i}^0$ ,  $G_{b,i}^0$  and  $\eta_b$  for (Rb-O-H)<sub>b</sub> and its chemical reactions**

Variables	Reaction 1 Eq. (190)	Reaction 2 Eq. (191)	Reaction 3 Eq. (192)	Rb-O-H cycle variation (b)
$\Delta H_{b,i}^0$ [kJ]	366.48	54.48	-135.13	420.96 <sup>1</sup> to 285.83 <sup>2</sup>
$\Delta S_{b,i}^0$ [J/K]	67.15	90.10	6.06	163.31
$\Delta G_{b,i}^0$ [kJ]	346.47	27.63	-136.93	237.16
$\eta_b$ [%]	-	-	-	67.89 <sup>1</sup> to 100 <sup>2</sup>

1-Whitout recovering the energy released from Equation (192) - ( $\Delta H_{\max}$  and  $\eta_{\min}$ ).

2-Recovering the energy released from Equation (192) - ( $\Delta H_{\min}$  and  $\eta_{\max}$ ).

Source: the author.

**TABLE 38 -  $\Delta H^0_{c,i}$ ,  $\Delta S^0_{c,i}$ ,  $\Delta G^0_{c,i}$  and  $\eta_c$  for (Rb-O-H)<sub>c</sub> and its chemical reactions**

Variables	Reaction 1 Eq. (193)	Reaction 2 Eq. (194)	Reaction 3 Eq. (195)	Reaction 4 Eq. (196)	Solidification Eq. (197)	Rb-O-H cycle variation (c)
$\Delta H^0_{c,i}$ [kJ]	77.60	366.48	-6.60	-135.13	-16.30	443.86 <sup>1</sup> to 285.83 <sup>2</sup>
$\Delta S^0_{c,i}$ [J/K]	13.15	67.15	133.64	6.06	-	220.00
$\Delta G^0_{c,i}$ [kJ]	73.68	346.47	-46.42	-136.93	-	236.79
$\eta_c$ [%]	-	-	-	-	-	64.39 <sup>1</sup> to 100 <sup>2</sup>

1-Whitout recovering the energy released from Equations (196) and (197) - ( $\Delta H_{\max}$  and  $\eta_{\min}$ ).

2-Recovering the energy released from Equations (196) and (197) - ( $\Delta H_{\min}$  and  $\eta_{\max}$ ).

Source: the author.

**TABLE 39 -  $\Delta H^0_{d,i}$ ,  $\Delta S^0_{d,i}$ ,  $\Delta G^0_{d,i}$  and  $\eta_d$  for (Rb-O-H)<sub>d</sub> and its chemical reactions**

Variables	Reaction 1 Eq. (198)	Reaction 2 Eq. (199)	Reaction 3 Eq. (200)	Rb-O-H cycle variation (d)
$\Delta H^0_{d,i}$ [kJ]	77.60	343.36	-135.13	420.96 <sup>1</sup> to 285.83 <sup>2</sup>
$\Delta S^0_{d,i}$ [J/K]	13.15	144.10	6.06	163.31
$\Delta G^0_{d,i}$ [kJ]	73.68	300.41	-136.93	237.16
$\eta_d$ [%]	-	-	-	67.89 <sup>1</sup> to 100 <sup>2</sup>

1-Whitout recovering the energy released from Equation (200) - ( $\Delta H_{\max}$  and  $\eta_{\min}$ ).

2-Recovering the energy released from Equation (200) - ( $\Delta H_{\min}$  and  $\eta_{\max}$ ).

Source: the author.

**TABLE 40 -  $\Delta H^0_{e,i}$ ,  $\Delta S^0_{e,i}$ ,  $\Delta G^0_{e,i}$  and  $\eta_e$  for (Rb-O-H)<sub>e</sub> and its chemical reactions**

Variables	Reaction 1 Eq. (201)	Reaction 2 Eq. (202)	Rb-O-H cycle variation (e)
$\Delta H^0_{e,i}$ [kJ]	366.48	-80.65	366.48 <sup>1</sup> to 285.83 <sup>2</sup>
$\Delta S^0_{e,i}$ [J/K]	67.15	96.16	163.31
$\Delta G^0_{e,i}$ [kJ]	346.47	-109.30	237.16
$\eta_e$ [%]	-	-	77.99 <sup>1</sup> to 100 <sup>2</sup>

1-Whitout recovering the energy released from Equation (202) - ( $\Delta H_{\max}$  and  $\eta_{\min}$ ).

2-Recovering the energy released from Equation (202) - ( $\Delta H_{\min}$  and  $\eta_{\max}$ ).

Source: the author.

## Results of all chemical reactions for all variations of the Cs-O-H cycle

Tables 41 to 45 are obtained after implementing Equations (102) to (185) for all variations (a, b, c, d and e) of the Cs-O-H cycle described in section 6.1.4 together with thermodynamic data for cesium compounds from Table 21, as explained in section 6.2. The results related to all configurations of the cesium-oxygen-hydrogen procedure in Tables 41 to 45 are combined to build Table 25 in section 6.4.

**TABLE 41 -  $\Delta H_{a,i}^0$ ,  $S_{a,i}^0$ ,  $G_{a,i}^0$  and  $\eta_a$  for (Cs-O-H)<sub>a</sub> and its chemical reactions**

Variables	Reaction 1 Eq. (186)	Reaction 2 Eq. (187)	Reaction 3 Eq. (188)	Condensation Eq. (189)	Cs-O-H cycle variation (a)
$\Delta H_{a,i}^0$ [kJ]	137.68	454.60	-157.63	-148.82	592.28 <sup>1</sup> to 285.83 <sup>2</sup>
$\Delta S_{a,i}^0$ [J/K]	41.60	272.80	14.71	-	329.11
$\Delta G_{a,i}^0$ [kJ]	125.28	373.30	-162.01	-	336.57
$\eta_a$ [%]	-	-	-	-	48.25 <sup>1</sup> to 100 <sup>2</sup>

1-Whitout recovering the energy released from Equations (188) and (189) - ( $\Delta H_{\max}$  and  $\eta_{\min}$ ).

2-Recovering the energy released from Equations (188) and (189) - ( $\Delta H_{\min}$  and  $\eta_{\max}$ ).

Source: the author.

**TABLE 42 -  $\Delta H_{b,i}^0$ ,  $\Delta S_{b,i}^0$ ,  $G_{b,i}^0$  and  $\eta_b$  for (Cs-O-H)<sub>b</sub> and its chemical reactions**

Variables	Reaction 1 Eq. (190)	Reaction 2 Eq. (191)	Reaction 3 Eq. (192)	Cs-O-H cycle variation (b)
$\Delta H_{b,i}^0$ [kJ]	362.73	56.09	-132.99	418.82 <sup>1</sup> to 285.83 <sup>2</sup>
$\Delta S_{b,i}^0$ [J/K]	70.84	91.04	1.43	163.31
$\Delta G_{b,i}^0$ [kJ]	341.62	28.96	-133.41	237.16
$\eta_b$ [%]	-	-	-	68.24 <sup>1</sup> to 100 <sup>2</sup>

1-Whitout recovering the energy released from Equation (192) - ( $\Delta H_{\max}$  and  $\eta_{\min}$ ).

2-Recovering the energy released from Equation (192) - ( $\Delta H_{\min}$  and  $\eta_{\max}$ ).

Source: the author.

**TABLE 43 -  $\Delta H_{c,i}^0$ ,  $\Delta S_{c,i}^0$ ,  $\Delta G_{c,i}^0$  and  $\eta_c$  for (Cs-O-H)<sub>c</sub> and its chemical reactions**

Variables	Reaction 1 Eq. (193)	Reaction 2 Eq. (194)	Reaction 3 Eq. (195)	Reaction 4 Eq. (196)	Solidification Eq. (197)	Cs-O-H cycle variation (c)
$\Delta H_{c,i}^0$ [kJ]	68.84	362.73	-1.99	-132.99	-10.76	431.57 <sup>1</sup> to 285.83 <sup>2</sup>
$\Delta S_{c,i}^0$ [J/K]	20.80	70.84	90.01	1.43	-	183.08
$\Delta G_{c,i}^0$ [kJ]	62.64	341.62	-28.81	-133.41	-	242.03
$\eta_c$ [%]	-	-	-	-	-	66.23 <sup>1</sup> to 100 <sup>2</sup>

1-Whitout recovering the energy released from Equations (196) and (197) - ( $\Delta H_{\max}$  and  $\eta_{\min}$ ).

2-Recovering the energy released from Equations (196) and (197) - ( $\Delta H_{\min}$  and  $\eta_{\max}$ ).

Source: the author.

**TABLE 44 -  $\Delta H_{d,i}^0$ ,  $\Delta S_{d,i}^0$ ,  $\Delta G_{d,i}^0$  and  $\eta_d$  for (Cs-O-H)<sub>d</sub> and its chemical reactions**

Variables	Reaction 1 Eq. (198)	Reaction 2 Eq. (199)	Reaction 3 Eq. (200)	Cs-O-H Cycle variation (d)
$\Delta H_{d,i}^0$ [kJ]	68.84	349.98	-132.99	418.82 <sup>1</sup> to 285.83 <sup>2</sup>
$\Delta S_{d,i}^0$ [J/K]	20.80	141.08	1.43	163.31
$\Delta G_{d,i}^0$ [kJ]	62.64	307.93	-133.41	237.16
$\eta_d$ [%]	-	-	-	68.24 <sup>1</sup> to 100 <sup>2</sup>

1-Whitout recovering the energy released from Equation (200) - ( $\Delta H_{\max}$  and  $\eta_{\min}$ ).

2-Recovering the energy released from Equation (200) - ( $\Delta H_{\min}$  and  $\eta_{\max}$ ).

Source: the author.

**TABLE 45 -  $\Delta H_{e,i}^0$ ,  $\Delta S_{e,i}^0$ ,  $\Delta G_{e,i}^0$ , and  $\eta_e$  for (Cs-O-H)<sub>e</sub> and its chemical reactions**

Variables	Reaction 1 Eq. (201)	Reaction 2 Eq. (202)	Cs-O-H cycle variation (e)
$\Delta H_{e,i}^0$ [kJ]	362.73	-76.90	362.73 <sup>1</sup> to 285.83 <sup>2</sup>
$\Delta S_{e,i}^0$ [J/K]	70.84	92.47	163.31
$\Delta G_{e,i}^0$ [kJ]	341.62	-104.45	237.16
$\eta_e$ [%]	-	-	78.79 <sup>1</sup> to 100 <sup>2</sup>

1-Whitout recovering the energy released from Equation (202) - ( $\Delta H_{\max}$  and  $\eta_{\min}$ ).

2-Recovering the energy released from Equation (202) - ( $\Delta H_{\min}$  and  $\eta_{\max}$ ).

**Source: the author.**